Technological and design aspects of the processing of composites and nanocomposites, Vol. I

Technological and design aspects of the processing of composites and nanocomposites

Volume I

Technological and design aspects of the processing of composites and nanocomposites

Volume I

Lublin University of Technology
University of Minho
Technical University of Košice

TECHNOLOGICAL AND DESIGN ASPECTS OF THE PROCESSING OF COMPOSITES AND NANOCOMPOSITES

Volume I

Monography

edited by

Prof. **Janusz W. Sikora**, Ph.D., D.Sc.
Lublin University of Technology

Assoc. Prof. **Ľudmila Dulebová**, Ph.D., D.Sc.
Technical University of Košice

Košice
Technical University of Košice
2018

Scientific-Practical International Workshop
under a Project H2020-MSCA-RISE-2016-734205

This project has received funding from the European Union's Horizon 2020 research and innovation programme under the Marie Skłodowska-Curie grant agreement No 734205–H2020-MSCA-RISE-2017

Reviewed by:
Prof. Ernest Gondár, Ph.D., D.Sc., Slovak University of Technology in Bratislava, Slovakia
Wiesław Jan Frącz, Ph.D., D.Sc., Rzeszów University of Technology, Poland
Mykola Brailo, Ph.D., D.Sc., Assoc. Prof. , Kherson State Maritime Academy, Ukraine

Publisher:
Technical University of Kosice, Fakulty of Mechanical Engineering, Letna Str. 9 , 040 01 Kosice, Slovakia

Production Editor:
František Greškovič, Ľudmila Dulebová

Printed by:
Technical University of Kosice, Letna Str. 9, Kosice, Slovakia

ISBN 978-80-553-2773-0

PREFACE

Nowadays it is difficult to imagine further development of science without nanotechnologies and technologies of processing of polymer materials since in many research areas one runs out of research possibilities and opportunities of knowledge acquisition.

The contents of this monograph constitutes only a small part of scientific issues discussed by the participants of the NEWEX project in the second year of its duration. The main objective of the NEWEX project entitled "Investigation and development of a new generation of machines for the processing of composite and nanocomposites materials" is the exchange of researchers from the institutions participating in the project, and hence the development of their professional careers and promotion of international and inter-sector cooperation between EU countries institutions. Another objective is to foster, improve and develop permanent international and inter-sector collaboration between academic research centres (Lublin University of Technology, Technical University of Kosice, University of Minho) and industrial organizations (Zamak-Mercator LLC and SEZ-Krompachy a.s., Dirmeta UAB). Participants of the project share their knowledge, get to know modern technologies of manufacturing polymer composites by extrusion and injection molding.

This monograph contains results of the research activities of participants of the NEWEX project and presents the problems concerning the studies of optimization and simulation of the extrusion and injection process, as well as the properties of polymers filled with fillers and nanofillers, on the matrix of mainly polypropylene, polyethylene and polyvinylpyrrolidone.

We hope that this publication will be useful to a wide group of people from the industry of plastics processing and it should also useful for scientific employees dealing with technologies and processing of polymer composites and nanocomposites.

Janusz W. Sikora
Ľudmila Dulebová

TABLE OF CONTENT

A. Gaspar-Cunha[1], José A. Covas[1], M. Fernanda P. Costa[2], Lino Costa[3]

OPTIMIZATION OF SINGLE SCREW EXTRUSION

Abstract: *Multi-objective evolutionary optimization algorithms (MOEA) are used for the optimization of plasticating single screw extrusion. For this purpose, a specific MOEA is linked to available process modelling routines. The methodology is used to set the operating conditions and identify the screw geometry for a specific case study, thus demonstrating the practical utility of this approach.*
Keywords: *extrusion process, optimization, Pareto chart*

1. Introduction

The optimization of single screw extrusion is a difficult task as it involves taking into attention several conflicting objectives [1-3]. Two major practical challenges are the definition of the optimal operating conditions and/or the identification of the geometrical parameters yielding the best process performance. Traditionally, a trial-and-error approach combined with empirical knowledge has been used for this purpose. Also, some attempts based on mathematical models coupled to statistical analysis have been applied [4-6]. Nevertheless, a more efficient approach is to handle single screw extrusion as an optimization problem where different conflicting objectives are to be considered simultaneously [1, 3, 7]. In such a case, Multi-objective Evolutionary algorithms (MOEA), such as the Reduced Pareto Set Genetic Algorithm (RPSGA) [1, 2], can be used. Generally, the outcome of these methodologies is a group of solutions approaching the set of Pareto optimal solutions, which represents different trade-offs between the objectives. Decision making strategies can be implemented to assist the decision maker to select, from the Pareto optimal set, the more suitable solutions for the single screw extrusion process.

This chapter discusses the application of a multi-objective optimization methodology based on evolutionary algorithms for the definition of the operating conditions and/or the geometry of a single screw extruder for a representative case study.

2. Optimization problem formulation

The optimization of the single screw extrusion requires coupling different tools that will create a comprehensive system being able to consider the response of the extruder to the appropriate set of input parameters. Thus, the MOEA is

[1)] *Department of Polymer Engineering, Institute for Polymer and Composites, University of Minho, Guimarães, Portugal, agc@dep.uminho.pl*
[2)] *Department of Polymer Engineering, Centre of Mathematics, University of Minho, Guimarães, Portugal,*
[3)] *Department of Polymer Engineering, Algoritmi Research Centre, University of Minho, Guimarães, Portugal.*

coupled to a modelling routine of plasticating extrusion, which must be able to compute the values of the relevant objectives for a given set of equipment geometry and dimensions, operating conditions and polymer properties. The modelling routine is presented in more detail in chapter 1 and in references [1, 2]. It describes mathematically the plasticating sequence by a set of balance equations that are coupled to a rheological constitutive law and a set of boundary conditions [2].

The most relevant objectives (extruder performance) are generally considered to be the mass output (Q), the length of screw required for melting the polymer (Z_t), the melt temperature at the die exit (T_{exit}), the mechanical power consumption (*Power*) and the degree of mixing. The latter may be quantified by the weighted-average total strain (*WATS*), a measure of distributive mixing. Usually, the aim is to maximize Q and *WATS* and minimize Z_t, T_{exit} and *Power*. The values attained by these objectives depend on the values of the decision variables. There are two groups of variables (Figure 1). One corresponds to the operating conditions of the extruder, specifically the screw speed (N), and the temperature profile of the heater bands in the barrel (T_{b1}, T_{b2}, T_{b3}). The range of variation of the former depends on the mechanical power system (motor and reduction gear) of the extruder. The lower and upper bounds for the range of temperatures of the heater bands are the polymer melting temperature and the onset of degradation, respectively. The other group of variables comprises the geometrical parameters,

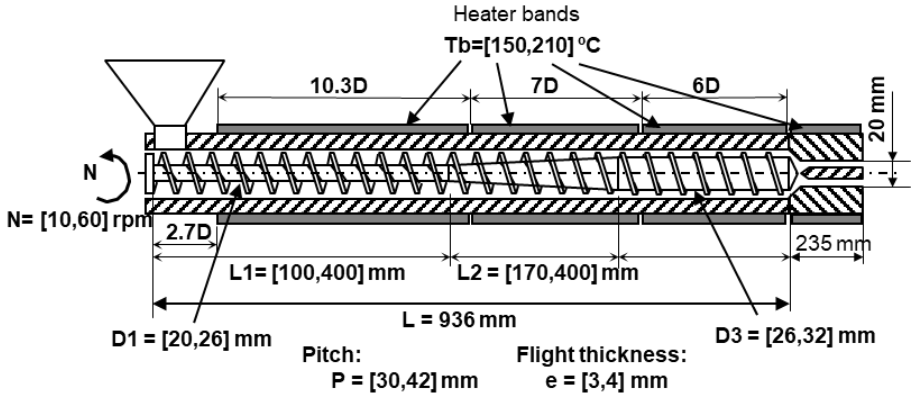

Fig. 1. Operational and geometrical variables to be optimized

which encompass the internal screw diameter of the feed (D_1) and metering zones (D_3), the axial lengths of the feed (L_1), compression (L_2), and metering zones (L_3), the flight thickness (e) and the screw pitch (p). The ranges of variation of the geometrical parameters are usually defined based on empirical knowledge. For example, if the compression zone is too short, the rate of decreasing channel depth downstream could become higher than the melting rate, resulting in material

clogging. Conversely, since the shallower the screw channel the higher the melting rate, a very long compression zone will result in an unnecessarily long melting stage. It should be noted that all these decision variables are continuous.

As noted above, the aim is to optimize several conflicting criteria simultaneously. This implies, for example, increasing the screw speed which will bring out higher outputs, but also lower quality of mixing and greater energy consumption. Therefore, there is no single solution that optimizes all criteria, but instead a set of solutions that represents different trade-offs between them. This type of problems can be formulated as a multi-objective optimization problem (MOP). A general mathematical formulation of a MOP can be written as follows:

$$\begin{aligned} \underset{x\in R^n}{\text{minimize}} \quad & f(x) \equiv (f_1(x), \dots, f_m(x)) \\ \text{subject to} \quad & c_i(x) \geq 0, i \in I \\ & c_i(x) = 0, i \in E \\ & lb \leq x \leq ub \end{aligned} \tag{1}$$

where, $f: R^n \to R^m$ are the m objective functions, $c_i: R^n \to R$ are the constraint functions and I and E are two finite sets of indices. For $i \in I$, c_i are the *inequality constraints* and for $i \in E$, c_i are the *equality constraints*. lb and ub are the vectors of the lower and upper bounds on the decision variables, respectively.

A point x that satisfies the constraints is called a *feasible point*. The set of feasible points is defined by:

$$\Omega = \{x \in R^n: c_i(x) \geq 0, i \in I; c_i(x) = 0, i \in E; lb \leq x \leq ub\}.$$

Thus, the multi-objective optimization problem (1) can be rewritten more compactly as:

$$\underset{x\in\Omega}{\text{minimize}} \ (f_1(x), \dots, f_m(x)) \tag{2}$$

In multi-objective optimization, the solutions are compared in terms of dominance. The following definitions are used [8].

Definition 1 (Pareto dominance): Given $x, y \in \Omega$, the point x is said to dominate point y, denoted by $x \prec y$, if and only if

$f_i(x) \leq f_i(y)$, for all $i \in \{1, \dots, m\}$ and $f_j(x) < f_j(y)$ for at least one $j \in \{1, \dots, m\}$.

Definition 2 (Pareto optimality): Let $x^* \in \Omega$ be a feasible point; x^* is Pareto optimal if there is no vector the point $y \in \Omega, y \neq x^*$ that

$f_i(y) \leq f_i(x^*)$, for all $i \in \{1, \dots, m\}$ and $f_j(y) < f_j(x^*)$ for at least one $j \in \{1, \dots, m\}$.

The set of the images of the Pareto optimal set is called the *Pareto optimal front*. Mathematically, any maximization objective can be converted as a minimization one since $\max f_i(x)$ is equivalent to $-\min -f_i(x)$. Hence, in this chapter any maximization objective will be reformulated as a minimization one.

In the context of the optimization of a specific single screw extrusion process, the objective functions f_i, for $i \in \{1, \dots, m\}$, can be normalized taking into consideration reference values for them in the search space of the real problem. Thus, the objective functions can be re-scaled to the same order of magnitude in the interval [0,1], the normalized objectives being computed for all $i \in \{1, \dots, m\}$ by:

$$F_i(x) = \begin{cases} \dfrac{f_i(x) - f_i^{min}}{f_i^{max} - f_i^{min}} & \text{if } f_i^{min} \le f_i(x) \le f_i^{max} \\ 1 \end{cases} \qquad (3)$$

where $f_i^{min} = \min_{x \in \Omega} f_i(x)$ and $(f_1^{min}, \dots, f_m^{min})$ is called the *objective ideal vector*, and each component f_i^{max} of the vector $(f_1^{max}, \dots, f_m^{max})$ is an estimation of the *nadir objective vector* obtained from a payoff table [10]. For normalized objectives, a maximization objective can also be reformulated as a minimization objective as follows:

$$\max_{x \in \Omega} F_i(x) = \min_{x \in \Omega} \left(1 - \frac{f_i(x) - f_i^{min}}{f_i^{max} - f_i^{min}}\right) \qquad (4)$$

This reformulation is adopted in this work. The single screw optimization problem is a bound constrained multi-objective optimization problem. To simplify the formulation, the decision variables are denoted by $x = (N, T_{b1}, T_{b2}, T_{b3}, D_1, D_3, L_1, L_2, e, p)$. For the extruder size range and layout illustrated in Figure 1 and assuming the processing of a typical thermoplastic polyolefin (High Density Polyethylene (HDPE), the lower and upper bounds vectors are $lb = (10,\ 150,\ 150,\ 150,\ 20,\ 26,\ 100,\ 170,\ 3,\ 30)$ and $ub = (60,\ 210,\ 210,\ 210,\ 26,\ 32,\ 400,\ 40,\ 4,\ 42)$, respectively. The minimum and maximum values of the objective functions are defined based on the practical experience with this equipment and material. Table 1 presents normalized objective functions, for generic values of f^{min} and f^{max}.

Table 1. Objective functions to be optimized

Description	Aim	f^{min}	f^{max}	Normalization
Mass output - Q (kg/hr)	maximize	1.0	20.0	$F_1(x) = 1 - \frac{f_1(x) - f_1^{min}}{f_1^{max} - f_1^{min}}$
Length – Z_t (m)	minimize	0.2	0.9	$F_2(x) = \frac{f_2(x) - f_2^{min}}{f_2^{max} - f_2^{min}}$
Melt temperature - T_{melt} (ºC)	minimize	150.0	210.0	$F_3(x) = \frac{f_3(x) - f_3^{min}}{f_3^{max} - f_3^{min}}$
Power consumption - *Power* (W)	minimize	0.0	9200	$F_4(x) = \frac{f_4(x) - f_4^{min}}{f_4^{max} - f_4^{min}}$
Mixing degree - *WATS*	maximize	0.0	1300	$F_5(x) = 1 - \frac{f_5(x) - f_5^{min}}{f_5^{max} - f_5^{min}}$

Thus, the mathematical formulation of the single screw multi-objective optimization problem is given by

$$\begin{aligned} \underset{x \in R^{10}}{\text{minimize}} \quad & (F_1(x), F_2(x), F_3(x), F_4(x), F_5(x)) \\ \text{subject to} \quad & lb \leq x \leq ub \end{aligned} \tag{5}$$

where the $F_i(x)$, for $i \in \{1,2,3,4,5\}$, are given in Table 1.

3. Multi-objective Optimization Methods

Different approaches for solving multi-objective optimization problems are reported in the literature [8, 10]. One approach includes the use of scalarization methods. In these methods, the multi-objective optimization problems are reformulated as single objective optimization using a scalarized function that depends on the set of parameters, such as weights or reference points. Different sets of parameters must be used to obtain different approximations to the Pareto optimal solutions. Thus, in this type of approach several single optimization problems must be solved.

For example, in the weighted sum scalarization method, the MOP in equation (3) is reformulated using an aggregated function, as follows:

$$\begin{aligned} \underset{x \in R^{10}}{\text{minimize}} \quad & \sum_{i=1}^{5} w_i F_i(x) \\ \text{subject to} \quad & lb \leq x \leq ub \end{aligned} \tag{6}$$

where $w_i \geq 0$ are the weights, and $\sum w_i = 1$. One advantage of these methods is the possibility of being solved using the simpler single objective optimization

algorithms available in the literature. Nevertheless, these methods have some drawbacks. They require the definition of appropriate sets of values for the parameters that depend on the problem. Additionally, to approximate the Pareto optimal front of the multi-objective problem, solving several single objective optimization problems can be computationally expensive.

Alternatively, Evolutionary Algorithms (EAs) can be used instead [9, 10]. EAs are particularly suited to deal with the multi-objective nature of real problems since they work with a population of candidate solutions (or vectors), rather than with a single solution point. Moreover, EAs have the ability to seek the global optimum, avoiding being trapped in local optima. In Multi-objective Evolutionary algorithms (MOEAs), some mechanisms are used to promote the convergence towards the Pareto front. It is also possible to implement diversity preserving techniques during the search, to obtain a representative and diverse set of compromise solutions. Thus, MOEAs can provide, in a single run, approximations to several Pareto optimal solutions, representing different trade-offs between the objectives.

The Reduced Pareto Set Genetic Algorithm (RPSGA) is a MOEA that has been used successfully to optimize single screw extrusion [1-3, 7, 11]. RPSGA uses a clustering technique to reduce the number of solutions and to guarantee their good distribution along the Pareto front during the search procedure. Initially, a population of points is generated randomly. At each generation, several operations are performed. First, the solutions of the population are evaluated (*i.e.*, the values of the objectives are computed). Next, a clustering technique is applied to reduce the number of non-dominated solutions (*i.e.*, approximations to the Pareto front) based on ranks. Then, a linear ranking function is used to compute the fitness value of the solutions. This value depends on the rank of each solution in the population, which is related to its performance, location and non-domination condition. The best individuals are selected for reproduction using a roulette wheel selection. For the reproduction, a SBX recombination operator and polynomial mutation are used [11]. The iterative process stops when a pre-defined maximum number of generations is reached. Details about RPSGA can be found in [11].

MOEAs are easy to implement, explore the entire search space and, consequently, are able to escape from local optimal solutions and can be easily adapted to work in the optimization in different conditions.

4. Numerical Results

In this section, the RPSGA is used to optimize the single screw extrusion problem defined in Figure 1 and Table 1. Seven different scenarios, identified in Table 2, are considered to optimize the operating conditions and the screw geometry. In scenarios 1 to 4, the operating conditions of the extruder are optimized using only two objectives. These correspond to bi-objective optimization problems, that are relevant to check if the solutions produced by the

RPSGA are suitable for the extrusion process. Moreover, the results obtained are simpler to analyze, enable an easier visualization of the trade-offs between the solutions, as well as easier selection of the best solution to use from the set of the dominated solutions obtained. In the case of the scenarios 5 to 7, all five objectives were considered. Concerning the decision variables, in scenarios 1 to 5 only the operating conditions are considered, in scenario 6 only the geometrical parameters are optimized, whilst scenario 7 includes both types of decision variables are used.

Table 2. Scenarios for single screw extrusion optimization

Scenarios	Objectives	Decision variables
1	(Q, Z_t)	$x = (N, T_{b1}, T_{b2}, T_{b3})$
2	(Q, T_{melt})	$x = (N, T_{b1}, T_{b2}, T_{b3})$
3	(Q, *Power*)	$x = (N, T_{b1}, T_{b2}, T_{b3})$
4	(Q, *WATS*)	$x = (N, T_{b1}, T_{b2}, T_{b3})$
5	(Q, Z_t, T_{melt}, *Power*, *WATS*)	$x = (N, T_{b1}, T_{b2}, T_{b3})$
6	(Q, Z_t, T_{melt}, *Power*, *WATS*)	$x = (D_1, D_3, L_1, L_2, e, p)$
7	(Q, Z_t, T_{melt}, *Power*, *WATS*)	$x = (N, T_{b1}, T_{b2}, T_{b3}, D_1, D_3, L_1, L_2, e, p)$

The thermal, physical and rheological characteristics (the shear rate and temperature dependence of the viscosity are modelled by the Carreau-Yasuda equation) for a High Density Polyethylene, HDPE (grade ALCUDIA TR-135, manufactured by Repsol) are presented in Table 3:

$$\eta = \eta_0[1 + (\lambda\dot{\gamma})^{\alpha}]^{(n-1)/\alpha} \qquad (7)$$

The values chosen for the parameters of the RPSGA used resulted from previous empirical studies [1, 3, 11]: 50 generations; crossover probability of 0.8; mutation probability of 0.05; internal and external populations with 100 individuals; limits of the clustering algorithm set at 0.2; and number of ranks set at 30.

Table 3. Properties of the HDPE ALCUDIA TR-135, manufactured by Repsol

Density	Solids	ρ_s	495.0	$kg\ m^{-3}$
	Melt	ρ	854.4	
Thermal Conductivity	Solids	k_s	0.186	$W\ m^{-1}\ ^{\circ}C^{-1}$
	Melt	k_m	0.097	
Specific Heat	Solids	C_s	2350	$J\ kg^{-1}$
	Melt	C_m	2535	
Melting	Heat	H	167x10^3	$J\ kg^{-1}$
	Temperature	T_m	119.9	℃
Carreau-Yasuda equation	Viscosity	η_0	18000	$Pa\ s$
		E/R	10000	K
		$\hat{\lambda}$	0.70	s
		a	1.70	
		n	0.30	
		T_0	463.15	K

Figure 2 shows the Pareto fronts obtained for scenarios 1 to 4 (left column in Figure 2) and the two-dimensional projections of the Pareto front for scenario 5 (right column in Figure 2). In the first case, since only two objectives are optimized simultaneously, the algorithm converges to a curve, the Pareto front, that defines the trade-offs between the objectives in a two-dimensional space. For example, in scenario 2 the higher the output the higher is the melt temperature, as the viscous dissipation becomes more important. In scenario 5, the algorithm works in a 5-dimensional objective space. To visualize the trade-offs among the objectives, four two-dimensional projections of the Pareto front are drawn (right column in Figure 2). In such a case, it is important to note that some points that seem to be dominated in a given two-dimensional representation are non-dominated in another two-dimensional projection. In Figure 2, points P1 to P5 identify the best values for each objective, respectively. For example, point P1 identifies the maximum value of the output, while point P2 is the minimum value of the length of the screw required for melting.

Tables 4 and 5 show the decision variables and the corresponding objective functions values for these solutions. For instance, the maximum output for scenarios 1 to 4 is 8.57 kg/h, whilst for scenario 5 it attains just 7.69 kg/h, a reduction of 10.2%. This shows that the existence of several objectives (in scenario 5) may hinder attaining better/higher values of the individual objectives. Table 6 presents the relative difference between the values of the objectives for scenario 5 and scenarios 1 to 4 (in percentage). As it can be seen, for some objectives, in scenario 5 it was actually possible to improve some values (melt temperature and mechanical power consumption objectives).

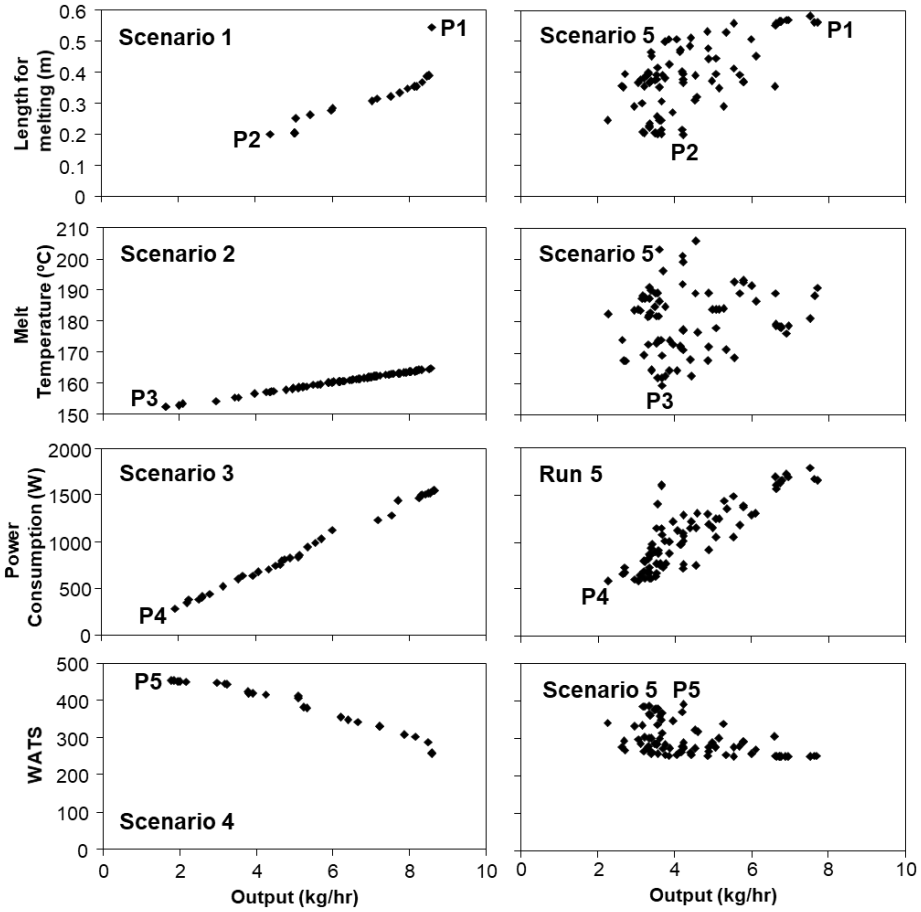

Fig. 2. Comparison between the Pareto fronts for scenarios 1 to 4 (left column) and the two-dimensional projections of the Pareto front for scenario 5 (right column)

Table 4. Solutions with the best values for each objective function for scenarios 1 to 4

	Operating conditions				Objectives				
	N (rpm)	T_{b1} (°C)	T_{b2} (°C)	T_{b3} (°C)	Q (kg/h)	Z_t (m)	T_{melt} (°C)	*Power* (W)	*WATS*
P1	59.4	210	196	199	**8.57**	0.544	206	1694	256
P2	28.8	203	200	197	4.37	**0.200**	202	1051	406
P3	10.7	150	202	150	1.64	0.323	**152**	296	297
P4	11.6	204	201	207	1.91	0.198	205	**276**	398
P5	12.3	209	154	150	1.77	0.145	157	524	**454**

Table 5. Solutions with the best values for each objective function for scenario 5

	Operating conditions				Objectives				
	N (rpm)	T_{b1} (°C)	T_{b2} (°C)	T_{b3} (°C)	Q (kg/h)	Z_t (m)	T_{melt} (°C)	*Power* (W)	*WATS*
P1	54.2	188	170	177	**7.69**	0.562	191	1654	254
P2	29.5	185	184	162	4.22	**0.201**	177	1292	392
P3	25.4	151	188	157	3.66	0.215	**160**	1598	369
P4	14.7	170	178	189	2.26	0.246	183	**586**	342
P5	29.5	185	184	162	4.22	0.200	177	1292	**392**

Table 6. Relative differences between the values of the objectives of scenario 5 and those of scenarios 1 to 4 (in %)

	Objectives				
	Q (kg/h)	Z_t (m)	T_{melt} (°C)	*Power* (W)	*WATS*
P1	**-10.2**	-3.2	7.2	2.3	-1.1
P2	-3.5	**-0.5**	12.5	-22.9	-3.5
P3	123.0	33.4	**-4.8**	-439.5	24.4
P4	18.5	-24.7	11.1	**-112.3**	-14.2
P5	138.5	-38.7	-12.7	-146.7	**-13.7**

A similar analysis of the results can be done for scenarios 6 and 7. Figure 3 shows the two-dimensional projections of the Pareto front for scenario 6. The clouds of non-dominated solutions indicate the existence of a compromise between all the objectives. Table 7 presents the geometrical parameters corresponding to the best values for each objective function. Table 8 identifies the operating conditions and geometrical parameters corresponding to the best values for each objective function for scenario 7. Finally, Table 9 shows the relative difference between the values of the objectives for scenario 7 and scenarios 1 to 4 (in percentage). In scenario 7, all the objectives were improved, except the length of screw required for melting.

Table 7. Optimal point corresponding to the best values for each objective function for scenario 6

	Geometrical parameters					
	L_1 (mm)	L_2 (mm)	D_1 (mm)	D_3 (mm)	p (mm)	e (mm)
P1	131	259	22.1	27.9	38.7	3.1
P2	101	183	22.0	31.7	32.2	3.3
P3	168	301	21.8	32.0	37.0	3.5
P4	390	365	21.7	30.9	40.7	3.1
P5	101	181	21.9	31.9	31.1	3.4

Table 8. Optimal point corresponding to the best values for each objective function for scenario 7

	Operating conditions				Geometrical parameters					
	N (rpm)	T_{b1} (ºC)	T_{b2} (ºC)	T_{b3} (ºC)	L_1 (mm)	L_2 (mm)	D_1 (mm)	D_3 (mm)	p (mm)	e (mm)
P1	58.1	189	198	172	174	266	23.3	27.3	38.1	3.5
P2	24.1	207	195	177	143	305	24.2	26.8	37.6	3.3
P3	19.7	152	180	156	204	248	25.0	31.1	36.2	3.1
P4	10.9	161	196	152	270	290	25.1	29.4	37.9	3.3
P5	46.8	183	179	173	138	220	25.0	31.2	41.4	3.5

Table 9. Relative differences between the values of the objectives of scenario 7 and those of scenarios 1 to 4 (in %)

	Objectives				
	Q (kg/h)	Z_t (m)	T_{melt} (°C)	*Power* (W)	*WATS*
P1	61.9	-9.2	-0.9	-18.0	-39.8
P2	32.2	-27.9	-12.7	46.8	-23.1
P3	-5.3	-77.4	1.0	49.6	0.6
P4	8.5	-54.6	12.6	36.1	-22.2
P5	63.6	-66.0	-5.8	-35.8	20.5

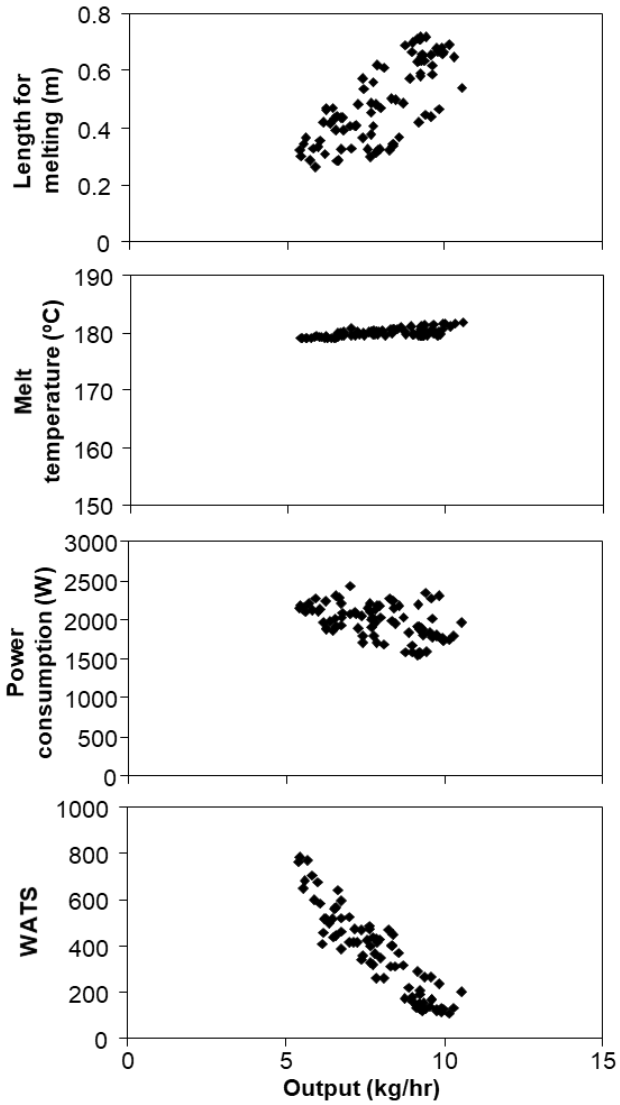

Fig. 3. Two-dimensional projections of the Pareto front for scenario 6

5. Decision Making

The decision maker (DM) must select the most suitable solution for the single screw extrusion problem from the Pareto optimal set. In this context, decision making strategies can be used to assist the DM [11]. In this work, the weighted sum method is used with different sets of weights to identify solutions according to the DM preferences. In practice, it is possible to define a tolerance (ϵ) that allows to reduce the region of the solutions.

For each scenario studied in the previous section, different sets of weights were used and an ϵ = 0.1. For instance, Figure 4 top shows the original Pareto front for scenario 1 (upper left side in Figure 2) and Figure 4 bottom presents the solutions obtained for three sets of weights, considering the DM preferences. The set of weights are $w_1 = (0.8, 0.1)$, $w_2 = (0.5, 0.5)$, and $w_3 = (0.2, 0.8)$, the corresponding solutions being denoted in the graph as a), b) and c), respectively. As it can be seen, the method is sensitive to the preferences of the DM. For example, as the output weight is decreased, the lower is the output of the solutions.

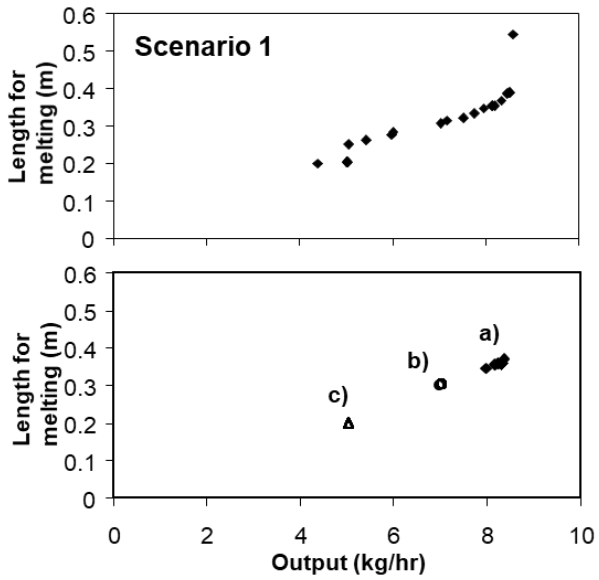

Fig. 4. Pareto front for scenario 1 (top) and the solutions obtained for three sets of weights (bottom)

Figure 5 presents the two-dimensional projections of the solutions obtained using the weighted sum method for scenario 5, considering two sets of weights: $w_1 = (0.8, 0.05, 0.05, 0.05, 0.05)$ and $w_2 = (0.2, 0.2, 0.2, 0.2, 0.2)$. Again, when the output weight decreases, the lower is the output of the solutions. Furthermore, the Pareto solutions are concentrated in smaller regions when compared with those obtained initially for scenario 5 (see Figure 2).

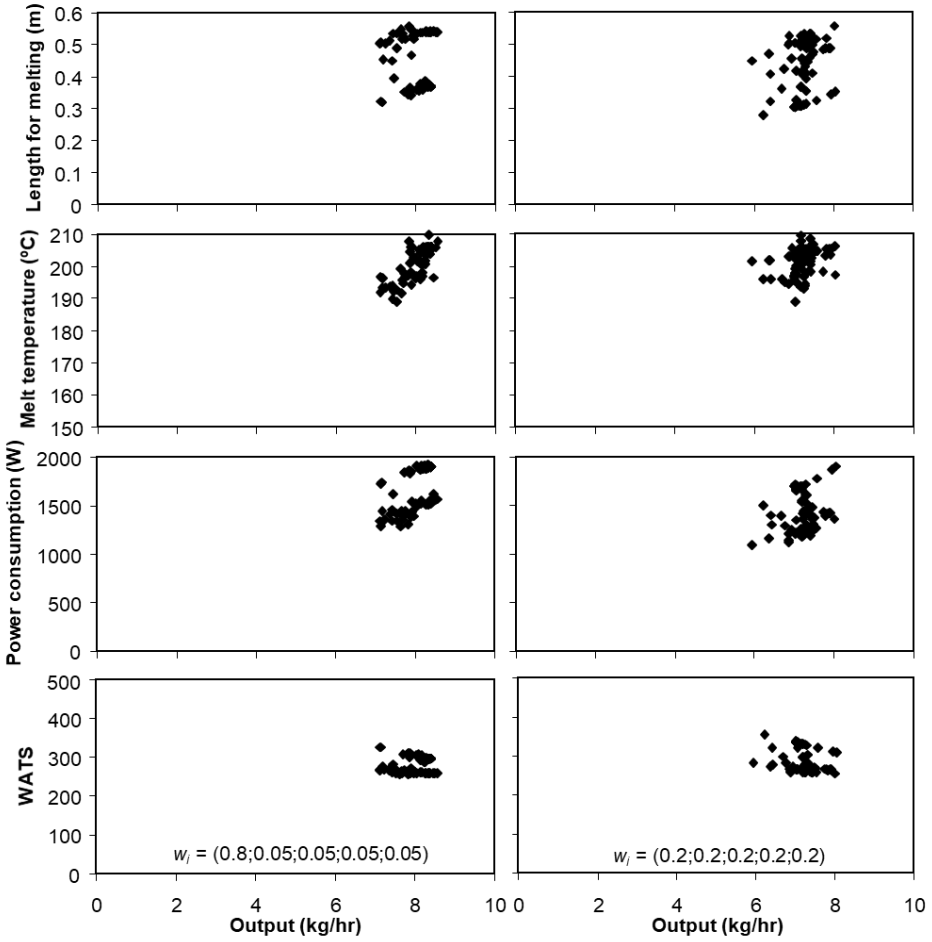

Fig. 5. Two-dimensional projections of the solutions obtained for two sets of weights for scenario 5

6. Conclusions

Traditionally, the optimization of single screw extrusion is performed based on empirical knowledge, often combined with trial-and-error procedures. Tentative extrusion experiments, or machining of screws, are performed until a desirable performance is obtained. This is costly and inefficient. Instead, setting the adequate operating conditions, or defining the screw geometry, can be assumed as an optimization problem. This chapter introduced a scientific approach to solve correctly and efficiently an important class of practical technological problems, including single screw extrusion.

Single screw extrusion was modelled as a multi-objective optimization problem, where the aim is to optimize its performance, as measured by several

relevant objectives. This problem involves different conflicting objectives, that depend on the operating conditions, or geometrical parameters, or both. The optimization method proposed was able to solve satisfactorily the problem and the solutions are viable and in agreement with current process knowledge (experimental validation is difficult and costly for obvious reasons). Finally, a decision making strategy incorporating the DM preferences was applied to assist the selection of solutions in the Pareto front.

Acknowledgements

This project has received funding from the European Union's Horizon 2020 research and innovation programme under the Marie Skłodowska-Curie grant agreement No 734205 – H2020-MSCA-RISE-2017.

7. References

[1] Covas, J. A., Gaspar-Cunha, A., Polymer Extrusion - Setting the Operating Conditions and Defining the Screw Geometry. Optimization in Polymer Processing, Nova Science Publishers, 87-113, 2011.

[2] Covas, J. A., Gaspar-Cunha, A., Oliveira, P. An optimization approach to practical problems in plasticating single screw extrusion. Polym Eng Sci, 39: 443-456, 1999.

[3] Covas, J. A., Gaspar-Cunha, A., Optimisation-based design of extruders, Plastics, Rubber and Composites, 33: 9-10, 416-425, 2004.

[4] Chung, C. I., A Scientific Approach to Screw Design, Journal of Reinforced Plastics and Composites, 17: 12, 1096 – 1109, 1998.

[5] Rauwendaal, C., Scale-up of single screw extruders. Polym Eng Sci, 27: 1059-1068, 1987.

[6] Potente, H., Existing Scale-up Rules for Single-screw Plasticating Extruders, Int. Polym. Proc., 6: 267–278, 1991.

[7] Gaspar-Cunha, A., Covas, J. A., The Design of Extrusion Screws: An Optimization Approach. International Polymer Processing, 16: 3, 229-240, 2001.

[8] Miettinen, K., Nonlinear Multiobjective Optimization. Kluwer Academic Publishers, Boston, 1999.

[9] Deb, K., Multi-Objective Optimization using Evolutionary Algorithms, Wiley, Chichester, UK, 2001.

[10] Multiobjective Optimization: Interactive and Evolutionary Approaches. Branke, J.; Deb, K.; Miettinen, K.; Slowinski, R.; Ed.; Lecture Notes in Computer Science, Springer-Verlag, Berlin, Heidelberg, 2008.

[11] Gaspar-Cunha, A., Ferreira, J., Covas, J. A., Fonseca, C., Extending Optimization Algorithms to Complex Engineering Problems. Optimization in Polymer Processing, Nova Science Publishers, 59-83, 2011.

A. Gaspar-Cunha[1], José A. Covas[1], Janusz Sikora[2]

MODELLING THE EFFECT OF GROOVED BARRELS ON THE PERFORMANCE OF SINGLE SCREW EXTRUDERS

Abstract: *Single screw extruders containing grooved barrels are used in many industrial extrusion lines, for example to manufacture plastics pipes and blown film. Through an increase of the drag friction forces between the polymer and the barrel, the conveying capacity of the screw is enhanced, yielding higher outputs and better process stability. This chapter presents and assesses computationally models for considering the effect of the presence of longitudinal or helical grooves near to the inlet port of the barrel of single screw extruders. The results obtained demonstrate that the existence of grooves clearly improves the performance of the extruder.*

Keywords: *computer modelling, calculations, extruder, grooved feed section*

1. Introduction

The underlying mechanism of solids conveying along the channel of a single screw extruder is well established [1-3]. Assuming that the solids form a cohesive plug maintaining good contact with the surrounding metallic surfaces (i.e., inner barrel wall, screw root, and pushing and trailing flights), the effect of the friction coefficients between the solids and the barrel, f_b, and between the solids and the screw, f_s, must be considered. Their relative magnitude will influence the corresponding dragging forces and, consequently, the displacement of the plug along the barrel. If $f_s > f_b$, the polymer will stick to the screw and slip on the barrel. Thus, the material will not move forward and the output is nil. Contrarily, if $f_b > f_s$, the material slips on the screw, progressing axially. This explains why, in practice, the surface of the screw channel is polished, while that of the barrel is kept relatively rough. The higher the difference between the friction coefficients, the higher the output. This prompted the concept of a grooved barrel near to the entry port of the extruder: if $f_b >> f_s$, not only the output is high, but it is also more stable [3], i.e., less dependent on fluctuations in melting, melt viscosity and die resistance. During the 1960's the concept found practical application in Germany, and progressively extended to european equipment manufacturers, especially for the extrusion of pipes and blown-film. Due to the popularity achieved, conventional extruders became known as "smooth bore extruders" in contrast with "grooved feed extruders".

Groove-feed extruders are still not very popular in the U.S.A., probably because they also have a number of disadvantages/requisites:

[1)] *Department of Polymer Engineering, Institute for Polymer and Composites, University of Minho, Guimarães, Portugal, agc@dep.uminho.pl*

[2)] *Faculty of Mechanical Engineering, Department of Technology and Processing of Polymer in Lublin, Nadbystrzycka 36 st., 20-618 Lublin, janusz.sikora@pollub.pl*

- The grooves should be relatively short (generally, lesser than 5D), in order to limit the pressure generated (which increases exponentially downstream) - this can reach 100 - 300 MPa; also, abrasion and mechanically resistant materials should be used for machining screw and barrel;
- Conversely, the friction forces generated will dissipate heat and could induce premature melting of the material, i.e., insufficient pressure generation; thus, it is important to assure the capacity of cooling the grooves via a circulating fluid and the existence of a thermal barrier with the remaining of the barrel;
- Higher friction forces require more torque for the same screw speed, i.e., a more powerful motor and a higher energy consumption;
- Screws with small compression ratio are usually mandatory, in order to limit the pressure generated; however, these screws have lower melting efficiency;
- The performance of the grooves is very sensitive to the characteristics of the solids; generally, they are not suitable to processing soft pellets (such as those of thermoplastic elastomers), powders and regrinds, due to possible plugging;
- The presence/flow of pellets in the grooves may affect the self-cleaning time of the extruder.

Due to the practical importance of the topic, numerous theoretical and experimental studies have been performed during the last forty years on groove feed extruders [3-11]. Two major modelling approaches have been developed, one assuming a global coefficient of friction resulting from the geometry of the grooves, while the other considers contribution of the flow of pellets inside the grooves. Due to the possibility of using analytical solutions, this chapter adopts the first approach. Four models proposed in the open literature are assessed in terms of their suitability and their sensitivity to changes in geometric parameters. Finally, the effect of the geometry of the grooves on the performance of a laboratorial extruder will be studied, with the aim of generating data that later could be compared with values obtained experimentally.

2. Geometry of the grooves

Grooves can be longitudinal or helical, as illustrated schematically in Figure 1. They are generally distributed evenly around the perimeter of the inner barrel wall. The cross-section can be rectangular, semi-circular, semi-drop shaped, or saw-toothed, but the former seems to be the most popular due its simpler machining. Usually, the depth of the grooves (h_N) decreases gradually from a maximum value at the entrance (h_{N0}) to zero at the outlet:

$$h_N = h_{N0} - A\, Z_N \tag{1}$$

where A is the slope and Z_N is the length. This solution minimizes the probability of the pellets being retained in the grooves. While longitudinal grooves create a

higher global friction coefficient, the helical solution induces the same effect, and the helix angle creates a positive drag component for the material inside the grooves.

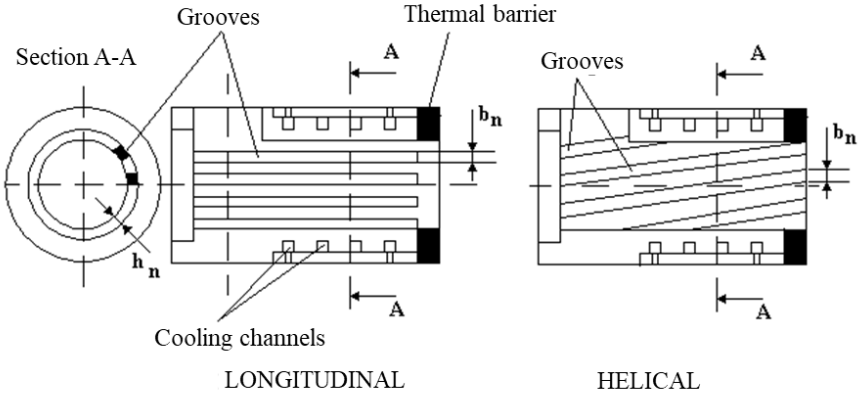

Fig. 1. Longitudinal and helical grooves in the barrel

3. Models assuming a global friction coefficient in the grooves

This approach assumes that the friction coefficient for a smooth bore extruder, f_b, can be replaced by a larger global, or equivalent, friction coefficient in the presence of grooves, f_{ef}. As shown in Figure 2, in the presence of grooves, three friction coefficients play a role in the transport of the solids: polymer-barrel, f_b, polymer-screw, f_s, and polymer-polymer, $f_{p\text{-}p}$. Therefore, this approach ignores the dynamics of flow in the grooves.

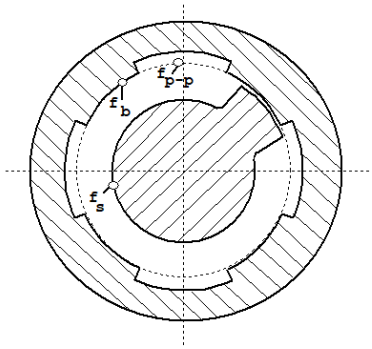

Fig. 2. Friction coefficients in the presence of grooves

Goldacker [11] proposed an equation for f_{ef} that contains the contribution of f_b and $f_{p\text{-}p}$:

$$f_{ef} = f_b + \left(f_{p-p} - f_b\right)\frac{B}{\pi D_b} \tag{2}$$

where D_b is the internal diameter of the barrel and B is the total grooves width, given by:

$$B = b_N N_N \tag{3}$$

This method does not consider the number of grooves nor their depth, whose influence has been shown as considerable [6, 8]. To overcome this, Potente [5] proposes the following equation:

$$f_{ef} = f_b + \left(f_{p-p} - f_b\right)\frac{B}{\pi D_b}\left\{1 - \exp\left[-\alpha\left(\frac{h_N}{B}N_N\right)^{\beta}\right]\right\} \tag{4}$$

α and β are empirical constants that are approximately equal to 5 and 0.9, respectively [5]. If the coefficients of friction in the inner surface of the barrel, f_b, and at the base of the grooves, f_{Na}), are different ($f_{Na} \geq f_b$>), the equation becomes:

$$f_{ef} = \left[f_b + \left(f_{p-p} - f_b\right)\frac{B}{\pi D_b}\right]\left\{1 - \exp\left[-0.65\left(\frac{f_{Na}}{f_b} - 1\right)^{1.2}\right]\right\} + \left[f_b + \left(f_{p-p} - f_b\right)\frac{B}{\pi D_b}\left\{1 - \exp\left[-5\left(\frac{h_N}{B}N_N\right)^{9}\right]\right\}\right]\exp\left[-0.65\left(\frac{f_{Na}}{f_b} - 1\right)^{1.2}\right] \tag{5}$$

Rautenbach and Peiffer [6, 7] performed force balances for an element of the solid plug in the channel and assumed the validity of the Hooke's Law. Neglecting the effects of inertia and gravity, as well as the distribution of transverse stresses in the downchannel direction, for the coordinate system shown in Figure 3, they obtained the following expression for a balance of the friction forces acting on the grooves:

$$f_{ef} = \frac{1}{e^{A^+\varphi_E} - 1}\sum_{n=1}^{M}\left\{f_b\left[e^{A^+\left(n\varphi_F + (n-1)\varphi_N\right)} - e^{A^+(n-1)(\varphi_N + \varphi F)}\right] + f_{p-p}\left[e^{A^+ n(\varphi_N + \varphi F)} - e^{A^+\left(n\varphi_F + (n-1)\varphi_N\right)}\right]\right\} \tag{6}$$

where:

$$M = \frac{\varphi_E}{\varphi_F + \varphi_N} \tag{7}$$

φ_E is the adimensional screw channel length:

$$\varphi_E = 2\pi E\cos\theta_b \tag{8}$$

φ_N is the angle shown in Figure 3:

$$\varphi_N = arctg \frac{b_N}{D_B} \tag{9}$$

φ_F is the angle shown in Figure 3:

$$\varphi_F = \frac{2\pi - N_N \varphi_N}{N_N} \tag{10}$$

A^+ is ~ 0.5, E is the number of screw turns facing grooves and θ_b is the screw helix angle.

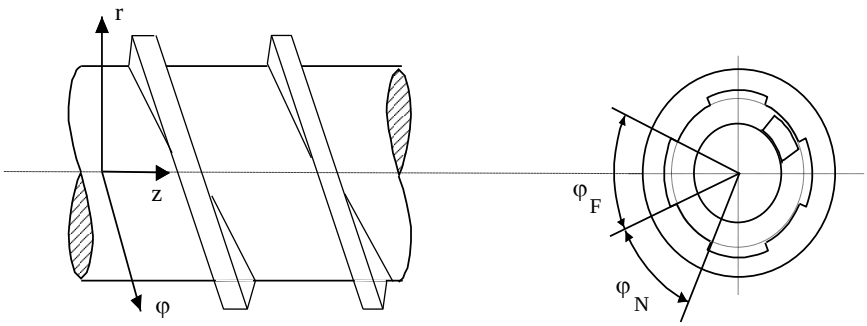

Fig. 3. System of coordinates and geometrical parameters for the model proposed by Rautenbach and Peiffer [6, 7]

Grünschloβ [8] considered the presence of transverse flow of polymer granules in the grooves (see Figures 4 and 5). He observed that the latter becomes significant when the ratio h_N/b_N is small (Figure 5). Thus, two situations may occur:

- If h_N/b_N is greater than a critical value, the average friction coefficient is obtained from equation 2;
- Otherwise, its value varies between the value given by equation 2 and f_b (Figure 6); in this case, higher pressures develop along the grooves.

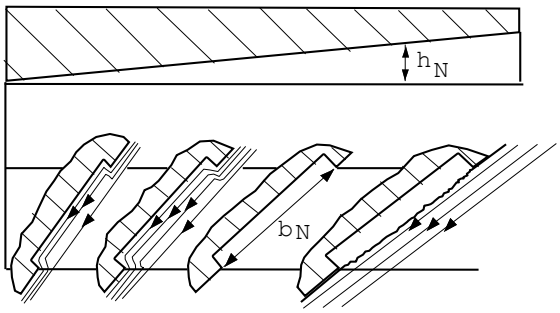

Fig. 4. Transverse flow of polymer granules in the grooves

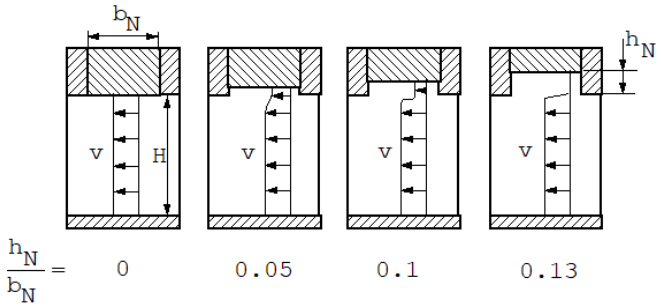

Fig. 5. Velocity profiles in the screw channel and transversal to the grooves

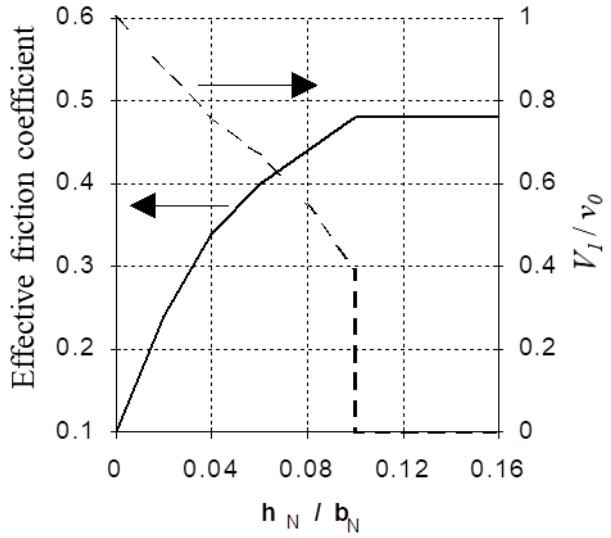

Fig. 6. Coefficient of friction and velocity of the solid bed as a function of h_N/b_N (f_b = 0.11 and f_{p_p} = 0.48)

These observations were used to build the model represented in Figure 7. The model assumes that the total power consumed to maintain the flow naturally adjusts to a minimum value ($P_{Ges\ min}$).

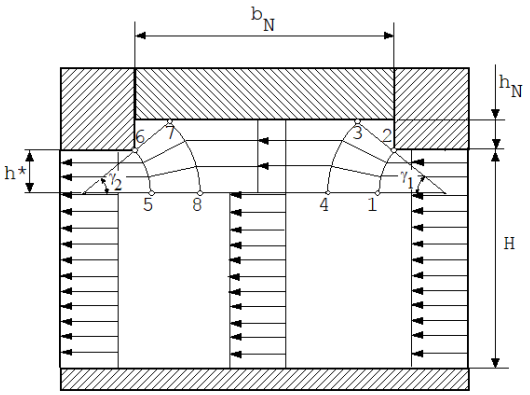

Fig. 7. Model illustrating the transversal flow in the grooves

The total power (P_{Ges}) is due to the deformations in zones 1 to 4 and 5 to 8, the deflections in zones 1-2, 3-4, 5-6 and 7-8 and the friction at zones 1-4, 5-8, 2-3, 6-7, 3-7, and 4-8:

$$P_{Ges} = 4P_{1-2} + 2P_{1-2-3-4} + 2P_{1-4} + 2P_{2-3} + P_{3-7} + P_{4-8} \tag{11}$$

Where P_i represents a dimensionless power consumption. These values depend on γ_1, γ_2 and h^*, and can be obtained from the following equations, for $\gamma_1 = \gamma_2 = \gamma$:

$$P_{1-2} = \frac{h^*}{b_N}\frac{\sin^2(\omega-\phi)}{tg\gamma}\left(\sqrt{1+\frac{tg^2\gamma}{\sin^2(\omega+\phi)}}-1\right) \tag{12}$$

$$P_{1-2-3-4} = \frac{h^*}{b_N}\ln\left(1+\frac{h_N}{h^*}\right) \tag{13}$$

$$P_{1-4} = \frac{h_N^2}{2b_N\sin\gamma\left(h^*+\frac{h_N}{2}\right)} \tag{14}$$

$$P_{2-3} = \frac{h^* h_N}{b_N\sin\gamma\left(h^*+\frac{h_N}{2}\right)} \tag{15}$$

$$P_{3-7} = \frac{h^*}{h^* + h_N} \frac{f_{Na}}{f_{p-p}} \left(1 - \frac{2h_N}{b_N tg\gamma}\right) \tag{16}$$

$$P_{4-8} = \frac{h^*}{h^* + h_N} \left(1 + \frac{2h^*}{b_N} \left(\frac{1}{tg\gamma} - \frac{1}{\sin\gamma}\right) - \frac{2h_N}{b_N \sin\gamma}\right) \tag{17}$$

where h^* is the level of divergence of the grooves, γ is the angle of the deformation zone (Figure 7) and ω is the angle of the grooves, equal to arctan of A. P_{Ges} depends on γ and h^*. Then, it is necessary to minimize P_{Ges}=f**(**γ**,** h^***)** using a numerical minimization method. One possibility is to adopt the Rosenbrock algorithm [12], which is convenient for the optimization of functions with several variables.

The coefficient of friction acting on the area of the grooves (f_e) can be obtained from:

$$f_e = f_{p-p} P_{Ges\min} \tag{18}$$

Finally, the average effective friction coefficient is obtained by substituting f_{p-p} by f_e in expression 2:

$$f_{ef} = f_b + (f_e - f_b) \frac{B}{\pi D_b} \tag{19}$$

4. Effect of the geometry of the grooves

4.1 Geometry and polymer properties

The extruder to be used in the calculations has a square pitch screw with a diameter of 36 mm and a *L*/*D* ratio equal to 26. Sleeves 4D long (144 mm) containing grooves with different geometries can be exchanged. In all cases, the grooves have a maximum depth at the beginning, which decreases linearly downstream until cancelling out. Table 1 presents the various configurations used for the grooves.

Table 1. Geometry of the grooves tested

Configuration	N_N	b_N (mm)	N_N*b_N (mm)
1	12	5.0	60
2	10	6.0	60
3	8	7.5	60
4	6	10.0	60
5	4	15.0	60
6	12	4.0	48
7	12	6.0	72

The polymer used in the calculations is a High-Density Polyethylene, a thermoplastic typically used for pipes and blown film, with the friction properties shown in Table 2.

Table 2. Friction coefficients for HDPE

Friction coefficient polymer- barrel	0.45
Friction coefficient polymer- screw	0.25
Internal friction coefficient	0.669

4.2 Results with the various calculation methods

The four calculation methods presented in the previous section were used to determine the value of the global friction coefficient, f_{ef}, for the groove geometries of Table 1. Figure 8 shows the effect of h_N/b_N on f_{ef} for configuration 1. As expected, the models of Goldacker and Rautenbach are insensitive to channel depth. In the case of the model of Potente, f_{ef} varies continuously; two regimes are present for the model of Grünschloβ, i.e., when $h_N/b_N < 0.06$, f_{ef} takes one value, whereas for the remaining values of h_N/b_N the coefficient of friction is the same as that given by the Goldacker model. Indeed, both models use equations 2 and 23 when $P_{Ges\ mín}$ converges to 1.

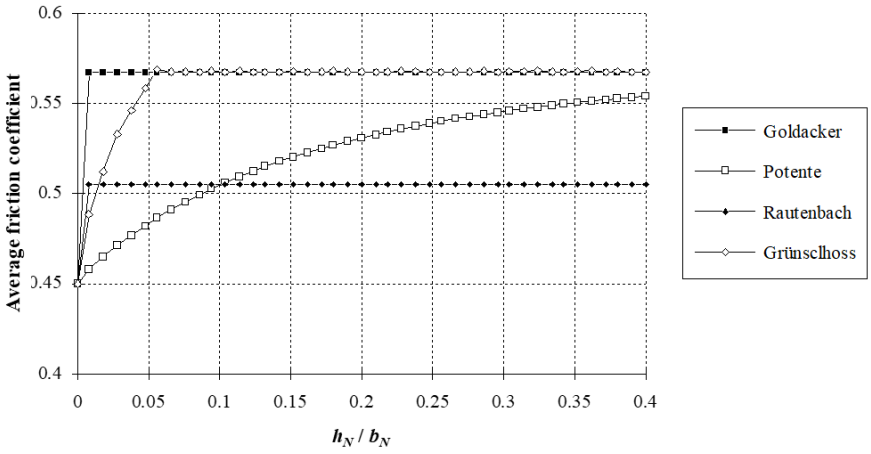

Fig. 8. Effect of h_N/b_N on the average friction coefficient according to various calculation models

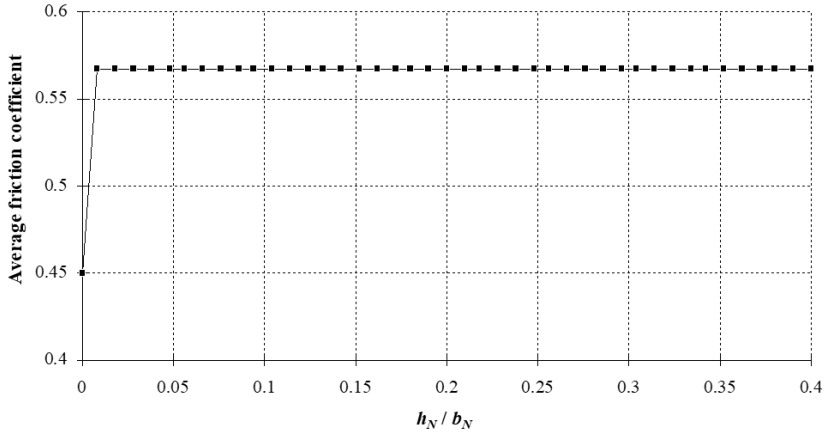

Fig. 9. Average friction coefficient calculated by the Goldacker model (configurations 1 to 5)

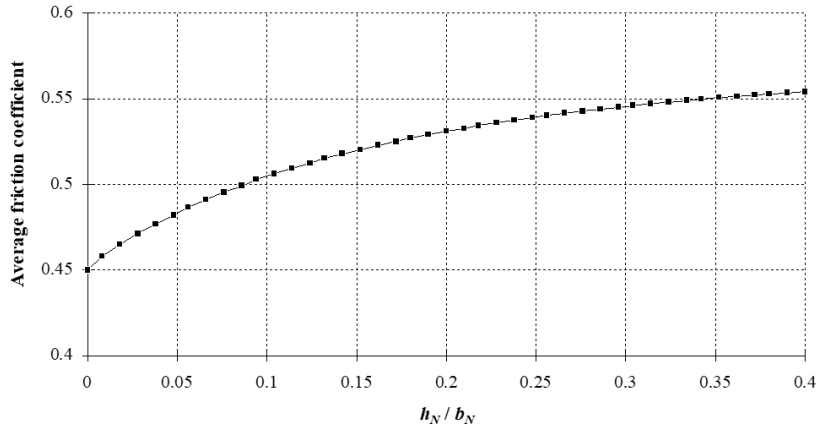

Fig. 10. Average friction coefficient calculated by the Potente model (configurations 1 to 5)

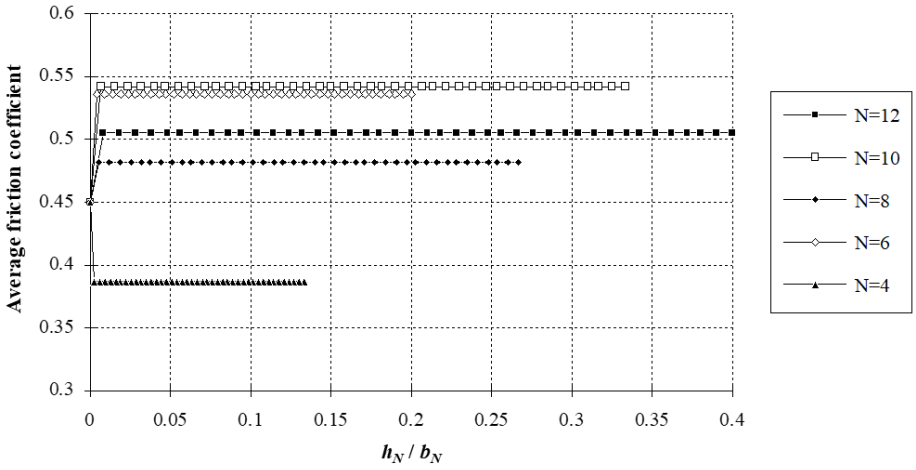

Fig. 11. Average friction coefficient calculated by the Rautenbach model (configurations 1 to 5)

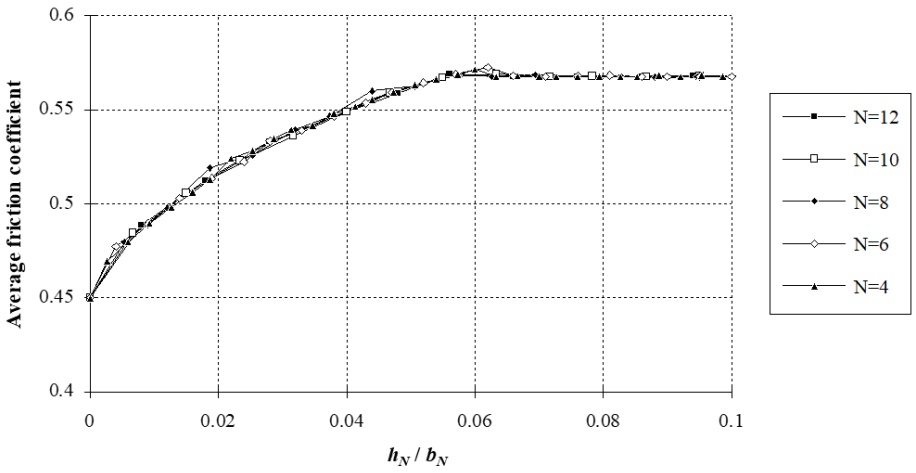

Fig. 12. Average friction coefficient calculated by the Günschloβ model (configurations 1 to 5)

As seen in Figures 13 to 16, all the models are sensitive to variations in the total width of the grooves, B. Furthermore, a proportionality exists between both, as demonstrated in Table 3.

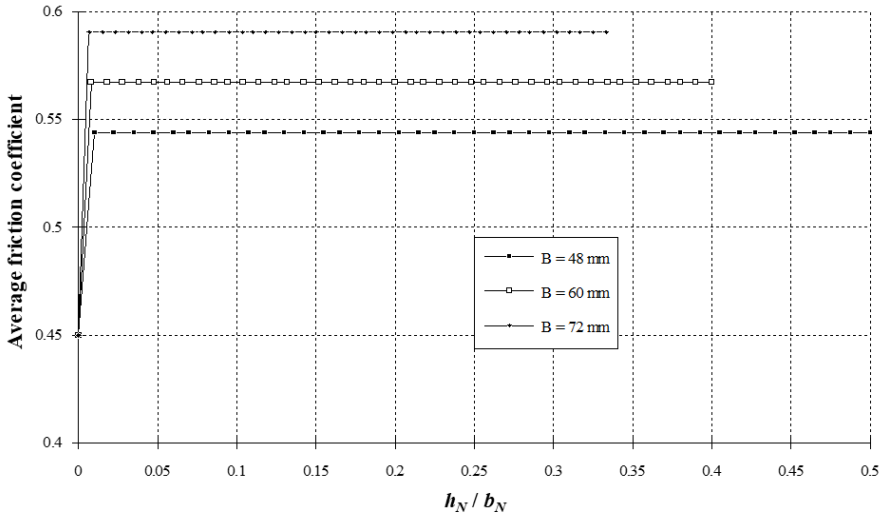

Fig. 13. Effect of the total width of the grooves on the average friction coefficient (Goldacker model)

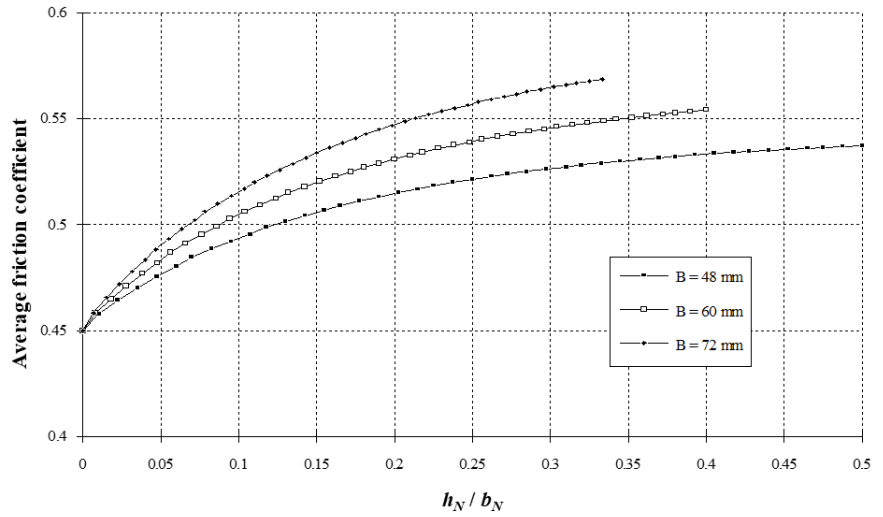

Fig. 14. Effect of the total width of the grooves on the average friction coefficient (Potente model)

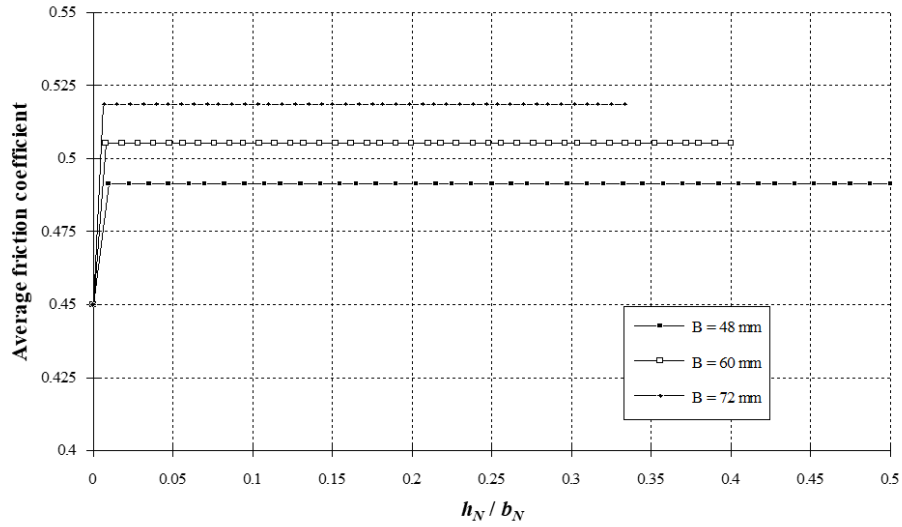

Fig. 15. Effect of the total width of the grooves on the average friction coefficient (Rautenbach model)

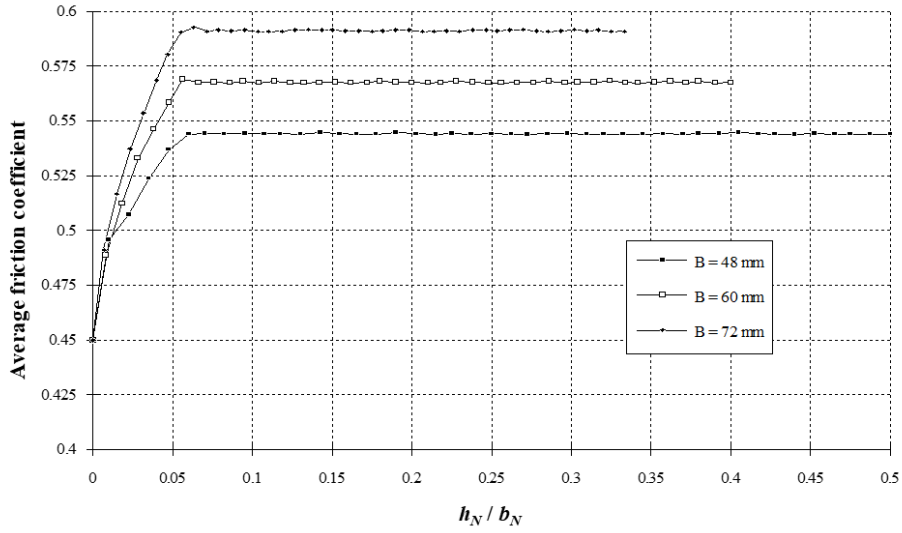

Fig. 16. Effect of the total width of the grooves on the average friction coefficient (Grünschloß model)

Table 3. Proportionality between f_{ef} and B

Model	*B* (mm)	f_{ef} (máximo)
Goldacker	48/60/72	0.544/0.567/0.591
Potente	48/60/72	0.537/0.554/0.569
Rautenbach	48/60/72	0.491/0.505/0.519
*Grünschlo*β	48/60/72	0.544/0.568/0.591

Finally, Figure 17 shows the effect of the coefficient A^+ of the Rautenbach model on the value of f_{ef}. As shown, a variation of A^+ from 0.1 to 0.9 produces a change between 0.551 and 0.482 in f_{ef}.

Globally, these results show that the model of Potente is able to consider simultaneously the effect of the total width of the grooves (*B*) and of their depth (h_N), while remaining take in only the effect of one of these parameters.

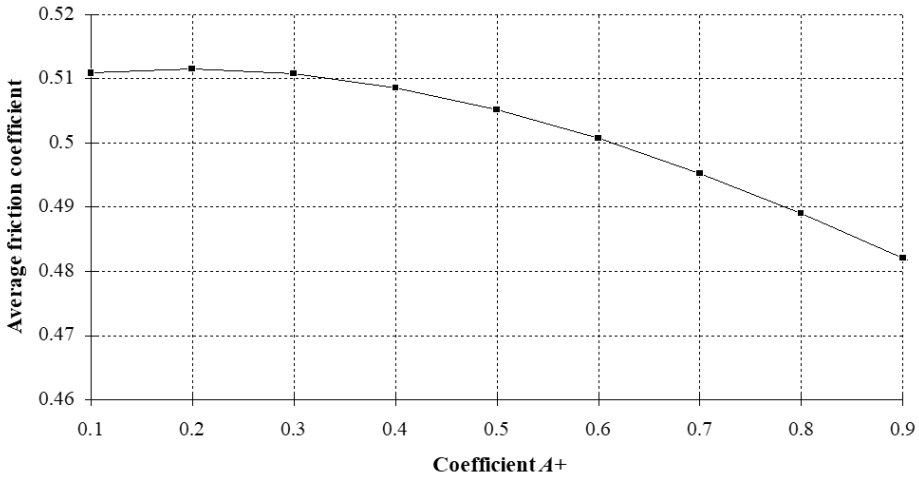

Fig. 17. Influence of A^+ in the average friction coefficient

4.3 Influence on plasticating extrusion

As discussed above, a higher friction coefficient between the polymer and the barrel will generate higher positive drag forces, hence higher pressure generation and higher output. Therefore, it is interesting to perceive what is the effect of the various methods to calculate f_{ef} on the predictions of a global modelling package of plasticating single screw extrusion (for details see the relevant chapter). The answer is given in Table 4, which shows that the models that yield a higher effective friction coefficient (Goldacker and Grünschloβ) also induce a higher throughput.

Table 4. Predicted outputs when using different calculation methods for the effect of the grooves

Calculation methods	Output (kg/hr)
Without grooves	8.06
Goldacker	8.32
Potente	8.07
Rautenbach	8.07
*Grünschlo*β	8.17

5. Application to a case study

This section uses one of the calculation methods above (the model of Potente), to study the effect of the geometry of the grooves on the performance of a laboratorial extruder. The aim is to generate data that later could be compared with values obtained experimentally.

5.1 Extruder, material and operating conditions

The layout of the extruder is represented in Figure 18. The three-zone screw has a diameter, D_{screw} = 25 mm, a L/D ratio of 25 and a square pitch. The lengths of the feed, compression and metering zones are 8D, 8D and 9D long, respectively. The internal screw diameter is 16.6 mm and 22.0 mm, respectively, in the feed, D_{i1}, and metering, D_{i3}, zones; the longitudinal length of the grooves, L_g, is 100 mm. A simple circular die is coupled at the end.

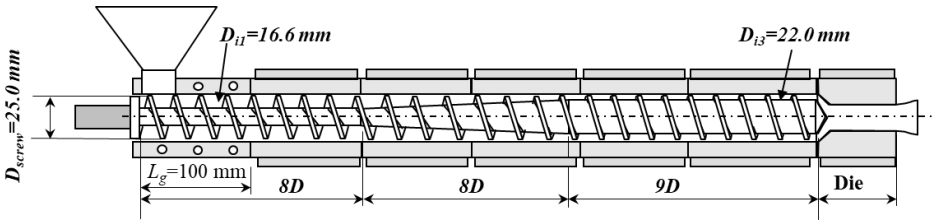

Fig. 18. Extruder layout

Table 5 shows the diverse geometries utilized. They could also correspond to different positions of devices allowing to adjust continuously the geometry of the grooves. In such a case, G1a represents the position when the grooves have the maximum value for the initial depth, h_{N0}, while G1d represents the case when this depth is nil.

Table 6 presents the relevant properties of the polymer used, a Low-Density Polyethylene (grade Malen E FGAN 18-D003 produced by LyondellBasell). The melt viscosity (Figure 19) was measured by capillary rheometry, the data being fitted to a power law with an Arrhenius temperature dependence:

$$\eta = \eta_0 \, \gamma^{(n-1)} e^{-a(T-T_0)} \tag{20}$$

Table 5. Geometry of the grooves studied

Geometry	b_N **(mm)**	h_{N0} **(mm)**	N_N	L **(mm)**	$B = N_N * b_N$ **(mm)**
G1a	6.0	6.0	4	100.0	24
G1b	6.0	4.0	4	100.0	24
G1c	6.0	2.0	4	100.0	24
G1d	6.0	0.0	4	100.0	---
G1e	6.0	6.0	5	100.0	30
G1f	6.0	4.0	5	100.0	30
G1g	6.0	2.0	5	100.0	30
G1h	6.0	0.0	5	100.0	---

Table 6. Main properties of LDPE (Basel Malen E FGAN 18-D003)

Properties			**LDPE**	**Unity**
Density	*Apparent*	ρ_0	495.0	kg/m^3
	Solid	ρ_s	921.0	kg/m^3
	Melt	ρ_m	854.4	kg/m^3
Friction coefficients	*Internal*		0.67	---
	Hopper		0.30	---
	Barrel		0.40	---
	Screw		0.20	---
Thermal conductivity	*Solid*	k_s	0.141	W/m ºC
	Melt	k_m	0.078	W/m·ºC
Specific Heat	*Solid*	C_s	3160.0	J/kg
	Melt	C_m	2682.0	J/kg
Melting heat		h	1.03 x 10^6	J/kg
Melting temperature		T_m	113.0	ºC
Viscosity: Power law with Arrhenius temperature dependence		n	0.27	---
		η_0	3.7e4	Pa/s
		a	0.005	1/°C
		T_0	170.0	°C

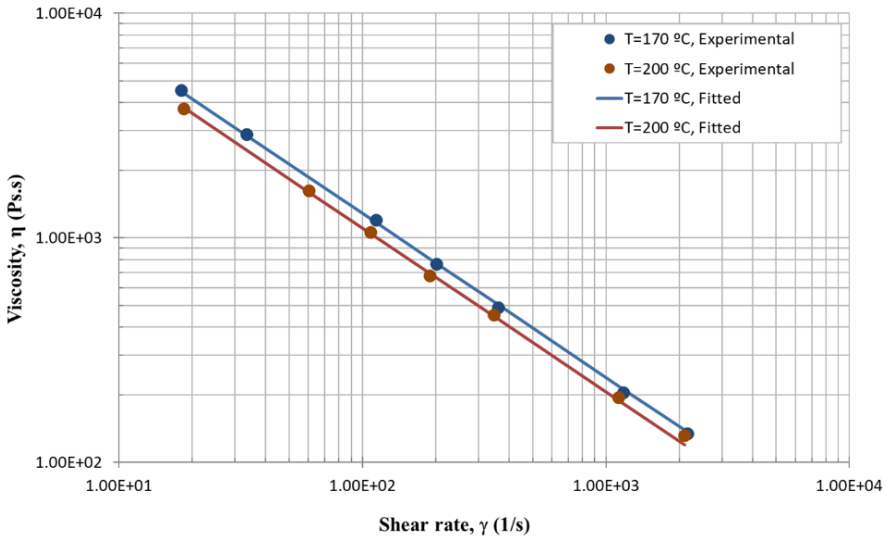

Fig. 19. Rheological data for LDPE (Basel Malen E FGAN 18-D003)

In all calculations, the operating conditions were fixed. The screw speed was 120 rpm; the barrel set temperature profile during the first 5D (corresponding to the length of the grooves) varies linearly from 30 ºC and 70ºC in order to prevent melting of the polymer and is constant and equal to 170ºC in the remainder of the barrel and die.

6. Results

Figure 20 presents the axial development of pressure, *P*, solids width (*X/W*, where X is the width of the solids and W is the channel width), and maximum temperature in the solids, $T_{s\ max}$, together with the barrel temperature profile imposed, T_{Barrel}, for the geometry G1a. Table 7 shows the values of global extruder responses: output, average melt temperature at die exit, mechanical power consumption, length required for melting, degree of distributive mixing (quantified by *WATS*, a measure of the average total of the melt in the extruder [13]), and viscous dissipation (ratio between the maximum and the barrel temperatures). Observation of the temperature graphs in Figure 20 shows that $T_{s\ max}$ raises faster than T_{Barrel} due to the high rate of heat generated by friction. Consequently, the length of the solids conveying stage reduces and so does the pressure generation, which reaches only less than 9 MPa. As expected, the maximum pressure is attained near the end of the compression zone of the screw. Most of the melting stage develops along the compression zone and is completed before the metering zone.

The Potente model used to calculate f_{ef} is only sensitive to values of h_N/b_N < 0.1 (see Figure 14). For geometries G1a to G1c, B = 24, thus h_N/b_N = 0.3 at the

beginning of the grooves (h_{N0} = 2); this ratio becomes small only towards the end of the grooves, where the effect of f_{ef} on the pressure profile is minor. Therefore, the results for these three cases are very similar (Table 6).

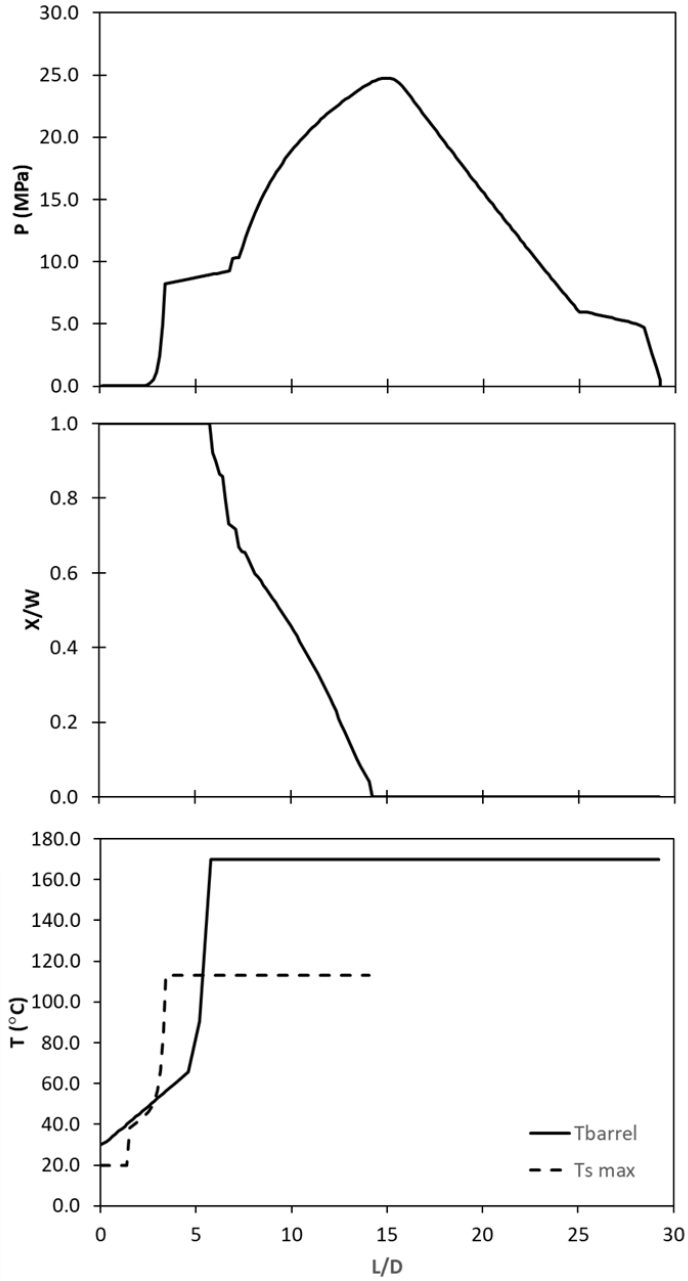

Fig. 20. Results obtained when using grooves with the geometry G1a (Table 5)

Table 7. Results for the geometries G1 in Table 5

Geometry	Output (kg/hr)	T_{melt} (°C)	Power consumption (W)	$L_{melting}$ (L/D)	*WATS*	Viscous Dissipation
G1a	5.43	188.5	2647	14.21	302.6	1.53
G1b	5.38	188.6	2597	14.17	303.1	1.54
G1c	5.38	188.6	2630	13.69	299.5	1.54
G1d	5.34	188.9	2278	14.64	308.0	1.46
G1e	5.47	188.3	2728	14.21	301.8	1.53
G1f	5.46	188.3	2669	13.83	299.2	1.51
G1g	5.35	188.3	2709	13.88	301.2	1.53
G1h	5.34	188.9	2278	14.64	308.0	1.46

Geometry G1e exhibits grooves with bigger depth and total width. As seen in Figure 21, the pressure can reach approximately 10 MPa, as expected. Conversely, G1d and G1h, where grooves are absent, are capable of inducing lower pressures than the remaining (Figure 22). As demonstrated in Figure 23, the various groove geometries will induce distinct pressure generations. Values between 6 MPa and 10 MPa will be obtained at the end of solids conveying. In turn, they will influence the remaining thermomechanical history of the material in the extruder, yielding the differences summarized in Table 7.

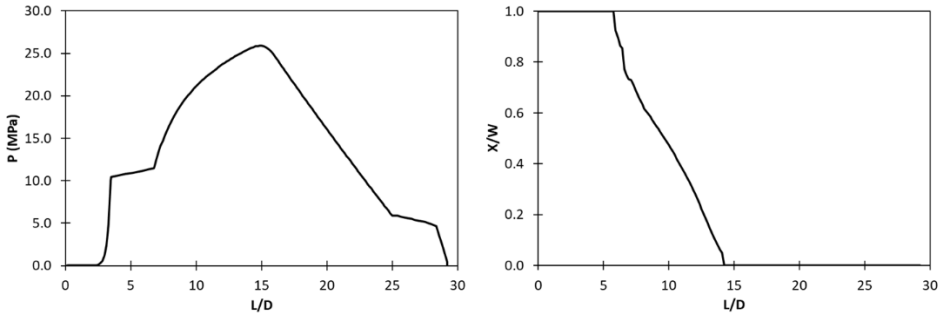

Fig. 21. Results obtained when using grooves with the geometry G1e (Table 5)

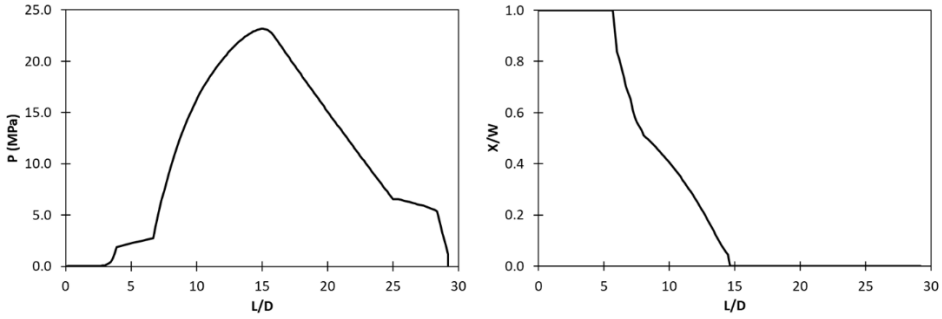

Fig. 22. Results obtained when using grooves with the geometries G1d and G1h (Table 5)

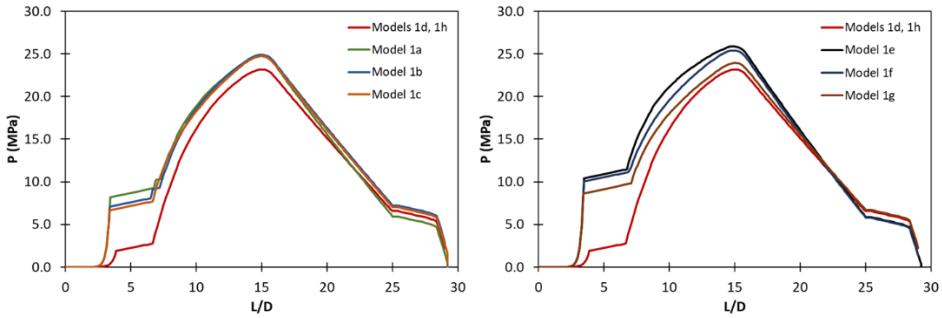

Figure 23. Pressure profiles for the geometries G1 (in Table 6)

7. Conclusions

The presence of grooves in the initial part of the barrel can affect significantly the performance of single screw extruders. Modelling their effect would enable the development of suitable and reliable process modelling routines. One possible approach is to calculate the global friction coefficient between barrel and polymer, f_{ef}, that is created by the presence of the grooves. The more sensitive f_{ef} would be to the geometrical parameters of the grooves, the better. This chapter assessed the suitability of four calculation methods of f_{ef}. It was shown that the equation developed by Potente considers both the width and depth of the grooves, whilst the model of Goldaker has the strongest influence on the plasticating sequence.

The examples discussed showed that the presence of the grooves does indeed improve the performance of the extruder in terms of pressure generation and output, but their geometry, particularly depth and the total width, greatly influences the behaviour.

Acknowledgements

This project has received funding from the European Union's Horizon 2020 research and innovation programme under the Marie Skłodowska-Curie grant agreement No 734205 – H2020-MSCA-RISE-2017.

8. References

[1] H. Darnell, E.A.J. Mol, SPE J., 12, 20, 1956
[2] Tadmor, Z.; Klein, I., "Engineering Principles of Plasticating Extrusion", Van Nostrand Reinhold, Ney York, 1970
[3] Rawendaal, C., "Polymer Extrusion", Hanser Publishers, Munich, 1986
[4] Boes, D.; Krämer, A.; Lohrbäccher, V.; Scheneiders, A., Kunststoffe Germ. Plast., 80, 6, 659, 1990
[5] Potente, H., Kunststoffe Germ. Plast., 75, 7, 439, 1985
[6] Rautenbach, R., Peiffer, H., Kunststoffe Germ. Plast., 72, 3, 137, 1982
[7] Rautenbach, R., Peiffer, H., Kunststoffe Germ. Plast., 72, 5, 262, 1982
[8] Grünschloss, E., Kunsttoffe Germ. Plast., 74, 7, 405, 1984
[9] Potente, H., Kunststoffe Germ. Plast., 78, 4, 355, 1988
[10] Potente, H., Koch, M., Intern. Polym. Process., 4, 4, 288, 1989
[11] Goldacker, E., Diss. RWTH Aachen, 1971
[12] Rosenbrock, H.H., The Computer Journal, 3, 3, 175, 1960
[13] G. Pinto, Z. Tadmor, Polym. Eng. Sci., 10, 279, 1970

José A. Covas[1], A. Gaspar-Cunha[1]

MODELLING OF FLOW AND HEAT TRANSFER, MIXING AND MORPHOLOGY DEVELOPMENT IN PLASTICATING SINGLE SCREW EXTRUSION OF POLYMER SYSTEMS

Abstract: *Models for flow and heat transfer, morphology development of liquid-liquid and solids-liquid systems and mixing assessment in conventional single screw extruders are introduced. Their computer implementation and interdependence are explained. Representative predictions are discussed with the aim of illustrating the capability of these models as wells as showing the typical response of single screw extruders.*
Keywords: *extrusion, extruder, flow, mixing, modelling, morphology, polymer systems*

1. Introduction

Single screw extruders are a crucial element of the extrusion lines used for the manufacture of plastics products such as tubular and flat films, sheets, pipes & tubing, profiles, wire & cable, mono and multifilaments, fibers, nets, bottles and other hollow containers, etc. Their role is to pump towards the shaping die a homogeneous melt at the highest possible constant rate. To accomplish this, the machine must be able to receive the raw material in powder or granular (the most frequent) form, melt it, homogenize it (both in terms of temperature and composition), and generate the pressure necessary for extrusion at the anticipated rate. The term *plasticating* applied to single screw extrusion designates the sequence of physical phenomena experienced by the polymer from the moment it enters the extruder until it exits the die.

The performance of single screw extruders is determined by the material properties, the geometrical/constructive features of the machine and the operating conditions selected (usually, screw speed and axial temperature profile). If a specific process behavior could be predicted rather than determined experimentally (this usually involves a significant number of expensive and time consuming trial and error attempts), better screw designs, higher quality products and greater outputs could be achieved faster and cheaper. Therefore, not surprisingly, plasticating single screw extrusion has been extensively studied both in academia and industry. Initially (between the 1950s and the 1960s), efforts were made to understand the physical phenomena developing along the screw. Various attempts to model (parts of) the process were also published (between the 1960s and 1980s) [1-6]. Later, a number of overall models of plasticating extrusion were progressively made available as commercial software packages.

[1)] *Department of Polymer Engineering, Institute for Polymer and Composites University of Minho, Guimarães, Portugal, agc@dep.uminho.pl*

The present chapter presents an overall model of plasticating extrusion that was conceived to balance completeness and precision of the predictions with reasonable computational costs. In turn, this model was subsquently coupled to other algorithms that yield supplementary data about the process. One example is process optimization, which will be dealt with in a separate chapter.

Moreover, although models of plasticating extrusion assume the presence of a specific homopolymer, currently more complex material systems are processed, such as compounds comprising polymers and specialized additives, polymer blends, polymer composites and nanocomposites. In most cases, upon melting and subsequently downstream, a multiphase liquid–liquid or liquid-solid morphology develops. It is well accepted that the final morphology determines the performance of the material under service conditions. Therefore, it is important to predict the progress of the morphology of liquid–liquid or solid-liquid systems during plasticating extrusion. This can be done by implementing a morphology development model and coupling it to a plasticating model, which will deliver information on local flow conditions (velocities, temperatures and residence times). Morphology development models for liquid-liquid and solid-liquid systems will be presented in this chapter. Finally, the data supplied by such models can be used to assess the mixing capability of a particular extruder, both in terms of distributive and dispersive mixing.

The present chapter is structured in three main parts. First, models for flow and heat transfer (i.e. plasticating), morphology development and mixing assessment are introduced. They are preceded by a presentation of the geometry assumed for the calculations. The second part explains the computer implementation of the above models. In general, this involves coupling the routine for flow and heat transfer to one of the other algorithms. Finally, the third part discusses some representative results.

1. Modelling the process

1.1 Geometry

Figure 1 illustrates the typical layout of a standard single-screw extruder. It consists essentially of a hollow long barrel (with a length to diameter ratio, L/D, typically equal to or above 24), inside which one Archimedes-type screw rotates at a controllable constant speed (the machine comprises also a DC or AC drive motor, a speed reducing gear and a control panel, which are not represented in the figure). A shaping die is coupled to one end of the barrel, while the raw material is fed by a lateral hole at the opposite end (commonly known as feed throat), on top of which a hopper is fixed. The latter usually consists of a vertical column with straight and/or inclined sections and contains the raw material to be processed, usually in pellet form. The screw shown in the Figure 1 has a constant pitch and a variable channel depth, thus producing three geometrically distinct zones. From hopper to die, one can identify a feed zone (with constant channel depth), a compression zone (with decreasing channel depth) and a metering zone

(where the screw is shallower). Heater bands surround the barrel and die. Together with thermocouples and temperature controllers, they allow to set and maintain a specific axial temperature profile. At constant geometry, changing the set temperatures and/or the screw speed, will create distinct thermomechanical environments inside the machine.

The flow channel linking the feed throat to the die (i.e., the free volume inside the barrel to be occupied by polymer) is helical, with the pitch of the screw, an approximately rectangular cross-section, and a depth that is either constant or gradually decreasing, depending on the lengthwise location. Therefore, the simplest straight progress of a pellet or fluid element along this channel is mathematically described by the equation of helix, if a Cartesian coordinate system, for example with its origin positioned at the start of the extruder is assumed. If the flow is more complex, equations will become inevitably also more complicated. This difficulty originated three classic assumptions that are habitually adopted when modelling single screw extrusion. One concerns the cinematics, two refer to the geometry of the system:

a) Although the screw rotates inside a motionless barrel, the opposite is assumed, i.e., the screw is considered as stationary, and the barrel is assumed to rotate in the opposite direction at the same angular velocity;
b) The helical channel and the barrel are considered as unwrapped. In other words, the helical channel becomes a rectangular channel whose lateral walls are the pushing and trailing flights of the screw, and the bottom is the screw root (in reality, the helical geometry causes the helix angle to depend on radius, but the distortion caused upon unwrapping is disregarded). The depth changes along the length, as seen above. Likewise, the barrel becomes a flat surface sliding on top of the rectangular screw channel towards the die. Considering assumption a), this sliding motion makes an angle relative to the channel, which is the screw helix angle;
c) Given a) and b), the Cartesian coordinate system can now be attached to the stationary screw channel; axes x,y,z correspond to directions across the channel, upwards and along the channel, respectively.

As a result of these assumptions, a movement of material straight along the channel is now simply described by the equation of a straight line. These assumptions are thus quite convenient and will be adopted in this chapter.

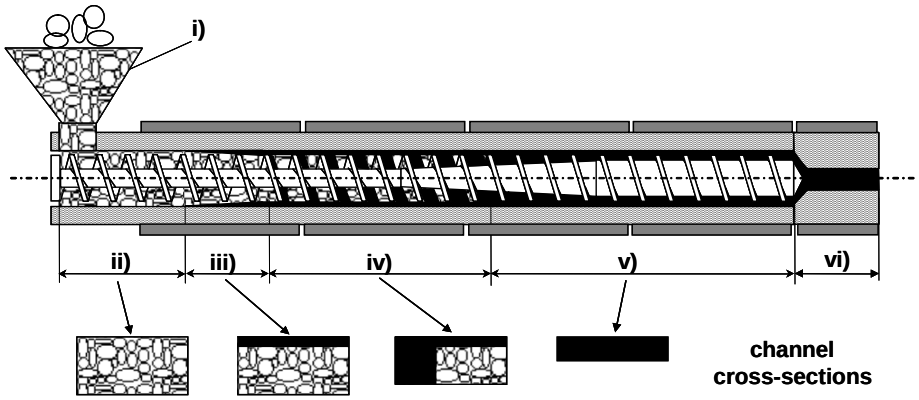

Fig. 1. Geometrical layout of a single screw extruder and plasticating sequence; the pellets are stored in the hopper and fed through a lateral opening in the barrel; they advance along the screw and are progressively melted, the melt exists the die at the opposite end; (i) to vi) represent process stages identified in the text)

1.2 Modelling flow and heat transfer

To model the plasticating process of the polymer inside a single screw extruder, it is first necessary to identify the physical phenomena developing from the instant the material enters the channel until it emerges from the die. These are schematically illustrated in Figure 1. The pellets enter the channel via the hopper by gravity-induced flow. Then, the material is dragged along the screw due to friction (it slides along the screw due to the friction created by the inner barrel surface) until it melts. Melting is initiated near to the inner barrel surface due to the combined effect of heat conduction from the barrel and mechanical energy dissipation due to the friction forces. Melting of the bulk solids develops gradually following a well-ordered mechanism that involves the segregation of the melt from the surviving solids. Due to the relative barrel-screw movement, the melt formed near to the inner barrel wall accumulates in a melt pool that co-exists side by side with the solid bed. The width of the former increases progressively along the channel, while that of the latter reduces, until all the material is molten. In the last portion of the screw, the melt advances following a helical pattern, generating pressure and some degree of distributive mixing, until it flows through the die taking approximately the desired shape. Extensive experimental research demonstrated that this sequence of phenomena is quite general, although the rate of development and the extent of each stage are affected by the operating conditions, material properties and channel geometry. Consequently, as shown in Figures 1 and 2, plasticating extrusion can be taken as the sequence of the following individual stages (also known as functional zones):

i) gravity-induced *solids conveying* in the hopper;
ii) *drag solids conveying* in the initial screw turns;

iii) *delay in melting*, due to the growth of a thin melt film between the solids and the channel wall(s);
iv) *melting* according to a specific mechanism;
v) *melt conveying*, consisting of a helical flow pattern of the fluid towards the die;
vi) *die flow*.

Each of these stages is described mathematically by a set of general equations, together with the relevant constitutive laws and boundary conditions. In turn, all the stages are linked by appropriate boundary conditions, thus yielding a global coherent plasticating model.

The hopper consists of a sequence of vertical and/or divergent columns holding thousands of loose pellets with various shapes, an average particle size, and a particle size distribution. The pellets descend due to gravity, enter the channel of the rotating screw and then progress downstream with a complex velocity profile due to friction with the barrel, with the screw walls and between pellets, due to gravity, and due to particle-particle and particle-wall collisions. The packing density and temperature of the particles increase progressively until the solids form a cohesive elastic solid-plug. The flow of the individual pellets in the hopper and in the initial screw turns can be computed numerically by means of the discrete element method (DEM) [7, 8]. Mass output, volume fraction, average residence time, residence time distribution and velocity profiles (in the cross-channel and down-channel directions) can be predicted, but only after a significant computation effort. In practice, this approach has been used to study solids conveying independently, but has never been linked to the remaining plasticating stages because of the resultant excessive computation times. It has been demonstrated that the free flow capacity of a hopper is much higher than the actual discharge rate verified when it is mounted on top of the feed opening of an extruder [4]. Thus, a static vertical pressure profile may be assumed and calculated using the analysis proposed by Walker [9], which is based on a force balance on an elemental horizontal bulk solids slice. The pressure at the bottom of the hopper represents inlet condition of the sceew channel. Drag solids conveying (see Figure 2) is usually modelled assuming the sliding of a non-isothermal elastic solid plug between two parallel plates (barrel and screw root) with different friction coefficients. The thermal effect results from the contribution of conduction from the hot barrel and of friction near to the polymer/metal interfaces [10, 11]. The pressure generated between the screw inlet and the subsequent process stage is determined from force and torque balances made on differential down-channel elements. Pressure rises exponentially along the channel, the increase being linked to the relative value of the fiction coefficients [12].

A delay zone (delay in melting, Figure 2) is often presumed as developing after drag solids conveying [13]. Indeed, friction and heat transfer will ultimately lead to the melting of the solids near to the inner barrel wall (and later, at the

solids/screw interface). A film is then formed. When, due to the relative screw-barrel movement, this molten material can no longer flow backwards through the gap between the barrel and the screw tip, or through the spaces between contiguous pellets, a melt pool is formed near to the active flight and the melting stage initiates [14]. Thus, the delay zone can be sub-divided into two sequential phases. First, a melt film is formed near to the barrel wall (Figure 2, delay in melting-B). In the calculations, the friction force for drag solids conveying is replaced by a shear stress applied by the film on the solid bed. The film thickness and temperature can be obtained by solving the relevant forms of the momentum and energy equations, taking in heat convection in the down-channel and radial directions and heat conduction in the radial direction. In the second phase, films of molten material are created near to the screw channel walls (films B, D and E in Figure 2, delay in melting-B). From a modelling point of view, this can be viewed as a special state of melting, which develops while the width of melt film B remains smaller than the channel height [15].

Tadmor and Klein [1] developed a melting model based on the important experimental observations reported by Maddock [16] in the fifties. Subsequently, several variants were proposed with the aim of relaxing progressively some of the initial assumptions, and thus make the model more realistic. As illustrated in Figure 2 (melting), Lindt *et al* [17, 18] assumed the existence of the main melt pool (B), of a film (C) separating the barrel and the solid plug (A), and molten films separating the solid plug from the lateral and bottom screw walls (D,E). Constant down-channel solid bed velocity and cross-channel flow recirculation were also postulated. Flow and heat transfer in each of the 5 regions were described by different forms of the momentum and energy equations, coupled to the relevant boundary conditions and force, heat and mass balances [15].

The precise description of the flow of molten polymer during melting and melt conveying requires a full 3D analysis. However, if the overall modeling of the plasticating sequence is to be associated with morphology development and optimization, the necessary computational times would become unreasonable. Thus, melt conveying is often assumed as a two-dimensional non-isothermal flow of a non-Newtonian fluid. Considering that flow is incompressible and both flow and temperature are fully developed in the down and cross-channel directions, and that the viscosity is described by a Carreau-Yasuda law, the mass conservation, momentum and energy equations are solved, coupled to the relevant boundary conditions. Domingues *et al* [19] compared the predictions produced by this approach with those obtained by a 3D analysis using the ANSYS Polyflow® software [20]. The average differences associated with V_x, V_y, and V_z (the velocities in the x, y, and z directions, respectively) were 10.4%, 2.9%, and 6.5%, respectively, thus supporting the utilization of the simplified approach.

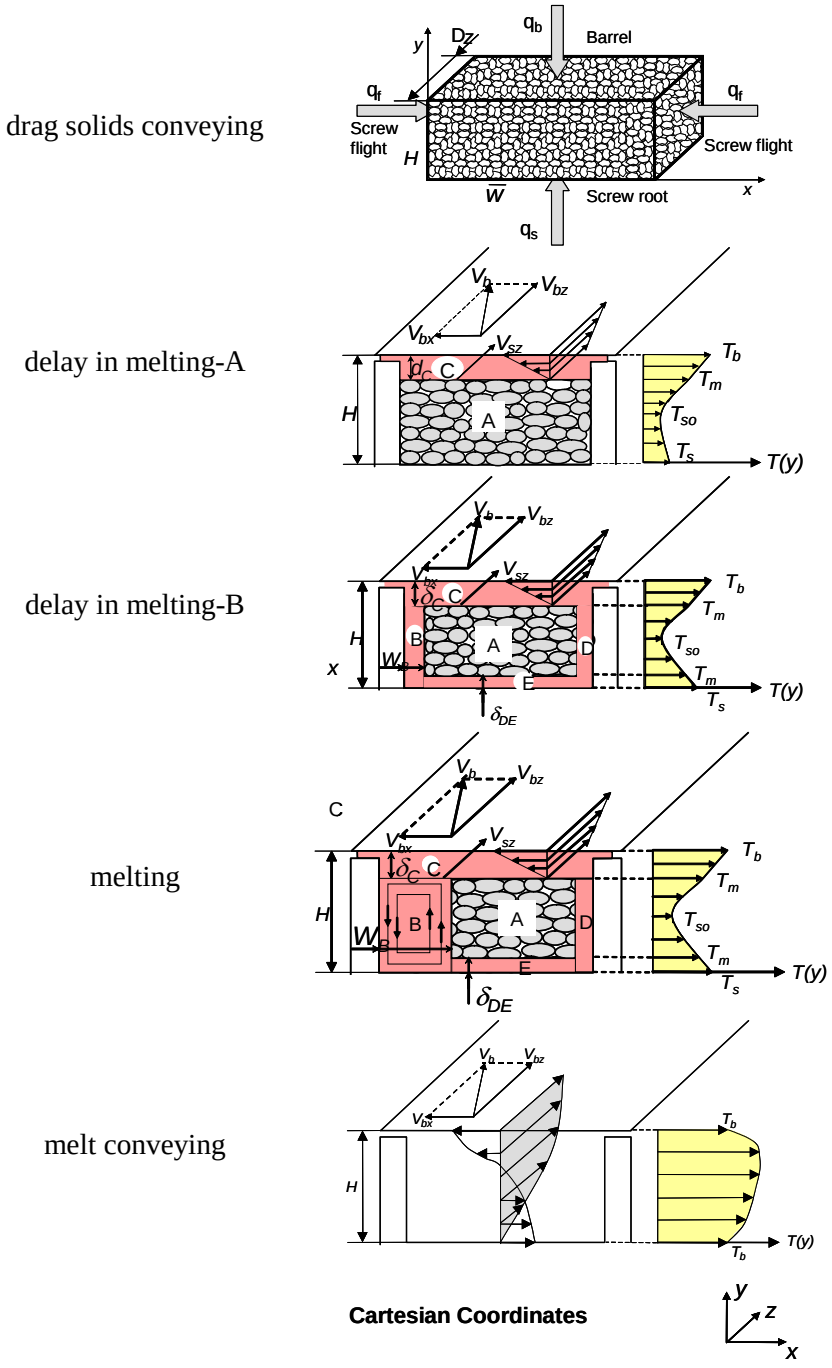

Fig. 2. Physical models for the functional zones developing along the screw channel in plasticating single screw extrusion

1.3 Modeling morphology development in liquid-liquid systems

Since the material or materials to be extruded are generally fed as solids in the hopper, a mathematical description of the development of the morphology of a multiphase liquid–liquid system along the screw must encompass the melting and melt conveying zones, and consider the relevant deformation, break-up and coalescence phenomena usually associated to these systems [21]. The break-up and coalescence processes compete against each other, and it is the overall result of this contend that determines the final drop size distribution.

A number of Maddock-type experiments were performed with immiscible and compatibilized Polyamide/Polypropylene blends, under a variety of operating conditions and screw profiles [22]. The authors reported that the melting stage follows a more complex mechanism than that accepted for homopolymers (and discussed in the previous section). Instead, a competition between a Tadmor-type model involving the co-existence of a melt pool and a solid bed and melting of individual solid pellets suspended in the melt was observed. This is probably related to the fact that the polymers had distinct melting temperatures and rheological properties. Since a melting model for this hybrid sequence is not currently available, melting of the major component (the one with higher concentration) will be assumed, and uniformly distributed suspended drops of the minor component will be inserted [19] at the pace of melting. The morphological model aims at estimating the evolution of the dimensions of these entities along the screw channel.

During flow, the suspended droplets will be subjected to affine deformation due to shear, i.e., they will stretch progressively. For a simple shear flow, the growth in length (L) can be correlated with the shear deformation (γ) and the initial drop diameter (d) through [19]:

$$L = \begin{cases} \left(1 + \frac{\gamma^2}{2} + \frac{\gamma}{2}\sqrt{4+\gamma^2}\right)^{0.5} \cdot d & \text{if} \quad \gamma < 5 \\ \gamma \cdot d & \text{if} \quad \gamma \geq 5 \end{cases} \tag{1}$$

The size of the droplets may be reduced by erosion or break-up. The former consists in the removal of small fragments from the drop surface, but this usually embodies a minor effect and will be disregarded here. Break-up occurs when the viscous forces are sufficiently higher than the interfacial tension and act during enough time. The ratio between the viscous forces (given by $\eta_c * \dot{\gamma} * r$, which represent matrix viscosity, shear rate and drop radius, respectively) and the interfacial tension (υ_{12}) is known as the Capillary number (Ca). The Ca required for break-up is usually known as critical Ca (Ca*). The time required for drop break-up (t_b) is given by [19]:

$$t_b = \frac{2\eta_c r}{\upsilon_{12}\Omega} Ln\left(\sqrt{\frac{r}{\alpha}}\right) \quad (2)$$

where Ω is a long function [21], λ is an index whose value depends on flow type (it assumes the value of 1 for extensional, 0.5 for shear, and 0 for rotational flow), *p* is the ratio between the viscosity of the dispersed phase and that of the matrix (η_d/η_c) and α is the amplitude of the initial deformation. Grace [23] established a well-known correlation between Ca* and *p* for a spherical drop suspended in a homogeneous steady flow. When Ca > 2 Ca*, the initial droplet deforms extensively and bursts into numerous smaller droplets; when Ca*< Ca < 2 Ca*, the droplet is expected to break into two equal spherical droplets [24]. In the case of low Reynolds numbers, a third smaller droplet can also be created and reportedly has a volume of 10–17% of that of the initial droplet [25].

When two drops collide and move jointly in a shear flow during enough time, coalescence may take place, i.e., the droplets can merge into a single larger entity. For calculation purposes, two successive steps of the process are assumed: (i) the collision of two equal drops and (ii) the exclusion of the polymer film separating them, which will flow into the main stream. The coalescence probability (P_{coal}) can be defined as the product of the probability of the two drops colliding (P_{coal}), with the probability of film exclusion between the drops (P_{exc}) [26]:

$$Pcoal = \exp\left(-\frac{\pi}{8\dot{\gamma}\phi t_{loc}}\right) \quad (3)$$

$$P_{exp} = \exp\left[-\frac{\sqrt{3}}{4}\left(\frac{r}{h}\right)p.Ca^{3/2}\right] \quad (4)$$

Equation (4) is valid for p∼1. Φ is the volume fraction of the dispersed phase, t_{loc} is the local residence time and *h* is the critical value at which the liquid film breaks.

The phenomena taken into consideration along this section must be interrelated with a proper description of the flow developing along the extrusion screw, since information on the onset and length of the melting zone, velocities, temperatures and residence times are necessary to predict the morphology development.

1.4 Modelling agglomerate dispersion in solid-liquid systems

The solid particles added to polymers upon processing (e.g., fillers, fibers) usually consist of agglomerates with a hierarchical structure: agglomerates are clusters of aggregates, and these contain numerous primary particles. Cohesive forces hold these structures together. Consequently, the dispersion of these assemblies can only occur when the hydrodynamic stresses developed during flow along the screw (σ_m) overcome their cohesive strength (σ_c). Dispersion can take place through erosion (small fragments detach from the outer surface of the agglomerate) and/or rupture (the agglomerate fragments into aggregates). In principle, the critical stress for erosion is smaller than that required for rupture, but erosion is a much slower process. Based on these concepts, Manas-Zloczower and co-workers [27] proposed the concept of a fragmentation number (Fa), defined as the ratio σ_m/σ_c, and suggested (for silica agglomerates of various densities suspended in low molecular weight polymers) that erosion takes place when $2 \leq Fa < 5$, while rupture occurs rapidly when $Fa \geq 5$. These limits will be adopted here, due to the lack of experimental data on the cohesive strength of most agglomerates used in polymer processing (including calcium carbonate, titanium dioxide, carbon black, carbon nanotubes, organoclays, exfoliated graphite, etc).

Even at high Fa, there is a finite probability associated with the break-up of agglomerates, which is defined as $P_{break} = \lambda^*\Delta t$, with $\lambda^*\Delta t << 1$, where λ is a probability per unit time, proportional to the surface area of the agglomerate. The time interval Δt is set as a function of screw speed [28]:

$$\Delta t = \frac{kH}{\pi N D_b} \tag{5}$$

P_{break} increases with increasing residence time and agglomerate size. There is an obvious parallelism between Fa and P_{break} and Ca and t_b (see previous section) for liquid-liquid systems.

This dispersion model must be coupled to a numerical model of plasticating extrusion and applied to the melting and melt conveying zones. As in the procedure developed for liquid-liquid systems, a number of initial agglomerates are inserted in the melt pool proportionally to the rate of melting. At the end of melting, the total number of inserted agglomerates corresponds to the filler concentration in the system. The dynamics of particle size distribution are calculated from the location where fillers are inserted until the screw tip.

1.5 Assessing mixing

Mixing, i.e., the reduction of spatial composition non-uniformity, is generally an important process pre-requisite for optimal product performance. It can be achieved through two routes. The spatial arrangement of the formulation

components can be improved by imposing a certain shear deformation history, this being known as distributive mixing. The latter depends on the interfacial area generated, which is proportional to the applied strain (defined as the product of shear rate and residence time). Thus, knowing the velocity field, it is possible to map the total strain for the various fluid elements in the screw channel. This was done, for example, by Pinto and Tadmor [29], who computed the degree of distributive mixing during melt conveying using a weighted-average total strain (WATS), assuming isothermal Newtonian flow between parallel plates. A review of other mixing calculation approaches can be seen in [5,6,21]. Composition non-uniformity can also be improved by decreasing the size of at least one of the components of the formulation (for example, droplets of the minor phase for an immiscible polymer blend, or solid agglomerates in the case of a filled system, as discussed above). This means that the computation of dispersive mixing in single screw extrusion requires the complete identification of the size, shape, orientation, and spatial location of every particle or droplet of the minor component along the flow channel. In this section, general mixing indices are proposed to quantify the degree of distributive and dispersive mixing in single-screw extruders. They are obtained by coupling a description of the flow in the screw from hopper to die to the models of morphology evolution previously discussed. Thus, processing of liquid-liquid and solid-liquid systems are dealt with individually.

In the case of liquid-liquid systems, the degree of distributive mixing can be estimated using the concept of striation thickness [6,21]. As seen previously, during the affine deformation of a droplet subjected to a simple shear flow, its length increases gradually as described by equation (1). A similar expression can be derived for the width of the drop, B [21,28]. In these equations, the drop diameter (d) changes if the drop breaks. Therefore, if d_i is the initial drop diameter, B/d_i represents the width reduction. The degree of distributive mixing may be quantified by [28]:

$$mix_{dist} = \frac{\sum_{j}^{N}\left[\left(\frac{d}{d_i}\right)_j \times \left(1-\frac{B}{d_i}\right)_j\right]}{\sum_{j}^{N}\left(\frac{d}{d_i}\right)_j} \tag{6}$$

where N is the total number of drops. Similarly, the degree of dispersive mixing can be defined as:

$$mix_{disp} = \frac{\sum_{j}^{N}\left[\left(\frac{d}{d_i}\right)_j \times \left(1-\frac{d}{d_i}\right)_j\right]}{\sum_{j}^{N}\left(\frac{d}{d_i}\right)_j} \tag{7}$$

For solid-liquid systems, distributive mixing can be measured using an entropic measure, such as the Shannon entropy, as proposed by Manas-Zloczower and co-workers [27]. Dividing the system in M equal sub-regions, the Shannon entropy can be calculated from:

$$S = -\sum_{j=1}^{M} p_j \log p_j \tag{8}$$

where p_j is the probability of finding a particle in sub-region j. The Shannon entropy is maximized when the probability of finding a particle in each sub-region is the same and is nil when all the particles are located in a single sub-region. A Shannon entropy normalized to its maximum value can be used as a distributive mixing index:

$$mix_{dist} = \frac{-\sum_{j=1}^{M} p_j \, log \, p_j}{log(M)} \tag{9}$$

The global degree of dispersive mixing can be estimated from Eq. (7), where d now represents the diameter of the solid agglomerates.

2. Computer Implementation

As seen above, the global plasticating extrusion model describing flow and heat transfer between hopper and die must encompass a number of individual stages that are linked sequentially through appropriate boundary conditions. Output is one of the unknowns of the problem. Therefore, as seen in Figure 3, before proceeding with calculations along small down-channel screw increments, an initial output is guessed from volumetric considerations. During the calculations, the local development of solids conveying, melting, or melt conveying is detected and velocity and temperature profiles ate computed. Once the calculations are completed, if the predicted pressure drop at the die exit is not

sufficiently small (theoretically, it should be nil), the output is changed and a new iteration is performed, the process being repeated while necessary. The results obtained include global process parameters, such as mass output, mechanical power consumption, axial length of screw required for melting, average melt temperature, degree of distributive mixing (WATS) and maximum viscous dissipation (ratio of maximum melt temperature to local barrel temperature), as well as the progress along the screw of a few variables, like solids and melt pressure, relative presence of solids, melt temperature, and mechanical power consumption.

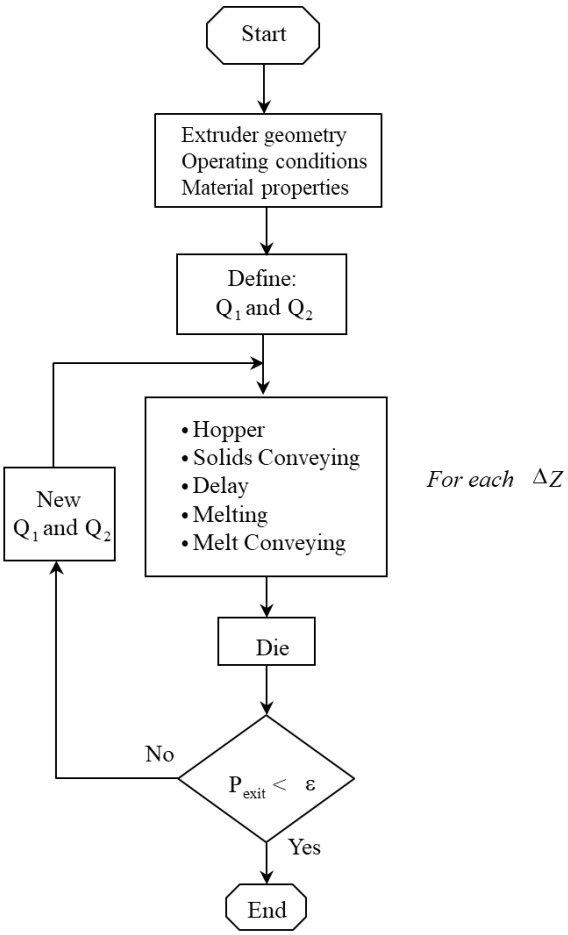

Fig. 3. Flowchart for modelling flow and heat transfer along the screw

The evolution of the morphology for liquid-liquid or solids-liquid systems, as well as the estimation of the resulting degree of distributive and/or dispersive

mixing involves an interrelation with the description of flow and temperature tackled above. Figures 4 and 5 depict the corresponding flowcharts. For liquid-liquid structures, the main steps are the following (Figure 4):

a) Compute velocity and temperature profiles in the screw channel;
b) Compute the local viscous forces and compare the maximum with the interfacial tension of the minor component; if it is high enough, the time for breakup is calculated;
c) Compare the local residence time with the breakup time; if break-up occurs, the droplet is replaced by smaller spherical ones;
d) Test for coalescence probability - if it is likely, set the new drop dimensions;

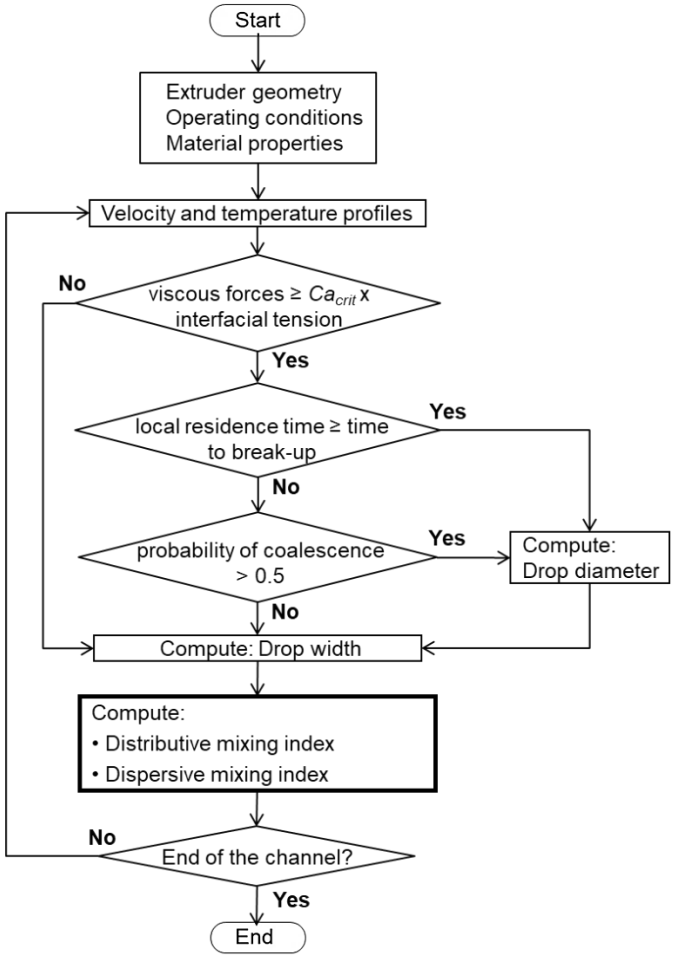

Fig. 4. Algorithm for predicting morphology evolution and mixing for a liquid–liquid system

e) If the drop does not break nor coalesce, calculate its new width;
f) Repeat the calculations in the remaining fractions of the same channel cross section;
g) Evaluate the mixing indices for the channel cross-section under consideration;

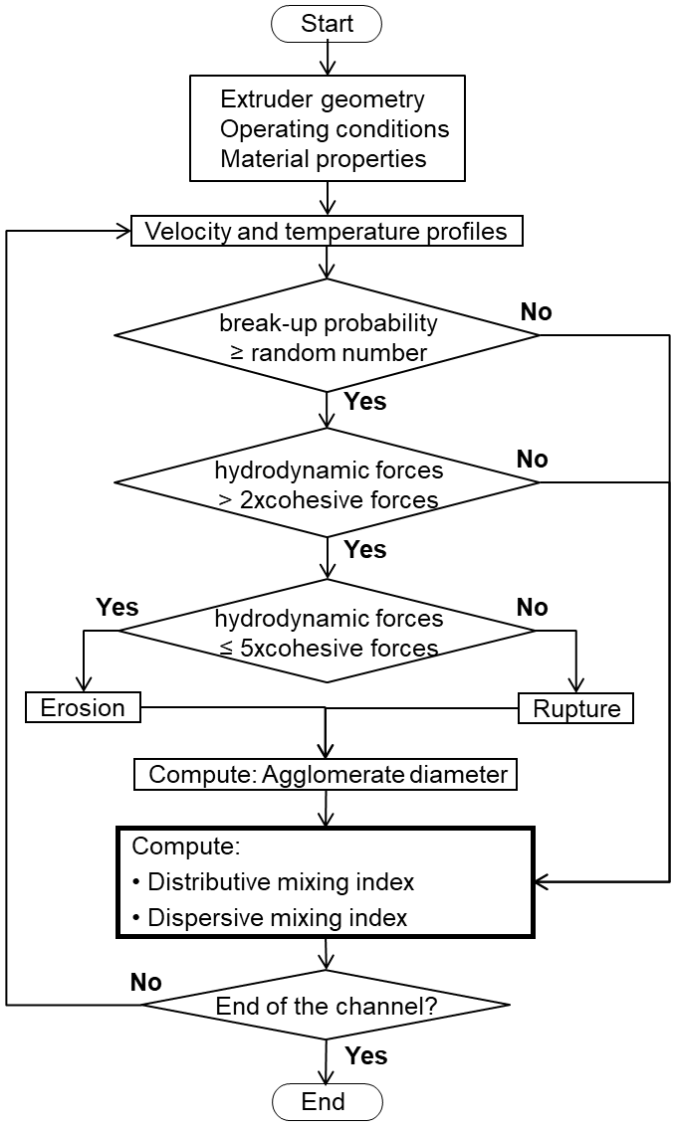

Fig. 5. Algorithm for predicting morphology evolution and mixing for a liquid–liquid system

h) Repeat the above steps for a downchannel increment, until reaching the outlet.

For solid-liquid systems, the sequence of calculations is (Figure 5):

a) Compute velocity and temperature profiles in the screw channel;
b) Apply a Monte Carlo scheme to determine a breakup probability, which is then compared with a random number in the interval [0,1]; if it is higher, breakup can occur; c) Compute the fragmentation number and set the dispersion mode;
d) Estimate new particle dimensions;
e) Same as steps f) to h) above.

3. Selected Results

This section presents a few illustrative results obtained when applying the algorithms presented so far to specific material/extruder/operating conditions combinations.

Figure 6 portrays the axial evolution of pressure and of the relative presence of solids (in terms of the ratio between the solids width, *X* and the channel width, *W*). X decreases progressively downstream, hence only a portion of the channel downstream works fully filled with melt. As a radar plot, Figure 7 shows the influence of screw speed on mass output, mechanical power consumption, axial length of screw required for melting, average melt temperature, degree of distributive mixing (WATS) and maximum viscous dissipation (ratio of maximum melt temperature to barrel temperature) for a specific set of imput conditions. An increase in screw speed produces an increase in mass output, but at the cost of additional mechanical power consumption, greater viscous dissipation (and melt temperatures) and lower mixing quality (generally, WATS deteriorates as the screw speed increases, since a shorter channel section becomes available for mixing due to the gradual lower melting rates and shorter residence times).

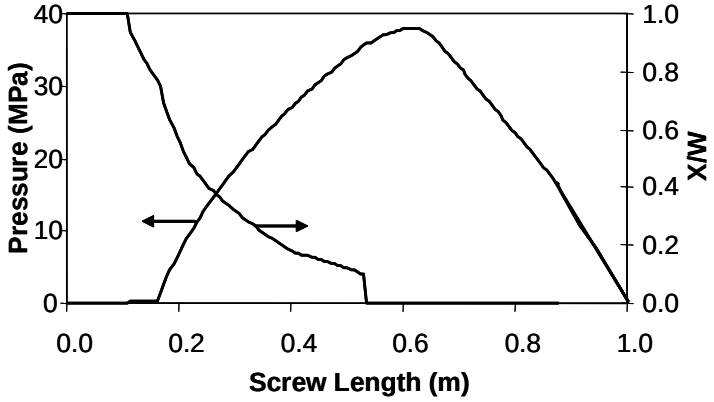

Fig. 6. Axial profiles of pressure and relative presence of solids (at 60 rpm)

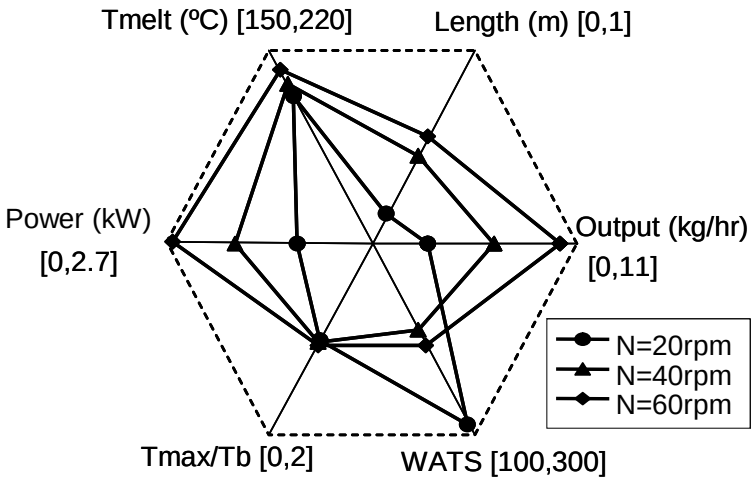

Fig. 7. Influence of screw speed on various process parameters for a specific material and extruder geometry

Figure 8 concerns the evolution of the morphology of a liquid-liquid system (typically, an immiscible polymer blend), for different values of the viscosity ratio *p* of the components. The graph on top represents the development of the average drop size, d, together with the corresponding standard deviation, whereas the chart at the bottom shows the progress of the average drop length, L. Melting extends approximately from L/D = 7 to L/D = 18, i.e., it contributes significantly to dispersion. As observed by Grace [23], as the ratio p decreases, drop break-up occurs under higher shear rates, but the time for drop break-up also decreases and dispersion becomes more effective. This is confirmed in Fig. 8 for values of p of 1 and 10^{-2}. For lower values of p, the time for drop break-up tends to zero, but dispersion becomes less important because it requires higher shear rates than those attained under the operating conditions considered.

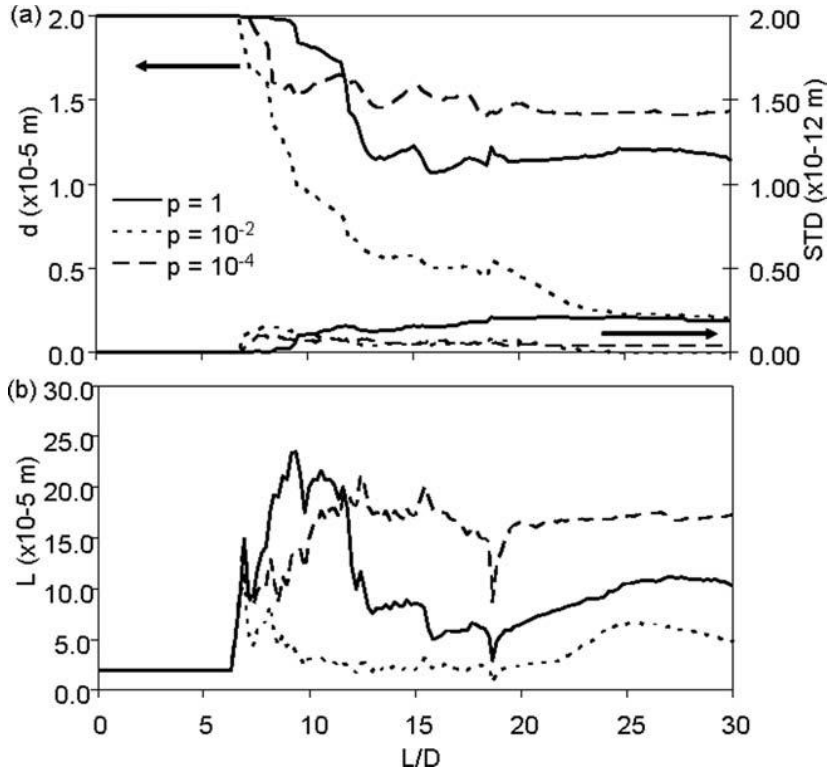

Fig. 8. Effect of the viscosity ratio on the average drop diameter (a) and drop length (b) of the minor phase

Figure 9 demonstrates the dynamics of the progress of the dimensions of solid particles suspended in a melt for a particular solids-liquid system. All fluid elements follow helical patterns along the channel; each of the 4 images correspond to the flow times indicated. The (unwrapped) rectangular channel corresponds to the metering zone of a screw, the flow developing vertically upwards. At the inlet, 1000 agglomerates with an uniform size of 100μm are assumed as regularly distributed. The progressive conversion of these agglomerates into aggregates and then into primary particles is evident. At short residence times, the primary particles should be formed from the erosion of bigger particles. At the outlet, 20% of the agglomerates survive, and a range of particle sizes is present (aggregates are about 50μm in diameter, primary particles between 1 and 4 μm) [28]. This type of predictions has a physical equivalence, despite the difficulty in performing an experimental validation [28].

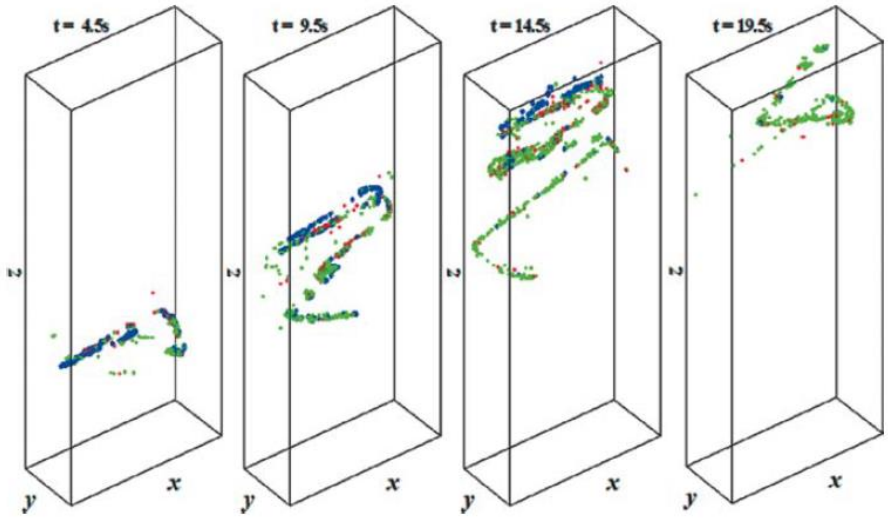

Fig. 9. Flow (vertically upwards) in the metering zone of the (unwrapped) screw; during the helical flow the parent agglomerates (blue) are progressively broken into aggregates (green) and primary particles (red)

Figure 10 displays examples of the evolution along the screw of the global mixing indices for two different screw speeds (50 and 200 rpm). As observed above for liquid-liquid systems, the melting stage can have a significant contribution to mixing (albeit this being often ignored in the calculations published in the literature). This role should be expected, given the relatively high shearing rates developing in melt films (surrounding the solid plug) and melt pool (particularly towards the end of the compression zone of the screw). As the screw speed increases, the melting zone usually becomes longer, thus further increasing its importance to mixing.

Distribution and dispersion continue along the melt conveying zone. In this particular example, the dispersion of the liquid-liquid system advances gradually, as breakup requires not only enough shear stresses, but also sufficient residence time. In the case of the solid-liquid system, dispersion by erosion seems to be followed by the distribution of the particles just generated.

The relative unsteadiness of the curves in the melting stage, as well as the eventual decrease of the actual value of a mixing index along the screw axis, are due to the insertion of new suspended material during melting of the matrix, as part of the calculation algorithms presented in the preceding sections. Please note that upon melting of the matrix, the average size of the particles/droplets results from the balance between their dispersion and the number and size of the new entities injected into the system. As these new entities are not deformed and are

assumed as uniformly distributed in the melt, they also affect negatively the local distribution.

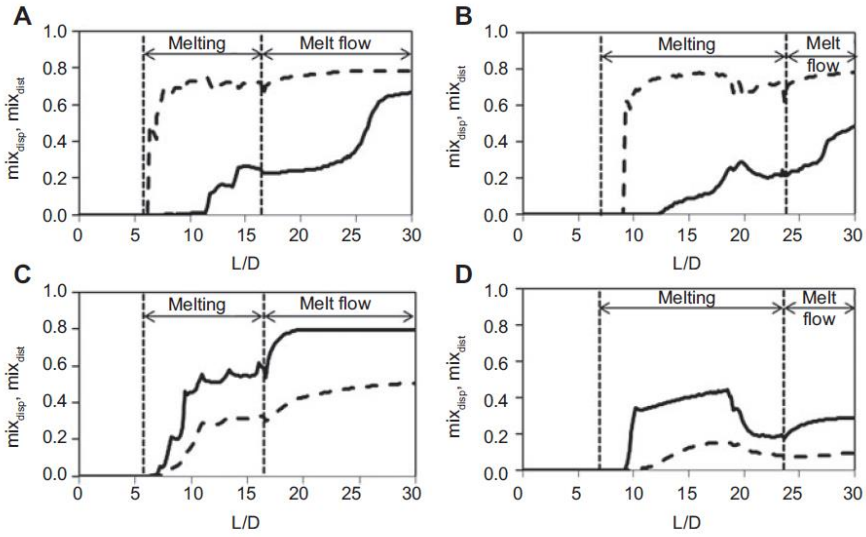

Fig. 10. Axial evolution of distributive (broken lines) and dispersive (solid lines) global mixing indices along a single screw extruder. (A) Liquid-liquid system, screw rotating at 50 rpm; (B) liquid-liquid system, screw rotating at 200 rpm; (C) solid-liquid system, screw rotating at 50 rpm; (D) solid-liquid system, screw rotating at 200 rpm

4. Conclusions

Single screw extruders are one of the most important processing equipments used by the industrial plastics sector. They accept the raw material as powder or pellets, melt it and generate the pressure necessary for a continuous flow through the shaping die. The performance of these machines depends on their geometry/construction, material properties and operating conditions. However, the interrelationship between these is far from obvious. Therefore, the design of improved screws, or the selection of the appropriate operating conditions for the successful manufacture of a given product from a specific polymer system, will greatly benefit from the support of precise process modelling tools.

It is currently possible to couple descriptions of flow and heat transfer along the screw to models describing the development of the morphlogy of complex polymer systems, such as polymer blends and composites. Thus, processors can now acquire a detailed picture of the process for a given set of input conditions and thus make more informed decisions. Also, these routines can be used for processing optimization, which will be dealt with in a separate chapter.

Acknowledgements

This project has received funding from the European Union's Horizon 2020 research and innovation programme under the Marie Skłodowska-Curie grant agreement No 734205 – H2020-MSCA-RISE-2017.

5. References

[1] Z. Tadmor, I. Klein, Engineering Principles of Plasticating Extrusion, Van Nostrand Reinhold, New York (1970)

[2] C C Chung, Extrusion of Polymers Theory and Practice, 2nd ed., Hanser Publishers, Munich (2000)

[3] C. Rauwendaal, Polymer Extrusion,5th ed. Hanser Publishers, Munich (2014)

[4] M.J. Stevens, J.A. Covas, Extruder Principles and Operation, 2nd ed., Chapman & Hall, London (1995).

[5] D G Baird, D I Collias, Polymer Processing Principles and Design,2nd ed., John Wiley & Sons, Inc., Hoboken, New Jersey (2014)

[6] Z Tadmor, C Gogos, Principles of Polymer Processing, 2nd ed., Wiley-Interscience, John Wiley & Sons, Inc., Hoboken, New Jersey (2006)

[7] Michelangelli, O. P., Gaspar-Cunha, A., & Covas, J. A. (2014). The influence of pellet-barrel friction on the granular transport in a single screw extruder. Powder Technology, 264(9), 401–408.

[8] Michelangelli, O., Yamanoi, M., Gaspar-Cunha, A., & Covas, J. A. (2011). Modelling pellet flow in single extrusion with DEM. Journal of Process Mechanical Engineering, 225(Part E), 255–268.

[9] D.M. Walker, An Approximate Theory for Pressures and Arching in Hoppers, Chem. Eng. Sci., 21, pp. 975-997 (1966).

[10] E. Broyer, Z. Tadmor, Solids Conveying in Screw Extruders – Part I: A modified Isothermal Model, Polym. Eng. Sci., 12, pp. 12-24 (1972).

[11] Z. Tadmor, E. Broyer, Solids Conveying in Screw Extruders – Part II: Non Isothermal Model, Polym. Eng. Sci., 12, pp. 378-386 (1972).

[12] H. Darnell, E.A.J. Mol, Solids Conveying in Extruders, SPE J., 12, pp. 20-29 (1956).

[13] L. Kacir, Z. Tadmor, Solids Conveying in Screw Extruders – Part III: The Delay Zone, Polym. Eng. Sci., 12, pp. 387-395 (1972).

[14] J-F Agassant, P Avenas, P J. Carreau, B Vergnes, M Vincent, Polymer Processing Principles and Modelling, 2nd ed., Carl Hanser Verlag, Munchen, Germany (2017)

[15] Gaspar-Cunha, A. (2009). Modelling and Optimisation of Single Screw Extrusion Using Multi-Objective Evolutionary Algorithms (1st ed.). Koln, Germany: Lambert Academic Publishing.

[16] B.H. Maddock, A Visual Analysis of Flow and Mixing in Extruder, Soc. Plast. Engs. J., 15, pp. 383-394 (1959).
[17] J.T. Lindt, B. Elbirli, Effect of the Cross-Channel Flow on the Melting Performance of a Single-Screw Extruder, Polym. Eng. Sci, 25, pp. 412-418 (1985).
[18] B. Elbirli, J.T. Lindt, S.R. Gottgetreu, S.M. Baba, Mathematical Modelling of Melting of Polymers in a Single-Screw Extruder, Polym. Eng. Sci., 24, pp. 988- 999 (1984).
[19] Domingues, N., Gaspar-Cunha, A., & Covas, J. A. (2010). Estimation of the morphology development of immiscible liquid–liquid systems during single screw extrusion. Polymer Engineering and Science, 50(11), 2194–2204.
[20] ANSYS, Inc, www.ansys.com
[21] I Manas-Zloczower (ed.) Mixing and Compounding of Polymers, 2nd ed., Hanser Publishers, Munich, 521 (2009).
[22] Domingues, N., Gaspar-Cunha, A., & Covas, J. A. (2012). A Quantitative Approach to Assess the Mixing Ability of Single Screw Extruders for Polymer Extrusion. Journal of Polymer Engineering, 32(2), 81–94.
[23] H.P. Grace, Dispersion phenomena in high viscosity immiscible fluid systems and application of static mixers as dispersion devices in such systems, Chem. Eng. Commun., 14, 225 (1982).
[24] P G Lafleur, B Vergnes, Polymer Extrusion, John Wiley & Sons, Inc, Hoboken, USA (2014)
[25] Y.M. Stegeman, Time Dependent Behavior of Droplets in Elongational Flows, PhD Thesis, Tech. Univ. Eindhoven, The Netherlands (2002).
[26] L. Delamare, B. Vergnes, Computation of the morphological changes of a polymer blend along a twin-screw extruder, Polym. Eng. Sci., 36, 1685 (1996).
[27] Scurati, A., Feke, D.L., Manas-Zloczower, I., Analysis of the Kinetics of Agglomerate Erosion in Simples Shear Flows, Chem. Eng. Sci., 60, p. 6564-6573 (2005)
[28] Domingues, N., Gaspar-Cunha, A., Covas, J. A., Camesasca, M., Kaufman, M., & Manas-Zloczower, I. (2010). Dynamics of Filler Size and Spatial Distribution in a Plasticating Single Screw Extruder – Modeling and Experimental Observations. International Polymer Processing, 25(3), 188–198.
[29] G. Pinto, Z. Tadmor, Mixing and Residence Time Distribution in Melt Screw Extruders, Polym. Eng. Sci., 10, pp. 279-288 (1970).

Ľudmila Dulebová[1], José A. Covas[2]

EFFECT OF NANOCLAY ON PROPERTIES OF POLYMER NANOCOMPOSITES

Abstract: *Polymer nanocomposites is a rapidly growing area of nanoengineered materials, providing lighter weight alternatives to conventional, filled plastics with additional functionality associated with nanoscale specific, value added properties. This contribution deals about the study of influence of montmorillonite in polypropylene matrix on selected properties of PP/MMT nanocomposites. Polypropylene marked Mosten PND 33-301 and two types of commercial montmorillonite nanofillers type Cloisite 20A and Cloisite 3010 were used for experiments. Concentrate containing of nanofiller in the PP polymer matrix was performed on Buhler twin-screw extruder BTSK 20/40D. Mechanical properties of prepared samples by injection molding were tested on tensile test and Charpy impact test before and after degradation in simulated climatic ageing. DSC analysis and study of the structure of tested materials were conducted.*
Keywords*: polymer nanocomposites, injection moulding, polypropylene, montmorillonite*

1. Introduction

Polymer/clay nanocomposites are materials composed of a polymer matrix and nanometer size clay particles. They exhibit significant improvements in tensile modulus and strength and reduced permeability to gases and liquids, as compared with the pure polymer. These property improvements can be realized, while retaining clarity of the polymer without significant increase in density, since the typical clay loading is 2–5%. Composites that exhibit a change in composition and structure over a nanometer length scale have been shown to afford remarkable property enhancements, relative to conventional microcomposites [1].

Polymer nanocomposites show major improvements in mechanical properties, gas barrier properties, thermal stability, fire retardancy, and other areas.

There are many factors that affect the polymer nanocomposite properties:

- Synthesis methods such as melt compounding, solvent blending, in-situ polymerization, and emulsion polymerization,
- Polymer nanocomposite morphology,
- Types of nanoparticles and their surface treatments,

[1)] *Department of Engineering Technologies and Materials, Faculty of Mechanical Engineering, Technical University of Kosice, Masiarska 74, 040 01 Kosice, Slovakia, ludmila.dulebova@tuke.sk.*

[2)] *Department of Polymer Engineering, Institute for Polymer and Composites University of Minho, Guimarães, Portugal,*

- Polymer matrix such as crystallinity, molecular weight, polymer chemistry, and whether thermoplastic or thermosetting [2].

There are different types of commercially available nanoparticles that can be incorporated into the polymer matrix to form polymer nanocomposites. Depending on the application, the researcher must determine the type of nanoparticle needed to provide the desired effect. These are the most commonly used nanoparticles:

- Montmorillonite organoclays (MMT)
- Carbon nanofibers (CNFs)
- Polyhedral oligomericsilsesquioxane (POSS®)
- Carbon nanotubes [multiwall (MWNTs), small-diameter (SDNTs),and single-wall (SWNTs)]
- Nanosilica (N-silica)
- Nanoaluminum oxide ($A1_20_3$)
- Nanotitanium oxide (TiC^)
- Others. [2,3]

2. Structure and Properties of Clay

Most commonly used type of layered silicate is montmorillonite (MMT) natural smectic clay 2:1 phyllosilicate [3]. Hectorite and saponite are also classified as layered silicates [4]. Owing to high surface area and aspect ratio, MMT clays are of special interest for preparing nanocomposites [5]. The structure of MMT consist of stack of crystalline sheets [6]. Crystal lattice of these sheets comprises two-dimensional layers where octahedral layer of alumi-num or magnesium is surrounded by two external tetrahedral layers (2:1) [7]. The thickness of each sheet is considered around 1 nanometer (nm) [3] while the lateral dimension of individual layers may differ from 30 to 2000 nm depending on the particular silicate [8]. Stack of platelets is held together by electrostatic forces with interlayer distance called d-spacing between the platelets [9]. The interlayer is also characterized by negative sur-face charge where counterions are attracted to the net negative charge within the clay platelets [9]. The exchange of simple inorganic cations is very much depended upon surface charge density which is known as cation ex-change capacity (CEC) expressed by meq/100g [7]. Localization of nega-tive charge is not constant and may vary from layer to layer. Therefore, it is beneficial to consider CEC as an average value of entire crystal [10].

3. Structure of MMT

Silica is the dominant constituent of the montmorillonite clays, with alumina being essential. The chemical structure of montmorillonite clays is illustrated in Figure 1, showing its sheet structure consisting of layers containing the tetrahedral silicate layer and the octahedral alumina layer. The tetrahedral silicate

layer consists of SiC_4 groups linked together to form a hexagonal network of the repeating units of composition Si_4O_{10}. The alumina layer consists of two sheets of closely packed oxygens or hydroxyls, between which octahedrally coordinated aluminum atoms are imbedded in such a position that they are equidistant from six oxygens or hydroxyls. The two tetrahedral layers sandwich the octahedral layer, sharing their apex oxygens with the latter. These three layers form one clay sheet that has a thickness of 0.96 nm. The chemical formula of the montmorillonite clay is $Na_{1/3}(Al_{5/3}Mg_{1/3})$ $Si_40_{10}(OH)_2$. In its natural state Na^+ cation resides on the MMT clay surface [5-7].

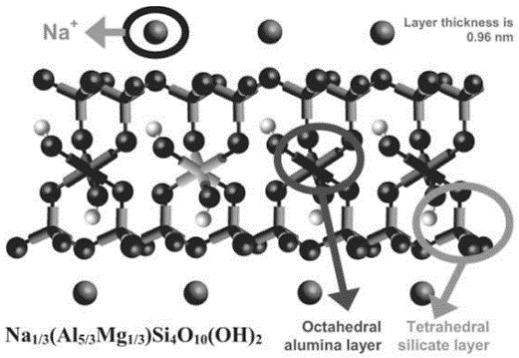

Fig. 1. Chemical structure of montmorillonite nanoclays

4. Degradation of polymers

Degradation of the polymers under the influence of temperature, light, humidity and oxygen leads to changes in structures such as the increase in crosslinking, reducing the degree of polymerization, oxidation or recrystallization of the molecular chains [11-13]. The result of the ageing process are reversibly or irreversibly a deterioration of processing and changing of properties [14, 15]. The irreversible changes are related to the chemical transformations, they are taking place as a result of depolymerization, crosslinking, oxidation, degradation. Reversible changes are classified to physical transformation (absorption and desorption, relaxation and recrystallization) [16].

Ageing tests which enable the evaluation of the degree of changes in the performance (mechanical strength, hardness, brittleness, elasticity, color, texture, reliability, durability) occurring in the polymers is carried out under the conditions for this specially designed and controlled, for example, increased temperature, humidity, mechanical fatigue or exposure to light and different kinds of radiation [11]. Significant deterioration in the mechanical properties of polyolefins are observed after two weeks of accelerated ageing at increased temperature, and for engineering polymers after a month [14].

5. Experimental work

Material

Aim of this paper is to describe the change of selected mechanical properties of PP/MMT nanocomposites. As the polymer matrix material polypropylene marked Mosten PND 33-301 was used. For these experiments, montmorillonite nanofillers were chosen Cloisite 20A and Cloisite 301 with various concentrations in the PP polymer matrix.

Nanofiller Cloisite 20A is montmorillonite modified with a quaternary ammonium salt, moddified by hydrogenated tallow (2M2HT ~65% C18; ~30% C16; ~5% C14), Anion: Chlorid.

Nanofiller Cloisite 3010 is bentonite treated with a surfactant (supplied by Sud-Chemie), used surface modificator –dimethyl benzyl hydrogenated tallow alkyl ammonium.

Preparation of polymer nanocomposite

The processing of materials - various concentrations of nanofiller in the PP polymer matrix - was performed on Buhler twin-screw extruder BTSK 20/40D.

Configuration of extruder BTSK 20/40D:

- Screw configuration: K3,
- Torque: 32Nn,
- Temperature of the melt in the screw head: 208ºC,
- Input power: 0.54kW,
- Screw speed: 250 rpm,
- Melt pressure in the screwhead: 1 bar,
- Temperature zones :190 °C, 200 °C, 200 °C, 200 °C, 195 °C,
- Cooling: air.

Samples for tests were molded at injection molding machine type ARBURG Allrounder 370S under ISO standards.

Methodology of experiments

Mechanical properties of prepared samples were tested on tensile test machine TiraTest 2300 under STN ISO 527-1 standard. Impact strength of material was tested by Charpy impact hammer under EN ISO 179-1 standard. For hardness measurements were used portable hardness tester Shore D under ISO EN 868.

To investigate the influence of low temperatures to studied material, the test samples were degraded at low temperature (-20ºC) for 1440 hours. Subsequently, the material was tested directly without conditioning in a low temperature.

Determination of mechanical properties after degradation caused by UV radiation took place in the UV chamber test according to EN ISO 4892-3. The total exposure time amounted of 60 days in 18 hour cycles set to switch from 4.00 to 22 o'clock in the overall exposure time of 1080 hours. Labeling of used materials for tests is described in Table 1.

Table 1. Labeling of used materials for tests

Material	Label
PP Mosten PND 33-301	PP
PP + 2% CLOISITE 20A	PP/A2
PP + 4% CLOISITE 20A	PP/A4
PP + 6% CLOISITE 20A	PP/A6
PP + 2% CLOISITE SE 3010	PP/B2
PP + 4% CLOISITE SE 3010	PP/B4
PP + 6% CLOISITE SE 3010	PP/B6

6. Results and discusion

Assessment of the properties of polypropylene / clay nanocomposites

Values of tensile strength of material polypropylene / clay nanocomposites materials are shown on Figure 2.

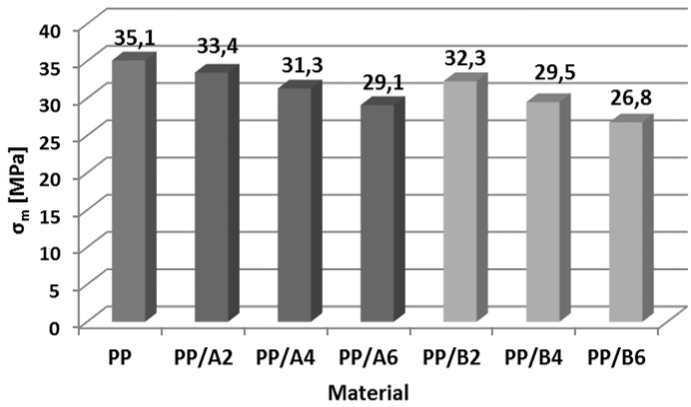

Fig. 2. Tensile strength of materials PP/A and PP/B

Based on the measured values, we can conclude that the addition of nanofiller Cloisite 20A or Cloisite SE 3010 into the polymer matrix had no positive effect on tensile strength and elongation of material. Addition of 6% of Cloisite 20A caused a decrease in tensile strength of 17.1%. Also adding a small amount of filler Cloisite 20A at a rate of 2% caused reduction in yield strength of the material by 4.7%. Material with 6% of organically modified Cloisite SE 3010 showed decrease in tensile strength of 23,7%.

Study of influence of addition the Cloisite fillers on resulting impact strength were obtained positive results (Figure 3).

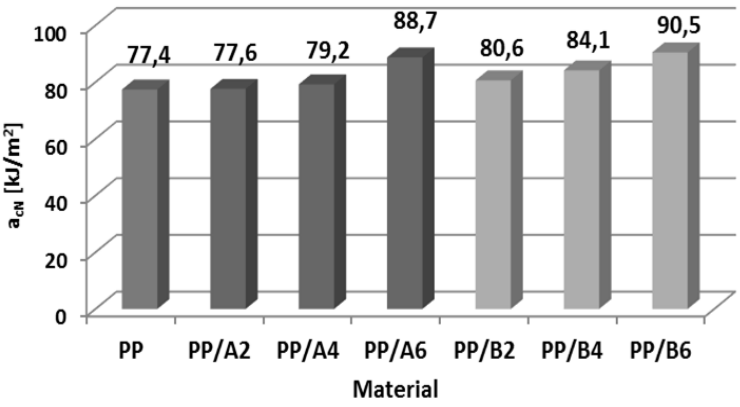

Fig. 3. Impact strength of materials PP/A and PP/B

Addition of nanofiller Cloisite 20A at rate of 6% achieved an increase in impact strength of the material by 14.6% from the original 77.4 kJ.m^{-2} to 88.7 kJ.m^{-2}. The material containing 6% filler Cloisite SE 3010 showed increase of impact strength of 16.9%.

Degradation of PP/MMT material at low temperatures

Changes of mechanical properties after degradation are shown in Figure 4 and Figure 5 at sample of PP.

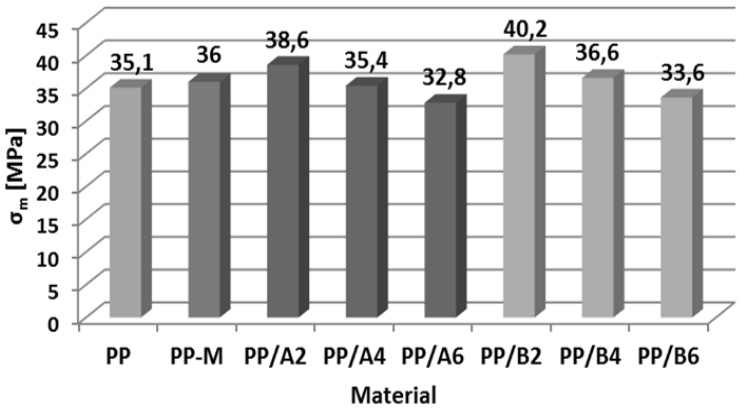

Fig. 4. Tensile strength of materials PP/A and PP/B after degradation

As illustrated on Figure 4, after exposure of material to low temperatures, the samples shows increase of tensile strength, what is desirable for automotive industry. Also the impact strength test showed increase at all samples filled with

MMT nanofillers (Figure 5). At pure PP there was reduction of impact strength by 26.7%, while material filled with 6% of Cloisite 20A showed increase of 44.6% and material filled with 6% of Cloisite 3010 even showed increase of impact strength by 55.9%.

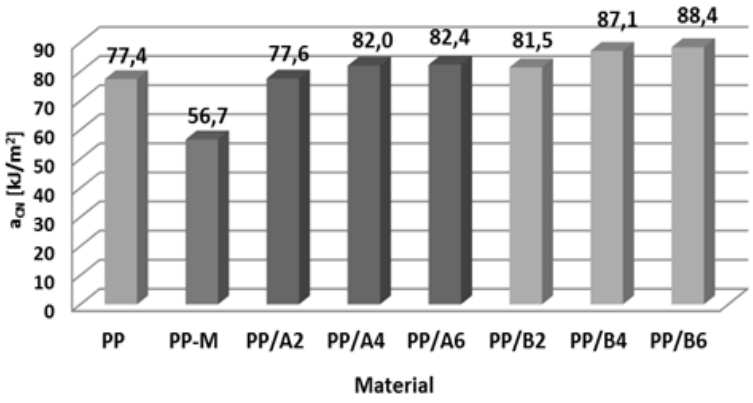

Fig. 5. Impact strength of materials PP/A and PP/B after degradation

Degradation of PP/MMT material at UV chamber

The test materials were subsequently tested at UV chamber, specifically testing the mechanical properties (tensile strength, impact strength). Figure 6 shows to influence the tensile strength of the investigated materials after exposure to UV radiation. Figure 7 displays the change of impact strength of test materials after UV degradation.

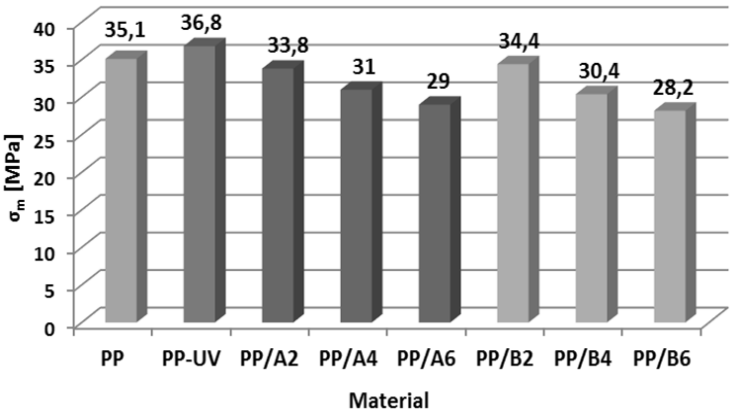

Fig. 6. Tensile strength of materials PP/A and PP/B after UV degradation

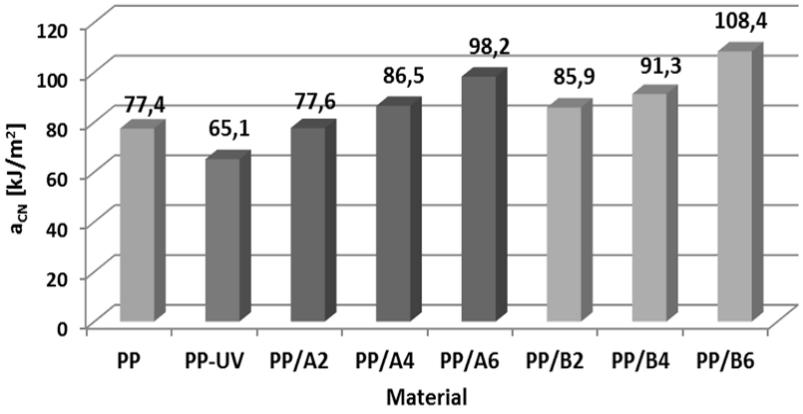

Fig. 7. Impact strength of materials PP/A and PP/B after UV degradation

Examination of the UV degradation effect on the mechanical properties show varying degrees of influence on various materials after exposure to UV radiation. This phenomenon can be explained by the distribution of particles in the volume of the cross-section of the material to prevent the complete penetration of UV radiation. Pure polypropylene is susceptible to chain degradation due to heat and UV radiation. Oxidation is the most frequently observed on a tertiary carbon atom in each repeating unit. First, there is the initial formation of the free radicals, which then reacts with oxygen, followed by chain cleavage and allows for the formation of aldehyde and carboxylic acids. After degradation, network of cracks and hairline infringement occurs. Addition of nanofillers also reduced the breaking strength of the material, in comparison to the material, which was not exposed to UV radiation. Tensile strength has shown that UV radiation had no noticeable effect to influence of mechanical properties compared to those obtained in previous studies. But in case of default material tensile strength was reduced (-10.3 %), as well as impact strength (-15.9 %). Material containing 6 % Cloisite 20A filler showed an increase in the impact strength of 50.8 % and at filler Cloisite 3010 was observed improvement of impact strength by 66.5 % compared to the material exposured to UV radiation.

TGA and DSC analysis

TGA and DSC analysis was performed on a TA Instruments Q600 SDT Simultaneous analyzer. From each material sample was taken if the approximate dimensions of 3x3x3 mm to fit into aluminum pans. Subsequently, the samples were weighed on a microbalance weight in the chamber of the device and the device was reseted. Measures were carried out by increments of 20 °C/min from 30°C to 250°C. The recorded data were subsequently transferred to TA Universal

Analysis. Through the analysis and integration curves were recorded melting points, as well as weight loss material. The results of TGA and DSC analysis of PP / Cloisite 20A is described in Table 2.

Table 2. The results of TGA and DSC analysis of material PP/Cloisite 20A

Material	Weight reduction [%]	Temperature T_m [°C]	Heat flow [J/g]
PP	+0.15390	176.87	75.52
PP/A2	-0.15820	177.51	75.52
PP/A4	-0.08317	176.48	75.06
PP/A6	-0.09538	180.05	76.99

The results of DSC analysis shown in Table 2 shows that the heat consumption of all test materials was very similar. For a system containing 6% of a filler, an increase of melting temperature of 3.18°C, which is indeed the minimum value, but evokes a change in the heat transfer system.

DSC analysis on Figure 8 shows, that heating the tested materials to melting temperature T_m shows deviations. Temperature T_m at pure polypropylene was achieved in heating time 7.93 min, while at the PP/6% Cloisite 20A this temperature was achieved after 8.35 min, which evokes an increase in resistance to elevated temperatures and also the possibility of exposure of the material to higher temperatures for longer time without transmission solid state to the molten state.

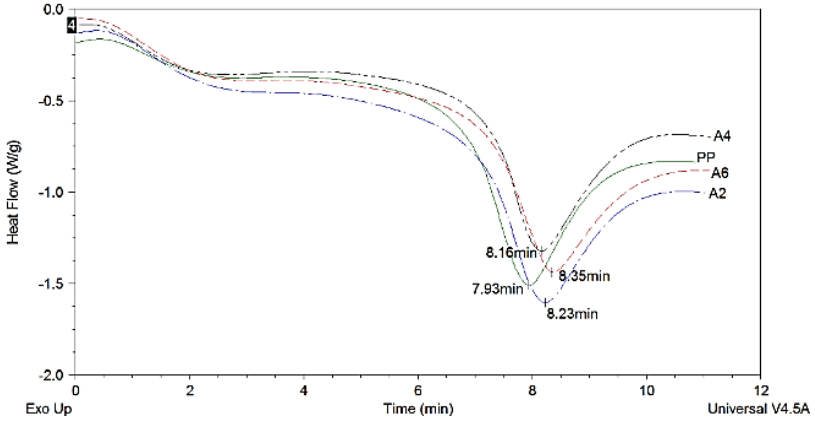

Fig. 8. DSC analysis of PP/Cloisite 20A material

Summary evaluation of TGA and DSC analysis of PP / Cloisite SE 3010 is expressed in Table 3.

Table 3. The results of TGA and DSC analysis of material PP/Cloisite 3010

Material	Weight reduction [%]	Temperature T_m [°C]	Heat flow [J/g]
PP	+0.15390	176.87	75.52
PP/B2	-0.16520	179.71	72.81
PP/B4	-0.07057	176.73	97.22
PP/B6	-0.58550	175.81	94.61

TGA and DSC analysis of PP/B6 material with the addition of 6% nanofiller Cloisite SE 3010 shows that the effect of heating to a temperature of 250°C directed in a loss of 0.5855% weight of the material.

From an examination of dependence of the heat flow (DSC) due to the heating time on Figure 9 implies that the temperature T_m was at pure polypropylene achieved in heating time 7.93 min. The nanocomposite PP/B2 reached temperature T_m after 8.12 min, at PP/B4 system temperature T_m was reached after 8.36 min and the system PP/B6 filled with 6% of filler Cloisite SE 3010 reached T_m after 8.39 min, which evokes an increase in resistance to elevated temperatures and also the possibility of exposure of the material to high temperatures for an extended period of time without sneaking from the solid state to the molten state.

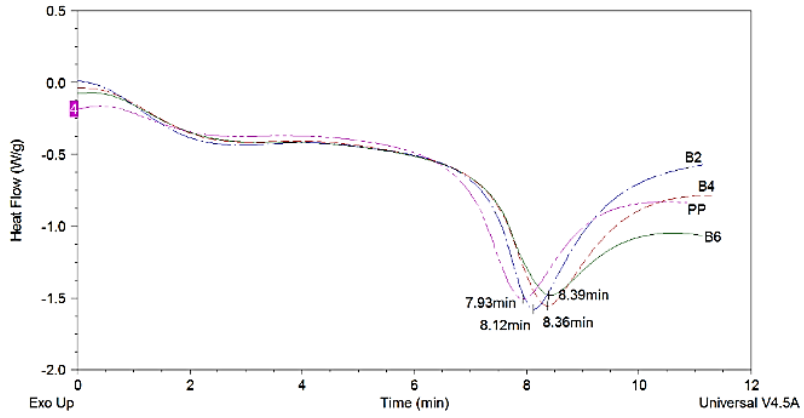

Fig. 9. DSC analysis of PP/Cloisite 3010 material

SEM Microspopy

Figure 10 shows structure of pure polypropylene observed on SEM microscope TESLA BS 340.

SEM image of material PP/A6 (Figure 11) shows that exfoliation of filler was not performed sufficiently. There are visible clumps of filler, undigested filler and also visible air bubbles in the material, on average 1-2μm diameter. These bubbles may result from the treatment of material, or as residual traces of moisture in the material. In the case of clusters of already fragmented filler is probable cause inappropriateness of the compatibilizer - quaternary ammonium salt. For further investigation will be the matrix/filler supplied with compatibilizer to increase the hydrophilicity of polypropylene.

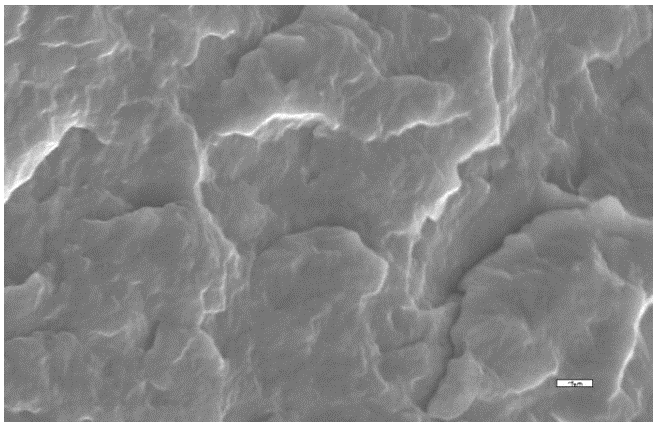

Fig. 10. Structure of pure material PP

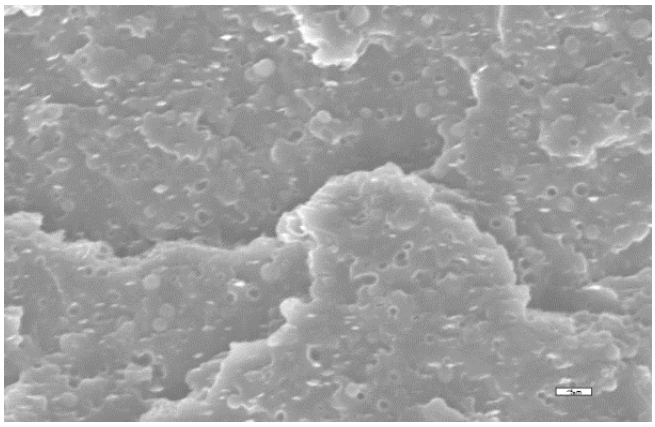

Fig. 11. Structure of material PP/A6

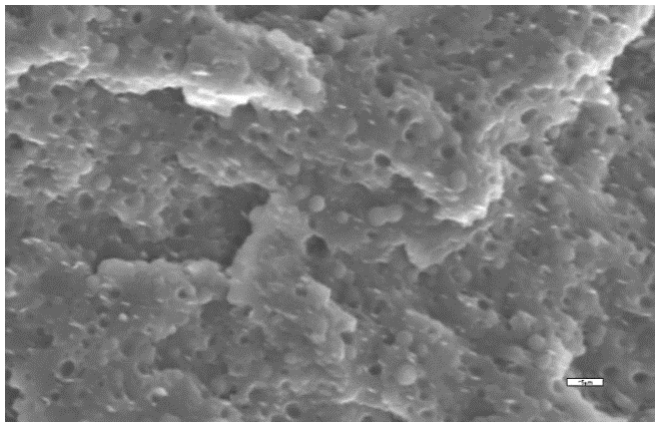

Fig. 12. Structure of material PP/B6

The SEM image on Figure 12 shows the structure of PP / Cloisite SE 3010, where they are clearly visible clumps of filler in the matrix. Clumps of fillers are uniformly dispersed within the base matrix. Pictured are clearly visible clumps of filler and also turgidity after clusters.

7. Conclution

Polymer nanocomposites is a rapidly growing area of nanoengineered materials, providing lighter weight alternatives to conventional, filled plastics with additional functionality associated with nanoscale specific, value-added properties. Significant research is needed to figure out the behaviour of nano-interfaces, and this field can still be considered to be in its beginnings.

This contribution deals about the study of influence of montmorillonite in polypropylene matrix. As it was pointed out in experimental part of this article, preparation of polymer nanocomposites is difficult and can lead into preparation of microcomposites, when adhesion forces between matrix and filler are not strong enough. In our case, some of the properties were positively influenced, but properties like tensile strength decreased. This decrease was than explained by SEM images, where visible clumps of filler and undigested filler were found. Next goal in our progress will be to supply the matrix/filler with compatibilizer to increase the hydrophilicity of polypropylene.

Acknowledgements

This project has received funding from the European Union's Horizon 2020 research and innovation programme under the Marie Skłodowska-Curie grant agreement No 734205 – H2020-MSCA-RISE-2017.

References

[1] Okamoto M., Morita S., Taguchi H., Kim Y.H., Kotaka T., Tateyama H., Synthesis and structure of smectic clay/poly (methyl methacrylate) and clay/polystyrene nanocomposites via in situ intercalative polymerization, Polymer, 2000, 41, 3887–3890.

[2] Duleba B., Greškovič F., Application of clay based nanofillers at polymers nanocomposites, In: Technological and design aspects of extrusion and injection moulding of thermoplastic polymer composites and nanocomposites. Volume I., Lvov. 2013, 127-139.

[3] Lepoittevin, B., Pantoustier, N., Devalckenaere, M., Alexandre M., Calberg C., Jérôme R., et al., Polymer/layered silicate nanocomposites by combined intercalative polymer-ization and melt intercalation: a masterbatch process, Polymer, 2003, 44, 2033–2040.

[4] Ahmadi S.J., Huang Y.D., Li W., Synthetic routes, properties and future applications of polymer-layered silicate nanocomposites, Journal of Materials Science, 2004, 39, 1919–1925.

[5] Herrera-Alonso J.M., Sedlakova Z., Marand E., Gas barrier proper-ties of nanocomposites based on in situ polymerized poly (n-butyl methacrylate) in the presence of surface modified montmorillonite, Journal of Membrane Science, 2010, 349, 251–257.

[6] Nazarenko S., Meneghetti P., Julmon P., Olson B.G., Qutubud-din S., Gas barrier of polystyrene montmorillonite clay nanocomposites: Effect of mineral layer aggregation, Journal of Polymer Science Part B: Polymer Physics, 2007, 45, 1733–1753.

[7] Bhiwankar N.N., Weiss R.A., Melt intercalation/exfoliation of pol-ystyrene-sodium-montmorillonite nanocomposites using sulfonated pol-ystyrene ionomer compatibilizers, Polymer, 2006, 47, 6684–6691.

[8] Bharadwaj R.K., Modeling the barrier properties of polymer-layered silicate nanocomposites, Macromolecules, 2001, 34, 9189–9192.

[9] Su S., Wilkie C.A., Exfoliated poly (methyl methacrylate) and polystyrene nanocomposites occur when the clay cation contains a vinyl monomer, Journal of Polymer Science Part A: Polymer Chemistry, 2003, 41, 1124–1135.

[10] Dobránsky J., Baron P. Kočiško M., Běhálek L., Vojnová E., Solving depressions formed during production of plastic molding, Metalurgija, 2015, 54, 496-498.

[11] Jachowicz T., Krzyżak A., Wpływ starzenia naturalnego na wybrane właściwości rur z polietylenu, MOTROL 2009,11c, 70 – 76

[12] Běhálek L., Seidl M., Dobránsky J., Crystallization of polylactic acid composites with banana and hemp fibres by means of DSC and XRD methods, Applied Mechanics and Materials, 2014, 616, 325-332.

[13] Dobránsky J., Baron P., Kočiško M., Vojnová E., Monitoring of the influence of moisture content in thermoplastic granulate on rheological

properties of material, Applied Mechanics and Materials, 2014, 616, 207-215.
[14] Dulebová Ľ., Krasinskyi V., Qualitative evaluation of selected mechanical properties of composites produced by injection molding after degradation. In: Technological and design aspects of extrusion and injection moulding of thermoplastic polymer composites and nanocomposites: Volume 2. Košice, 2014, 78-90.
[15] Malon H., Martin J., Castejon L., Mechanical behavior variation of an isotactic polypropylene copolymer subjected to artificial ageing, Edited by F. Dogan: Polypropylene, InTech 2012, 49-62.
[16] Gahleitner M., Fiebig J., Wolfschwenger J., Grein C., Processing and morphology effects on long-term stability of polypropylene. SEM X International Congress & Exposition on Experimental & Applied Mechanics 2004.

Ľudmila Dulebová[2], Anna Rudawska[3], A. Gaspar Cunha[4]

THE MECHANICAL PROPERTIES OF LOW-DENSITY POLYETHYLENE WITH NANOFILLER MASS CONTENT

Abstract: *Nanocomposites are a new class of composites that are particle-filled composites in which at least one dimension of the dispersed particles is in the nanometer range. One of the interesting aspects of the use of nanofillers is the low concentration of that filler that needs to be added to the polymer system to obtain desired property improvements. This contribution presents the results of research from basic processing and mechanical properties of nanocomposites with Low-Density Polyethylene (LDPE) matrix. Nanocomposites based on low-density polyethylene (LDPE), containing 2, 4 and 6wt% of Halloysite nanotubes (HNT), were prepared by melt-mixing. Nanocomposites were filled with 5 wt% Polyethylene grafted with maleic anhydride (PE-graft-MA) as a compatibility factor. The specimens for testing were prepared by injection molding and their selected mechanical properties were tested by static tensile test, Charpy impact test and Shore hardness test.*

Keywords*: Low-Density Polyethylene, nanofillers, Halloysite nanotubes, mechanical properties*

1. Introduction

Nanotechnology is a rapidly growing interdisciplinary field of knowledge, spanning many areas of research. There are always critical needs for lighter, stronger, less expensive, and more versatile materials to meet the demands of industrial consumers. The synthesis of polymer nanocomposite is an integral aspect of polymer nanotechnology. Polymer nanocomposite has been known as one of the early success stories of realizing the potential of nanomaterial as reinforcement filler to improve the properties of neat polymers. By adding the nano sized organic compounds, the properties of polymers are improved [1, 2, 3]. Properties of the nanocomposites produced are depending on the inorganic materials present in the polymers matrix [4]. Reinforcing thermoplastic polymers with nanoparticles to form nanocomposites is a way to increase the usage of polymeric materials in engineering applications by improving their mechanical properties, namely elastic modulus and yield stress with filler contents as low as

[2)] *Department of Engineering Technologies and Materials, Faculty of Mechanical Engineering, Technical University of Kosice, Masiarska 74, 040 01 Kosice, Slovakia, ludmila.dulebova@tuke.sk*

[3)] *Lublin University of Technology, Department of Production Engineering, 36 Nadbystrzycka St., 20-618 Lublin, Poland, a.rudawska@pollub.pl*

[4)] *Department of Polymer Engineering, Algoritmi Research Centre, University of Minho, Guimarães, Portugal*

5–10 wt% [5, 6, 7]. There are different types of commercially available nanoparticles that can be incorporated into the polymer matrix to form polymer nanocomposites [8, 9].

Optimizing polymeric materials by the addition of a small filler content with nanometer-scale dimensions has been the focus of many industrial and academic studies. The introduction of filler contents to polymeric materials has been found to significantly increase the mechanical, barrier, thermal, and electrical properties,[10,11] and in general, the better the dispersion of nanoparticles (NPs) and the more effective the polymerparticle interface, the greater the obtained reinforcing effect. Among the NPs studied, the most prominent are the lamellar clays, such as montmorillonite (MMT) and carbon nanotubes (CNTs). Halloysite is a tubular aluminosilicate with two interesting characteristics: a chemical composition similar to montmorillonite, and a nanotubular geometry similar to CNTs.Because of these features, its use as a reinforcing filler in polymer nanocomposites has attracted considerable interest in recent years [12, 13].

Material and structural parameters of nanofiller such as shape, size, aspect ratio, concentration etc play important role for properties of nanocomposites. Quality of interface between particles and matrix are no less important. Presence of rigid filler usually deteriorates strength and toughness of polymeric materials [14]. Quality dispersion of nanoparticles in matrix plays key role for an improvement of impact properties of nanocomposites. Dispersed systems are generally in thermodynamically non-equilibrium state. Surface free energy reduction is driving force for termination of dispersion state and aggregations growth (coagulation) [15]. Suitable treatment of particle surface can prevent coagulation of particles during compounding of the polymer composites [16]. Nanocomposites are possible to sort by geometric shape of reinforcement to (Fig.1):

- Nanoparticle-reinforced composite ($CaCO_3$, TiO_2, SiO_2…),
- Nanofibre-reinforced composite (carbon nanotubes - CNT, halloysite - HNT),
- Nanoplateled-reinforced composite (organically modified clay, expanded graphite).

Recently, halloysite nanotubes have become the subject of research attention as a new type of additive for enhancing the mechanical and thermal performance of polymers [8, 12]. Halloysite can be mined from the consequent deposit as a raw mineral. Common halloysites can be found in form of fine, tubular structures with a length of 300~1500 nm, and inner diameter and outer diameters of 15-100 nm and 40-120 nm, respectively [13]. With their high aspect ratio and reasonable mechanical strength, HNTs are a potential alternative to carbon nanotubes (CNTs) as a reinforcing filler for polymers because HNTs are much less expensive than CNTs [7].

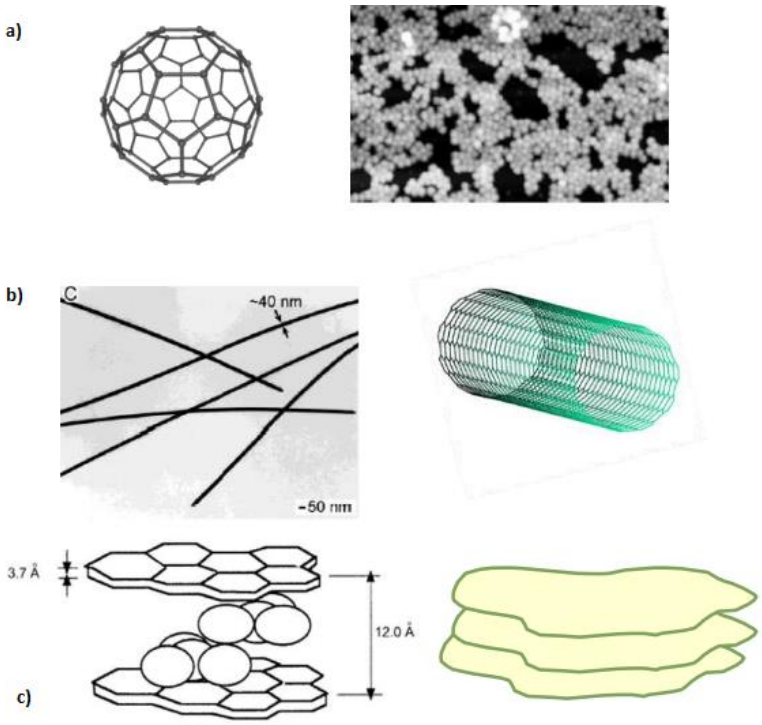

Fig. 1. Geometric shape of reinforcement: a) particulate filler, b) fibrous filler, c) layered filler

Mechanical properties of plastics

Where plastic components are designed to withstand stress, the mechanical characteristics of a material have a particularly important role to play [17]. The fundamental mechanical material properties include:

- Strength: dimension for the resistance of a material to external stress.
- Formability: the capacity of a material to become deformed under external stress.
- Rigidity: dimension for the resistance of a material to deformation.
- Toughness: dimension for the energy absorption capacity of a material under external stress.

These material characteristics are generally determined by briefly applying tensile load in one direction with a tensile test. The results of tensile test is stress (б) – strain (ε) curve (Fig. 2). The stress-strain curve relates the applied stress to the resulting strain and each material has its own unique stress-strain curve.

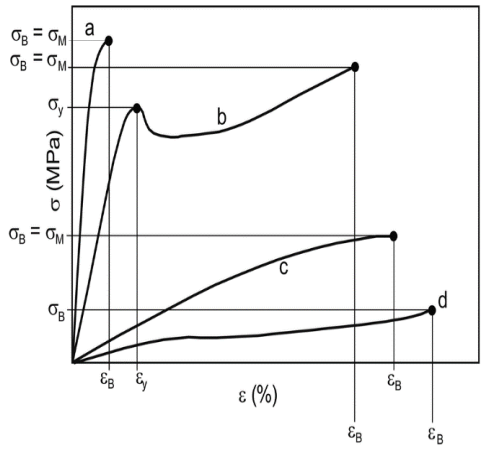

Fig. 2. Stress – strain curve of plastics: brittle plastics (curve a), tough plastics (curve b, c), soft, elastic plastics (curve d)

With an increase of strength, the tension increases according to the formula (1) and the extension is varied according to the formula (2):

$$б = F/ A_0 \quad (1)$$

$$\varepsilon = \frac{L-L_0}{L_0} = \frac{\Delta L}{L_0} \quad (2)$$

where: б - engineering stress [MPa], F- applied load [N], A_0 – original cross sectional area [mm^2], L_0 – original length before test [mm], L- final length after test [mm].

During tensile test, the most significant factors are tensile strength σ_M (the tensile stress at maximum force), tensile stress at break σ_R (the tensile stress at the moment of break) and elongation ε (the change in length ΔL in relation to the original length L_0 of the specimen at any point during testing, the elongation at maximum force is described as ε_M, elongation at break as ε_R) as shown on Fig.2.

The Charpy impact test is a standardized high strain-rate test which determines the amount of energy absorbed by a material during fracture. Calculate the Charpy impact strength of notched samples - a_{cN} - expressed in $kJ.m^{-2}$, with notches C, using the following equation:

$$a_{CN} = \frac{E_C}{h \,.\, b_N} \,.\, 10^3 \quad (3)$$

where: E_c - the corrected energy absorbed by breaking the test sample [J]; h is the thickness of the test sample [mm]; b_N is the remaining width of the test sample [mm].

2. Experimental work

In the present study, low-density polyethylene (LDPE) / halloysite nanotubes (HNT) nanocomposites were prepared and tested. Mechanical properties namely elastic modulus, tensile strength, impact strengt and hardness of the nanocomposites were investigated. Nanocomposites were filled with 5wt% Polyethylene grafted with maleic anhydride (PE-graft-MA) as a compatibility factor.

Production of specimens

A large number of products are produced by injection molding. In injection molding process, the compounded samples are preheated in cylindrical chamber to a temperature at which it can flow and then it is forced into a cold, closed mold cavity by means of quite high pressure, which is applied hydraulically through the ram or screw type plunger. The screw rotates to pick up the material and melt it, mix the melt and deliver it to the closed mold. The screw is then moved forward to force a fixed volume of the molten polymer into the closed mold. After melting, material is solidified in the cool mold, the screw rotates and moves backward to charge the polymer for the next cycle.

The specimens for testing were made by injection molding on injection molding machine type Arburg Allrounder 320 C 500 – 170 (Fig.3). The cavity has a shape of paddles testing and the following dimensions: length L_1 =150 mm, L_0 = 50 mm, a width of from b_2 to b_1 =10=20 mm, depth a= 4 mm.

Fig. 3. Injection moulding machine Arburg Allrounder 320 C used for testing
1 – tool system, 2 – plasticizing system, 3 – drive system, 4 – control devic

The injection process of the polymer nanocomposites were performed under the following conditions:

- the temperature of the heating zones of the plasticizing system of the injection moulding machine, starting with the hopper, equalled 100, 140, 160, 170 and 180 ^{o}C,
- the temperature in the feed opening zone was set at 30 ^{o}C,
- the total time of the injection process cycle equalled 34.16 second, including the cooling time of 20 second,
- injection pressure: 100 MPa,
- the holding pressure equalled 85 MPa,
- the temperature of the injection mould was set at 18 ^{o}C.

Materials for experiments

The polymer used in the experimental tests was Low- Density Polyethylene (LDPE) marketed under the trade name Malen E symbol FGAN 18-D003, produced by Basell Orlen Polyolefins Company. Linear low density polyethylene (LLDPE) is an important thermoplastic for the applications such as electric wire, cable, film, pipe and container [13]. However, its applications are limited, especially due to its relatively low strength, low softening point and flammability resistance. Therefore, it is necessary to modify LLDPE with the incorporation of nanofillers to get improved mechanical properties, flame retardancy as well thermal stability.

Some of the properties of the polyethylene, as specified by the manufacturer are listed in Table 1.

Table 1. *The selected properties of the test polymer LDPE (producer data)*

Property	Value
Density 23 ^{o}C, kg/m^{3}	921
Melt flow rate (190 ^{o}C; 2,16 kg), g/10 min	0.28
Tensile strength at break, MPa	21
Tensile strain at break, %	360
Tensile modulus, MPa	220
Vicat softening temperature, $^{\circ}$C	93
Shore D hardness 15s, $^{\circ}$ShD	50

The material LDPE was modified by Halloysite nanotubes (HNT). Halloysite nanotubes (HNT), by Sigma-Aldrich Company, in the form of powder of the grain diameter from 30 to 70 nm and length 1-3 μm, specific surface 64 m^{2}g^{-1} and density 2530 kg.m^{-3} were used as filler.

Polyethylene grafted with maleic anhydride (PE-graft-MA), by Sigma-Aldrich Company, as a compatibility factor was used. Its melt temperature was 105 ^{o}C and density 920 kg.m^{-2}.

Material for experiments was blended at the three volume concentrations of 2, 4 and 6 wt% of HNT within LDPE matrix and volume concentration of 5wt% of compatibility factor in LDPE polymer.

Methods

Studies of selected mechanical properties of the moldings obtained with the change of HNT amount in LDPE matrix include measurements of tensile strength ($б_M$), strain at strength (ε_M), Charpy impact strength (a_{CN}) and Shore hardness (ShD).

Tension testing in the static tension test of the obtained injection moulds with various amount of filler in the form of standardized specimens used in strength testing was conducted using a standard testing machine manufactured by TIRA GmbH (symbol TIRAtest 2300). Testing of obtained polyethylene specimens was conducted according to EN ISO 527-1:2012 standard; the accuracy of the test was 1N, and the speed of tension was 100 mm/min., temperature at testing in the laboratory was 22 ^oC. The results are an arithmetic average of five measurements.

The hardness testing was conducted according to the hardness measurement procedure described in the EN ISO 868:2005 standard. Plastics and ebonite – determining hardness using interference. The tests were conducted by using a Shore durometer (Shore method). This method has many advantages, among others the measurements are obtained quickly and easily on a small surface area of the tested polymer specimen, and the measurement is precise. The measuring tool has a relatively simple design, and the method itself is one in which the polymer specimen does not undergo destruction. Five hardness measurements were made on each specimen and the final result is an arithmetic mean of these measurements.

The Charpy impact strength test was performed according to EN ISO 179-1:2010 Plastics - Determination of Charpy impact properties - Part 1: Non-instrumented impact test. This standard specifies a method for determining the Charpy impact strength of plastics under defined conditions. A number of different types of samples and test configurations are defined. Different test parameters are specified according to the type of material, the type of test sample and the type of notch. The results of impact strength are an arithmetic mean of ten measurements according to standard. Rectangular samples of 80 x 10 x 4 mm were made by injection molding, samples notch were type C (notch radius r_N = 0.10 mm ± 0.02 mm). The test was performed on device Charpy impact hammer type PSW60/500.

3. Results and Discussion

Strength test results for obtained polyethylene specimens are presented graphically as a plots of the mass content of the nanofiller HNT with the addition (5%) of a compatibilizing agent as a function of the following variables: Young's modulus E, tensile strength $б_M$, tensile strain at strength ε_M. The figures below show the relationships between the mass content of the nanofiller HNT and the

following parameters tensile strength $б_m$ (Fig. 4) and tensile strain at strength ε_m (Fig. 5) for the injection molded specimens obtained in the experiment.

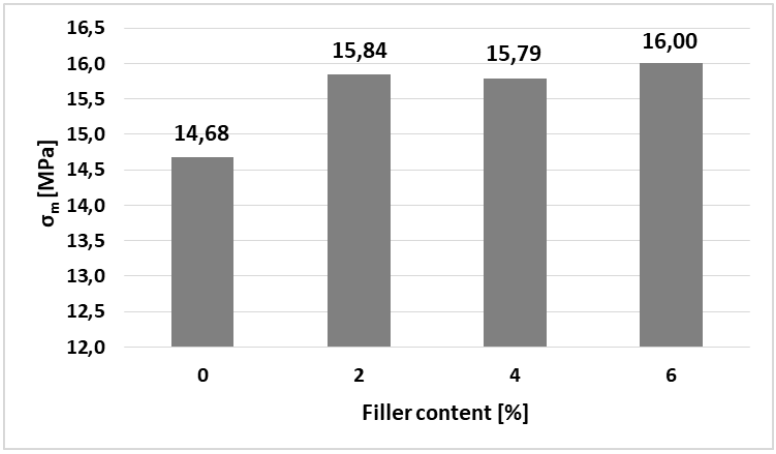

Fig. 4. The relationship between tensile strength and the mass content of the nanofiller with the addition (5%) of a compatibilizing agent

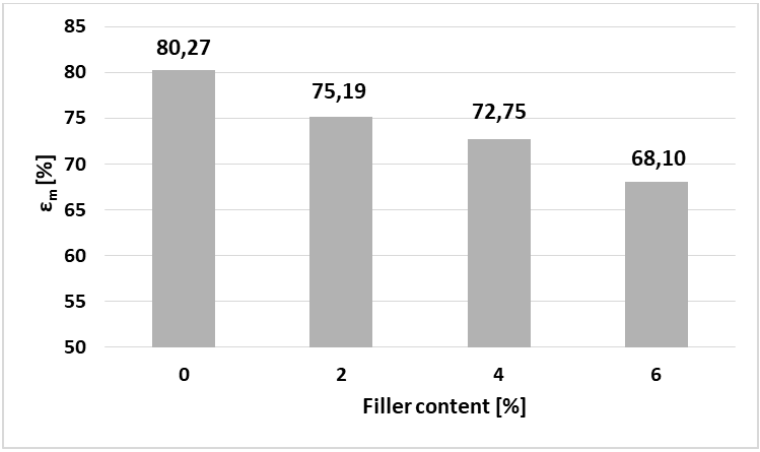

Fig. 5. The relationship between strain at strength and the mass content of the nanofiller with the addition (5%) of a compatibilizing agent

Figure 4 presents the relationship between tensile strength and the mass content of the HNT in the matrix LDPE material with the addition (5%) of a compatibilizing agent. Based on these results it can be concluded that the highest tensile strength was measured for the material LDPE filled 6% HNT (16 MPa) and lowest tensile strength was measured for the material LDPE filled 4% HNT (15.79MPa). Tensile strength at HNT content of 2wt% and 5% PE-graft-MA it is

higher by 7.9 % compared with the LDPE material and at HNT content of 6wt% and 5% PE-graft-MA is higher by 9.0 % compared with the pure LDPE material. The difference between the measured values of the tensile strength (σ_m) was minimal. The value tensile strength was increased by adding the filler content into the LDPE material.

The relationship between strain at strength and the mass content of the nanofiller with the addition (5%) of a compatibilizing agent is shown on Fig.5. Based on strain at strength results it can be concluded that the highest strain at strength was measured for the material LDPE (80.27%) and lowest strain at strength value was measured for the material LDPE with 6% HNT and 5% PE-graft-MA (68.10%). Strain at strength at HNT content of 2wt% and 5% PE-graft-MA it is smaller by 6.3 % compared with the LDPE material and at HNT content of 6wt% and 5% PE-graft-MA is smaller by 15.2 % compared with the LDPE material. The value strain at strength was decreased by adding the filler (HNT) and compatibility factor (PE-*graft*-MA) into the LDPE material.

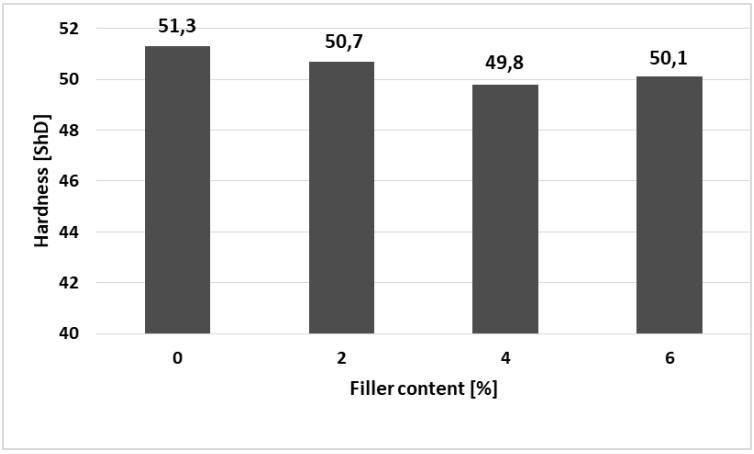

Fig. 6. The relationship between hardness and the mass content of the nanofiller with the addition (5%) of a compatibilizing agent

Figure 6 presents the relationship between Shore hardness and the mass content of the HNT in the matrix LDPE material. Based on these results it can be concluded that the highest Shore hardness value was measurement for the LDPE material (51.3 ShD). After addition of 2 to 6wt% nanofillers and 5% PE-graft-MA to the LDPE material, the hardness value was reduced. For example hardness value 49.8 ShD was measurement for the material LDPE with 4% HNT and 5% PE-graft-MA. Shore hardness at HNT content of 2wt% and 5% PE-graft-MA it is smaller by 1.16 % compared with the LDPE material, at HNT content of 4wt% and 5% PE-graft-MA is smaller by 2.9 % compared with the LDPE material and at HNT content of 6wt% and 5% PE-graft-MA is smaller by 2.3 % compared with

the LDPE material. The hardness was decreased by adding the nanofiller and the compatibility factor PE-graft-MA into the LDPE material. The difference between the measured of the hardness values was minimal.

The relationship between Charpy impact strength and the mass content of the nanofiller HNT with the addition of a compatibilizing agent is shown in Fig. 7.

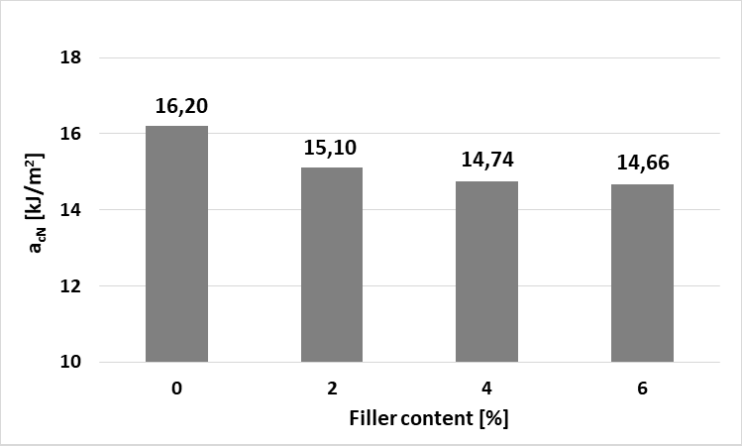

Fig. 7. The relationship between impact strength and the mass content of the nanofiller with the addition (5%) of a compatibilizing agent

Based on these results it can be say that the highest impact strength value was measurement for the material pure LDPE (16.20 kJ/m^2). After addition of 2 to 6wt% nanofillers and 5% PE-graft-MA to the LDPE material, the impact strength values of tested materials were decreased. Impact strength at material LDPE with HNT content of 2wt% and 5% PE-graft-MA was measured smaller by 6.8 % compared with the LDPE material. Impact strength at material LDPE with HNT content of 6wt% and 5% PE-graft-MA is smaller by 9.5 % compared with the LDPE material.

4. Conclusions

This study investigated the influence of Halloysite nanotubes (HNT) and PE-graft-MA within a Low- Density Polyethylene (LDPE) matrix on the mechanical properties. The mechanical properties of specimens made by the injection molded were determined. The results of the tests conducted in this study on the effect of the mass content of the nanofiller (2, 4, 6wt %) with the addition (5%) of a compatibility agent demonstrated that the amount filler and compatibility factor PE-graft-MA has minimum effect on the mechanical properties of the polymer. The selected mechanical properties of the polyethylene (tensile stress, strain at strength) determined in a static tensile strength test were changed by adding filler.

The tensile strength was increased by adding the filler and PE-graft-MA and strain at strength was decreased by adding the filler and PE-graft-MA into the LDPE material. The hardness of the tested materials remained almost constant over the test but showed a tendency to decrease. Added of the filler into LDPE material had no significant effect on hardness of tested materials. The largest deterioration of the investigated properties was observed for the tested material by the Charpy impact test where the impact strength values of tested materials were decreased about 9.5%.

Reinforcing thermoplastic polymers with nanotubes to form nanocomposites is a way to increase the usage of polymeric materials in engineering applications by improving their mechanical properties.

Acknowledgement

This project has received funding from the European Union's Horizon 2020 research and innovation programme under the Marie Skłodowska-Curie grant agreement No 734205 – H2020-MSCA-RISE-2017.

References

[1] Ch. Y. Chee, N. L. Song, L.Ch. Abdullah, T. S. Y. Choong, A. Ibrahim, T. R. Chantara, Characterization of Mechanical Properties: Low-Density Polyethylene Nanocomposite Using Nanoalumina Particle as Filler, Journal of Nanomaterials, 2012 (2012), 6 pages.

[2] E. Joussein, S. Petit, G. Churchman, B. Theng, D. Righi, B. Delvaux, Halloysite clay minerals - a review, Clay Minerals 40 (2005),383-426.

[3] L. Dulebova, T. Garbacz, V. Krasinskyi, B. Duleba, The influence of modifying HDPE on properties of the surface, Materials Science Forum, 818 (2015), 101-104.

[4] B. Theng, M. Russell, G. Churchman and R. Parfitt, Surface properties of allophane, halloysite, and imogolite, Clays and Clay Minerals 30 (1982), 143-149.

[5] J. Jancar, Review of the role of the interphase in the control of composite performance on micro- and nano-length scales. Journal of Materials Science, 43 (2008), 6747-6757.

[6] L.S. Sutherland, R.A. Shenoi, S.M. Lewis, Size and scale effects in composites: I. Literature review. Composites Science and Technology, 59(1999), 209 - 220.

[7] P. C. Ma, N.A. Siddiqui, G. Marom, J. K. Kim, Dispersion and functionalization of carbon nanotubes for polymer-based nanocomposites: A review. Composites Part A: Applied Science and Manufacturing, 41 (2010), 1345-1367.

[8] A. Lagashetty, A. Venkataraman, Polymer nanocomposites, Resonance, (2005), 49–60.

[9] Y. C. Ching, I. I. Yaacob, Effect of polyurethane/nanosilica composites coating on thermo-mechanical properties of polyethylene film, Materials Technology, 27 (2012), 113–115.
[10] S. C. Tjong, Structural and mechanical properties of polymer nanocomposites, Mater. Sci. Eng.: 53, (2006), 73–197.
[11] C. A. G. Beatrice, R. M. V. Alves, M. C. Branciforti, R. E. S. Bretas, Rheological, mechanical, optical, and transport properties of blown films of polyamide 6/residual monomer/montmorillonite nanocomposites, J. Appl. Polym. Sci. 116 (2010), 3581–3592.
[12] U. A. Handge, K. Hedicke-Höchstötter, V. Altstädt, Composites of polyamide 6 and silicate nanotubes of the mineral halloysite: influence of molecular weight on thermal, mechanical, and rheological properties, Polymer 51 (2010), 2690–2699.
[13] M. Du, B. Guo, D. Jia, Newly emerging applications of halloysite nanotubes: a review, Polym. Int'l 59 (2010), 574–582.
[14] R. N. Rothon, Particulate-filled polymer composites, Rapra Technology Ltd., UK, 2003.
[15] E. D. Shchukin et al., Colloid and Surface Chemistry, Elsevier, Netherlands, 2001.
[16] Y. Wang et al: Interfacial interactions in calcium carbonate–polypropylene composites. 2: Effect of compounding on the dispersion and the impact properties of surface-modified composites, Polymer Composite, Vol. 25 (2004), 451.
[17] J. Bussink, Engineering Plastics. In: Lemstra P.J., Kleintjens L.A. (eds) Integration of Fundamental Polymer Science and Technology-3. Springer, Dordrecht, (1989), 43-50.

Karolina Głogowska[1], Łukasz Majewski[1]

THE EFFECT OF ADDITION OF NANOTUBES TO THE THERMAL PROPERTIES AND PROCESSING POLYETHYLENE

Abstract: *In the last two decades, polymer nanocomposites based on unmodified or modified mineral nanofillers have attracted a great deal of attention both in science and industry. A large majority of these nanocomposites were prepared on the basis of natural and synthetic smectites, such as montmorillonite, halloysite, hectorite or laponite. Importantly, low nanofiller content (1—10 wt %) is usually sufficient to achieve significant enhancement of physical properties or flame retardancy of nanocomposites. The paper presents the results of melt flow rate (MFR), Vicat softening temperature (VST) and heat distortion temperature (HDT) analysis of low density polyethylene nanocomplex in the form of nanotubes with a mass fraction of 2% to 6%, in relation to the matrix with the addition (5 %) and without any compatibilizer.*
Keywords*: nanofiller, polymer blend, modification*

1. Introduction

Up to now, most polymer nanocomposites with mineral fillers have been based on MMT with platelet structure. Recently, naturally occurring halloysites with a unique tubular form, known as halloysite nanotubes, have attracted extensive interest [1, 2, 3]. The cylindrical shape of the tubes results from a mismatch in the two-layered alignment of the constituent sheets of silica and alumina. Sometimes, halloysites also form spheroidal. Halloysite is a layered mineral with the empirical formula $Al_2 [Si_2O_5] (OH) 4 \cdot 2H_2O$, containing in its structure a number of natural nanotubes with a high value of the shape factor, and packs of plates (Fig. 1) [4]. Nanotube nanofillers, due to their structure and specific physicochemical properties, gather the interest of both researchers and manufacturers. They can be widely used in various industries, such as: electronic, electrotechnical, optical, etc. There are many different types of nanotubes that are synthesized, but the most important are: carbon nanotubes, metallic and inorganic [5, 6, 7, 8, 9]. The inorganic group includes halloysite nanotubes (HNT-halloysite nanotubes) [10].

[1] *Faculty of Mechanical Engineering, Department of Technology and Processing of Polymer in Lublin, Nadbystrzycka 36 st., 20-618 Lublin, k.glogowska@pollub.pl; l.majewski@pollub.pl*

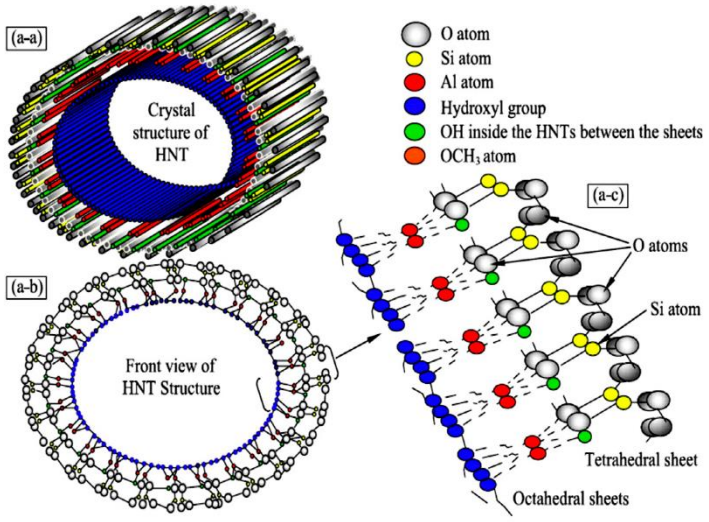

Fig. 1. Schematic presentation showing the crystalline structure of halloysite - in which, three different views (a–a, a–b, and a–c)

The mechanical, thermal, rheological, barrier and other properties of HNT modified polymers depend on two most important factors: the degree of dispersion of the filler particles and the compatibility of the polymer with the nanofiller. With non-polar polymers, such as raw rubber or polypropylene, halloysite nanotubes are incompatible. The improvement of compatibility can be achieved by grafting non-polar macromolecules of maleic anhydride or surface modification of halloysite nanotubes [12, 13].

The aim of the presented research was to determine the effect of powder nanofiller on the melt flow rate, softening point and deflection of the filled polymer (PE-LD) depending on the mass fraction of the nanofiller.

2. Experimental

2.1 Test stand

Experiments were performed using an injection moulding machine Arburg Allrounder 320 C 500 – 170 (Fig. 2). The injection moulding machine has a cylindrical screw with a diameter of 30 mm and the length to diameter ratio of 20. The highest peripheral screw speed equals 42 m/min and its torque is up to 250 Nm. The screw is made as one-piece and single-flight, finished with a ring preventing the polymer from retreating to the plasticizing system during the injection of the polymer to the injection mould cavity. The barrel is also uniform and finished with an exchangeable injection nozzle.

The plasticizing system of the Arburg injection moulding machine has five heating zones of the same length and a cooled feed opening zone. It makes it

possible to inject into the forming cavity of the injection mould up to 80 cm^3 of polymer plasticized with maximum injection pressure of up to 200 MPa.

The ttransmission of the injection moulding machine is powered with three-phase alternating current with voltage of 400V and frequency of 50 Hz. The injection moulding machine ensures the clamping force of the mould of 500 kN. The area between the columns of the opening-closing tool with dimensions of 320 mm x 320 mm, and the size of tables of the movable and immovable subassembly of the injection mould is 550 x 550 mm. A two-part injection mould was mounted on the platens of the injection moulding machine. In one of its parts, the flow channels of the mould were created, that is sprue, runners and gates. The injection moulding machine has two mould cavities, with the shape and size in accordance with standardized specimens for strength testing. The second part of the mould is a flat plate that constitutes the closing of the first part. The mould is thermostatized with oil of the temperature in the range from 12 to 50 °C, flowing through the channels in the mould.

The temperature of the heating zones of the plasticizing system of the injection moulding machine, starting with the hopper, equalled 100, 140, 160, 170 and 180 ^oC while the temperature in the feed opening zone was set at 30 ^oC. The total time of the injection process cycle equalled 34,16 s, including the cooling time of 20 s. The composite polymer was injected into the mould at the pressure of 100 MPa and the holding pressure equalled 85 MPa. The temperature of the injection mould was set at 18 ^oC.

Fig. 2. Injection moulding machine Arburg Allrounder 320 C used for testing

Research stand for testing melt flow index (MFR) is the extrusion plastometer Zwick 4105.100 with additional equipments and analitical scale PRL TA14. The mass of samples obtained using the extrusion plastometer was determined by

means of an analytical balance of the type PRL T A14 and symbol WA 34, with the measuring range from 0 to 100g and measuring accuracy 0.00001 g.

The measurements of heat distortion temperature (HDT) and Vicat softening temperature (VST) were made using the Instron-manufactured CEAST HV3 provided with three work stations.

2.2 Materials

The polymer used in the experimental tests was low density polyethylene LDPE marketed under the trade name Malen E and symbol FGAN 18-D003, produced by Basell Orlen Polyolefins company (tab. 1). The PE used in the experiment is manufactured for extrusion. The recommended processing temperature for this product ranges from 170°C to 220°C.

Table 1. Basic properties of the tested polymer as given by the manufacturer

Property	Unit	Value
Density	kg/m^3	921
Melt flow rate (190 °C; 2.16 kg)	g/10 min	0.28
Tensile modulus	MPa	220
Tensile strain at break	%	360
Shore hardness	°Sh D	50
Vicat softening temperature B50 (50°C/h, 50N)	°C	93

Halloysite nanotubes (HNT), by Sigma-Aldrich company, in the form of powder of the grain diameter from 30 to 70 nm and length 1-3 μm, specific surface 64 m^2/g and density 2530 kg/m^3.

Polyethylene grafted with maleic anhydride (PE-*graft*-MA), by Sigma-Aldrich company, as a compatibilizer was used. Its melt temperature was 105 °C and density 920 kg/m^2.

2.3 Tested parameters

Given the objective of the study, we devised a set of key parameters describing the processing, thermal and granulometric properties of the tested material. The parameters were divided into four groups.

Resulting parameters:

- melt flow rate MFR, g/10min.
- heat distortion temperature HDT, °C;
- Vicat softening temperature, °C;

Variables:

- nanofiller type: halloysite nanotubes;
- weight in weight concentration of the nanofiller in the test piece: $\zeta = 2$; 4; and 6 %.

Constant parameters:

- geometry of the plasticizing unit, tools and injection mold:
- temperature of the injection mold 18°C:
- temperature along the plasticizing unit of the injection molding machine: 100, 140, 160, 170 and 180 °C;
- injection pressure: 100 MPa; holding pressure: 85 MPa; holding time: 6s, injection cycle time: 34,16s; cooling time: 20s;
- Vicat load 10N;
- oil bath heating rate 120 K/h.

Disturbing parameters:

- electric voltage: 219 – 241 V,
- relative air humidity: 55 – 65 %,
- ambient temperature: 20 – 24°C.

The results of the investigated direct twin-screw extrusion and injection molding processes revealed that the disturbing parameters have a negligible effect on the results of the measurements.

2.4 Methods

Measurements of melt flow rate (MFR) of a low-density polyethylene modified with a nanofiller in the form of nanotubes of the content from 2% to 6% by mass in relation to the matrix with the addition of 5% of compatibilizer and without it were made in accordance with ISO 1133-1:2011. Before measurements are started, the cylinder and the piston of the extrusion plastometer are heated to a set temperature (190 °C), which must be maintained for 15 minutes. Pellets of the nanocomposite are introduced into the cylinder and a weighted piston (2.16 kg) is placed in the cylinder; after about 4 min, the test material reaches the measurement temperature. Measurement (which involves cutting off pieces of the test material) starts when the bottom ring mark on the piston rod reaches the upper edge of the cylinder and ends when the top ring mark reaches the upper edge of the cylinder. During this time, extruded sections of the test material are cut off every 60s. When the cutting is completed and the polymeric composite extrudate has solidified, the sections are weighed, using an analytical balance, to an accuracy of 0.001g, and then the average mass of the extruded sections and the melt flow rate (MFR) are calculated from the formula:

$$MFR\ (T, m_{nom}) = 600\ m/t \qquad (1)$$

where: T – means test temperature in ^{o}C; m_{nom} – loading mass in kg; m – average mass of extruded polymer sections in grams; 600 is calculation coefficient (600s = 10 min) meaning cutting period of time in seconds, matched in relation to the tested polymer, in such a way that polymer section length is within the range from 10 to 20 mm.

The Vicat softening temperature (VST) test was performed according to ISO 306. Before being placed in measuring stations specimens were measured with a precision caliper to an accuracy of 0.01 mm. The specimen dimensions obtained were entered into the computer program which calculated the dedicated load for the given each specimen. VST was measured using the A50 method, in which a specimen is loaded with a force of 10 N and the temperature increase rate is 50 degrees C/h. After placing the specimens in the measuring stations, they were immersed in an oil bath, and the gauge needle's sensors were calibrated. The starting temperature of the process was 30 ^{o}C, and the maximum oil temperature was set at 120 ^{o}C. According to the norm, VST is a temperature in °C, at which the specimen is penetrated to a depth of 1 mm by a hardened steel needle with a circular cross-section of 1 mm2 under a specific load at a specific temperature increase.

The heat deflection temperature (HDT) test was performed according to ISO 75. Before being placed in measuring stations specimens were measured with a precision caliper to an accuracy of 0.01 mm. The specimen dimensions obtained were entered into the computer program which calculated the dedicated load for the given each specimen. The load causes constant bending stress which equals 0,45 MPa (defined by standard). After placing the specimens in the measuring stations, they were immersed in an oil bath, and the gauge deflection sensors were calibrated. The starting temperature of the process was 30 ^{o}C, and the maximum oil temperature was set at 120 ^{o}C. According to the standard the heat deflection temperature is the temperature at which the specimen deflects by a defined value (0,32 mm) because of constant bendig stress. After the deflection computer software called Visual Therm connected to the test station automatically stops the device, reports the results and draws the curve of penetration as a function of temperature growth. Heat Deflection Temperature results were used to calculate the arithmetic mean and standard deviation.

3. Results and discussion

3.1. Melt flow rate (MFR)

It was noted that regardless of the screw speed of the extruder, the melt flow rate and melt volume rate of the resulting polymer nanocomposites had increased 9 (Fig. 3). At a screw speed of 50 rev/min, the melt flow rate of the composite with a 2% nanofiller of halloysite nanotubes increases in comparison with virgin polymer from 0.318 g/10 min to 0.488 g/10 min, which is an increase of 53.45%. Further increase in the proportion of the nanofiller also increases the MFR to 0.608 g/10 min, which is more than 24%.

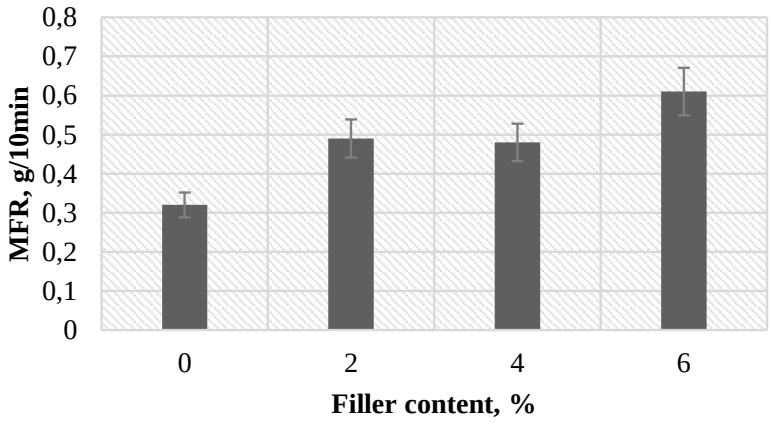

Fig. 3. Melt flow rate (MFR) of received nanocomposites in dependence on nanofiller mass content with the addition of 5% of compatibilizer

3.2. Vicat Softening Temperature and Heat Deflection Temperature

When studying Vicat Softening Temperature, the addition of nanofiller in the form of halloysite nanotubes into low density polyethylene causes a slight decrease of the studied temperature. The addition of 2% of nanofiller causes the decrease of VST by almost 0.2 degrees Celsius, while the addition of 6% of nanofiller results in the drop of VST by 0.5 degrees (Fig. 4). The introduction of 5% of compatibiliser into the composite results in a bigger VST decrease

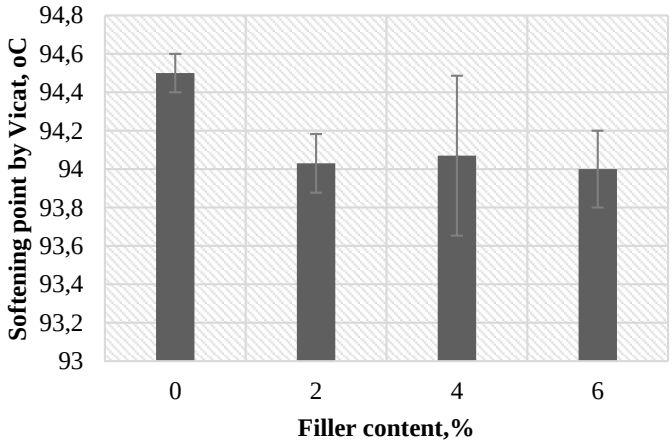

Fig. 4. Vicat softening temperature (VST) in dependence on nanofiller mass content without the addition of compatibilizer

therefore VST drops 1 degree Celsius with 2% mass participation of nanofiller and VST drops 2 degrees Celsius with 6% mass participation of nanofiller (Fig. 5). Fillers can form agglomerates where interactions between filler particles are scarce. Loose clusters of filler particles easily degrade, as long-term exposure to high temperature results in a gradual degradation of the polymer, which leads to its softening.

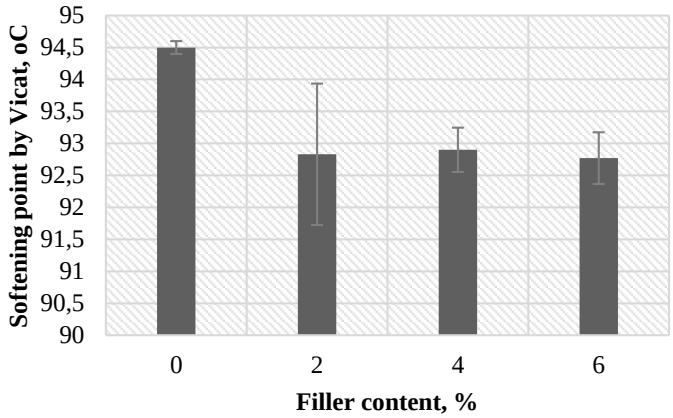

Fig. 5. Vicat softening temperature (VST) in dependence on nanofiller mass content with the addition of 5% of compatibilizer

As a result of the conducted tests it was stated that the addition of nanofiller in the form of halloysite nanotubes influences Heat Deflection Temperature in a positive way causing its slight increase, while the addition of compatibilizer

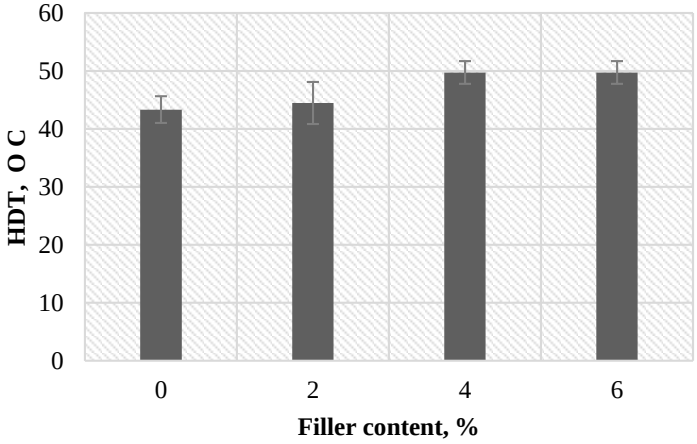

Fig. 6. Heat deflection temperature (HDT) in dependence on nanofiller mass content without the addition of compatibilizer

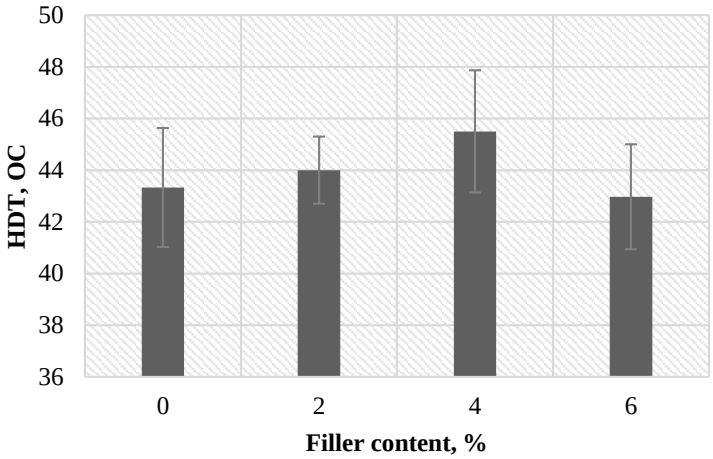

Fig. 7. Heat deflection temperature (HDT) in dependence on nanofiller mass content with the addition of 5% of compatibilizer

influences the addition of compatibilizer influences the value of temperature in a negative way by decreasing it (Fig. 6). The addition of 2% of nanofiller to low density polyethylene causes the increase of HDT by almost 2 degrees Celsius, while the addition of 6% of HNT results in almost 7 degrees Celsius increase of HDT. Additionally, the introduction of compatibilizer into the composite in the amount of 5% by mass causes the increase of HDT by almost one degree if the nanofiller equals 2% and the increase of HDT of 3.5 degrees Celsius if the nanofiller equals 6% (Fig. 7).

4. Conclusions

The preparation of polymer compositions is an interdisciplinary matter. When choosing a nanofiller and its amount, one should take into account various factors and parameters in the field of chemistry, physicochemistry of polymers, mechanics, rheology, material engineering, and even the design of processing machines. The right nanofiller and its appropriate proportions allow to achieve desired changes in selected properties. Therefore, it is important to study new compositions using previously unused fillers to discover blends with unprecedented properties.

The results of the preliminary tests confirmed that the nanofiller influences the processing and usage properties of polyolefins with its presence. Halloysite nanotubes can be promising nanofillers of polyolefins that could allow to obtain new and useful materials. For this reason, further research is planned, the aim of

which will be to analyse the effect of halloysite nanotubes on the structure and mechanical properties.

Acknowledgements

This project has received funding from the European Union's Horizon 2020 research and innovation programme under the Marie Skłodowska-Curie grant agreement No 734205 – H2020-MSCA-RISE-2017.

References

[1] Pasbakhsh P., Ismail H., Fauzi M. N. A, Bakar A. A., Influence of maleic anhydride grafted ethylene propylene diene monomer (MAH-g-EPDEM) on the properties of EPDM nanocomposites reinforced by halloysite nanotubes, Polymer Testing, 2009, 28/6, 548-559.

[2] Miltner H. E., Assche G. V., Pozsgay A., Pukánszky B. & Van Mele B., Restricted chain segment mobility in poly(amide) 6/clay nanocomposites evidenced by quasi-isothermal crystallization. *Polymer, 2006, 47/3,* 826 - 835.

[3] Bhattacharyya A. R., Sreekumar T. V., Liu T., Kumar S., Ericson L. M., Hauge R. H., Smalley R. E., Crystallization and orientation studies in polypropylene/single wall carbon nanotube composite. Polymer, 2003, 44/8, 2373 - 2377.

[4] Gorga R. E., Cohen R. E., Toughness enhancements in poly (methyl methacrylate) by addition of oriented multiwall carbon nanotubes. Journal of Polymer Science, 2004, 42, 2690 - 2702.

[5] Li C., Liu J., Qu X., Yang Z., A general synthesis approach toward halloysite-based composite nanotube. Journal of Applied Polymer Science, 2009, 112, 2647 - 2655.

[6] Ye Y., Chen H., Wu J. Ye. L., High impact strength epoxy nanocomposites with natural nanotubes. Polymer, 2007, 48, 6426 – 6433.

[7] Baochun G., Quanliang Z., Yanda L., Demin J., Structure and Performance of Polyamide 6/Halloysite Nanotubes Nanocomposites, Polymer Journal, 2009, 41, 835–842.

[8] Ismail H., Pasbakhsh P., Fauz, M.N.A., Abu Bakar A., Morphological, thermal and tensile properties of halloysite nanotubes filled ethylene propylene diene monomer (EPDM) nanocomposites. Polymer Testing, 2008, 27, 841–850.

[9] Marney D.C.O., Russell L.J., Wu D.Y., Nguyen T., Cramm D., Rigopoulos, N., Wright, N., Greaves, M., The suitability of halloysite nanotubes as a fire retardant for nylon 6. Polymer Degradation and Stability 2008, 93, 1971-1978.

[10] Liu M., Guo B., Du M., Jia D., Drying induced aggregation of halloysite nanotubes in polyvinyl alcohol/halloysite nanotubes solution and its effect on properties of composite film. Applied Physics A: Materials Science and Processing 2007, 88, 391–395.
[11] Albdiry M. T., Yousif B. F., Role of silanized halloysite nanotubes on structural, mechanical properties and fracture toughness of thermoset nanocomposites, Materials & Design, 2014, 57, 279-288.
[12] Ismail H., Pasbakhsh P., Ahmad Fauzi M.N., Abu Bakar A., The effect of halloysite nanotubes as a novel nanofiller on curing behaviour, mechanical and microstructural properties of ethylene propylene diene monomer (EPDM) nanocomposites. Polymer - Plastics Technology and Engineering 2009, 48, 313–323.
[13] Hedicke-Hochstotter K., Teck Lim G., Novel polyamide nanocomposites based on silicate nanotubes of the mineral halloysite. Composites Science and Technology 2008, 69, 3-4, 330-334,

Łukasz Majewski[4], Karolina Głogowska[4]

THE ANALYSIS OF THE IMPACT OF A COMPATIBILIZER ON THE HOMOGENISATION OF A LDPE/HNTs NANOCOMPOSITE

Abstract: *The rapid development in the field of material engineering makes it necessary to control material structure in the nanometric scale when modifying composite properties. In order to bring about the desired properties, the reinforcement phase must be dispersed properly in the matrix with the appropriate adhesion at the matrix-filler interface. To achieve that, various attempts to increase the specific surface of filler grains are made by activating the surface chemically or by covering with an intermediate, a compatibilizer. The aim of this study was to test the impact of a compatibilizer on the dispersion level of a nanofiller in the form of halloysite nanotubes (HNTs) in a low density polyethylene matrix.*
Keywords: *nanotubes, halloysite, homogenization, compatibilizer, nanocomposite*

1. Introduction

Nanotechnology is a quickly developing, interdisciplinary field of knowledge encompassing many research areas including physics, chemistry, biology, mechanics and even medicine. The interdisciplinary character makes it difficult to determine its exact subject scope and research areas, because virtually all technical fields involve issues associated with the nanometric scale [1,2]. The term nanotechnology was coined in 1974 by Norio Taniguchi as a name for treatment with accuracy smaller than 1μm. It is currently believed that nanotechnology deals with objects with at least one dimension below 100 nm [3, 4]. According to the author of [5], "new" nanotechnology should comply with three conditions:

- tested structures should have at least one dimension below 100nm,
- chemical and physical properties should be controllable in the manufacturing process,
- they must provide the possibility to be used for the construction of bigger objects.

In light of these definitions it is obvious that polymer nanocomposites (PNC) are a part of nanotechnology, as usually the dimensions at least one of their components are measured in nanometres – ranging from about 1 nm to a few hundred nm. Major studies on such systems began at the beginning of the last

[4)] *Lublin University of Technology, Faculty of Mechanical Engineering, Department of Polymer Processing and Technology; 36 Nadbystrzycka St; 20-618 Lublin, Poland*

decade of the 20th century and made continuous progress for 10 years, while in 2002 already half of all studies on PNC involved those with polymer matrix [3].

The most frequently used nano-additives in polymer material processing are aluminosilicate nanofillers: montmorillonite and halloysite. Recently, kaolinite materials have attracted considerable attention, owing to the fact that they are very commonly found in nature, being the main element of the earth's crust. Such materials can be successfully used to manufacture organic-inorganic hybrid materials used in various branches of industry and environmental protection [6-8]. Nanofillers may come in different shapes, e.g. plates, grains, needles, fibres or nanotubes. Usually many types of nanotubes are synthesized, the most important of them being inorganic and metallic carbon nanotubes [10,11]. The inorganic group includes e.g. halloysite nanotubes.

Halloysite is a hydrated aluminosilicate with a density of (2.0–2.2) g/cm³ and chemical formula $Al_2[Si_2O_5](OH)_4 \cdot 5H_2O$. Due to its characteristic structure, halloysite exhibits features of both layered and tubular nanofillers. The morphology of a halloysite grain depends on its origin, especially the conditions during crystallisation in the geological environment. This mineral consists of silicon tetrahedra and aluminium octahedra making up a porous, spatial structure. Individual plates are separated by a gap, where the absorbed ions and particles (including water) loosely connected to the surface of the plate mainly by hydrogen bonds may occur. It may contain traces of chromium, iron, magnesium, nickel and copper. It is a white, yellow, green or red powder. The main halloysite deposits are in Russia, Belgium, Germany, France and Poland (Dunino near Legnica). It is characterised by considerable porosity and specific surface, high ion exchange capacity, ease of chemical and mechanical processing and minor amounts of impurities. Small number of -OH groups found on the surface causes halloysite nanotubes to disperse well in polymers and the produced nanocomposites have many specific properties. About 30% of the material's structure is composed of stiff, straight nanotubes (called halloysite nanotubes – Fig. 1) with a diameter of 10–150 nm and length of about 2 μm, which means it could be a more economical and ecological alternative for still rather expensive carbon nanotubes [6, 10-14].

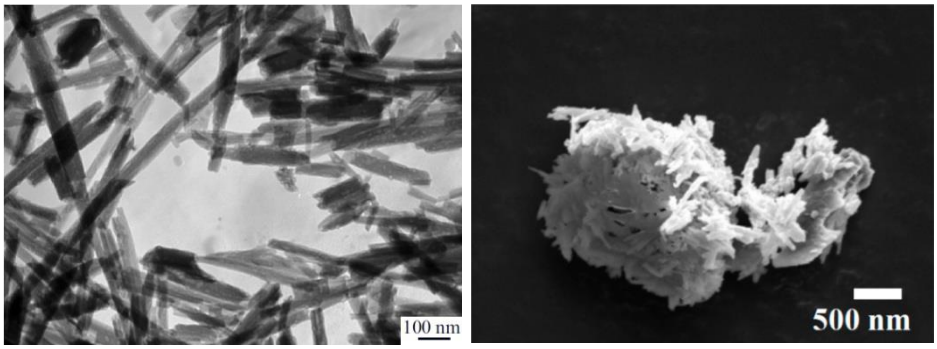

Fig. 1. TEM and SEM images of halloysite nanotubes [9,10]

Apart from the components' physicomechanical properties, the properties of polymer composites as construction materials are also highly influenced by the size of the dispersed phase interface and the character of interactions between the continuous and dispersed phase. As many studies and experiments have proved, the mechanical properties of a composite increase when the filler's aspect ratio increase and its transverse dimension decreases. The filler's specific surface increases and the sum of impact forces between the polymer matrix and the filler particles increases. This is why nanocomposites obtain great mechanical properties even containing little amounts nanofiller, comparable to 3-5% of weight. The improvement of properties depends to a great extent on the dispersion of the filler in the polymer matrix [13-15].

The aim of this study was to conduct a microscopic analysis of the decomposition of halloysite nanotubes in low density polyethylene matrix and examine the impact of the used compatibilizer on the character of the decomposition.

2. Test stands

The specimens for studies of degree of homogenization and microscope studies of the material structure were obtained by using an injection moulding machine Arburg Allrounder 320 C 500 – 170. The injection moulding machine has a cylindrical screw with a diameter of 30 mm and the length to diameter ratio of 20. The temperature of the heating zones of the plasticizing system of the injection moulding machine, starting with the hopper, equalled 100, 140, 160, 170 and 180°C while the temperature in the feed opening zone was set at 30°C. The total time of the injection process cycle equalled 34.16 s, including the cooling time of 20 s. The composite polymer was injected into the mould at the pressure of 100 MPa and the holding pressure equalled 85 MPa. The temperature of the injection mould was set at 18°C. The specimens obtained in the process of

injection moulding were used for tension strength testing. Specimens obtained in the injection moulding process were ruptured during a static tensile test on a TIRAtest 2300 tensile testing machine. The following testing parameters were applied: initial force 0.1 MPa and testing speed 50 mm/min.

The specimens were sputtered in the Quorum Q150T ES sputter coater prior to the experiment (Fig. 3). It is used for plasma sputtering of thin carbon or metallic layers, facilitating the examination in a high-definition scanning electron microscope (SEM) and transmission electron microscope (TEM).

Scanning Electron Microscope Nova NanoSEM 450 produced by FEI (Fig. 2) was used to measure degree of polymer homogenization and microscope laboratory studies of the material structure. SEM a is high resolution microscope operating in high and low vacuum mode. It is used for testing the structure, phase and chemical content in a wide range of enlargement. The microscope can operate in SE (secondary electrons) mode and BSE (backscattered electrons) mode.

Fig. 2. High resolution Scanning Electron Microscope Nova NanoSEM 450 from FEI

The application of through-the-lens low energy electron detector (TLD), multisectoral concentric BSE detector and e-beam deposition ensures very good

working parameters at low voltage acceleration. An integrated plasma cleaning system and cryogenic trap reduce the specimen contamination. These microscopes are characterized by unique operating parameters in low vacuum mode – helix detector of secondary electrons provides direct imaging of non-conductive and biological specimens with the resolution higher than 2 nm. They are also optimised to electron litography (fast electrostatic system of beam deflection) and to transmission high energy electron detector (STEM) imaging (movable detector HAADF/DF/BF).

3. Materials

The polymer used in the experimental tests was low density polyethylene LDPE marketed under the trade name Malen E and symbol FGAN 18-D003, produced by Basell Orlen Polyolefins company. According to the data provided by the producer, this material exhibits the following properties: density – 921 kg/m^3, melt flow rate (190°C; 2.16 kg) = 0.28 g/10 min, tensile strength at break – 21 MPa, tensile strain at break – 360 %, Tensile modulus – 220 MPa, Vicat softening temperature – 93°C, Shore hardness D – 50°ShD. The PE used in the experiment is manufactured for extrusion. The recommended processing temperature for this product ranges from 170°C to 220°C.

Halloysite nanotubes (HNT), by Sigma-Aldrich company, in the form of powder of the grain diameter from 30 to 70 nm and length 1-3 μm, specific surfacej 64 m^2/g and density 2530 kg/m^3.

Polyethylene grafted with maleic anhydride (PE-graft-MA), by Sigma-Aldrich company, as a compatybilizer was used. Its melt temperature was 105°C and density 920 kg/m^2.

4. Research methodology

Seven series of specimens consisting of injection mouldings were prepared for the study. Table 1 shows the exact chemical composition of the specimens.

Table 1. Composition of the tested composites

No.	PE-LD Malen E FGAN 18-D003, g	Halloysite nanotubes HNT, g (%)	Compatibilizer PE-graft-MA, g (%)
1	700	0%	0%
2	700	14g (2%)	0%
3	700	28g (4%)	0%
4	700	42g (6%)	0%
5	700	14g (2%)	35g (5%)
6	700	28g (4%)	35g (5%)
7	700	42g (6%)	35g (5%)

Specimens were ruptured to obtain fractured surfaces for microscopic observation. The fractured surfaces were cut off with a guillotine and taped to slides compatible with the microscope stage. The specimens were attached to the stage of the microscope, which was then placed in the Quorum Q150T ES sputter coater along with the specimens. There, in an argon atmosphere, a thin (10 nm thick) layer of gold was sputtered onto the surface of the specimens, which facilitated observation under the microscope (Fig. 3).

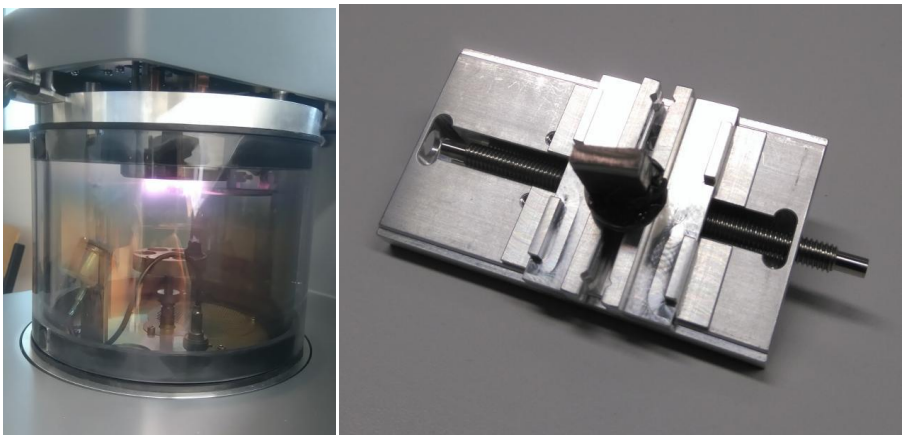

Fig. 3. Process of gold sputtering and the specimen after sputtering

Prepared in this way, the specimens were placed on a mobile and rotating microscope stage mounted on a retractable drawer (Fig. 3 and Fig. 4). Once the specimens were in the chamber and the chamber was closed, the air was extracted.

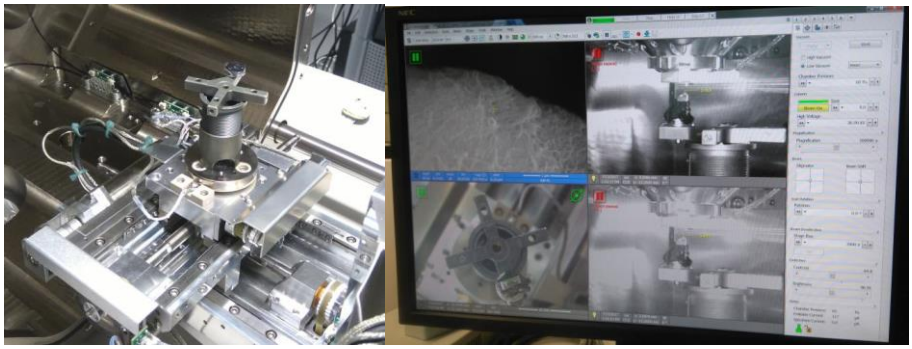

Fig. 4. Parts of Scanning Electron Microscope: microscope stage and image on the computer screen

Observations were carried out in low vaccum (60 Pa). The distance of the specimen from the detector, the exact position of the detector above the specimen, and the parameters of the scan beam could be monitored on the screen (Fig. 4).

5. RESULTS

Figures from 5 to 11 show the results of microscopic observantions (SEM) of polymer composites containing halloysite nanotubes and an optional addition of a compatibilizer. Figure 5 shows the surface of pure polyethylene without additives. The surface is homogeneous without visible inclusions, even at large magnifications.

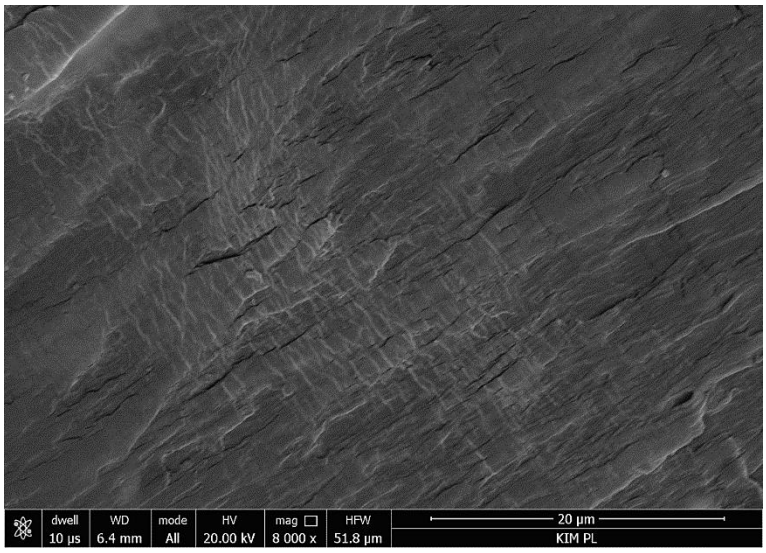

Fig. 5. Image showing polyethylene without the addition of nanotubes and compatibilizer

Figure 6 shows the fractured surface of a composite containing 2% of nanotubes, and Figure 7 is an image of a composite with 2% of nanotubes and 5% of compatibilizer. In both cases, nanotube agglomerates of various sizes (from several to a dozen μm) are visible on the polymer surface. Given the size of the nanotubes themselves, the size of the agglomerates is quite large. Enlargements of Figure 6 show the way the agglomerates are embedded in the matrix. The polymer does not cling fast to their surface, which may indicate poor adhesion of the agglomerates to the polymer. In the next Figures (Fig. 8, Fig. 9, Fig. 10 and Fig. 11), the agglomerates are larger and more densely arranged with the increase of halloysite nanotubes in polymer matrix. It can be seen that they are abundant in places where the specimen has ruptured. A large concentration of nanotube agglomerates is observed in Figure 10. The enlargement shows that

only a small amount of the polymer has penetrated into the interior of the nanotube cluster. The presence of such structures will most likely adversely affect the properties of the entire composite.

Figure 11 also shows large agglomerates of nanotubes, up to a dozen μm, at the edge of the fractured surface. The presence of structures of this size may also adversely affect the strength of the material.

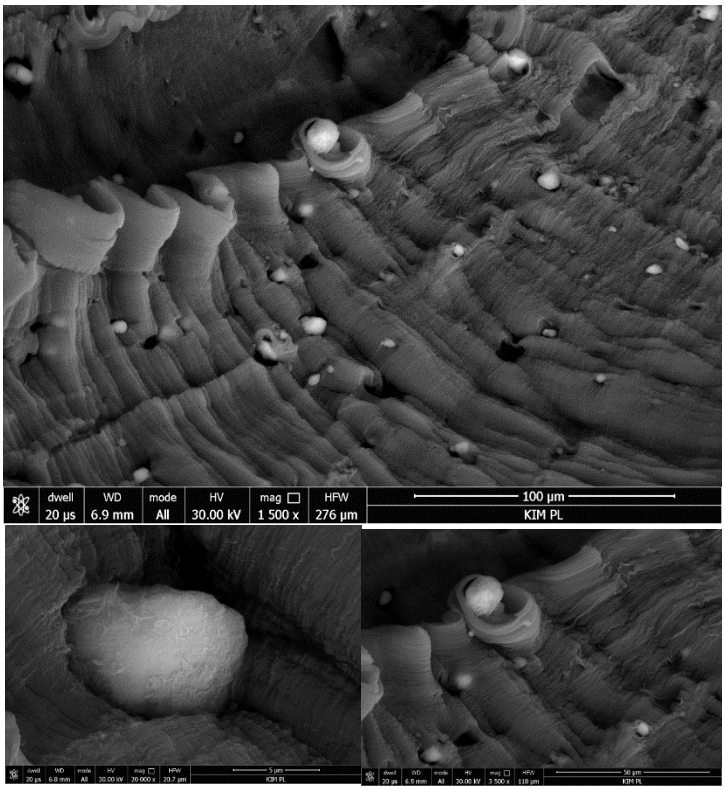

Fig. 6. Image showing polyethylene with 2% addition of nanotubes and two enlargements of nanotube agglomerates

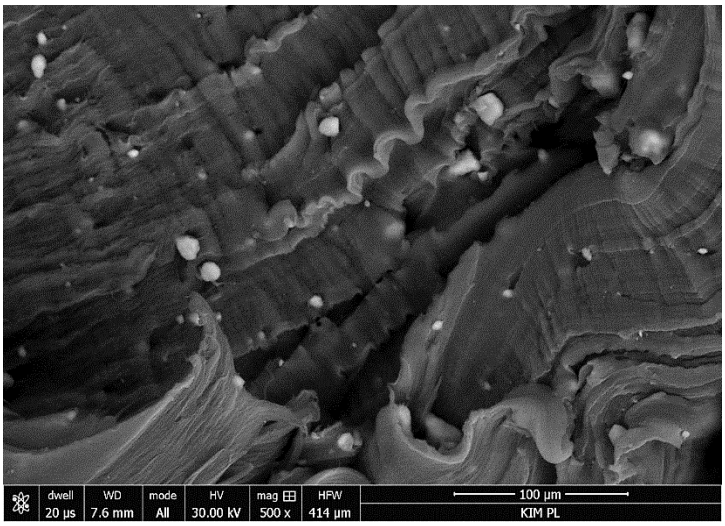

Fig. 7. Image showing polyethylene with 2% addition of nanotubes and 5% of compatibilizer

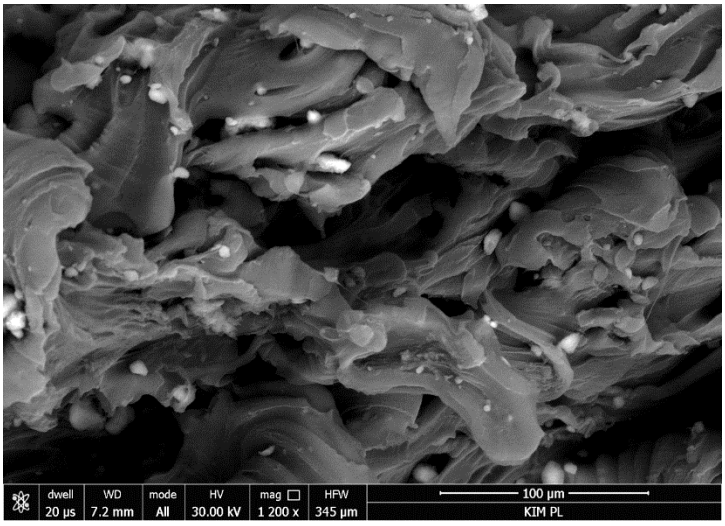

Fig. 8. Image showing polyethylene with 4% addition of nanotubes

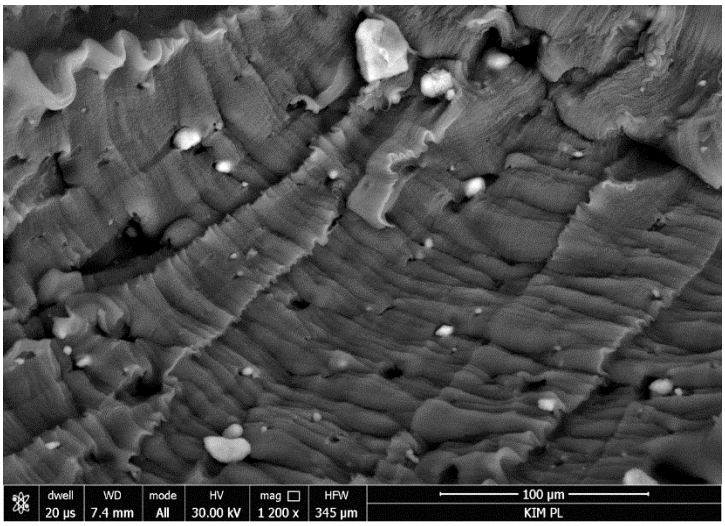

Fig. 9. Image showing polyethylene with 4% addition of nanotubes and 5% of compatibilizer

One can see tiny needle-like structures that match the dimensions of the nanotubes as provided by the manufacturer. In most cases, however, the nanotubes are clustered into large agglomerates, sized several to a dozen µm. The last Figure 12 shows nanoparticle agglomerates mechanically separated from the polymer matrix from a cluster so large that it was visible to the naked eye. Small, needle-like structures can be seen, matching the dimensions of nanotubes provided by the manufacturer. Still, they mostly appear in big agglomerates of a few to a dozen µm. There is an analogy between the observed agglomerates and the nanotubes in Fig. 1.

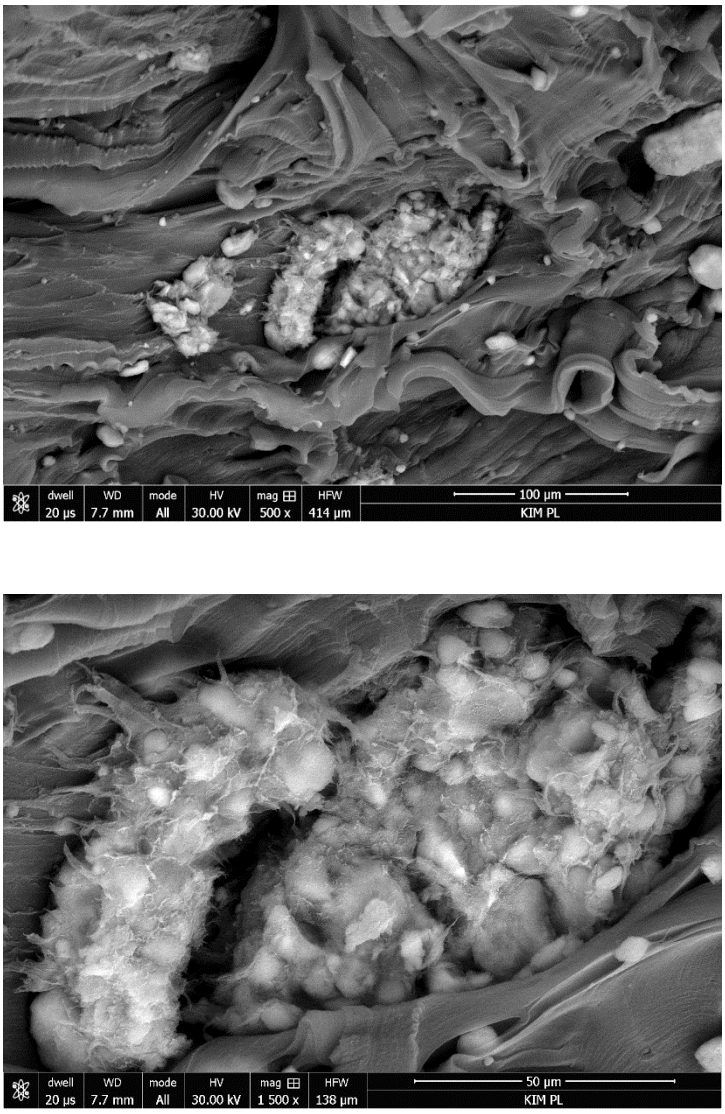

Fig. 10. Image showing polyethylene with 6% addition of nanotubes and enlargement of halloysite nanotube agglomerate

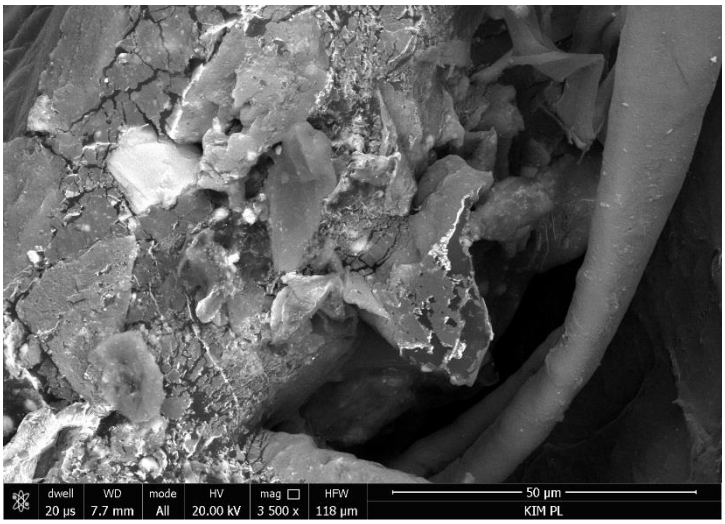

Fig. 11. Image showing polyethylene with 6% addition of nanotubes and 5% of compatibilizer

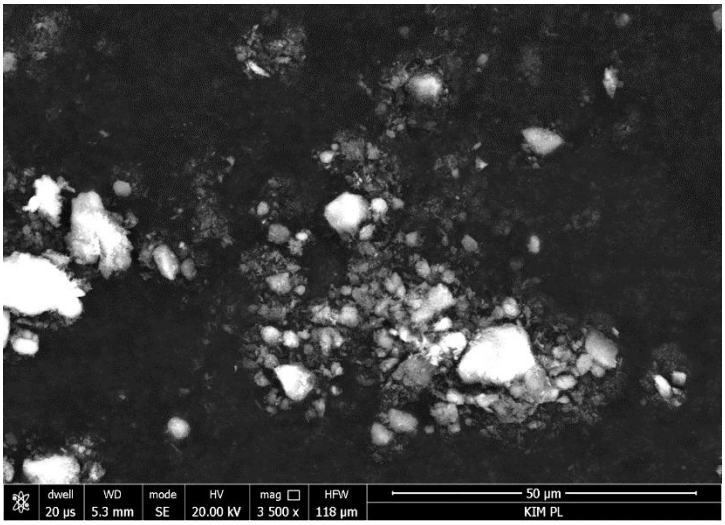

Fig. 12. Nanotubes agglomerates separated from polymer

To verify the results, the obtained images were compared to those obtained by other authors examining halloysite nanotubes dispersion with SEM. Figure 13 is a SEM image from paper [16], depicting the decomposition of halloysite nanotubes in a polilactic acid matrix. One can clearly see agglomerates of nanotubes of size and appearance corresponding to those obtained in this paper.

Despite the presence of agglomerates of 20-30 μm in size, the authors of those papers define the dispersion level as good.

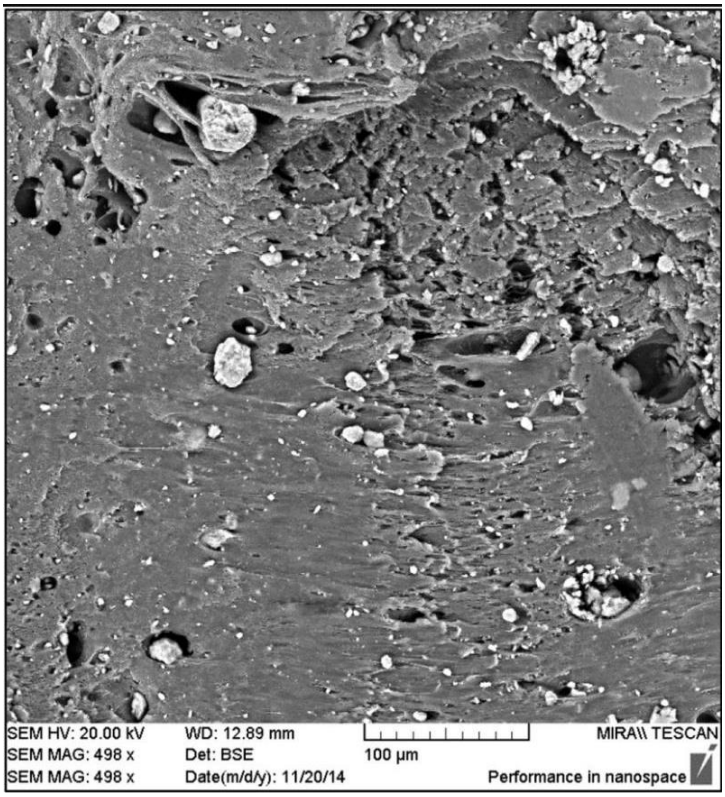

Fig. 13. Decomposition of halloysite nanotubes in a polilactic acid matrix, SEM image [16]

The image of halloysite nanotube cluster obtained in [17] can be seen in Fig. 14. The authors describe the impact of halloysite nanotube contents on EPDM properties. On the basis of this image, they describe the face-to-face and face-to-edge interaction of nanotubes and their influence on tensile strength and brittleness of the composite. They claim that the image allows to assume that the nanofiller was dispersed correctly in the polymer matrix. Surprisingly, the authors of [17] applied the magnification of merely 5000x.

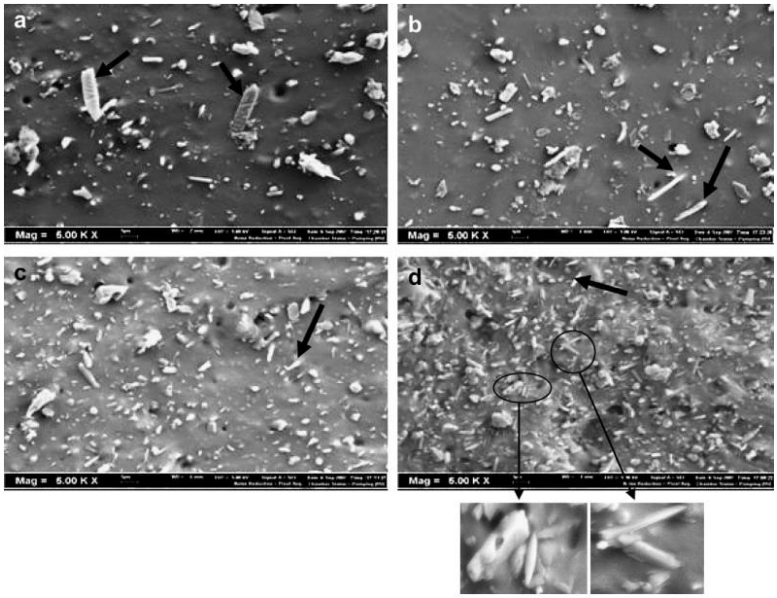

Fig. 14. Tensile fracture surfaces of EPDM/HNT nanocomposites with (a) 5 phr, (b) 10 phr, (c) 30 phr and (d) 70 phr (magnification 5000x) [17]

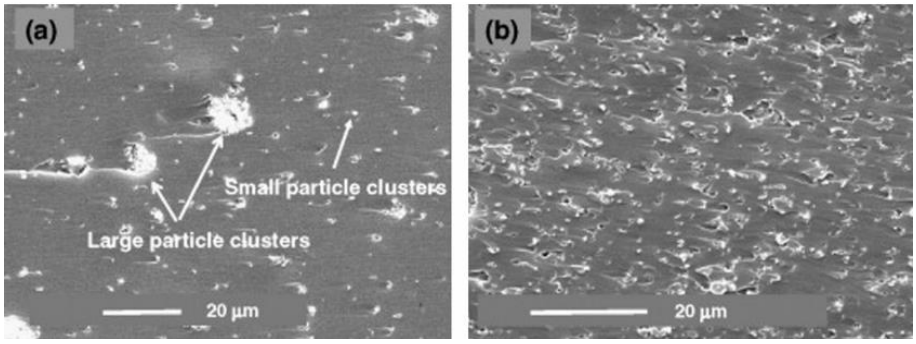

Fig. 15. Distribution of HNTs in HNTs–epoxy composites (10 wt.% HNTs) prepared by: (a) mechanical mixing and (b) ball milling homogenization [18, 19]

Works [18] and [19] describe SEM images depicting the decomposition of halloysite nanotubes in epoxy nanocomposites using two different homogenization methods (Fig. 15). The authors proved the superiority of ball milling over mechanical mixing homogenization. When the latter method was used, SEM images showed nanotube agglomerates of considerable size.

6. Conclusion

We may assume that the presence of agglomerates during the halloysite nanotubes manufacturing of nanocomposites is not unusual. Many papers describe the presence of such nanotube clusters reaching even several dozen micrometres in size and still define the dispersing level as good.

On the basis of the conducted microscope observations it is not possible to state clearly how compatibilizer influences the correctness of nanotubes distribution in polyethylene matrix. In specimens with compatibilizer and in those without its addition, agglomerates of nanotubes appeared and they were of considerable sizes in relation to the sizes quoted by the producer. The degree of homogenization of the obtained polymer material is not high. Also the adhesion of nanotubes to polymer surface is poor but this statement requires an additional research to be confirmed.

Acknowledgements

This project has received funding from the European Union's Horizon 2020 research and innovation programme under the Marie Skłodowska-Curie grant agreement No 734205 – H2020-MSCA-RISE-2017.

References

[1] Olejnik M.: Nanokompozyty polimerowe – rola nanododatków. Techniczne Wyroby Włókiennicze, 16, 3/4, 2008, 25-31.

[2] Abdullayev E., Lvov Y.: Halloysite clay nanotubes as a ceramic „skeleton" for functional biopolymer composites with sustained drug release. Journal of Materials Chemistry B, 23, 2013, DOI: 10.1039/c3tb20059k

[3] Kacperski M.: Nanokompozyty polimerowe. Kompozyty (Composites), 3, 7, 2003, 225-232.

[4] Malina D., Sobczak-Kupiec A., Wzorek Z.: Nanobiotechnologia – dziś i jutro. Chemik, 65, 10, 2011, 1027-1034.

[5] Stix G.: Małe jest wielkie. Świat Nauki, 11, 2001, 24.

[6] Wierzbicka E., Legocka I., Wardzińska-Jarmulska E., Szczepaniak B., Krzyżewski M.: Funkcjonalizowany nanonapełniacz polimerów – otrzymywanie, charakterystyka i zastosowanie. Polimery, 61, 10, 2016, 670-676.

[7] Liu M., Guo B., Du M.: Properties of halloysite nanotube-epoxy resin hybrids and the interfacial reactions in the systems. Nanotechnology, 45, 18, 2007, 1-9.

[8] Vahedi V., Pasbakhsh P.: Instrumented impact properties and fracture behaviour of epoxy/modified halloysite nanocomposites. Polymer Testing, 39, 100, 2014, 101-114.

[9] Saharudin M. S., Wei J., Shyka I., Inam F.: Biodegradation of halloysite nanotubes-polyester nanocomposites exposed to short term seawater immersion. Polymers, 9, 8, 2017, doi:10.3390/polym9080314.
[10] Kelar K., Olejniczak J., Mencel K.: Modyfikacja poliamidu 6 haloizytowymi nanorurkami. Polimery, 58, 1, 2013, 18-23.
[11] Kelar K., Mencel K.: Wpływ obróbki cieplnej na strukturę i właściwości nanokompozytów poliamid 6/nanorurki haloizytowi. Przetwórstwo Tworzyw, 5, 2014, 405-409.
[12] Olejniczak J., Szostak M.: Struktura i właściwości PA6 modyfikowanego haloizytowymi nanorurkami. Przetwórstwo tworzyw, 4, 2016, 321-330.
[13] Li C., Liu J., Qu X., Yang Z.: A general synthesis approach toward halloysite-based composite nanotubes. Applied Polymer Science, 112, 5, 2009, 2647-2655.
[14] Ye Y., Chen H., Wu J., Ye L.: High impast stength epoxy nanocomposites with natural nanotubes. Polymer, 48, 2007, 6426-6433.
[15] Królikowski W., Rosłaniec Z.: Nanokompozyty polimerowe. Kompozty (Composites), 4, 9, 2004, 3-16.
[16] Chen Y., Geever L., Higginbotham C., Killion J., Lyons S., Devine D.: Reinforced polylactic acid for use in high-strength biodegradable medical implants. Plastic Research Online, 2016, DOI: 10.2417/spepro.006218
[17] Ismail H., Pasbakhsh P., Ahmad Fauzi M. N., Abu Bakar A.: Morphological, thermal, and ten sile properties of halloysite nanotubes filled ethylene propylene diene monomer (EPDM) nanocomposites. Polymer Testing, 27, 2008, 841-850.
[18] Liu M., Jia Z., Jia D., Zhou C.: Recent advance In research on halloysite nanotubes – polimer nanocomposite. Progress In Polymer Science, 39, 2014, 1498-1525.
[19] Deng S., Zhang J., Ye L.: Halloysite-epoxy nanocomposites with improved particle dispersion through ball mill homogenisation and chemical treatment. Composite Science and Technology, 69, 2009, 2497-2505.

Ivan Gajdoš[5], Emil Spišák[5], František Greškovič[5], Janusz Sikora[6]

CALCULATION OF LONG FIBERS BREAKING AND DISTRIBUTION IN INJECTION MOLDED PARTS WITH CAE ANALYSIS

Abstract: *As the technology of digital prototyping becomes more sophisticated, demand on accurate results of fibers breaking and fibers distribution in molding rises. To solve this task several predictions models are implemented in CAE software Autodesk Simulation Moldflow insight (ASMI). This paper describes adopted models within ASMI and introduces some other experimental techniques for validation of fiber distribution.*
Keywords: *injection molding, CAE, fibers distribution, composites*

Introduction

Use of fiber reinforced thermoplastics composites has significantly increased in recent years in the automotive, aviation and space industry due to the requirement of weight reduction. Weight reduction in means of transport is desirable from economic and ecological point of view.

Long fiber-reinforced thermoplastic (LFRT) composites have become wide used lightweight automotive materials since they satisfy safety and durability requirements at low cost. The configuration of the reinforcing fibers, including fiber orientation, fiber length, and fiber concentration, ultimately affects the mechanical performance of the finished part [1]. Ability to accurately predict fiber orientation is essential for accurately determining mechanical properties and dimensional stability of LFRT products.

As the mechanical and thermal properties of LFRT products are strongly dependent on fiber orientation and distribution, prediction of the fiber orientation is drawing more and more attention in CAE. The fiber orientation distribution is important for building microstructure models of composite strength [2,3], warpage and shrinkage, thermal conductivity [4], etc. Prediction of fiber orientation is quite difficult for parts manufactured by injection molding made from long fiber reinforced polymer because the fibers are able to bend during the processing [5]. The fiber orientation in injection molded parts is affected by the shear and extensional flows during processing, leading to the creation of a layered structure. Some studies showed that the layered structure plays an significant role in the mechanical behavior of the composites [4, 5].

[5)] *Technical University of Košice, Mäsiarska 74,040-01 Košice, Slovak Republic, e-mail: ivan.gajdos@tuke.sk, emil.spisak@tuke.sk, frantisek.greskovic@tuke.sk*
[6)] *Faculty of Mechanical Engineering, Department of Technology and Processing of Polymer in Lublin, Nadbystrzycka 36 st., 20-618 Lublin, Poland*

During past recent decades, many researchers [6,7] have used destructive ways of characterizing fiber orientation. Usually, the molding was cut and polished in order to take a microphotograph of the ellipse mark of the fibers left on the cross section, which was used for image analysis. Such technique is still being used by many researchers because of its simplicity and low cost. I case of short fibers, each ellipse mark indicates one single fiber because the fiber is straight in the composite. On the other hand, a single elliptical mark cannot be used to describe the direction of a long fiber because the fiber leaves different sizes of ellipse in the cross section at different locations due to its bending in the matrix. In 1995, H. Yaguchi etc. [8] proposed a non-destructive method based on soft X-ray photographs for short fibers. The fibers and matrix were distinguished by the gray value of the pixels in the image. On the boundary between the fiber and matrix, the pixels would have different gray value than the adjacent one. However, this method provided the fiber orientation information on the projection plane only.

As computer technology continues to advance, X-ray computed tomography (X-ray CT) is proposed, which is based on a series of radiographic projections taken at varying angles [9]. It provides an increasingly practical solution to characterize fiber orientation. Using X-rays as a penetrating probe, this technology affords detailed microstructure information from almost any material (Fig.1). Also, the technique eliminates tedious sample preparation and associated artifacts.

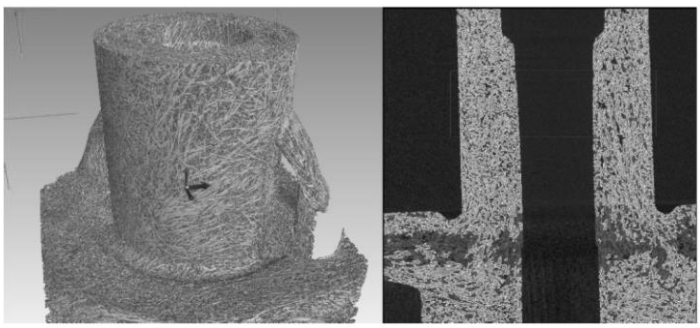

Fig. 1. CT scan of injection molded part with orientation of glass fibers

2. Theoretical Background

Most experiments carried out on injected molded parts show two skin layers with preferential orientation parallel to the flow direction and a core region with orientation perpendicular to the flow and in the plane of the part [10]. It is known that in a pure shear flow, fibers orient mainly in the flow direction, whereas in extensional flows, they orient in the direction of extension. Injection molded parts have usually constant thickness, which is much lower than the other dimensions.

Therefore, shear deformations are dominant, and this explains the skin layers. A divergent flow is responsible for the core layer. This happens at the gate that is at the junction between the feeding channel and the cavity itself, whose cross-section is larger than that of the channel. Prediction of fiber orientation and fiber breakage during injection molding is an important challenge. Local anisotropic mechanical properties can be deduced, improving structural computation precision for part design.

Fiber orientation prediction involves determining the spatial distribution of fibers, for each element and as a function of location through the part thickness.

While injection molded fiber-reinforced thermoplastics constitute a major commercial application of short fiber composite materials, the modeling of the process is more complex than in other applications as parts are usually thin and shorter fibers are often used. Other aspects such as the three-dimensional orientation of the fibers and the significant orientation variations across the part also contribute to the complexity of the problem.

During the filling of an injection molding die, three flow regions normally exist (Fig.2). These regions are: 3D region near the gate (Region A), lubrication region (Region B), where no significant velocities out of the main flow plane exist and where the majority of the flow is contained and fountain flow region at the flow front (Region C).

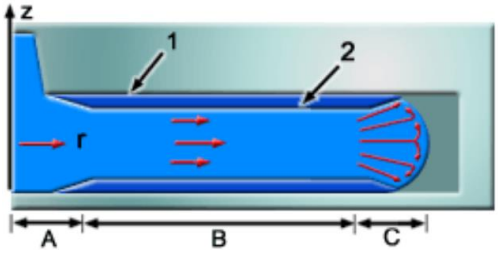

Fig. 2. Flow regions during filling. (1) Mold wall; (2) Frozen layer

During molding, the fiber orientation at a position is controlled by the fluid motion in two different ways:

- Flow-deduced orientation (a kinematic term)
- Flow-convected orientation (an advection term)

When modeling this, the accuracies of these separate terms depend on the accuracy of the determined velocity gradient and orientation gradient respectively. The effect of flow behavior on fiber orientation is complex, but two rules of thumb have been demonstrated (Fig.3):

- Shearing flows tend to align fibers in the direction of flow.

- Stretching flows tend to align fibers in the direction of stretching. For a center-gated disk, the stretching axis is perpendicular to the radial flow direction

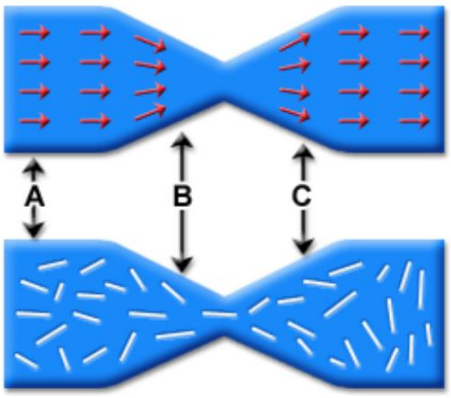

Fig. 3. Effect of stretching flows on fiber alignment. A = Entrance: Random fibers, B = Converging flow: Flow aligned fibers, C = Diverging flow: Transverse alignment

It has been found that the orientation of fibers in injection molded composites is layered, with a core created by in-plane fiber motion during mold filling. For a radial flow case (as in a center-gated disk), there is an in-plane stretching flow and the core layer contains fibers aligned in the stretching direction. For a case where no stretching applies, as for a strip mold, the orientation set by the flow at the gate is simply convected down the flow length with little change, giving:

- Shell layers on either side of the core, with a flow aligned orientation caused by gapwise shearing.
- Skin layers at the mold surface: when thick frozen layers form during filling, orientation is set by the fountain flow, at a value between that of the core and shell layers.

The number, thickness and type of layers depending on the location in the part and the part geometry. In addition to the above, it is observed that:

- Processing conditions and material behavior do affect the orientation.
- The filling speed is the process parameter that most influences fiber orientation. Faster injection speeds cause thicker core layers and thinner skin layers.
- The fiber average aspect ratio and concentration also influence the fiber orientation. With increased fiber aspect ratio and concentration, the flow-aligned orientation in the shell layer increases.

There are three factors which must be considered by the analysis program for a fiber-filled material. They are:

- The general fluid dynamics of the molten polymer.

- The effects of the molten polymer on the fibers.
- The inter-fiber interactions.

The general fluid dynamics of the molten polymer is dealt with using Autodesk Simulation Moldflow's regular Fill+Pack analysis algorithm, but the effects of the molten polymer on the fibers and the interaction of the fibers requires the use of an equation of motion for rigid particles in a fluid suspension.

3. Numerical models for prediction of fiber orientation

Numerical prediction of three-dimensional fiber orientation during mold filling is based on an equation of motion for rigid particles in a fluid suspension. The analysis consists of two identifiable terms:

- The hydrodynamic term.
- The interaction term.

The hydrodynamic influence on particle motion is described by Jeffery's equation assuming infinite aspect ratio. This theory strictly applies to dilute suspensions but has been shown to provide useful qualitative agreement with experimental data.

The interaction term has been proposed by Folgar and Tucker and is incorporated to model the randomizing effect of mechanical interactions between fibers. It has the form of a diffusion term with the frequency of interaction being proportional to the magnitude of the strain rate. The effect of the interaction term is to reduce highly aligned orientation states predicted by Jeffery's model for some flow conditions, providing improved agreement with experimental observations [11].

4. Definition and prediction of fiber orientation

Calculation of three dimensional fiber orientations is performed concurrent with the mold filling analysis on the same finite element mesh. Each triangular element may be considered as consisting of several layers subdividing the local molding thickness. Each layer is identified by the grid point through which it passes. The midplane of the molding passes through grid point 1. An orientation solution is calculated at each layer for each element in the mesh. In this way it is possible to observe the variation in orientation distribution on a set of planes parallel to the mold surface through the cross-section of the molding. The three-dimensional orientation solution for each element is described by a second order tensor. The three-dimensional orientation solution for each element is described by a second order tensor. The fiber orientation tensor is derived from the concept of fiber angle probability distribution, as shown in Figure 4, and the orientation average, of a single fiber unit vector’s component products.

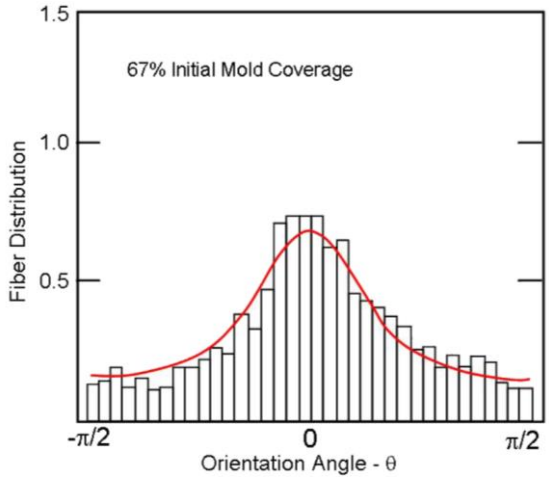

Fig. 4. Schematic view of fiber angle distribution [13]

For graphical representation, the fiber orientation tensor in any coordinate system can be described with its nine components in the coordinate system (tensor A of Figure 5), or by its eigenvalues (λ_1, λ_2 and λ_3 (Tensor B of Figure 4) in a coordinate system described by its eigenvectors e1, e2, e3 (Tensor C in Figure 4). The eigenvectors indicate the principal directions of fiber orientation and the eigenvalues give the statistical proportions (0 to 1) of fibers aligned with respect to those directions. This information is used to define an orientation ellipsoid which fully describes the probability distribution of fibers for any location and / or time of interest. A general orientation ellipsoid is also shown in Figure 4.

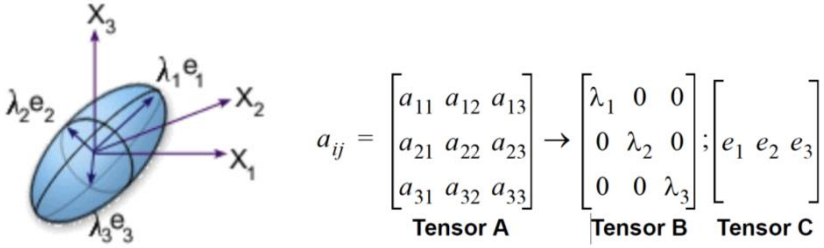

Fig. 5. Orientation ellipsoid and second order tensor for fiber orientation calculation

For display purposes, this 3D ellipsoid is projected onto the plane of each element to produce a plane ellipse. This creates a useful representation of orientation distribution, since the gapwise orientation components eliminated by projection are usually small. In this representation a near random distribution is

displayed as an ellipse tending to a circle while, for a highly aligned distribution, the ellipse degenerates to a line.

The second order orientation tensor a_{ij} provides an efficient description of fiber orientation in injection moldings. The tensor has nine components, with the suffixes for the tensor terms being:

- In the flow direction.
- Transverse to the flow direction.
- In the thickness direction.

Typically these axes apply:

- The X-Y (or 1-2) flow plane.
- The Z-axis in the thickness direction, out of the 1-2 flow plane.

The original nine components reduce to five independent components, due to:

- Tensor symmetry $a_{ij} = a_{ij}$ and
- A normalization condition $a_{11}+a_{22}+a_{33}=1$

These three major orientation components have been included in the orientation considerations:

- a_{11} fiber orientation in the flow direction, varying from 0 to 1.0.
- a_{22} fiber orientation transverse to flow, varying from 0 to 1.0.
- a_{33} tilt of orientation in the 1-3 plane, varying from -0.5 to 0.5.

A composite material of interest may be considered as particles or fibers suspended within a viscous medium. There may be mechanical and/or hydrodynamic interactions between the fibers. The suspension may be dilute, semi-concentrated or concentrated, as discussed below:

- A dilute suspension is one in which the fibers are never close to one another and do not interact.
- A semi-concentrated suspension would have no mechanical contact between the fibers, but the hydrodynamic interactions become significant.
- In a concentrated suspension, the fiber orientation behavior becomes very complex, since both mechanical and hydrodynamic fiber interactions apply.

Jeffery first modeled the motion of a single fiber immersed in a large body of incompressible Newtonian fluid. Jeffery's model applies only to suspensions that are so dilute that any inter-fiber interactions (even hydrodynamic interactions) are negligible.

An important measure for assessing suspension concentration is the average distance between the fibers. Considering fibers of diameter (d) and length (L), with an aspect ratio (L/d), a fiber concentration by volume (c) (or volume fraction

V_f) and having a uniform length distribution, a typical concentration classification scale is:

- Dilute $c<<(d/L)^2$
- Semi-concentrated $(d/L)^2<c<(d/L)$
- Concentrated $c > (d/L)$

Most commercial composites contain 10% to 50% fibers by weight, which can be regarded as being concentrated suspensions. For semi-concentrated suspensions, a model has been proposed by Dinh and Armstrong. The orientation of the fiber follows the bulk deformation of the fluid with the exception that the particle cannot stretch.

For concentrated suspensions, a term, called "the interaction coefficient" (or C_I), has been incorporated in the phenomenological model for fiber orientation proposed by Folgar and Tucker:

- Interactions among fibers tend to randomize the orientation.
- The term takes the same form as a diffusion term and since interactions only occur when the suspension is deforming, the effective diffusivity is proportional to the strain rate.
- The dimensionless C_I term determines the strength of the diffusion term.

Adding the rotary diffusion term to account for the fiber interactions has been found to improve the orientation predictions, since Jeffery's equation alone does not give qualitatively accurate predictions for fiber orientation. Until now, the Folgar-Tucker model has been the best available for fiber orientation modeling in concentrated suspensions. The model has been given in this form by Advani and Tucker:

$$\frac{\delta a_{ij}}{\delta t} + v_k \frac{\delta a_{ij}}{\delta x_k} = -\frac{1}{2}\left(w_{ik}a_{kj} - a_{ik}w_{kj}\right) + \frac{1}{2}\lambda\left(\gamma_{ik}a_{kj} + a_{ik}\gamma_{kj} - 2\gamma_{kl}a_{ijkl}\right) + 2C_1\gamma\left(\delta_{ij} - \alpha a_{ij}\right) \quad (1)$$

Where:

- α equals 3 for 3D and 2 for planar (2D) orientation
- v_k is the velocity component
- $1/2\omega_{ij}$ is the vorticity tensor and $1/2\gamma_{ij}$ is the deformation rate tensor
- λ is a constant that depends on the geometry of the particle
- δ_{ij} is a unit tensor
- C_I is the interaction coefficient

Fiber orientation model closure

The tensor form of the fiber orientation model from Advani and Tucker is not yet a suitable derivative for a second order orientation tensor, because it contains the fourth order tensor a_{ijkl}.

The derivative for a fourth order tensor contains a sixth order orientation tensor and so on. The only way to develop a suitable derivative is to approximate the fourth order tensor in terms of a second order tensor.
This approximation is called a "closure approximation". Various approximations have been tested by Advani and Tucker. However, the presence of the approximation itself may introduce some error into the simulation results. So the closure approximation is the most challenging problem associated with this model. No value of C_I can make the fiber orientation model expression fit all the orientation model components.

Examination of the Advani and Tucker fiber orientation model form indicates two ways to control the fiber orientation prediction accuracy:

- Find a more accurate closure.
- Find a new interaction model that considers the closure error.

While the first method would be preferred, no closure has been found to satisfactorily cover the range of shearing and stretching flows for a multi-decade range of C_I.

The effect of the closure approximation is to predict too much out-of-plane orientation. This result has been addressed by the fiber orientation model form proposed by Autodesk.

5. Fiber breakage model for long-fiber composites

The option to calculate fiber breakage when performing a fiber orientation analysis using a long-fiber composite material has been implemented. The fiber breakage model implemented was first proposed by Phelps and Tucker [12] as a statistical model which describes the probability of a fiber breaking due to buckling and shearing forces in a flow field. For a single fiber, the probability of breaking under the hydrodynamic forces can be expressed as:

$$P_i = C_b \dot{\gamma} max\left\{0, \left[1 - exp\left(1 - \frac{F_i}{F_{crit}}\right)\right]\right\} \tag{2}$$

$$\frac{F_i}{F_{crit}} = \frac{8\xi\eta_m\Gamma_i^4}{\pi^3 E_f d_f^4}\left(-\hat{D}:\hat{A}\right) \tag{3}$$

where $\hat{D}$ and $\hat{A}$ are the deformation rate tensor and fiber orientation tensor, respectively. Other variables are the properties of the fiber and matrix, except for ξ which is the drag factor.
The fibers, broken or not, have to follow a conservation law because they cannot disappear nor can they grow in a flow field. This conservation law can be expressed as:

$$\frac{dN(l,t)}{dt} = -P(l)N(l,t) + \int_l^L R(l,l')N(l,t')dl' \tag{4}$$

where L is the initial fiber length, $N(l,t)$ is number of fibers with length l at time t, $P(l)$is the scalar probability function of fiber length l, and $R(l,l')$ is the probability function of fiber length l breaking to form a fiber of length l' (where $l'<l$). It can be expressed as a Gaussian breakage profile, such as:

$$R(l,\acute{l}) = G_{norm}(l,\frac{\acute{l}}{2},S\acute{l}) \quad (5)$$

Where $G_{norm}(l,\frac{\acute{l}}{2},S\acute{l})$ is the Gaussian normal probability density function for the variable l with mean $l'/2$ and standard deviation Sl'. S is a dimensionless fitting parameter that can be used to control the shape of the Gaussian breakage profile.

6. Conclusion

As the concept of digital prototyping is becoming more widespread in area of production of injection molded parts, CAE analysis with fiber orientation prediction becomes important. Accurate prediction of fiber orientation, length and space distribution allows to gain precise information for calculation of molding shrinkage and warpage. Furthermore all those data can be exported and used in structural analysis. Fibers in moldings cause not heterogeneous mechanical properties in polymer and mapping those non-heterogeneous properties in structural analysis dramatically improves accuracy of results.

Acknowledgements

This project has received funding from the European Union's Horizon 2020 research and innovation programme under the Marie Skłodowska-Curie grant agreement No 734205 – H2020-MSCA-RISE-2017.

References

[1] Goris S, Osswald TA. Progress on the characterization of the process-induced fiber microstructure of long glass fiber-reinforced thermoplastics. In: SPE ACCE conference, technical papers, Michigan, USA; 7 September 2016.

[2] P. Shokri, N. Bhatnagar, Effect of packing pressure on fiber orientation in injection molding of ber-reinforced thermoplastics, Polymer Composites 28 (2) (2007) 214-223.

[3] S. Fu, B. Lauke, Effects of fiber length and fiber orientation dis- tributions on the tensile strength of short-fiber-reinforced poly- mers, Composites Science and Technology 56 (10) (1996) 1179-1190.

[4] A. Bernasconi, F. Cosmi, D. Dreossi, Local anisotropy analysis of in- jection mouldedfibre reinforced polymer composite, Composites Science and Technology 68 (12) (2008) 2574-2581.
[5] K. Ortman, D. Baird, P. Wapperom, A. Aning, Prediction of fiber orientation in the injection molding of long fiber suspensions, Polymer Composites 33 (8) (2012) 1360-1367.
[6] A. Bernasconi, F. Cosmi, D. Dreossi, Local anisotropy analysis of injection mouldedfibre reinforced polymer composite, Composites Science and Technology 68 (12) (2008) 2574-2581.
[7] R.S. Bay, C.L. Tucker III, Fiber orientation in simple injection moldings. Part I. Theory and numerical methods, Polymer Composites 13 (4) (1992) 317-331.
[8] H. Yaguchi, H. Hojo, D.G. Lee, E.G. Kim, Measurement of planar orientation of fibers for reinforced thermoplastics using image processing, International Polymer Processing 10 (3) (1995) 262-269.
[9] H. Shen, S. Nutt, D. Hull, Direct observation and measurement of fiber architecture in short fiber-polymer composite foam through Micro-CT imaging, Composites Science and Technology 64 (13-14) (2004) 2113-2120.
[10] Papathanasiou TD. Flow-induced alignment in injection molding of fiber-reinforced polymer composites. In: Papathanasiou TD, Guell DC, editors. Flow-induced alignment in composite materials. Cambridge: Woodhead Publishing Ltd; 1997. p. 113–65.
[11] Autodesk Moldflow Insight Performance THEORY & CONCEPTS FOR RELEASE 2010.
[12] Phelps, J.H., Processing-microstructure Models for Short- and Long-fiber Thermoplastic Composites. Ph.D. thesis, University of Illinois at Urbana-Champaign (2009).
[13] Advani, S.G., “Prediction of Fiber Orientation During Processing of Short Fiber Composites”, Ph.D. thesis, University of Illinois, Urbarna, IL (1987).

Andrzej Stasiek[1], Aneta Raszkowska-Kaczor[1], Marcin Bogucki[2]

CO-ROTATING TWIN SCREW EXTRUSION POLYPROPYLENE/TALC COMPOSITION

Abstract: *Literature analysis regarding to the twin-screw extrsion of polymer materials was carried out. Research of influence: angle of mutual position of cooperating cam disks, distance between cam discs from, rotational speed of screws and extrusion rate on torque on screw shafts, temperature of molten plastic in the head, were carried out. Statistical analysis of the results was obtained. The torque model is characterized by a very strong effect of interaction between the rotational speed and the distance between the cam disks. The temperature model of the material is characterized by a strong positive effect of rotational speed, a negative effect of curvature caused by a change in the distance between the cam disks and a negative effect of the extrusion efficiency.*
Keywords*: polypropylene, talc, extrusion, Response Surface Methodology, co-rotating twin screw extrusion*

1. Introduction

Polypropylene is a polymer belonging to the group of polyolefins [1]. Polypropylene, next to polyethylene, is one of the most commonly used materials [1]. Its application is found in many industry sectors, including automotive, toy and packaging. It is processed by injection, thermoforming, casting and extrusion [1]. Polypropylene is a partially crystalline material (the degree of crystallinity reaches up to 70%), it is characterized by higher stiffness and higher melting temperature [1]. It creates spiral chains that have a low tendency to cross each other. This mutual looping is responsible for the high strength of the alloy and therefore the polypropylene is characterized by low viscosity shear and deformation. There are three polypropylene structures: isotactic, syndiotactic and atactic [1]. The development of production techniques requires the use of modern construction materials. As a result, considerable interest in thermoplastic composites has been observed in recent years. Polymer composites are obtained as a result of physical modification, i.e. by adding to the polymer a suitable filler. Fillers are supplied in order to modify some properties of polymer materials, in particular their physical properties, as well as to lower the price of the product [2].

[1)] *Instytut IMPiB, Odział Przetwórstwa Materiałów Polimerowych w Toruniu, ul. M. Skłodowskiej Curie 55, 87-100 Toruń, Poland*
aneta.raszkowska-kaczor@impib.pl; a.stasiek@impib.pl
[2)] *Politechnika Lubelska, Katedra Automatyzacji, ul. Nadbystrzycka 38D, 20-618 Lublin, Poland, m.bogucki@pollub.pl*

The use of mineral fillers generally changes the following polymer properties: increase in density, increase in Young's modulus, increase or decrease in impact resistance [2].

The fillers are added to the polymeric materials already produced or during their processing [2]. Powder fillers are used primarily to improve selected mechanical, electrical, thermal, chemical, processing properties and to lower the price of the product [2].

Powder fillers are divided into inorganic and organic. Inorganic fillers include powders of metals or their alloys, glass, powders of aluminum, titanium, zinc, magnesium, potassium carbonates, barium and calcium, as well as powders of silicates, kaolin, mica talc [2].

For the production of materials with a high degree of filling (20-70% by weight), mainly co-rotating twin screw extruders are applied, which have a segmental structure of the plasticizing system. Such a structure allows to configure the system depending on the technological requirements of the process. For this purpose, segments are used: transporting, kneading, mixing gears [3].

The problem faced by plastics processing engineering is to determine whether the structural change of the machine part or the change in the level of control variables (ie extrusion conditions) will result in a desired beneficial effect in the form of eg increasing efficiency, reducing energy consumption or improving the properties of the processed material [4].

An effective way to solve the presented problems are experimental techniques, which are represented under the common term, namely Response Surface Methodology (RSM) [4]. The RSM is a complex, sequential research process that takes an advantage of achievements of the theory of experimental design [4].

The aim of the research is to determine the qualitative or quantitative dependence that expresses the relationship between the set of independent factors and an outcome variable [4].

The Response Surface Methodology is a type of research procedure according to which information obtained in first/previous experimental step are analyzed and then used to desing of the next sequence of experiments [4]. Doing so, an investigator has more and more accurate and conscious insight into the nature of the phenomenon under study. It is worth adding that the RSM is primarily used as a way of process and product optimization [4].

In the first phase of research, the problem is formulated and it is determined which of the factors affecting the studied process contribute to the variability of the outcome factor [4]. The next step of work is selection of the appropriate experimental program. This stage is very important, because when choosing a specific experimental design, it also decides on the accuracy of the approximation of the unknown response surface [4]. Then, realization of previous result takes place, this is, reconstructing the experimental design and measuring (or estimating) of outcome responses [4]. Having measurement results, the equation

of the examined response surface is determined, followed by the error discussion and statistical analysis of experimental results [4].

Co-rotating twin screw extrusion of the modified polypropylene is carried out at high shear rate of the polymer material. During this process degradation of the polymer material may occur [5]

Factors that influence the degree of material degradation include: local temperature values and its distribution along the plasticizing system, strain intensity in the plasticizing system, residence time in the plasticizing system [5]. Intensity of the above factors on the polymer material degradation depend on the construction of the plasticizing system and process conditions applied [5].

In order to reduce the shear rate in the plasticizing system, it uses modified kneading segments with bevelled cam discs, with decreasing cam disc, with reduced height of some cam disc ridges, with different angles between symmetry axes of cam disks, with increased distance between disks [5].

Co-rotating twin screw extruders are characterized by high mixing efficiency due to the high rotational screws speed and thus significant deformation of the material [6].

The modern screws are equipped in co-rotating systems based on the construction concept patented by Erdmenger [7]. The transport of polymer material in co-rotating twin screw extruders is induced, similarly as in single screw extruders, as a result of trailing flow assisted by the deflation of the back pressure flow [7].

2. Materials for research

Polypropylene Moplen EP 440G (produced by Basell Orlen, Płock) was used for the implementation of the tests, the characteristics of which are given in Table 1 [7].

To modify the polypropylene as a filler, Talc (symbol M15 (produced by Mondo Minerals) was supplied and mixed (density 2.75 g/cm3, bulk density 0.3 g /cm^3, hardness 1 according to the Mohs scale, form factor 5-100) [7, 9].
The properties of the polypropylene granules used are presented in Table 1.

Table 1. Characteristics of the polypropylene used [8]

Properties	Units	The values
Melt Flow Rate MFR (2.16, 190^{0}C)	g/10min	1.3
The tensile strength of σ_y	MPa	27
Relative elongation at yield point ε	%	8
Charpy notched impast	kJ/m^2	40
Softening temperature in (Vicata load 1kg)	^{0}C	150

3. Research plan

In carrying out the research work, the following plan was adopted:

- selection of the right research plan for the development of experimental models describing the variability of the properties of composites as a function of selected factors studied;
- basic research of the co-rotating process of twin screw extrusion of modified polypropylene: measurement of torque on screw shafts, temperature measurement of molten plastic in the head;
- determination of empirical models,
- summary and conclusions [5].

The operational range of input quantities were chosen as follow:
A - angle of mutual position of cooperating cam disks from -90º to 90º,
B - distance between cam discs from 0.5 to 4.5 mm,
n - rotational speed of screws from 420 to 660 min^{-1},
W - extrusion rate from 5 to 6 kg/h.

The efficiency of the co-rotating twin-screw extrusion process was controlled using gravimetric feeders. The extrusion process was run with incomplete filling of the screw channels [5].

This plan was chosen for the implementation of the above work for two reasons: it is preferred to the implementation of experiments in the field of machine technology and enabled the implementation of research in the accepted range of variability of input quantities [5].

In Table 2 levels of variability of independent variables used in the experiment is presented.

Table 2. Levels of variability of independent variables [5]

Factors	-α = -2	-1	0	1	α = +2
A	-90^0	-45º	0^0	45º	90º
B	0.5	1.5	2.5	3.5	4.5
n	420	480	540	600	660
W	5	5.25	5.5	5.75	6

Table 3. Experimental design expressed in terms of coded variables

Mark samples	A	B	n	W
P1	+1	-1	-1	-1
P2	-1	+1	-1	-1
P3	-1	-1	+1	-1

P4	+1	+1	+1	-1
P5	+1	-1	-1	+1
P6	-1	+1	-1	+1
P7	-1	-1	+1	+1
P8	+1	+1	+1	+1
P9	-2	0	0	0
P10	+2	0	0	0
P11	0	-2	0	0
P12	0	+2	0	0
P13	0	0	-2	0
P14	0	0	+2	0
P15	0	0	0	-2
P16	0	0	0	+2
P17	0	0	0	0

Table 4. Experimental design expressed in the natural units of measurements

Mark samples	A	B	n	W
P97	+45	1.5	480	5.25
P98	-45	3.5	480	5.25
P99	-45	1.5	600	5.25
P100	+45	3.5	600	5.25
P101	+45	1.5	480	5.75
P102	-45	3.5	480	5.75
P103	-45	1.5	600	5.75
P104	+45	3.5	600	5.75
P105	-90	2.5	540	5.5
P106	+90	2.5	540	5.5

P107	0	0.5	540	5.5
P108	0	4.5	540	5.5
P109	0	2.5	420	5.5
P110	0	2.5	660	5.5
P111	0	2.5	540	5
P112	0	2.5	540	6
P113	0	2.5	540	5.5

4. Conditions for extruding co-rotating twin screw

Polypropylene and talc composites were obtained by means of a research line equipped with co-rotating twin-screw extruder of the "BŰHLER" company, with a diameter of screws d = 20 mm and length L/d = 40 [7].

The test stand used to produce polypropylene and talc composites consisted of: gravimetric feeders, co-rotating twin screw extruder, cooling bath and granulator. In Figure 1. the configuration of screws is presented. In this configuration, the kneading research segment was installed, which is detailed shown in the Figure 2.

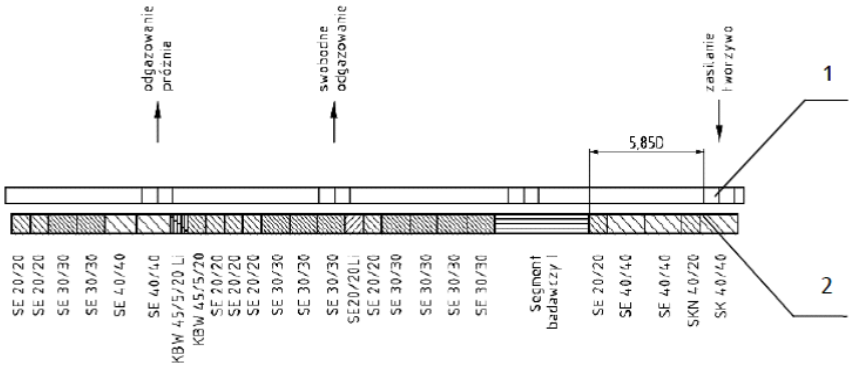

Fig. 1. The screw configuration used for the tests: 1 - cylinder, 2 - screw

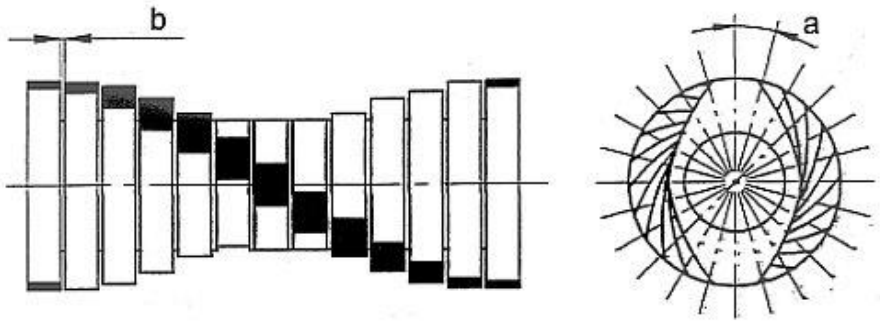

Fig. 2. The kneading research segment used in the configuration of screws

The kneading research segment used in the tests was characterized by the distance between the cam disks (b) and the mutual position of the cooperating cam disks (a). In each research segment, 13 cam disks of equal thickness were used [5].

5. Parameters of the co-rotating twin screw extruder

The extrusion process of polypropylene and talc composite was carried out with the parameters (input variables: A, B, n, W) presented in the table 4. In the process of extrusion of PP/talc composites, the temperature of all heating zones of the cylinder and head was 195ºC. The extruded polypropylene and talc composites were cooled in a cooling bath. The amount of talc filled was constant and amounted to 20% [5].

6. Test results

The results of the tests are shown in the table 5 and Table 6.

Table 5. Results of measurements of screw shaft torque

Pr.	1	2	3	4	5	6	7	8	9	10	mean
P97	18.9	18.6	18.6	18.6	18.6	18.2	18.2	18.6	18.2	18.6	18.51
P98	25.6	25.9	25.9	25.6	25.9	25.9	25.6	26.2	25.6	25.6	25.78
P99	22.7	23.0	23.0	22.7	22.7	22.4	22.7	22.4	23.0	22.7	22.73
P100	16.0	15.7	15.4	15.7	15.4	15.7	16.0	15.7	15.4	15.4	15.64
P101	19.2	18.9	19.2	18.9	19.5	18.9	19.2	19.5	18.9	19.2	19.14

P102	26.9	26.9	26.9	26.2	26.2	26.6	25.9	26.6	26.9	26.6	26.57
P103	23.4	23.0	23.4	23.7	23.7	23.7	23.4	23.4	23.4	23.7	23.48
P104	16	16	16	16	16.3	16	16	16	16	16.3	16.06
P105	23.0	23.0	23.0	23.0	23.0	23.4	23.4	22.4	23.0	23.0	23.02
P106	23.7	23.7	23.4	23.4	23.4	23.0	22.7	22.7	23.4	23.0	23.24
P107	20.8	20.8	21.8	21.4	21.8	21.8	21.4	21.4	21.8	21.4	21.44
P108	21.8	22.4	22.4	22.4	22.4	21.8	22.4	22.1	22.1	22.1	22.19
P109	24.0	24.6	24.0	24.0	24.0	24.0	23.7	24.0	23.7	23.7	23.97
P110	19.8	20.2	20.5	20.8	20.5	20.2	20.5	20.5	20.8	20.5	20.43
P111	20.8	20.5	20.8	21.4	21.1	21.4	20.5	21.1	21.1	20.8	20.95
P112	23.0	22.7	23.0	22.7	22.4	22.7	23.0	22.1	22.7	22.7	22.7
P113	22.1	22.1	21.8	21.8	21.4	21.4	21.8	21.4	21.4	21.8	21.7
P113 1	22.1	21.8	21.4	22.1	21.8	22.1	22.1	22.1	22.1	22.1	21.97
P113 2	21.8	22.1	21.8	21.4	22.1	22.1	22.1	22.1	21.4	21.8	21.87
P113 3	22.4	20.8	22.1	21.4	22.1	22.4	21.8	21.8	22.1	21.8	21.87
P113 4	21.1	21.1	20.8	20.8	21.1	20.8	21.4	20.5	21.4	21.1	21.01
P113 5	21.1	21.4	21.1	20.8	20.8	21.1	21.1	20.8	21.1	20.8	21.01

Table 6. Results of measurements of molten plastic temperature in the extrusion head

Pr.	1	2	3	4	5	6	7	8	9	10	Mean
P97	211	210	210	211	210	211	210	210	211	212	211
P98	210	210	211	212	210	209	210	210	211	210	210
P99	214	214	214	214	214	214	214	214	215	215	214
P100	217	216	217	217	218	217	217	218	218	217	217
P101	214	214	214	213	215	214	215	216	215	215	215
P102	214	215	213	214	213	213	213	214	214	214	214
P103	213	214	215	215	215	215	215	215	215	216	215
P104	220	221	221	221	222	222	221	221	221	222	221
P105	220	220	221	221	221	220	220	221	221	221	221
P106	219	218	219	220	220	220	220	220	220	220	220
P107	212	213	214	216	216	217	217	217	217	218	217
P108	215	216	217	216	217	216	217	217	217	217	217
P109	213	213	213	213	214	214	213	214	215	216	214
P110	225	225	226	226	227	228	228	228	228	228	227
P111	216	216	217	216	216	218	218	218	218	218	217
P112	222	223	223	223	223	223	224	223	224	223	223
P113	220	221	221	220	220	220	221	219	219	219	220
P113 1	219	220	220	220	220	220	221	221	221	221	220
P113 2	219	219	220	220	221	221	221	221	221	221	220

P113 3	218	217	220	219	220	220	221	221	222	222	220
P113 4	215	215	214	215	215	215	216	215	216	216	215
P113 5	215	215	216	215	216	216	215	215	215	215	215

Analysis of results

After analyzing the obtained results (Tables 5 and 6), it was found :

- the highest value of the extruder screws torque, namely 26.57 Nm were observed in the following process conditions: at the screw speed of 480 min^{-1}, the extrusion rate 5.75 kg/h, the angle of mutual position of the cooperating cam discs - 45º and the distance between the cam disks 3.5 mm.
- the lowest value of torque on the extruder screw shaft (15.64 Nm) was obtained during the extrusion process realized at a screw speed of 600 min^{-1}, an extrusion rate of 5.25 kg/h, an angle of mutual position of cooperating cam discs 45 ° and a distance between cam discs of 3.5 mm.
- the highest temperature of the molten material in the extrusion head (223 ºC) was obtained during the extrusion process carried out at the screw speed of 540 min^{-1}, extrusion rate 6 kg / h, the angle of mutual position of cooperating cam disks 0º and the distance between cam disks 2.5 mm.
- the lowest temperature value of the molten plastic in the extrusion head (210 °C) was obtained during the extrusion process realized at the screw speed of 480 min^{-1}, the extrusion rate 5.25 kg/h, the angle of mutual position of cooperating cam discs - 45º and the distance between the cam disks 3.55 mm.

7. The goal of experimental research

The aim of the experiments was to develop two empirical models describing the variability of torque observation and material temperature in extrusion head as a function of the variability of the studied factors: angle of mutual position of cooperating cam discs, distance between cam discs, speed rotational and extrusion rate.

Hartley's experimental design was adopted. Experimental design was based on fractional factorial 2^{4-1}IV design (so called kernel design) augmented with center and star design sets. The operational range of individual factors along with their corresponding symbols is summarized below.

A - angle of the mutual position of cooperating cam disks: (-90, 90), deg;
B - distance between cam discs: (0.5, 4.5) mm;
n - rotational speed of screws: (420, 660) min^{-1},
W - extrusion output: (5, 6) kg/h;

Table 7. Experimental design

System Experimental		Angle, α	Distance b, mm	Rotational speed n, min^{-1}	Extrusion output W, kg/h
1		45	1.5	480	5.25
2		-45	3.5	480	5.25
3		-45	1.5	600	5.25
4		45	3.5	600	5.25
5		45	1.5	480	5.75
6		-45	3.5	480	5.75
7		-45	1.5	600	5.75
8		45	3.5	600	5.75
17		-90	2.5	540	5.5
18		90	2.5	540	5.5
19		0	0.5	540	5.5
20		0	4.5	540	5.5
21		0	2.5	420	5.5
22		0	2.5	660	5.5
23		0	2.5	540	5
24		0	2.5	540	6
C		0	2.5	540	5.5

Experimental systems of the test program are shown in Table 7. It should be noted that as a result of the experiment, both the kernel and star design sets were not replicated. Repetitions of result measurements were made only for the center design sets. On this basis, the random variavility of the observations was estimated. This approach is often an experimental practice and is accounted for a significant reduction in research costs.

On the basis of the adopted research program and results of measurement of the output variables, empirical models in the form of a polynomial of many variables were determined, taking into account the constant, linear, two-factor and quadratic interactions terms - equation 1.

$$y = \beta_0 + \sum_{i=1}^{n} \beta_i x_i + \sum_{i=1}^{n} \beta_{ii} x_i^2 + \sum \sum_{i<j=2}^{n} \beta_{ij} x_i x_j + \varepsilon \qquad (1)$$

In the quoted equation, y denotes the resulting variable, and x with the corresponding index (i) or (j) represents the studied factor. The symbols β followed by indices indicate the coefficients of the empirical model.

The symbol ε stands for model error subject to the normal distribution N $(0, \sigma^2)$.

Statistical analysis of empirical models makes it possible to assess which of the factors studied and their corresponding linear, curvature and interaction effects have a critical influence on the variability of the examined response surface.

The results of the statistical analysis are then used to select the setting values or to optimize the extrusion process.

Based on the measurements given, corresponding to the adopted research plan, the coefficients of the terms of the regression equations of the output variables were estimated: torque and temperature of the material.

Each of the regression models was subjected to standard procedures for verifying the correctness of their construction: statistical tests of regression coefficients, analysis of the residuals of models and model adequacy checking.

Fig. 3 and Fig. 4 show the results of the residual analysis of the torque and temperature of material models, correspondingly. Each diagram presents probability-probability plots of residuals. The assumptions of the structure of empirical models require that the probability distribution of differences between the approximate values of the model and the values of measurements (the so-called model residues) are subject to normal distribution. The points on both charts accumulate around the line that determines the ideal fit of the model's residuals to the value of the normal distribution variable. Both drawings do not represent a significant deviation from the assumptions of the construction of empirical models

Tables 8 and 9 list the results of the variation analysis. The individual rows of the tables contain a statistical assessment of the contribution of individual elements of the regression equation (1).

The model terms whose contribution to model variability is comparable to the model error, this is probability level p greater than the arbitrarily adopted level of significance 0.05, were considered statistically insignificant.

Figures 5 and 6 illustrate the comprehensive results of statistical analysis in the form of Pareto analysis of the standardized effects, comparing the contributions of individual terms to the overall variability of regression models.

Each of the analyzed empirical models was characterized by a high value of the determination coefficient.

Table 8. Torque model - table of variance (the probability value of $\alpha = 0.05$ was assumed as the significance level of the test)

Model term	SS	df	MS	F	p
A(L)	0.242	1	0.2420	0.568	0.45
A(Q)	6.157	1	6.1573	14.458	0.00
(2)b(L)	2.813	1	2.8125	6.604	0.01
b(Q)	6.420	1	6.4203	15.075	0.00

(3)n(L)	62.658	1	62.6580	147.126	0.00
n(Q)	1.135	1	1.1353	2.666	0.10
(4)W(L)	23.180	1	23.1801	54.429	0.00
W, kg/h(Q)	6.228	1	6.2285	14.625	0.00
1L vs.2L	15.688	1	15.6876	36.836	0.00
1L vs.3L	1.073	1	1.0726	2.518	0.11
1L vs.4L	0.300	1	0.3001	0.705	0.40
2L vs.3L	549.452	1	549.4516	1290.155	0.00
2L vs.4L	0.036	1	0.0361	0.085	0.77
3L vs.4L	0.078	1	0.0781	0.183	0.66
Error	78.788	185	0.4259		
Total SS	1442.106	199			

Table 9. Material temperature model - table of variance (the probability value of α = 0.05 was assumed as the significance level of the test)

Model term	SS	Df	MS	F	p
A(L)	5.00	1	5.00	0.92	0.34
A(Q)	82.05	1	82.05	15.07	0.00
(2)b(L)	3.20	1	3.20	0.59	0.44
b(Q)	591.14	1	591.14	108.56	0.00
(3)n(L)	858.05	1	858.05	157.58	0.00
n(Q)	65.68	1	65.68	12.06	0.00
(4)W(L)	357.01	1	357.01	65.56	0.00
W, kg/h(Q)	82.05	1	82.05	15.07	0.00
1L vs.2L	39.01	1	39.01	7.16	0.01
1L vs.3L	28.06	1	28.06	5.15	0.02
1L vs.4L	19.01	1	19.01	3.49	0.06
2L vs.3L	97.66	1	97.66	17.93	0.00
2L vs.4L	10.51	1	10.51	1.93	0.17
3L vs.4L	9.11	1	9.11	1.67	0.20
Error	1007.38	185	5.45		
Total SS	3513.88	199			

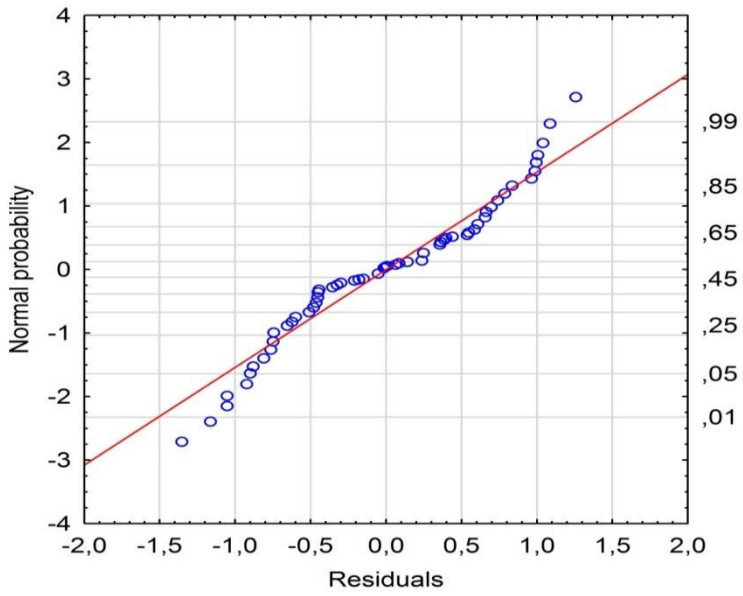

Fig. 3. Normal probability plot of residuals of the empirical model of torque

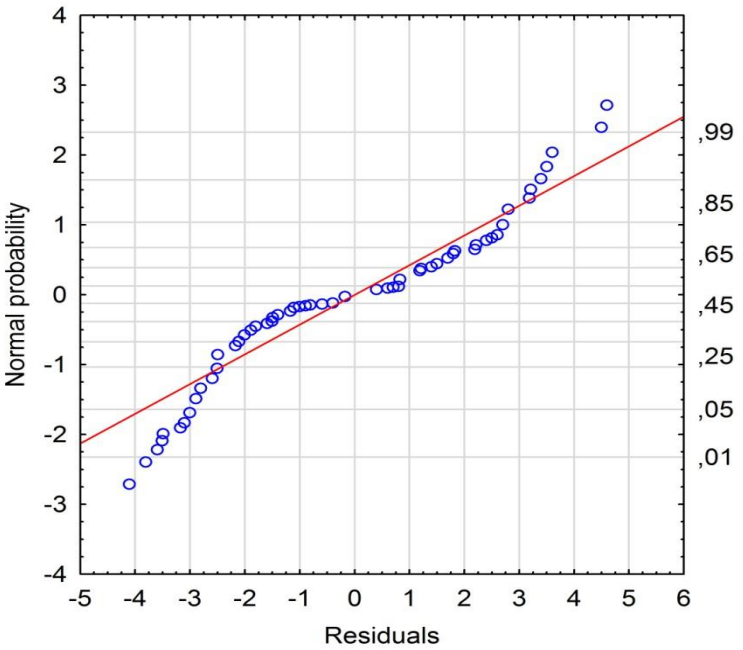

Fig. 4. Normal probability plot of residuals of the empirical model of temperature material

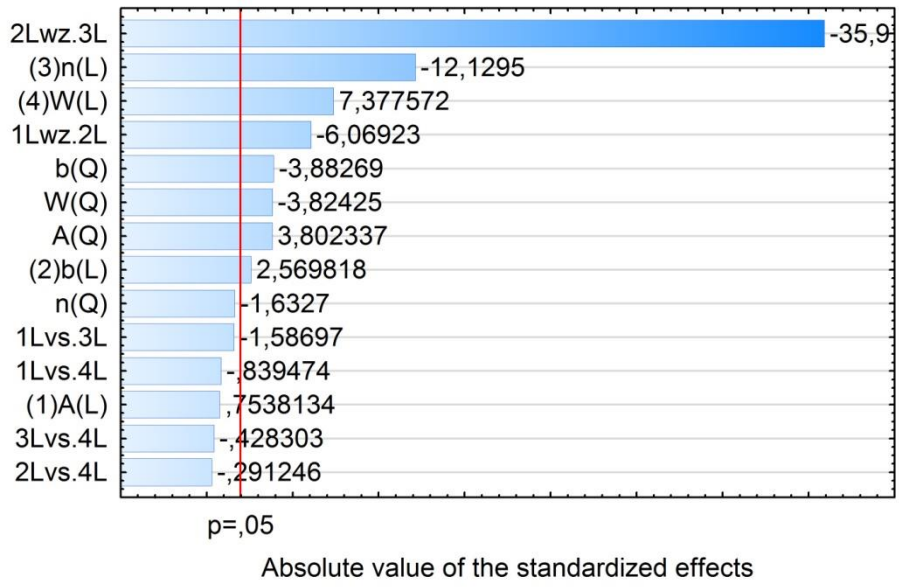

Fig. 5. Pareto analysis of the standardized effects of the torque model

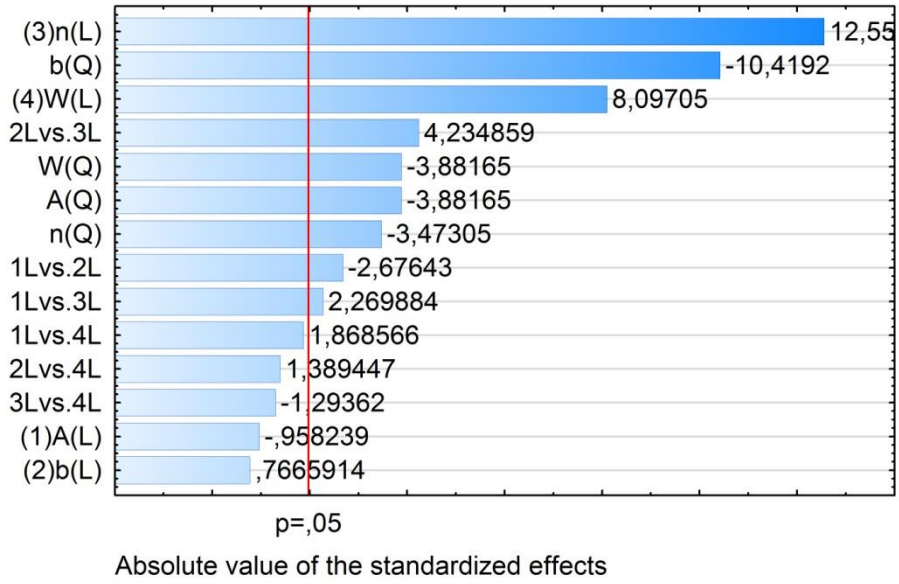

Fig. 6. Pareto analysis of the standardized effects of the material temperature model

8. The results of experimental research

The torque model is characterized by a very strong effect of interaction between the rotational speed and the distance between the cam disks. The effect of interaction between rotational speed and the distance between cam discs is also of great importance in explaining total variability (this effect is negative). Two other significant effects are the negative rotational speed effect and the positive extrusion rate effect.

Other effects of the model: the effect of curvature of rotational speed, the angle of mutual position of cooperating cam disks and the distance between cam discs, although they are statistically significant - they do not contribute much to the empirical model.

Figure 9 shows the strong effect of two-factor interactions between the rotational speed and the distance between the discs. The quoted comments are consistent with the results of the Pareto analysis of the standardized effects presented in Figure 5.

The temperature model of the material is characterized by a strong positive effect of rotational speed, a negative effect of curvature caused by a change in the distance between the cam disks and a negative effect of the extrusion efficiency.

In addition, the effect of the rotational speed influence on the temperature of the material depends on the level of variation in the distance between the disks, which is clearly shown in the 3D plot (Figure 7).

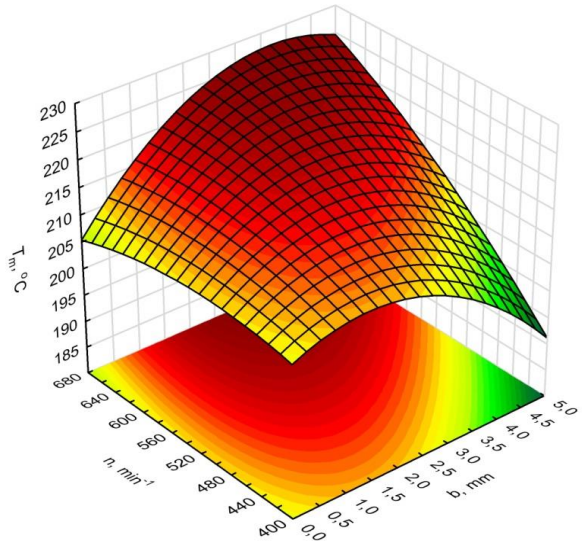

Fig. 7. Diagram of the cross section of the surface area of the temperature model response as a function of the rotational speed of the screw and the distance between the cam disks

A similar strong interaction effect is observed for two variables: extrusion rate and rotational speed – see: Figure 8.

The remaining effects, according to the analysis of variance, have a negligible contribution to the variability of the temperature model (see Pareto analysis - Figure 6).

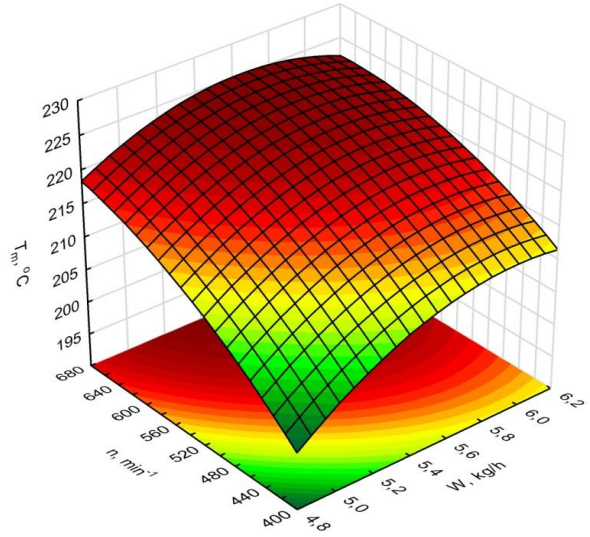

Fig. 8. Diagram of the cross-section of the surface of the temperature model response as a function of the extrusion efficiency and rotational speed of the screw

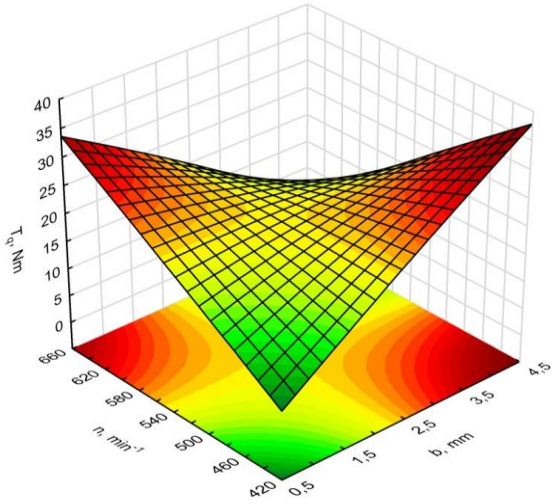

Fig. 9. Diagram of the cross-section of the surface of the torque model response as a function of the rotational speed of the screw and the distance between the cam disks

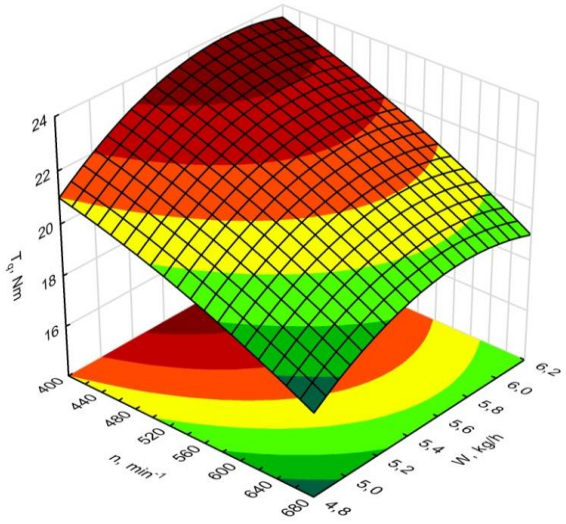

Fig. 10. Diagram of the cross-section of the response surface of the torque model as a function of the rotational speed of the screw and the extrusion rate

9. Conclusion

The lowest temperature value of the molten plastic in the extrusion head (210 °C) was obtained during the extrusion process realized at the screw speed of 480 min^{-1}, the extrusion rate 5.25 kg/h, the angle of mutual position of cooperating cam discs - 45º and the distance between the cam disks 3.5 mm.

References

[1] L. Nakonieczny, M. Zimowski „PP – właściwości i formowanie" PlastNews 11 2009, 32-34.

[2] A. Stasiek, D. Łubkowski, „Badania wpływu konstrukcji segmentów ślimaków wytłaczarek dwuślimakowych współbieżnych oraz parametrów technologicznych na proces wytłaczania polipropylenu modyfikowanego talkiem" Przetwórstwo Tworzyw 1/(133)/16 (styczeń – luty) 2010).

[3] A. Stasiek „Wpływ konstrukcji segmentów ślimaków wytłaczarek dwuślimakowych na charakterystykę procesu wytłaczania", Przetwórstwo Tworzyw 5/(119)13 wrzesień – październik 2007.

[4] J. Stasiek, K. Bajer, A. Stasiek, M. Bogucki, „Wytłaczarki dwuślimakowe współbieżne do kompozytów polimerowych. Metoda doświadczalnego badania procesu", Przemysł Chemiczny 91/2/(2012) 224-230.

[5] A. Stasiek, „Badania procesu współbieżnego dwuślimakowego wytłaczania modyfikowanego polipropylenu przy zmiennej geometrii ślimaków",

Rozprawa doktorska, Wydział Inżynierii Mechanicznej, Uniwersytet Technologiczno-Przyrodniczy, Bydgoszcz 2015, obroniona 2016.
[6] A. Stasiek, D. Łubkowski, M. Bogucki, „Badania procesu wytłaczania polipropylenu modyfikowanego talkiem", Przemysł Chemiczny 91/8(2012) 1625-1629.
[7] A. Stasiek, A. Raszkowska – Kaczor, K. Formela, Badania wpływu nieorganicznych napełniaczy proszkowych na właściwości polipropylenu", Przemysł Chemiczny 93/6(2014) 888-892).
[8] Materiały informacyjne firmy Orlen.
[9] Materiał informacyjny firmy Mondo Minerals.

Volodymyr Krasinskyi[1], Oleh Suberlyak[1], Viktoria Zemke[1], Yurii Klym[1], Ivan Gajdos[2]

REVIEW ON THE PROCESSING AND PROPERTIES OF NANOCOMPOSITES BASED ON THE MIXTURES OF POLYPROPYLENE AND MODIFIED POLYAMIDE

Abstract: *We established in the present work the regularities for obtaining homogeneous nanocomposites based on the mixture of PP/PA-6 with montmorillonite modified using PVP. In these nanocomposites, PA-6 and MMT contribute to the increase in thermal resistance of the material, while PVP improves compatibility between polar PA-6 and hydrophobic PP. On the basis of experimental data, it was found that the mixtures of polypropylene with polyamide modified by the montmorillonite-polyvinylpyrrolidone mixture are distinguished by the higher thermal resistance compared with the starting PP. It is established that the most suitable for application and processing is the mixture of polypropylene with modified polyamide in the ratio 70:30 % by weight, respectively.*

Keywords*: polypropylene, polyamide, montmorillonite, polyvinylpyrrolidone, mixture, nanocomposite, modification, recrystallization.*

1. Introduction

Creation of polymeric nanocomposites based on the polymers of structural designation is a relevant task at present. Of great interest in obtaining the polymeric nanocomposites is montmorillonite, as a nanoscale heterophase. Montmorillonite (MMT) – affordable raw material – is the main component (up to 85 %) of bentonite [1]. Montmorillonite has a special matrix structure that provides it with unique properties. In particular, in the aqueous environment the primary crystalline elements of montmorillonite are broken down into layers – nanoscale elements of the structure [2, 3].

At the end of 80s of the twentieth century, researchers from the concern Toyota obtained the first nanocomposite based on polyamide-6 and organomodified montmorillonite [4]. This composite was distinguished by increased physical-mechanical and thermal properties. The obtained results defined the prospects for such systems and caused an intensive development of research into this field. Today, the market of the layered-silicate polymeric

[1)] *Lviv Polytechnic National University, Department of Chemical Technology of Plastics, 12, Bandera Str., Lviv, 79013, Ukraine, e-mail: vkrasinsky82@gmail.com*

[2)] *Department of Cax Technologies,, Technical University of Košice, Mäsiarska 74, 040 01 Košice, Slovakia, e-mail: ivan.gajdos@tuke.sk*

nanocomposites is developing in the most intensive way with a volume about USD 950 million in 2014 [5].

The first attempts at creating composites based on polymers and aluminosilicates were made in 50s of the last century [6]. However, the introduction of approximately 40-50 % by weight of clays (bentonite, hector, etc.) did not lead to the improvement of properties of the polymeric material, first of all, because of the unsatisfactory dispersing of a silicate filler [7]. Significant progress in the creation of polymeric-silicate nanocomposites with improved physical and mechanical properties in comparison with the starting polymer and traditional dispersely-filled composites was achieved only in the 90s [8].

Recently, scientists have paid much attention to the mixtures based on polypropylene (PP) and polyamide (PA), mixing of which makes it possible to reduce negative characteristics of the starting polymers [9, 10]. In particular, nonpolar polypropylene during mixing with the polar highly hydrophilic polyamide significantly reduces water absorption of the material. Consequently, the effect of moisture on the mechanical and thermal properties of composites is reduced. On the other hand, mixing PP with PA allows expanding the temperature interval of material operation at negative temperatures (temperature of PE fragility reduces) [9].

However, obtaining a homogeneous mixture of PP with PA requires the use of compatibilizers, of a complex chemical structure, as a rule, namely low-ionized PP [10]. But, in this case, the probability of chemical cross-linking of macromolecules is increased as a result of the interaction between anhydrous groups with the peptide ones.

At the same time, paper [11] reported the possibility of obtaining a homogeneous mixture of polyamide with polyvinylpyrrolidone (PVP). This mixture is characterized by a high degree of crystallinity and the higher temperature of crystallization. At the same time, mechanical strength of the material after the modification is little changed. The homogeneity of the mixture is due to the physical interaction between polyamide and PVP based on hydrogen bonds. Such interaction reduces the polarity of both polymers, resulting in the manifestation of hydrophobic fragments of the chains. Formation of such material makes it possible to mix it with the hydrophobic polymers, in particular, with polypropylene (PP), without employing compatibilizers with a complex chemical structure.

In order to achieve a substantial improvement in the properties of the polymeric material, a uniform distribution of nanoparticles of silicate must be achieved in the polymeric matrix. The largest changes in the physical-chemical properties can be expected when introducing anisometric nanoscale filler to the polymer matrix [12]. Particles of lamellar aluminosilicates, in particular, of montmorillonite, have a significant anisometry [13].

Recently, researchers have been paying much attention to obtaining nanocomposites based on the thermoplastic polymeric matrices and a mineral high-polar aluminosilicate – montmorillonite [9, 12, 14, 15].

In article [16], the nanocomposites PP/montmorillonite are obtained by the intercalation of melt using a twin-screw extruder. Using a scanning electron microscope, the authors proved that MMT is dispersed evenly at the nanoscale. The test results of mechanical characteristics of such composites showed that strength at bending of the composites with a low content of MMT (2 % by weight) was higher than that of PP.

By using the method of intercalation from melt [17], the nanocomposites PP and layered silicate Na^+-montmorillonite (3 and 7 % by weight) were obtained with the polar modifier – a low-ionized PP of two types that differ in molecular weight and the content of polar groups. The modifier with low molecular weight and high content of polar groups (4 % by weight) contributes to the intercalation of PP, but it binds bad with it and worsens its thermal properties in the nanocomposite. A maximum difference between dynamic module of the nanocomposite with 3 % by weight of clay and the PP module is observed at 80 °C and is around 65 %. It is shown that the compatibility of nonpolar and polar polymers controls the crystal structure and thermal properties of the matrix mixture of polymers and can play a dominant role in the thermal-mechanical behavior of nanocomposites based on the partially crystalline polymers.

In paper [18], the surface of montmorillonite before mixing with PP is modified by a dispersing agent (DAG) with a high molecular weight. It is shown that DAG significantly affects the strength of mechanical properties. Results of the scanning electron microscopy reveal that MMT is dispersed in PP in the form of particles.

As we can see, in most cases, mixing PP with MMT leads to lower mechanical strength of the composite. Although one may note the growth of strength and thermal characteristics during introduction of 3 % by weight of MMT to PP, which is modified by the low-ionized PP [17].

At the same time, mixing a polar PA with a polar MMT provides increased rigidity and mechanical strength of the composite [19] and substantially increases temperature of the start of destruction [12].

Authors of article [20] demonstrated that the intercalated nanocomposite is formed during modification of polyamide-6 by nanosilicate.

The nanocomposites PP/PA-6/organomontmorillonite, obtained by the intercalation in melt [10], have higher strength at stretching and bending, compared to the unfilled PP, which is subsequently reduced with increasing content of a nanofiller. Impact viscosity of nanocomposites is higher than the impact strength of unfilled PP and reaches 9.61 kJ/m^2. In the presence of organomontmorillonite, the rate of crystallization of PP and PA-6 increases.

Given this, the authors propose a technique for obtaining a nanocomposite based on the mixture PP/PA-6 with enhanced temperature resistance, using the

positive effect of PVP and MMT on obtaining a homogeneous mixture [11] and improving temperature characteristics of the composite [12, 17]. For this purpose, it is proposed at first to obtain a nanocomposite based on PA-6 with MMT, which is intercalated by PVP. Next, to obtain a mixture based on PP and the synthesized nanocomposite. It is assumed that the application of MMT, intercalated by PVP, will contribute to the enhancement of thermostability of PA-6. At the same time, PVP, associated with PA-6, will contribute to an increase in the compatibility of polypropylene with polyamide, which will exclude the use of reactive compatibilizers with a complex chemical structure.

The purpose of present study was to investigate, applying the methods of thermogravimetric analysis, a correlation between thermal characteristics of the newly created nanocomposites based on the mixture PP/PA-6 with montmorillonite modified with the help of PVP, and to determine the optimal composition of a nanocomposite with the enhanced temperature resistance and a wide temperature interval of the viscous-fluid state.

2. Results and Discussion

In the present work, we used polypropylene (PP), Moplen HF501N mark (The Netherlands), with $MFI_{230/2.16}$=9.50 g/10 min, thermal resistance 155 ºC by Vick, density ρ^{20} = 0.900 g/cm^3, bulk density ρ_b = 0.53 g/cm^3.

Polyamide PA6-210/310 (Belarus) with $MFI_{230/2.16}$=19 g/10 min, melting temperature 215 ºC, density ρ^{20}=1.12 g/cm^3, relative viscosity 2.68. Before using, PA-6 was dried under vacuum at 90 ºC for 2 hours.

As a modifier for polyamide, we used the montmorillonite-polyvinylpyrrolidone mixture (MPM), obtained from the solution in the ultrasound field, with the ratio of components MMT:PVP=1:5 [21, 22].

To obtain the mixture, polyvinylpyrrolidone (PVP) with a molecular weight of 12600±2700 was used, softening point 140–160 °C, density 1.19 g/cm^3 at 20 °C, which was dried before mixing under vacuum at 60–70 °C for 2–3 hours.

We also used montmorillonite of the mark Fluka from the company SIGMA-ALDRICH with a surface area of 250 m^2/g and pH 4–5.

Thermal analysis of both the starting components and the compositions based on them was conducted using the derivatograph Q-1500D, connected to an IBM-compatible personal computer. The given device allows simultaneous determining the loss of mass (thermogravimetry – TG), the rate of weight loss (differential thermogravimetry – DTG) and thermal effects (differential-thermal analysis – DTA) for one sample. Research was conducted under dynamic mode in the ambient air. The samples were heated at a rate of 3 ºC/min. A batch was about 200 mg on average. Oxide of aluminum was a reference substance. Derivatographic study of the samples was conducted in a temperature range of 20–600 ºC.

The study objects were: sample 1 – pure PP; sample 2 – the composition PP:(PA-6/MPM) = 70:30 agglomerate; sample 3 – PP:(PA-6/MPM) = 70:30 – sample 2 after injection molding; sample 4 – the composition PP:(PA-6/MPM) = 30:70 – agglomerate; sample 5 – PP:(PA-6/MPM) = 30:70 – sample 4 after injection molding.

X-ray studies were conducted on the diffractometer DRON-4-07. Emitting lamps with a copper anode and an Ni-filter were used. The study was performed in the region of angles 2θ from 4 to 45θ, the length of measuring step was 0.10, period of pulse measurement 8 s.

In order to improve compatibility of montmorillonite with thermoplastic polymers, we previously obtained a mixture of montmorillonite with polyvinylpyrrolidone in the ratio MMT:PVP = 1:5, in the form of finely-dispersed powder in line with the procedure described in [21, 22].

It is known that the technique for mixing and the conditions of the implementation of the process exert a significant influence on the properties of the obtained mixtures. In order to obtain composites with a complex of high operational and technological characteristics, based on polypropylene and modified PA-6, the mixing was conducted in several stages.

At the first stage, a mixture was obtained based on polyamide (PA-6) and MPM in the ratio 90:10 % by weight. By mixing MPM in the melt of PA-6 during 15 min in the plunger-capillary plasticizer (nozzle diameter $d = 2.095 \pm 0.005$ mm) at a temperature of 230 °C and a load of 5 kg, we obtained strands, which were ground using a rotary-knife crusher.

At the second stage, the obtained agglomerate was dried under a vacuum at 80 °C and mixed mechanically with polypropylene in the ratios 30:70 and 70:30 % by weight. Next, in the thermoplastic automatic machine Kuasy 32/25, we performed the plastication of the obtained compositions at the following parameters: temperature by the sections of injection cylinder 170, 195, 230 °C, mixing time 4–5 min. The rods were obtained by the intrusion method, which were ground using a rotary-knife crusher.

At the third stage, the samples to be studied were obtained from the received compositions by injection molding, in the form of standard blades, in the thermoplastic automatic machine Kuasy 32/25 at the following optimal technological parameters: temperature in the sections of material cylinder of the molding machine – 170, 195, 235 °C; temperature of the molding shape – 68–70 °C; pressure of molding – 100 MPa; holding time under pressure – 6 s; holding time for cooling – 25 s.

Thermolysis of samples 2–5 is conducted at six stages (Table 1, Fig. 1). At stage 1, in the temperature range of 20–147 °C, the separation of physically bound water occurs. This process is accompanied by a slight weight loss of the samples and the emergence of not so deep endothermal effects on the DTA curves.

Samples 4, 5 have a much larger moisture content, due to the presence in their composition of a large amount of hygroscopic substances (PVP, MMT, PA-6).

Table.1. Results of thermogravimetric analysis of the composites samples

Sample	Thermolysis stage	Temperature range, ºC	Weight loss, %
1	I	140–170	–
	II	230–400	65.6
	III	400–600	34.4
2	I	20–126	0.74
	II	126–164	–
	III	164–211	–
	IV	211–328	**13.86**
	V	328–414	65.25
	VI	414–600	18.0
3	I	20–140	0.9
	II	140–160	–
	III	160–218	0.6
	IV	218–322	**7.1**
	V	322–439	77.9
	VI	439–600	13
4	I	20–147	2.62
	II	147–159	–
	III	159–241	3.23
	IV	241–349	**13.43**
	V	349–471	59.29
	VI	471–600	8.6
5	I	20–138	2.29
	II	145–163	–
	III	163–230	1.26
	IV	230–328	**14.53**
	V	328–463	73.55
	VI	463–600	8.52

In the temperature range of 126–164 ºC, at stage 2 of the thermolysis, the DTA curves of the compositions samples start to demonstrate an endothermic effect without a weight loss, which corresponds to the process of material melting (Fig. 1). This effect is the deepest for samples 2, 3, which are characterized by the higher content of PP, while for sample 4 an extremum of melting endoeffect is not clearly expressed.

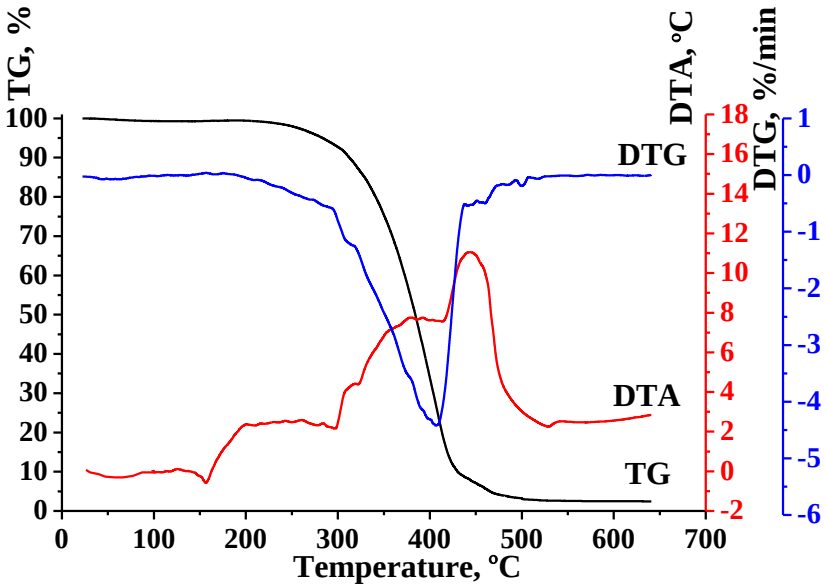
TG, %
DTA, °C
DTG, %/min
DTG
DTA
TG
Temperature, °C

a

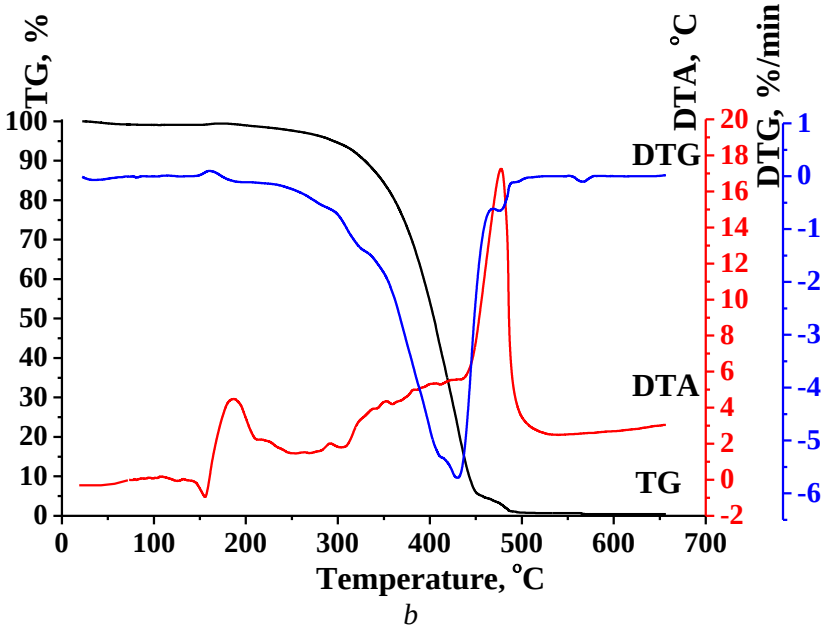
TG, %
DTA, °C
DTG, %/min
DTG
DTA
TG
Temperature, °C

b

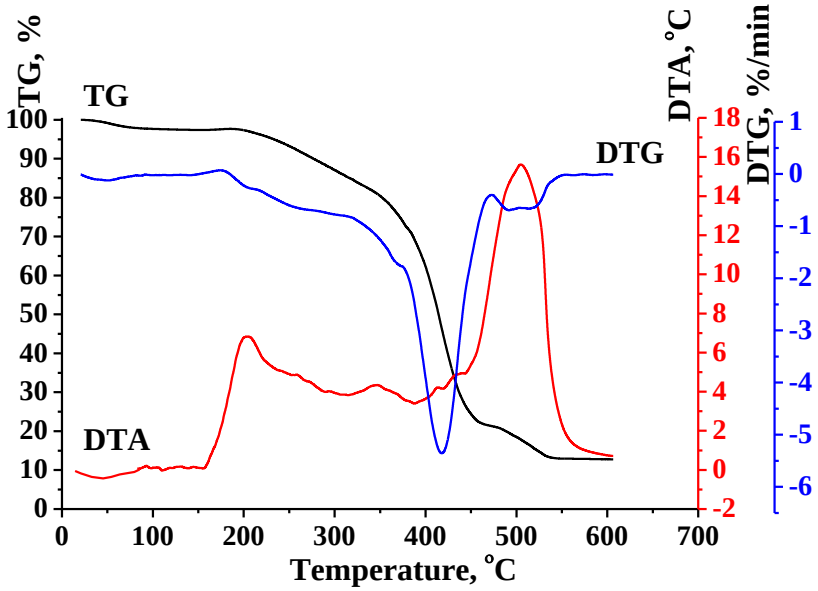

c

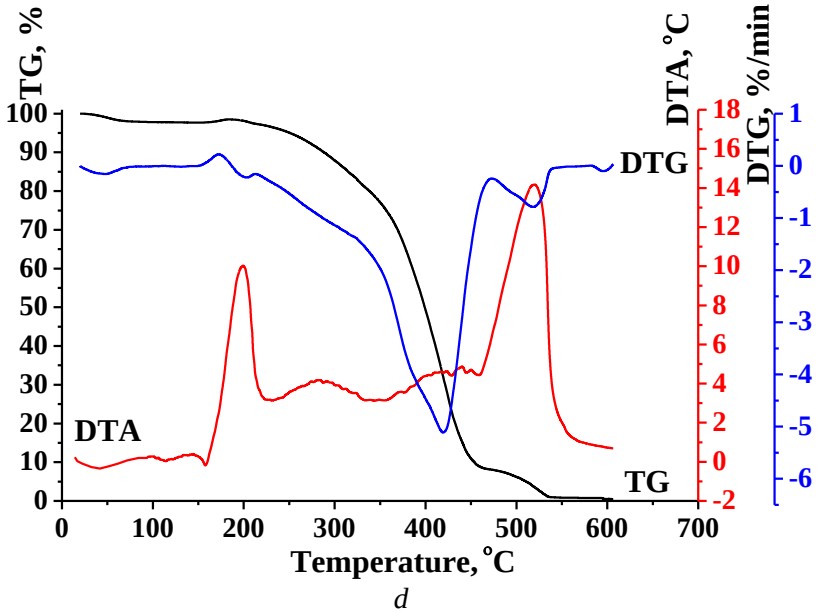

d

Fig. 1. Thermograms of composites samples based on polypropylene and polyamide-6, previously modified by the mixture montmorillonite- polyvinylpyrrolidone (MPM): a – sample 2 – the composition PP:(PA-6/MPM)=70:30 – agglomerate; b – sample 3 – PP:(PA-6/MPM)=70:30 – sample 2 after injection molding; c – sample 4 – the composition PP:(PA-6/MPM)=30:70 – agglomerate; d – sample 5 – PP:(PA-6/MPM)=30:70 – sample 4 after injection molding

At stage 3 of the thermolysis, in the temperature interval of 159–241 ºC, the DTA curves of samples 3–5 exhibit a clearly pronounced exothermic effect occurs (Fig. 1). This effect indicates, first of all, the intensity of the course of recrystallization processes of polyamide, modified by the montmorillonite-polyvinylpyrrolidone mixture. Crystalline phase of the modified PA-6, according to the results of an X-ray analysis, manifests itself at angles 2θ=20–30º (Fig. 2*a*). Moreover, for samples 3, 5, which have undergone repeated thermal treatment in the thermoplastic automatic machine, extrema of the effects are more intensive. This is explained by the fact that the rapid cooling of a material in the molding shape does not make it possible to form the natural crystal structure of the modified polyamide (Fig. 2*b*). A wide peak of this exoeffect for sample 4 indicates the formation of a supramolecular structure of the low level of organization and the high degree of polydispersity of the supramolecular structure. Additional confirmation of the course of recrystallization processes during thermolysis of the samples that have undergone repeated thermal treatment in the thermoplastic automatic machine are the significant differences in the radiographs of these samples (Fig. 2). In particular, in the radiograph of sample 3 (Fig. 2*b*), there are no peaks at all at angles 2θ=28.9º, 25.6º, 23.7º, and 21.1º, which are characteristic for sample 2 (Fig. 2*a*). The reaction of PVP oxidation is also not ruled out in this range of temperatures [23], which is accompanied by a slight weight loss of the samples (Table).

In the temperature interval of 211–349 ºC (stage 4 of thermolysis), there occur the processes of hydrolytic and oxide destruction of PVP and PA-6, which are accompanied by weight loss of the samples and the emergence of endothermic effects on the DTA curves. Samples 2, 3, which contain 30 % by weight of modified polyamide, are distinguished by the higher thermal resistance in comparison with the samples containing 70 % by weight of the modifier. Temperature of the onset of thermo-oxidation destruction of sample 3 is the highest and is within a range of 300 ºC (Fig. 1*b*). The samples of compositions containing the higher amount of modified PA-6 have a lower temperature of destruction, which, however, is higher than that of the sample of pure PP has (temperature of thermo-oxidation destruction of PP is 235 ºC) (Figs 1, 3). In the process of hydrolysis, samples 2, 3 lose weight less intensively (Table). Sample 3 has the highest thermal resistance, which loses only 7.1 % by weight in the process of destruction, in contrast to the rest of the samples of compositions whose weight loss at this stage is 13–15 %. Loss of weight by samples 2 and of pure PP (sample 1), which in this temperature range undergoes thermo-oxidation destruction processes, are almost identical. Samples 4, 5 are distinguished by the highest weight loss (Table). Thus, it is established that by using the mixing of PP with polyamide, which is modified by MPM, it is possible to increase thermal resistance of the composites against thermo-oxidation destruction. Effects of increasing the temperatures of thermo-oxidation destruction of compositions depend on the ratio of components and the method of processing. Such results

make it possible to increase considerably the intervals of temperature parameters of the injection molding process under the pressure of the designed composites, which will allow controlling in a wide range the operational properties of products.

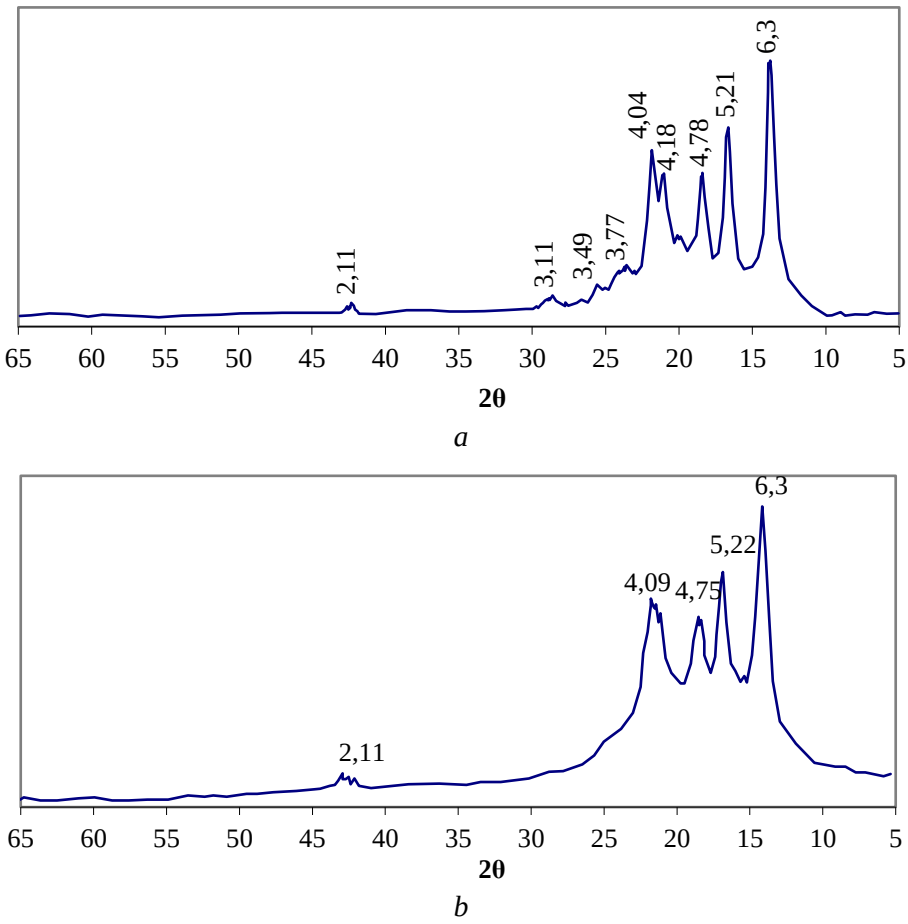

Fig. 2. Radiographs of the composites samples: a – the composition PP:(PA-6/MPM)=70:30 – agglomerate; b – PP:(PA-6/MPM)=70:30 – after injection molding

At stage 5 of the thermolysis of samples 2–5 in the temperature interval 322–471 ºC, there occurs a thermo-oxidation destruction of the hydrolysis products, which is accompanied by intensive weight loss and the emergence of exothermic effects on the DTA curves. Samples 3–5 lose weight less intensively in this region, while the exothermic effects are less intense and shifted to the region of higher temperatures compared to PP and sample 2.

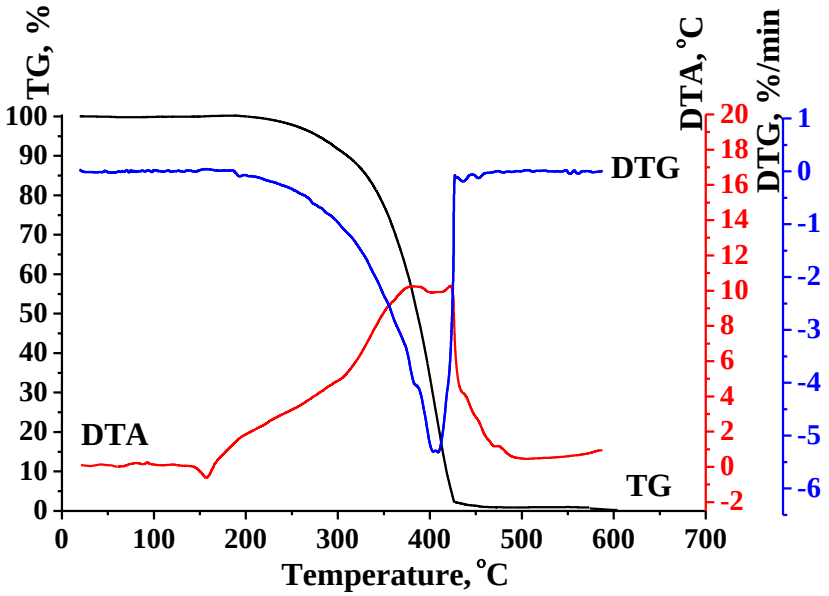

Fig. 3. Differential-thermal analysis of the sample of pure PP

At stage 6 of the thermolysis in the temperature interval 414–600 ºC, there is a combustion of the carbonated residue with the emergence of a clear exothermic effect on the DTA curves.

Thermolysis of the sample of pure PP takes place over 3 stages (Fig. 3). At stage 1, in the temperature interval 140–70 ºC, there is a process of sample melting without a weight loss. The DTA curve exhibits an endothermic effect with a maximum at temperature 157 ºC. At stage 2 of the thermolysis in the temperature range 230–400 ºC, a thermo-oxidation destruction of the sample occurs with intensive weight loss (Table 1), which finishes by the combustion of the destruction products. The DTA curves displays an exothermic effect with a maximum at temperature 386 ºC. At stage 3 of the PP thermolysis, in the temperature range 400–600 ºC, a combustion of the carbonized residue takes place, with the emergence of an exothermic effect on the DTA curve with a maximum at 422 ºC.

3. Conclusion

The regularities of obtaining nanocomposites based on the mixture PP/PA-6 with montmorillonite modified by using PVP were established. In these nanocomposites, PA-6 and MMT contribute to the improvement of thermal resistance of the material, while PVP improves compatibility of the polar PA-6 with a hydrophobic PP.

By analyzing results of the termogravimetric studies, it can be argued that the

nanocomposites were obtained on the basis of homogeneous mixtures of PP with the modified PA-6. Homogeneity of the mixtures is confirmed by the presence of one peak on the DTA curves (Fig. 1), which characterizes the process of polymers melting in the region of temperatures 126–164 ºC.

The nanocomposites obtained are characterized by the enhanced thermal resistance (temperature of the onset of thermo-oxidation destruction is 300 ºC compared with 235 ºC for the starting PP) and a wide region of the viscous-fluid state. Given this, such materials could be used for manufacturing structural products by traditional methods. The nanocomposites developed based on the mixtures of polypropylene and modified polyamide have wider temperature intervals of the viscous-fluid state – 126–300 ºC. This makes it possible, by changing the modes of processing, to influence the structure and properties of products, especially taking into account the difference in crystallization of the material depending on the conditions and the method of processing.

Taking into account an analysis of the scinetific literature and the effects of increasing temperature characteristics with a decrease in the amount of modified polyamide (Table 1, Fig. 1), the composites are promising that contain lower quantity of polyamide, modified by MPM. Therefore, in the future, we plan to undertake research into similar materials with small additions of the modified polyamide.

Based on the obtained results, it was established that the mixture of polypropylene with modified polyamide in the ratio 70:30 % by weight, respectively, is the most suitable for application and processing. Composites on the basis of such a mixture are characterized by highest thermal resistance – 300 ºC compared with 235 ºC for the starting PP.

References

[1] En-guang, Z. Effect of a high molecular weight dispersant on the properties of the montmorillonite/polypropylene composite material. Journal of the Daqing Petroleum Institute, 2009.

[2] Ahmad, M. B., Hoidy, W. H., Ibrahim, N. A. B., Al-Mulla, E. A. J. Modification of montmorillonite by new surfactants. J. Eng. Appl. Sci., 2009.

[3] Kiliaris, P., Papaspyrides, C. D. Polymer/layered silicate (clay) nanocomposites: An overview of flame retardancy. Progress in Polymer Science, 2010.

[4] Kovalevski, V. V., Rozhkova, N. N., Zaidenberg, A. Z., Yermolin, A. N. Fullerene-like structures in shungite and their physical properties. Mol. Mat., 1994.

[5] Mucha, M. Crystallization of isotactic polypropylene containing carbon black as a filler. Polymer, 2010.

[6] Zymankowska-Kumon, S. Assessment Criteria of Bentonite Binding Properties. Archives of Foundry Engineering, 2012.

[7] Youssef, A. M., Malhat, F. M., Abdel Hakim, A. A., Dekany, I. Synthesis and utilization of poly (methylmethacrylate) nanocomposites based on modified montmorillonite. Arabian Journal of Chemistry, 2017.
[8] Omurlu, C., Pham, H., Nguyen, Q. P. Interaction of surface-modified silica nanoparticles with clay minerals. Applied Nanoscience, 2016.
[9] Liang, M. R., Jiao, W. Y., Hui, H., Yi, Y. D. Research on Mechanical Properties and Crystallization Performance of PP/PA6/OMMT Composite Plastics Science and Technology, 2010.
[10] Guowang, H., Xiangfang, P. Research Progress of Preparation and Properties of Organic Montmorillonite Filled Polypropylene/PA6 Nanocomposites. Plastics Science and Technology, 2008.
[11] Gnatowski, A., Suberlak, O., Postawa, P. Functional materials based on PA6/PVP blends. Journal of Achievements in Materials and Manufacturing Engineering, 2006.
[12] Beatrice, C. A. G., Santos, C. R. dos, Branciforti, M. C., Bretas, R. E. S. Nanocomposites of polyamide 6/residual monomer with organic-modified montmorillonite and their nanofibers produced by electrospinning. Materials Research, 2012.
[13] Suberlyak, O. V., Krasins'kyi, V. V., Moravs'kyi, V. V., Gerlach, H., Jachowicz, T. Influence of Aluminosilicate Filler on the Physicomechanical Properties of Polypropylene-Polycaproamide Composites. Materials Science, 2014.
[14] Tesarikova, A., Merinska, D., Kalous, J., Svoboda, P. Ethylene-Octene Copolymers/Organoclay Nanocomposites: Preparation and Properties. Journal of Nanomaterials, 2016.
[15] Dulebova, L., Garbacz, T. The effect of particulate fillers on hardness of polymer composite. Advances in Science and Technology Research Journal, 2017.
[16] Chang, D., Li-hui, L., Jing, X., Kai-zhi, S. Effect of Low Frequency Vibration on Property of PP/MMT Blends. Polymer Materials Science & Engineering, 2006.
[17] Ji-Sheng, M., Shi-Min, Z., Zong-Neng, Q., You-Liang, H., Shu-Fan, Z. Microstructure and Morphology of PolypropyIene/Clay Nanocomposites Synthesized via Intercalative Polymerization. Chemical Journal of Chinese Universities, 2002.
[18] Zhou, L., Zhao, Y., Yang, M., Wang, D., Xu, D. Investigation on Photooxidative Degradation of Polypropylene/Organomontmorillonite Nanocomposites. Spectroscopy and Spectral Analysis, 2010.
[19] Huang, J. C., Zhu, Z. K., Ma, X. D., Qian, X. F., Yin, J. Preparation and properties of montmorillonite/organosoluble polyimide hybrid materials prepared by a one-step approach. Journal of Materials Science, 2001.

[20] Volkova, T. S., Isaev, A. Yu., Petrova, A. P. Osobennosti vliyaniya nanosilikatov na izmenenie svoystv razlichnyh polimernyh i kleyashchih sistem. Klei. Germetiki. Tekhnologyi, 2013.
[21] Krasinskyi, V., Suberlyak, O., Klym, Yu. Operational properties of nanocomposites based on polycaproamide and modified montmorillonite. Acta Mechanica Slovaca, 2016.
[22] Krasinskyi, V. V., Kochubei, V. V., Klym, Yu. V., Haidos, I. Termohravimetrychni doslidzhennia polivinilpirolidonu, modyfikovanoho montmorylonitom. Visnyk NU "Lvivska politekhnika", 2015.
[23] Suberlyak, O. V., Skorohoda, V. Y., Thir, I. G. Vliyanie kompleksoobrazovaniya na polimerizatsiyu 2-oksietilenmetakrilata v prisutstvyi polivinilpirrolidona. Vysokomolekulyarnye soedineniya, 1989.

Volodymyr Levytskyi[7], Ulyana Khromiak[8], Volodymyr Skorokhoda[7],
Khrystyna Levytska[7], Yurii Melnyk[7]

TECHNOLOGICAL ASPECTS OF OBTAINING AND PROPERTIES OF POLYVINYLPYRROLIDONE COPOLYMERS AND COMPOSITES

Abstract: *Kinetics of emulsion polymerization of hydrophilic vinyl monomers in the presence of polyvinylpyrrolidone and technological principles of their synthesis are determined. Reasonable technological parameters in the synthesis of copolymers are determined. Physicochemical properties of the synthesized copolymers (surface tension, the size of latex particles, pH) are determined. Synthesized graft copolymers were used to create high-adhesion polymer-monomer compositions. These compositions have high reactivity at room temperature. It can be regulated by the nature of the polymer matrix, the introduction of comonomers and fillers due to the influence of physicochemical factors on the process of polymer formation. The rate of polymerization and the degree of monomer conversion largely depend on the nature of the polymer matrix. The highest polymerization rate and the maximum degree of conversion are observed when using a copolymer of polyvinylpyrrolidone and polymethylmethacrylate. Materials based on the developed compositions are characterized by a low residual monomer content and high operational properties, such as surface hardness, Vicat softening temperature, adhesive bond strength to supports of different nature.*
Keywords: *vinyl monomers, polyvinylpirrolidone, emulsion polymerization, casting polymerization.*

1. Introduction

The contemporary development of science and technology requires the creation of new polymer materials with a corresponding set of special properties: high adhesion to supports of different nature, high physicomechanical, thermophysical and selective-sorption properties. These include low-toxic adhesive polymer-monomer compositions of medical and general technical purposes. Among the methods for preparation of such materials with the necessary properties the most interesting are those basing on the modification of known industrial polymers in polymerization processes. These methods make it possible to obtain polymer materials with the preferable set of technological and operational properties at rather low material and energy costs. The determining factor for the most of the technologies based on the preparation of modified polymeric materials is modifier. Polymers with high surface activity, good

[7] *Lviv Polytechnic National University, Department of Chemical Technology of Plastics, 12, Bandera Str., Lviv, 79013, Ukraine, e-mail: vlevytskyj@gmail.com*
[8] *Lviv State University of Life Safety, Department of Environmental Safety,35 Kleparivska str., Lviv, 79000,e-mail: ulanajukovska@gmail.com*

solubility in water and many aqueous organic media, high ability to complex formation, high sorption characteristics are used as modifiers [1, 2].

Polyvinylpyrrolidone (PVP) and its copolymers belong to such polymers. Due to their specific properties, additional opportunities for improving modern technologies [3, 4], obtaining of new functionalized materials [5] and expanding the branches of their use are opened.

Monomer-polymer compositions are widely used in a variety of industries especially as a basis for preparing materials with enhanced adhesion properties. Among such materials, acrylates based adhesives occupy a special place [6]. First of all, the increased interest in acrylates-containing glues is caused by their high operational properties: cure speed, adhesion to a variety of materials, strength and durability of adhesive compounds, their low toxicity [7]. In this regard, these materials are widely used in a variety of industries, namely, in medicine, dentistry, construction, engineering, automotive, electrical and textile industries [8]. It should be noted that the use of (meth) acrylic adhesives is expanding in current conditions to solve many technological tasks [9].

The main components of (meth) acrylic adhesives are (meth) acrylic monomers or polymers, initiating systems, hardeners, stabilizers, modifiers. Methyl methacrylate (MMA) is often used as the main monomer in the (meth) acrylic adhesives. It provides high adhesive strength and is a good solvent for a number of polymers. When combined with oils MMA makes it possible to glue untreated surfaces. MMA has several disadvantages, in particular, high volatility, pungent odor, fire risk. It is used in admixture with high boiling monomers such as hydroxyalkyl methacrylate, glycidyl methacrylate, methacrylates of higher alcohols: tetrahydro tetrahydrofurfuryl-, diethylaminoethyl-, 2-oxopropyl neopentyl- and other glycol methacrylates, and styrene [10-12].

The aim of the work is the development of functionalized materials based on graft copolymers of polyvinylpyrrolidone for high-adhesion methyl methacrylate-copolymer compositions.

2. Materials and methods

Copolymers were synthesized by emulsion polymerization of vinyl monomers in the presence of PVP, potassium persulfate or hydrogen peroxide at 60-70 °C and the ratio of monomer: aqueous phase = 1: 3. The kinetics of the emulsion polymerization of the test compositions was studied by dilatometric method for measuring the volume change of the reaction mixture during polymerization. IR studies were carried out on a spectrograph "Specord-75IR" at room temperature. The spectra were recorded at the same intensity and the same scan rate between 400 and 4000 cm^{-1}.

Ultrasonic investigations were carried out using Ultrasonic disintegrator UD-20 automatic (frequency 20 kHz, intensity $5 \cdot 10^4$ W) with cylindrical magnetostrictor. The ratio between its diameter and reactor diameter is 0.5. The

reactor equipped by thermostatic jacket is made of X18H9T stainless steel and has a volume of 100 ml. The volume of experimental sample is 40 ml.

The adhesive compositions were synthesized by the polymerization of MMA or a mixture thereof with other monomers in the presence of synthesized copolymers at room temperature. To determine the properties of the adhesive compositions, a number of studies were carried out. The conversion degree of the monomer was determined by the bromide-bromate method. The surface hardness and Vicat softening temperature of the samples were measured on the Heppler consistometer. Adhesion was determined according to ISO 527-5: 2009.

3. Results and discussion

3.1. Technological and kinetic features of emulsion polymerization of vinyl monomers in the presence of PVP

It has been established that the enhanced initiating ability of the series of (meth)acrylic monomers has graft copolymers of PVP. Copolymers were synthesized on the basis of PVP and vinyl monomers (MMA, vinyl acetate (VA), styrene) by emulsion polymerization. The emulsion polymerization of vinyl monomers is mostly carried out in the presence of emulsifiers that are surfactants of different nature [13-15]. The nature of the emulsifier and its concentration in the reaction medium greatly influence the mechanism and kinetics of the polymerization and therefore the technological features of the process and its productivity. This influence is caused by changes in the interphase characteristics of the polymerization system, adsorption phenomena at the phase boundary, as well as changes in the solubility of monomers in the dispersion medium with the active participation of the emulsifier. Emulsifiers have to meet a number of requirements [13, 14]: high surface activity, ability to micellization, non-toxicity.

Due to its properties and structure PVP can serve as an emulsifier in the processes of emulsion polymerization and also be an effective polymer matrix, which actively participates directly in the polymerization processes. It should be noted that the influence of the emulsifier on the regularities of the emulsion polymerization of vinyl monomers is primarily resulted in change in the interphase characteristics of the polymerization system and the solubility of the monomers in the reaction medium. On the basis of the conducted studies, it has been established that PVP macromolecules exhibit high surface activity on the interphase surface of water-vinyl monomer. This activity increases with a decrease in the polarity of the monomer in the VA-MMA-styrene series. This is evidenced by the nature of the interphase tension isotherms in the vinyl monomer-aqueous PVP solution system, the PVP adsorption dependences in the coordinates of the Langmuir equation, the maximum values of the Gibbs adsorption ($G_m = 2.14 \cdot 10^{-6}$ mol / m^2) and adsorption work ($W_{ad} = 48.8 \cdot 10^{-3}$ J / m^2) for styrene. PVP has different effects on the total (true and colloidal) solubility of vinyl monomers in aqueous solution.

The increase of the PVP concentration up to 0.2 mol / l monomer concentration, solubility of MMA increases from 0.15 to 0.22 mol / l, for VA it decreases from 0.33 to 0.18, and for styrene it is almost unchangeable. Obviously it is a consequence of specific intermolecular interactions in the system that will affect the polymerization processes in these systems.

High surface activity and solubilization ability of PVP prove its high efficiency as an emulsifier in the processes of emulsion polymerization of vinyl monomers (KKM PVP – 0.09-0.11 mole / liter monomer concentration).

The effect of the monomer nature, concentration factors, temperature and stirring rate on the kinetic regularities the of emulsion polymerization process of vinyl monomers in the presence of PVP was established. Emulsion polymerization of vinyl monomers in the presence of PVP is characterized by a different rate depending on the nature of the monomer (Fig. 1).

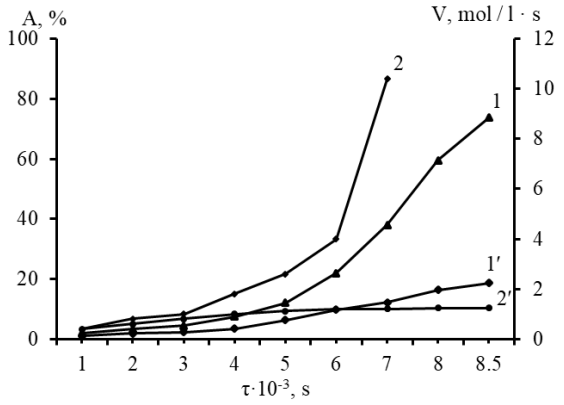

Fig. 1. Degree and rate of emulsion polymerization of vinyl monomers in the presence of PVP: 1, 1′ – A; 2, 2′ – V. 1, 2 – MMA. 1′, 2′ – styrene. $C_{mon.}$ = 0.99 mol / l; $C_{in.}$ = 2,81.10^{-3} mol / l; C_{PVP} = 0,09 mol / l; M_{PVP} = 28000; T = 323 K

The polymerization reaction rates for the monomer and initiator are 1.9 and 0.75, respectively, for MMA and 1.6 and 0.55 for styrene.

It was found that the polymerization rate of all the investigated vinyl monomers increases with increase in ratio of the monomeric and aqueous phases, the concentration of the initiator and the temperature. Dependence of the MMA polymerization rate on the particle size in the range of 70-200 nm is described by the equation:

$$V_{pol.MMA} = 1 \cdot 10^{-4} \cdot r^2 - 0.055 \cdot r + 5.603. \qquad (1)$$

Polymerization of the investigated monomers in the presence of PVP is significantly intensificed by ultrasound (US).

The polymerization under US treatment was studied at ratio polymer solution: monomer equal to 7:1 (wt/wt). All investigated monomers are polymerized in the presence of PVP under US treatment without induction period (Fig. 2). Moreover, the polymerization rate increases in the row butylacrylate < methylacrylate < styrene. For styrene the polymer yield exceeds 80 % already after 30 min from the reaction beginning.

The highest reaction ability of styrene is caused by its highest hydrophobicity. The most stiff and non-mobile polymeric chains of polystyrene, as well as the most indicative phase boundary (monomer - PVP aqueous solution) are formed on the basis of styrene. It is also necessary to take into account that in the most hydrophobic systems PVP shows the highest adsorptive activity on the phase boundary [7]. Such boundary favors the monomer solvation on PVP links and complex formation with transfer of charge which is polymerization activator [7].

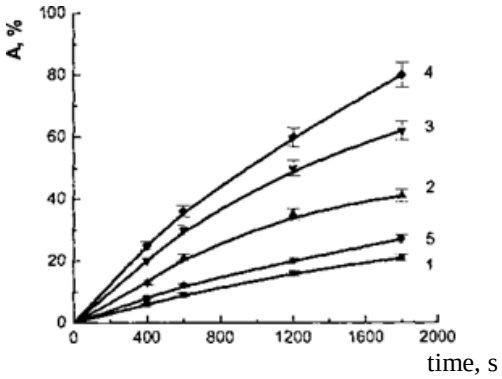

Fig. 2. Polymer yield (A) v.s. monomer nature. Monomers: butylacrylate (1); methylacrylate (2, 3) and styrene (4, 5). Concentrations (mol/1): 1 (1, 3-5) and 0.4 (2). PVP content (%): 1 (1-4) and 0 (5). $MW_{PVP} = 28\ 10^3$. T= 293 K

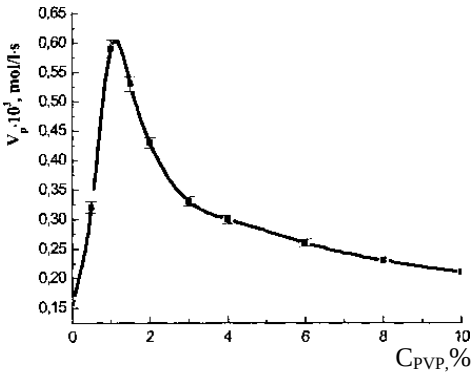

Fig. 3. Dependence of styrene polymerization rate on PVP concentration. T= 293 K; C_m = 1 mol/1; $MW_{PVP} = 28 \cdot 10^3$

The active role of phase boundary for the polymerization under US treatment is confirmed by the fact that polymerization of methacrylate with the concentration of 0.4 mol/l (the maximum concentration under which the homogeneous system is formed) proceeds slower than that with the concentration of 1 mol/1 (concentration under which the clear phase boundary monomer-PVP aqueous solution is observed; Fig. 2).

The effect of PVP amount in the aqueous phase on the polymerization rate becomes apparent at low concentrations and has extreme character with the maximum at PVP concentration of 1 wt % (Fig. 3). The obtained results are in good agreement with previous investigations about the effect of PVP concentrations in the aqueous phase on interphase polymerization of vinyl

monomers [8]. PVP optimum concentrations are 0.5-3 wt % taking into account the possibility of directed change of the polymerization rate.

As a result of polymerization, graft copolymers of PVP are formed in the investigated systems. This is evidenced by the physicochemical and IR spectroscopic studies. The IR spectra of synthesized methyl methacrylic copolymers (Fig. 4) have characteristic bands that are related to both the PVP links (1300 cm^{-1}, 1450 cm^{-1}, 1470 cm^{-1}, 1500 cm^{-1}) and PMMA (1140 cm^{-1}, 1160 cm^{-1}, 1180 cm^{-1}, 1200 cm^{-1}, 1220 cm^{-1}).

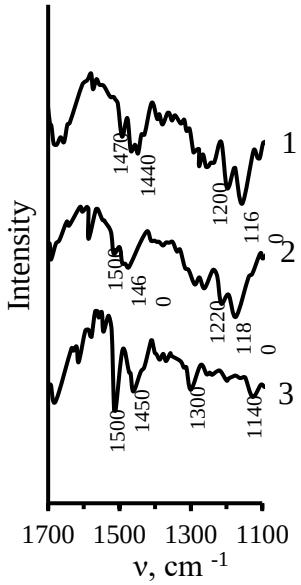

Fig. 4. IR spectra of PVP-gr-PMMA copolymers depending on the ratio of components in the synthesis and the drying temperature of the copolymer: MMA: PVP in the synthesis of the copolymer, mol / mol monomer concentration: 1, 2 - 3:1; 3 - 1: 1. T_d, K: 1- 313; 2, 3 - 343

The degree and effectiveness of grafting depend significantly on the conditions of the process, in particular the PVP concentration in the aqueous medium and the temperature of the process.

It has been established that the properties of latexes obtained by emulsion polymerization (surface tension, pH, particle radius) depend on the conditions of the process; the ratio of the monomeric and aqueous phases, the temperature, the concentration of the monomer and initiator, and the amount of PVP. As the concentration of the initiator increases and the temperature of the process decreases, the size of the latex particles and the pH decrease (Fig. 5).

The ratio between the components of the polymerization system and the mixing rate also has a significant effect on the size of latex particles. The size of the latex particles also depends on the nature of the monomer and, depending on the mixing rate, is described by the following equations:

for styrene – $r_{PVP-gr-PS} = -2 \cdot 10^{-4} \cdot V_{mix.}^3 + 0.0927 \cdot V_{mix.}^2 - 15.758 \cdot V_{mix.} + 988.58$, (2)

for MMA – $r_{PVP-gr-PMMM} = -9 \cdot 10^{-5} \cdot V_{mix.}^3 + 0.0517 \cdot V_{mix.}^2 - 9.6168 \cdot V_{mix.} + 666.24 \cdot$ (3)

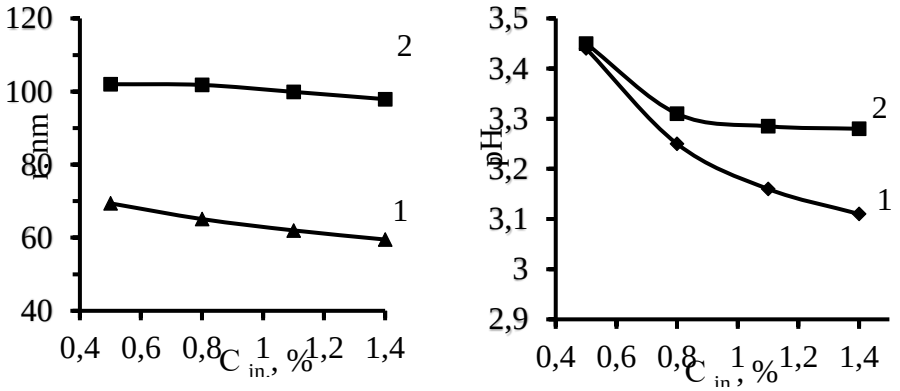

Fig. 5. Influence of synthesis conditions on the properties of copolymer latexes: a – r; b –pH. 1 – 323 K; 2 – 333 K

Synthesized PVP copolymers have sufficiently high sorption properties that can be controlled by polymerization conditions, primarily by the process temperature and the concentration of the initiator. As the polymerization temperature increases and the initiator concentration decreases, the sorption capacity of the copolymers decreases. Sorption ability of finely dispersed graft copolymers of polyvinylpyrrolidone and polystyrene (PVP-gr-PS) is greater, compared to the graft copolymer of polyvinylpyrrolidone and polymethylmethacrylate (PVP-gr-PMMA). With respect to heparin, it is $3.0 \cdot 10^5$ and $3.1 \cdot 10^4$ units / m^2, respectively, with respect to iodine - 36 and 32 mol / g. It can be used in the preparation of sorption materials for antiseptics, therapeutic insulating films and thrombus-resistant products.

3.2. The technological and physico-chemical basis for the development of methyl methacrylate-copolymer compositions and materials based on them

The emulsion polymerized graft copolymers of PVP were used as a polymer matrix for the preparation of MMA copolymer compositions cured by block polymerization.

The results of kinetic studies of MMA polymerization in the presence of finely dispersed PVP copolymers depending on the nature of the polymer matrix (PM) and the conditions for its synthesis are shown in Fig. 6.

The rate of polymerization and the degree of monomer conversion largely depend on the nature of the polymer matrix (Fig. 4). Polymerization of MMA occurs at a high rate and, depending on the nature of the polymer matrix, the monomer conversion rate of 70-90% is achieved in 10-15 minutes. The highest polymerization rate and the maximum degree of conversion are observed when using the PVP-gr-PMMA copolymer.

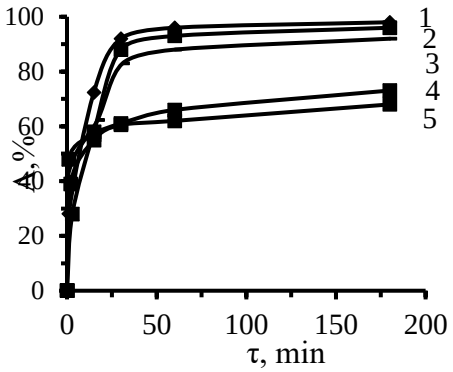

Fig. 6. Kinetic curves of polymerization of MMA compositions depending on the nature and conditions of PM synthesis: 1, 2, 4 - PVP-gr-PMMA; 3 - PVP-gr-PS; 5 - PMMA. The ratio of MMA: PVP in the synthesis of PM, mole / mole monomer concentration: 1-3 - 3: 1; 4 - 1: 1. T_d. PM, K: 1, 3, 5 - 313; 2, 4 - 343

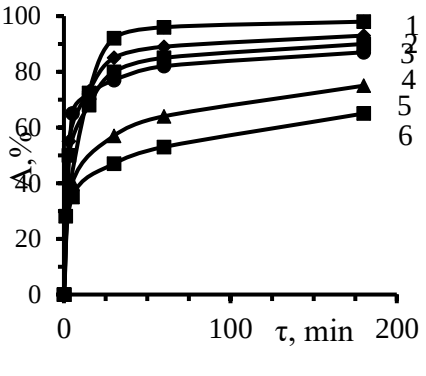

Fig. 7. Kinetic curves of MMA polymerization in the presence of PVP-gr-PMMA depending on nature and content of comonomer and filler. Comonomer; 2 – HEMA, 3 – GMA, 4 – VP. Filler: 5 – Al_2O_3, 6 – SiO_2. Comonomer content – 20 % (mas.). Filler content – 10 % (mas.)

It was found that the activity of the polymer matrix also depends on the conditions of its synthesis. A polymer matrix synthesized with a smaller amount of PVP exhibits significantly more activity during block polymerization of MMA. This, along with other factors, is a consequence of the greater affinity of the monomeric and polymeric phases. It should be noted that the drying temperature of the polymer matrix also affects its activity. The copolymers dried under milder conditions (313 K) show greater activity.

It is established that the kinetic regularities of the polymerization process are affected by the comonomer and mineral filler (Al_2O_3, SiO_2) (Fig. 7).

The addition of comonomers such as 2-hydroxyethylenemethacrylate (HEMA), glycidyl methacrylate (GMA) and vinylpyrrolidone (VP) to MMA leads to a decrease in the polymerization rate, regardless of the nature of the polymer matrix (PVP-gr-PMMA, PVP-gr-PS).

Depending on the nature of the polymer matrix and the monomeric phase, the ratio between phases and the presence of filler during polymerization under the investigated conditions, a number of stages can be distinguished in terms of physicochemical properties: sandy, sticky, dough-like, viscous, fully cured.

Duration of each of these stages for different systems based on the PVP-gr-PMMA copolymer is shown in Fig. 8.

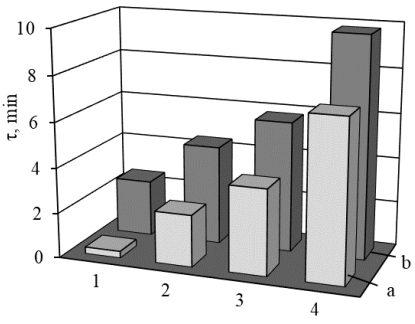

Fig. 8. Stages of polymerization of MMA – PVP-gr-PMMA compositions depending on comonomer nature: a – without comonomer; b – HEMA. Comonomer content – 20 % (mas.). 1 – sandy stage; 2 – sticky stage; 3 – dough-like stage; 4 – viscous stage

The sandy stage begins immediately after mixing the components, and depending on the temperature it can last from 30 s to 5 min. In this case, only the swelling of the finely divided polymer in the monomer begins. It occurs on the surface of the powder particles and depends on their dimensions. In this regard, the polymerization system has no plasticity and the material contains a large amount of unbound monomer. For some systems there is no sand stage. The sticky stage is characterized by the appearance of yarns, sticky mass properties and great ductility and flowability, with the material having high adhesion. The dough-like stage is characterized by high plasticity, low fluidity and lack of tackiness. At this stage, the reaction mass can be formed into different products. The rate of transition of the system from the plastic stage to the dough-like one for all polymer matrices is practically the same and increases with the increase in their dispersion. The viscous stage is characterized by the preservation of a given shape of the material, even with a short-term mechanical action and precedes the complete curing of the material. The duration of these stages determines the area of use of the developed compositions: either for glutinous materials, for compounds or for putty. The presence of this or that stage can be regulated by mixing times, by the ratio of the monomer and polymer phases. All these stages are the result of such chemical and physico-chemical processes between the polymeric and monomeric phases as wetting, swelling, dissolution, polymerization. These stages differ in the different degree of swelling of the polymer matrix, different ductility, fluidity, tackiness, and residual monomer content.

The technological recommendations were developed depending on the further use of the compositions. For glues the mixing time should not be more than 2-2.5 minutes, for putties - 3-4 minutes, for compounds - 5-6 minutes. To prevent the formation of air voids in the composition, it is necessary to add the monomer phase to the fine polymer powder in small portions.

The obtained modified materials on the basis of the developed MMA-copolymer compositions have with rather high operational properties, such as surface hardness, Vicat softening temperature, adhesive bond strength to supports

of different nature (Fig. 9).

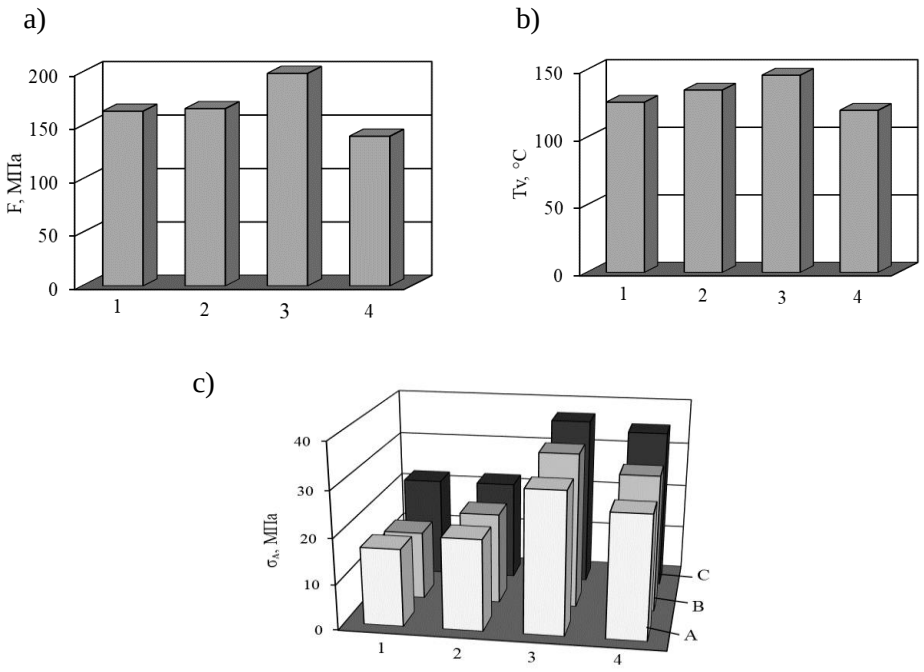

Fig. 9. Surface hardness (a), Vicat softening temperature (b) ma the strength of adhesive bonding (c) MMA – PVP-gr-PMMA compositionsdepending on comonomer nature: 1 – without comonomer; 2 – VP; 3 – GMA; 4 – HEMA. Nature of support material: A – steel/steel; B – ceramics/ceramics; C – steel/PMMA

It is established that the surface hardness and Vicat softening temperature depends on the nature and conditions of synthesis of the polymer matrix, and also on the nature of the comonomer. The addition of bifunctional GMA to the composition results in a significant increase in surface hardness and heat resistance. It may be caused by the formation of more structured materials. Vinylpyrrolidone increases these values, apparently as a result of the formation of a more uniform structure due to the better swelling of the copolymer that contains the PVP units in the monomeric phase. The introduction of comonomers with polar groups into the composition leads to an increase in the strength of the adhesive compound of polymethylmethacrylate materials.

The content of the filler has a significant influence on the surface hardness and Vicat softening temperature. The introduction of SiO_2 and the heat treatment at 333 K lead to an increase in the surface hardness (193 MPa) and Vicat softening temperature (126 °C).

However, process shrinkage (0.1 - 1.0 %), water absorption (0.8-1.2 %),

thermomechanical properties, chemical stability in acidic and alkaline media, are also dependent on the conditions of synthesis of the polymer matrix, the nature of the comonomer and filler. The materials that contain comonomers such as HEMA and VP, as well as copolymers with a large number of PVP units, ehibit increased water absorption. At the same time, heat treatment as a result of changes in the supramolecular structure leads to a decrease in water absorption. The calculated diffusion coefficients (7.0 ... $7.6 \cdot 10^{-7}$ sm^2/s), sorption coefficients (1.9 ... $2.3 \cdot 10^{-2}$ g/sm^3), permeability (17.1 ... $17.5 \cdot 10^{-9}$ $g \cdot sm/(sm^2 \cdot s)$ of chemical reagent (NaOH, H_2SO_4) in the sample indicate a sufficiently high chemical stability of the developed materials in acidic and alkaline media.

Polymerization of compositions HEMA-PVP in the presence of mineral fillers under the action of ultrasound was used to obtain porous osteoplastic composites. As mineral fillers, montmorillonite, hydroxyapatite and wollastonite were used. The results of kinetic studies of these compositions are presented in Table 1.

Table 1. Influence of ultrasound on the rate of polymerization of compositions (content of benzoyl peroxide – 1 мас. %, $AgNO_3$ – 1 мас. %, intensity 50 W, T = 298 K)

Polymer-monomer composition, wt. p			$V_p \cdot 10^3$, mol/l·s	«Limit conversion» of monomer, %	Time to achieve «limit conversion», s
HEMA	PVP	filler			
10	0	0	0	-	-
7	3	0	22	90	190
7	3	7 hydroxyapatite	104	94	40
7	3	7 wollastonite	118	96	35
7	3	7 montmorillonite	166	95	25

Studies have established that homopolymerization of HEMA in homogeneous conditions does not occur. In the presence of PVP without filler, the composition is polymerized at a moderate rate. Mineral fillers create a heterogeneous medium in compositions. As a result, in the presence of the filler under the action of ultrasound, polymerization occurs very quickly with the simultaneous foaming of the compositions. This provides additional technological advantages when creating a technology for the production of porous composites.

Studies have established that homopolymerization of HEMA in homogeneous conditions does not occur. In the presence of PVP without hydroxyapatite, the composition is polymerized at a moderate rate. Mineral fillers create a heterogeneous medium in compositions. As a result, in the presence of the filler under the action of ultrasound, polymerization occurs very quickly with the simultaneous foaming of the compositions. This provides additional technological advantages when creating a technology for the production of porous composites.

The use of ultrasound allows for polymerization at room temperature even in the presence of argentum salts in the reaction medium, which are known to slow down polymerization somewhat. Thus, by polymerization in the ultrasound field, a high degree of conversion of monomer into a polymer is achieved in a relatively short time. This will significantly intensify the process of obtaining porous composites and increase its productivity.

The presence of the salts of the argentum in the initial composition allows us to obtain silver nanoparticles in the composite structure and to give the composites the fungybactericidal properties [9].

4. Conclusions

Monomer-polymer compositions based on MMA and graft copolymers PVP-gr-PMMA or PVP-gr-PS have a high reactivity at room temperature. It can be regulated by the nature of the polymer matrix, the introduction of comonomers and fillers due to the influence of physicochemical factors on the polymerization process. Materials based on the developed compositions have low content of the residual monomer and sufficiently high operational properties such as surface hardness, heat resistance, adhesion to supports of different nature.

The developed materials can be used in various industries as compounds, adhesives, osteoplastic porous composites for replacement of damaged bone tissue and also in dentistry as components of filling materials, toning lacquers, protective coatings.

References

[1] Laila M. Al-Harbi, Samia A. Kosa, Musa K. Baloch, Qaisar A. Bhatti, and El-Sayed El-Badawey H. El-Mossalamy, Adsorption of Polyvinylpyrrolidone over the Silica Surface: As Affected by Pretreatment of Adsorbent and Molar Mass of Polymer Adsorbate, International Journal of Polymer Science, vol. 2016, Article ID 2417292, 9 pages, 2016. doi:10.1155/2016/2417292

[2] J. Sikora, V. Levytskyi, V. Moravsky, H. Gerlach, Twin screw extrusion with Expancel foaming agent, Journal of Polymer Engineering. vol. 33, no. 6, pp. 501-508, 2013.

[3] V. Levytskyi, A. Masyuk, D. Samoiliuk, L. Bilyi, T. Humenetskyi, Morphology and properties of polymer-silicate composites and polyester materials based on them, Materials Science, vol. 52, no. 1, pp. 17-24, 2016.

[4] V. Levytskyi, A. Masyuk, D. Katruk and M. Bratychak, Regularities of obtaining, morphology and properties of metal-containing polymer-silicate materials and polyester composites on their basis, Chemistry & Chemical technology, vol. 10, no. 1, pp. 35-40, 2016.

[5] V. Skorokhoda, Yu. Melnyk, V. Shalata, T. Skorokhoda, S. Suberliak, An investigation of obtaining patterns, structure and diffusion properties of biomedical purpose hydrogel membranes, Eastern-European Journal of Eenterprise Technologies, vol. 1, no. 6 (85), pp. 50-55, 2017.

[6] S. Davtyan, A. Tonoyan, A. Varderesyan, S. Muller, Frontal copolymerization in the presence of nano-particles, European Polymer Journal, vol. 57, pp. 182–186, 2014.
[7] Niels M.B. Smeets, Amphiphilic hyperbranched polymers from the copolymerization of a vinyl and divinyl monomer: The potential of catalytic chain transfer polymerization, European Polymer Journal, vol. 49, no. 9, pp. 2528–2544, 2013.
[8] A.M. Oliveira, K.L. Guimarães, N.N.P. Cerize,The role of functional [monomers on producing nanostructured lattices obtained by surfactant-free emulsion polymerization – A novel approach, European Polymer Journal, vol. 71, pp. 268–278, 2015.
[9] P. Klemarczyk, J. Guthrie, Advances in anaerobic and cyanoacrylate adhesives, Advances in Structural Adhesive Bonding. A volume in Woodhead Publishing Series in Welding and Other Joining Technologies, pp. 96–131, 2010.
[10] H. Kilambi, S.K. Reddy, L. Schneidewind, J.W. Stansbury, C.N. Bowman, Copolymerization and dark polymerization studies for photopolymerization of novel acrylic monomers, Polymer, vol. 48, no. 7, pp. 2014-2021, 2007.
[11] L. Liu, W. Feng, X. Lü, W.-K. Wong, First example of near-infrared (NIR) luminescent $Yb_4(Salen)_4$-containing metallopolymer through radical copolymerization with MMA (methyl methacrylate), Inorganic Chemistry Communications, vol. 75, pp. 29–32, 2017.
[12] S. Pal, B. Banoth, G. Rahithya, A. Dhawan, P. De, Copolyperoxides of 2-(acetoacetoxy)ethyl methacrylate with methyl methacrylate and styrene; Synthesis, characterization, thermal analysis, and reactivity ratios, Polymer, vol. 53, no. 13, pp. 2583-2590, 2012.
[13] H. Lutz, H.-P. Weitzel, W. Huster, 10.27 – Aqueous Emulsion Polymers, Polymer Science: A Comprehensive Reference, vol. 10, pp. 479–518, 2012.
[14] X. Liu, Z. Wu, F. Zhou, D. Li, H. Chen, Poly(vinylpyrrolidone-b-styrene) block copolymers tethered surfaces for protein adsorption and cell adhesion regulation, Colloid Surf B – Biointerf, vol. 79, pp. 452–459, 2010.
[15] K. Shen, D. Qi, Y. Li, X. Zhao, Y. Li, Controlled emulsion polymerization of styrene and methylmethacrylate in the presence of amphiphilic tertiary amine N-oxides, Colloids and Surfaces A: Physicochemical and Engineering Aspects, vol. 482, pp. 728–733, 2015.

Volodymyr Moravskyi[9], Iryna Dziaman[9], Andrii Masyuk[9], Anastasia Kucherenko[9], Oleksandr Grytsenko[9], Ludmila Dulebova[10]

TECHNOLOGY OF METALLIZATION OF POWDER-LIKE POLYMERS RAW MATERIALS

Abstract: *The technology of metallization of suspension powder-like PVC which includes its mechanical activation with subsequent copper plating of polymeric activated surface in chemical recovery solutions has been developed. The results of experimental studies of peculiarities of mechanical activation of powder-like polyvinylchloride with zinc are given. The influence of the ratio of powder-like polyvinyl chloride and finely dispersed zinc, the processing time and the degree of loading of the ball mill on the activation efficiency of the polymeric surface has been investigated. The kinetic regularities of the metallization of mechanically zinc-activated powder-like polyvinyl chloride in chemical recovery solutions are presented. The influence of the pH of the medium and amount of the metallic activator on the rate of copper deposition on the activated polymeric surface is investigated. It has been established that changing of the pH of medium can effectively influence at the process of metallization.*

Keywords: *metal-polymer composites, metal fillers, activation, polyvinyl chloride, zinc, ball mill, chemical recovery, reaction rate.*

1. Introduction

The widespread use of polymer composites is show by the analysis of trends in the development of promising materials and technologies. The particular interesting among these composites are electrically conductive metal-filled polymer materials [1, 2]. A wide range of practical use of such materials is due to the complex of their valuable properties [3]. In the simplest case, the electrically conductive metal filled polymer composite consists of finely dispersed metal particles that are uniformly distributed in the polymer matrix. The main disadvantage of such system is that at low concentrations of metal particles, they remain isolated from each other and do not contribute to the conductivity of the system. The next increase of concentration of the filler worsens the mechanical properties of the system.

Thus, the creation of polymer composites that combine good electrical and mechanical properties is a complex task and represents a significant practical interest. The creation of metal filled composite materials with high technological and operational properties requires the development of alternative technological solutions for their obtaining. The main disadvantage of traditional technologies

[9)] *National University Lviv Polytechnic, Department of Plastics Engineering, st. S.Bandera, 12, 79013 Lviv, Ukraine, e-mail: vmoravsky@gmail.com*

[10)] *Technical University of Kosice, Department of Engineering Technologies and Materials, Faculty of Mechanical Engineering, Mäsiarska 74, 040 01 Košice, Slovakia, e-mail: ludmila.dulebova@tuke.sk*

of the production of metal filled composites is a significant reduction of their mechanical properties, as well as high concentrations of reaching the percolation threshold [4]. We have developed a new technology of the production of metal-filled polymer composites by metallizing the initial polymeric raw material with its subsequent processing by standard methods directly in the product [5-7].

A result, the process of combining of components is greatly facilitated and a uniform distribution of the metal filler in the polymer matrix is provided. Also, this technology is highly effective, resource-saving technological process and characterized by a reduced of production cycle.

The developed technology is based on the use of mechanical activation of the polymeric surface to provide it with catalytic activity before metal deposition in chemical recovery solutions [8]. The use of such activation technologies avoids the main drawbacks of the classical metallization technology: a large number of previous operations of preparing the surface of the polymer to provide it catalytic activity and the use of dangerous and expensive reagents. In case of simultaneously processed in a ball mill polymer material with a powder-like metal-activator is possible to avoid the multistage process of chemical activation of the surface. This treatment provides the surface of the polymer by the catalytic activity is required to form the base layer of the metal in solutions of chemical recovery. The effectiveness of the mechanical activation method is determined by at least two factors: reducing the number of technological operations and reducing the number of expensive and harmful chemical reagents.

In the early stages of the development of the technology for the production of metal-filled polymer composites a granular polymer material was used [9, 10]. As the results showed, the significant disadvantage of the use of such raw materials is the limited content of metal that can be introduced into the final composite. A low specific surface area of granular materials does not allow the production of high-metal composites. An increase of the amount of metal can only be achieved by increasing its thickness on the surface of the granule, which is inexpedient. Proceeding from the above, it is necessary to increase the surface area of the output polymeric raw material, which can be achieved using polymers in the form of powder.

2. Investigation of the activation effectiveness of powder-like PVC

A significant difference in the size of the particles of the polymer and the metal-activator made possible the implementation of the process of activation of powder-like polyvinyl chloride with finely divided zinc (Fig. 1). The activation of the polymeric surface was carried out in a laboratory ball mill in a volume of 4 l with ceramic cylindrical grinding bodies and a speed of rotation of 100 rpm. Suspension PVC and fine zinc powder were loaded into the mill. During the rotation of the mill there was a fixation of the metal activator on the polymeric surface. The amount of PVC loaded in the mill was 50 g, zinc 3-15 g, the mass of milling bodies 1.5 kg.

The use of polymers in the form of highly dispersed powders poses a difficult task to study of the process of their activation. Since both the polymeric raw material and the metal-activator are highly dispersed powdered substances, it is impossible to predict whether occurs during of the activation process fixing of metal particles on the polymeric surface (activation), or a simple mechanical mixture of powdered substances is formed.

The formation of a mechanical mixture of powdered substances during processing in a mill is unacceptable. In this case, during the subsequent deposition of the metal in the solutions of chemical recovery will occur not on the polymeric surface, which eliminates all the advantages of the proposed technology (uniform distribution of the metal filler in the polymer matrix at the stage of formation of the product).

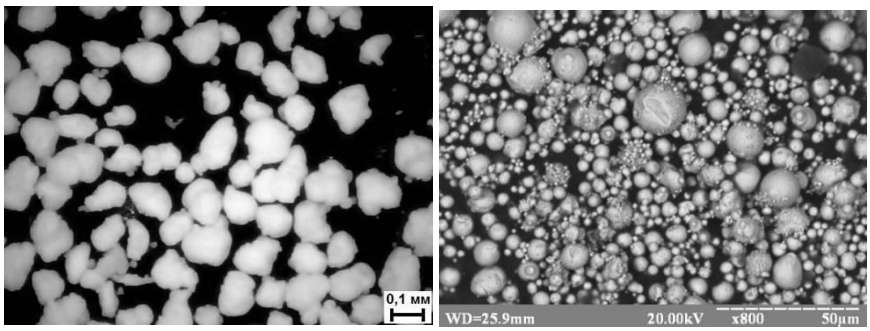

a) *b)*

Fig. 1. Microphotographs of suspension PVC (a) and zinc powder (b).

Investigation of the effectiveness of activation of powder-like polymers was carried out using a plant that provides the possibility of transferring the activated powder of a polymer into a fluidized state with simultaneous vibration exposure (Fig. 2). The simultaneous use of vibration and fluidization is needed to the condensation of a layer of a powder-like polymer under the action of vibration, which prevents the system from being split into separate fractions by density. The transfer of the test mixture to the fluidized state provides the necessary mobility of the components, which contributes to the rapid and maximally complete separation of the system by density.

Using only fluidization for system separation according to density is also less effective as a result of the presence of significant circulation flows, which, due to the small size of metal particles, contribute to the admixture of individual fractions.

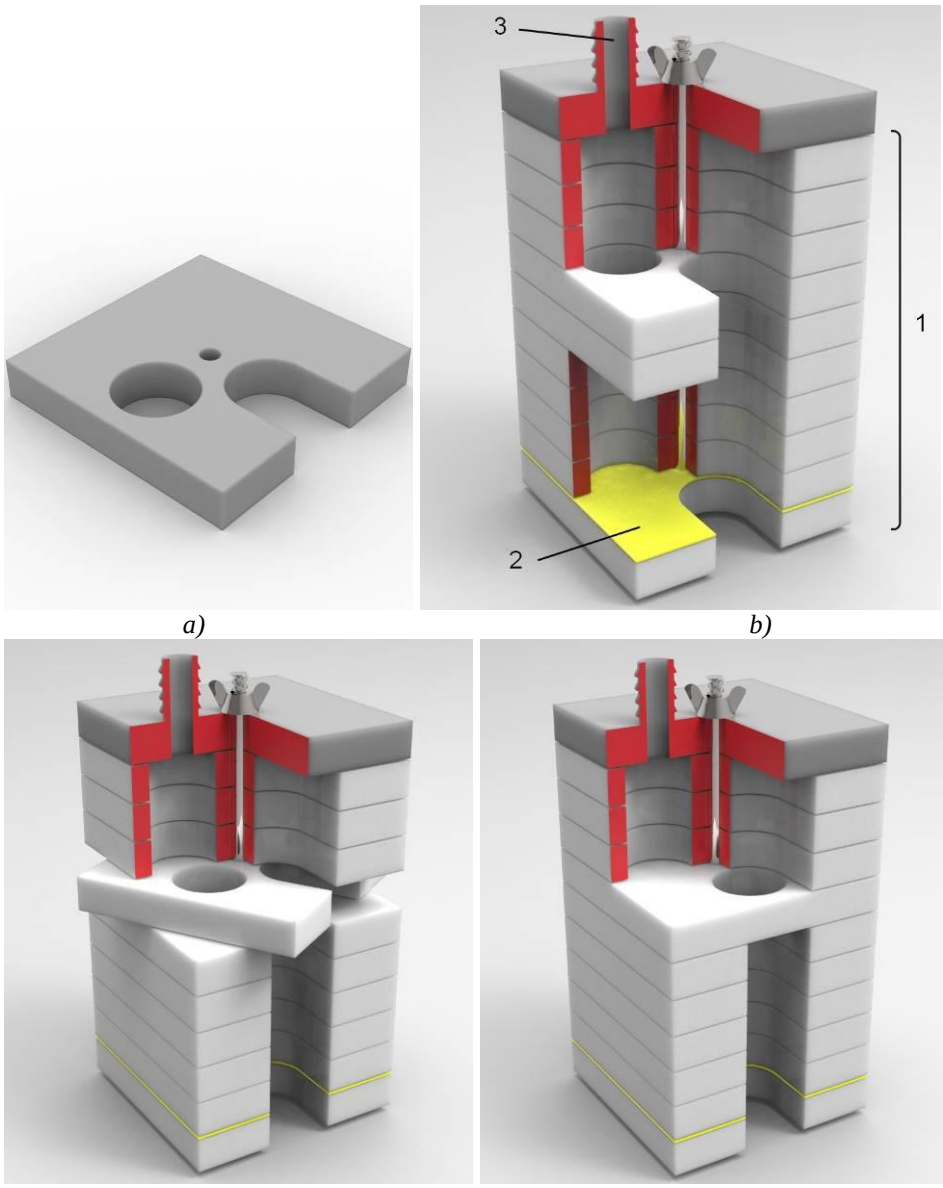

Fig. 2. The plant for investigating the activation efficiency of powder-like polymers a) rotating segment; b) the look of plant with local cuttings; c, d) rotation and position of the segment for unloading of separate fractions of activated polymer after separation: 1 - rotating segments, 2 - filter, 3 - supply of vacuum

The velocity of air flowing through the polymer layer must prevent the compaction and provide the required mobility of the components of the system

(polymer, metal, polymer with metal) for the possibility of their separation under the action of vibration and not cause a significant circulation in the layer, resulting in a density equalization by the height of the material layer. The design of the plant provides the opportunity after the mixing, unloading of individual fractions, which are divided by density of the height of the cylinder. After unloading, the percentages of metal in each fraction were determined. The fraction of the activated polymer was weighed to 0.00005 g, processed with 50% nitric acid and after filtering, washing and drying to constant weight again weighed. The activation efficiency was estimated by the difference in the percentage content of the metal in the upper fraction (X_U) and in the lower (X_L): $E = X_U / X_L$.

$$X_{U(L)} = \frac{m_F - m_T}{m_T} \cdot 100 \quad (1)$$

Where m_F is the mass of the fraction of the activated polymer, m_T is the mass of the fraction after digestion, washing and drying.

To determine the activation effectiveness of the powder-like polymeric raw materials, a number of studies on the activation of suspension of polyvinyl chloride powder with different amounts of finely divided zinc have been conducted (Fig. 3). The obtained results indicate that the activation efficiency increases with an increase in the amount of zinc in the mixture. This is due to the fact that at low amount of zinc, it's not sufficient for the uniform activation of all polyvinyl chloride. There is a certain amount of pure polymer that is unbound with zinc particles. With an increase in zinc content in the composition, the proportion of such unactivated PVC decreases, this leads to an increase of activation efficiency.

The dependence of the activation efficiency on the content of finely divided zinc has a maximum in the range of zinc content of 9-11 g. This is due to the increase in the amount of zinc unscrewed on the polymeric surface. The extra metal introduced into the mixture with PVC is not able to stick to its surface as a result of steric obstructions, which create already fixed particles on the surface of the metal. For a strong fixation of metal particles on a polymeric surface, a certain magnitude and direction of application of mechanical action (loading) is necessary, providing the necessary depth of penetration of a particle in a volume of a polymer. Schematically this assumption is shown in Fig. 4a.

With an increase in the amount of metal-activator conditions are created in which already fixed metal particles also perceive part of the load that acts on a new metal particle (Fig. 4 b). This reduces the penetration depth of the metal particle into the polymer and the make to impossibile of its firm fixation on the polymeric surface. The polymeric surface is characterized by the limit value of saturation, which is caused by steric obstacles.

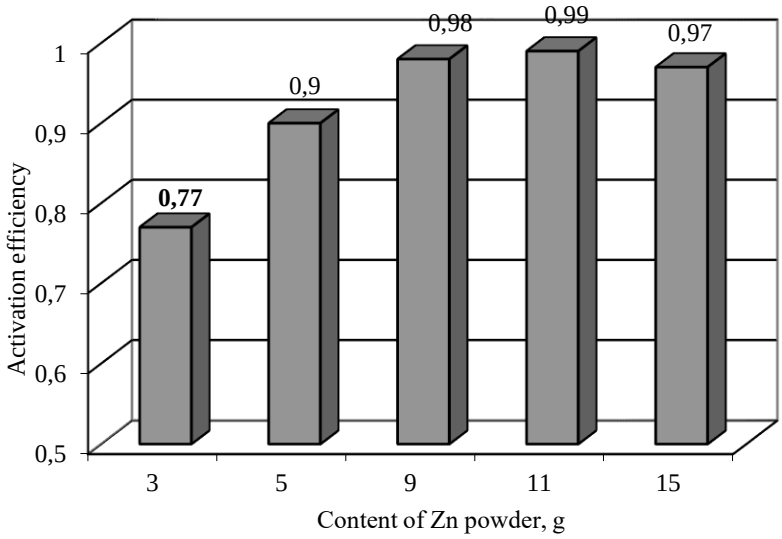

Fig. 3. Dependence of the activation efficiency on the content of finely divided zinc in a mixture with powder-like PVC. Processing time in ball mill 2 h.

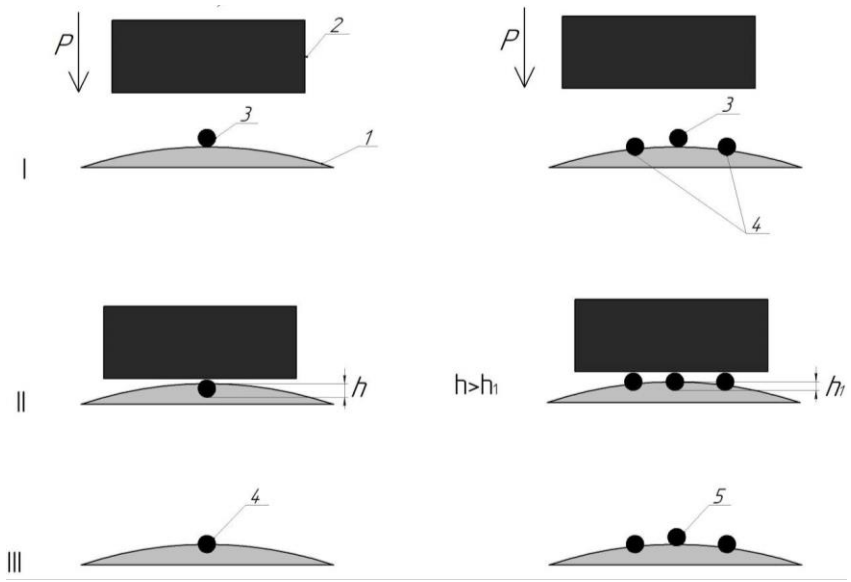

a) *b)*

Fig. 4. Schematic representation of the process of activating of the polymeric surface
a) fixing the metal particles on the polymeric surface,
b) influence of the fixed metal particles
1 – polymer particle, 2 – surface of a mill or inguinal body, 3 – metal-activator particle, 4 – fixed metal-activator particle, 5 – not fixed metal-activator particle.

To confirm this activation mechanism, microscopic studies were carried out using an optical microscope of mixtures of 50 g of PVC with 7, 9, 11 and 20 g of zinc after two hours of processing in a ball mill (Fig. 5). Microphotographs obtained using an optical microscope show that a mixture of 20 g zinc is characterized by practically the same distribution of metal-activator particles on a polymeric surface as compared to mixtures with lower metal content.

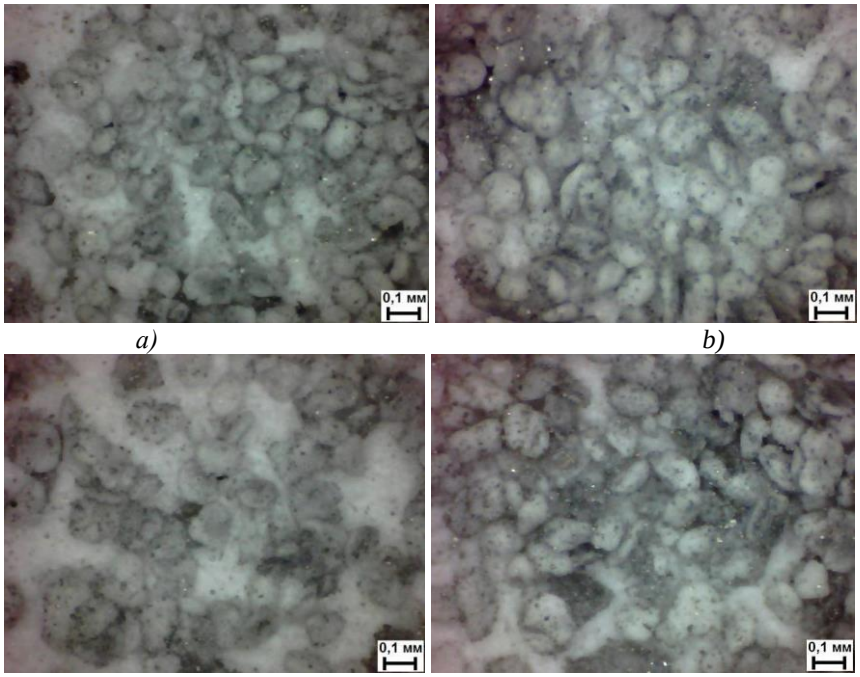

a) *b)*

c) *d)*

Fig. 5. Microphotographs of powder-like PVC activated by zinc. Processing time in ball mill 2 h. Zinc content: a) 7, b) 9, c) 11, d) 20.

Using a scanning electron microscope, it was possible to conduct an investigation of activated polyvinyl chloride in the mode of contrast on the average atomic number and to detect the spectrum of characteristic X-ray radiation of the regions corresponding to the highest atomic number (Fig. 6). The obtained results confirm the presence of zinc particles on the surface of polyvinylchloride, as evidenced by the presence of zinc and chloride peaks on the spectrum of characteristic X-rays.

To determine the effect of zinc content on the time when maximum activation efficiency was achieved during processing in a ball mill, mixtures of 50 g of PVC with 9 and 15 g of Zn (Fig. 7).

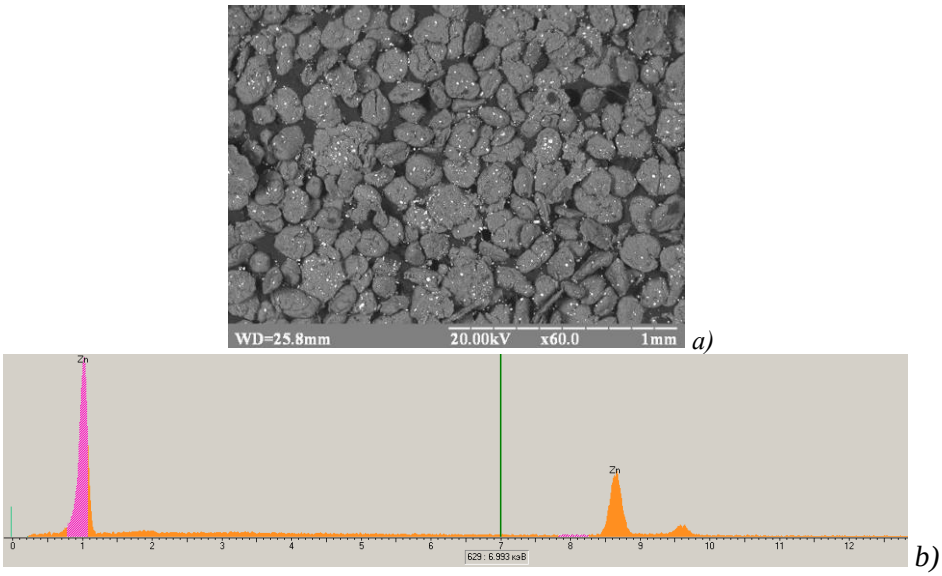

Fig. 6. a) Microphotographs of a surface of powder-like PVC activated by zinc obtained in the mode of contrast on the average atomic number; b) Spectrum of characteristic x-ray of the surface field corresponding to the highest atomic number of powder-like PVC. Processing time in ball mill 2 h. The content of zinc is 5 g

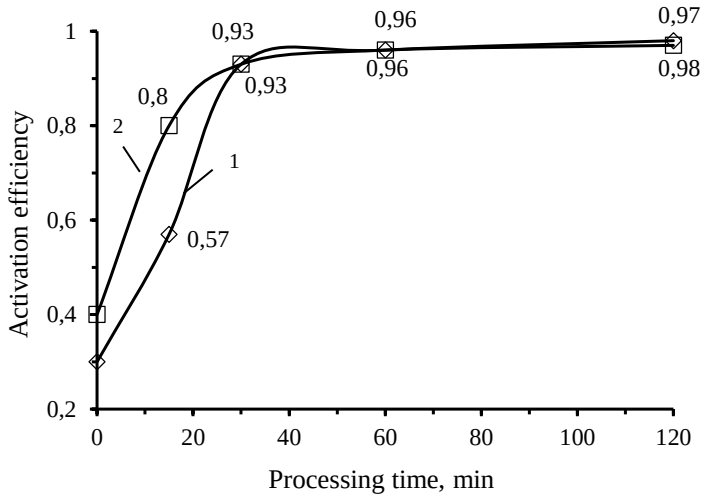

Fig. 7. The dependence of activation efficiency on processing time in the ball mill mix 50 grams of powder-like PVC 9 g Zn (1) and 15 g Zn (2)

The optimum processing time of the mixture in a ball mill is about 30 minutes and does not depend on the content of zinc in the mixture. The next increase of processing time significantly affects on the growth of activation efficiency and is inappropriate.

In order to intensify the activation process of powder-like PVC, a number of studies have been carried out with different speeds of ball mill (Fig. 8), as well as increased loading of grinding balls and a mixture of polymer with metal-activator (Table 1).

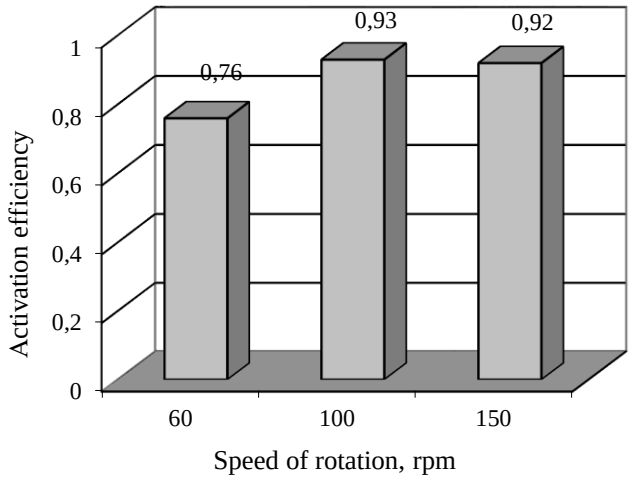

Fig. 8. Influence of the spin speed on the efficiency activation of the mixture of 50 g PVC and 9 g Zn. Processing time 30 min

The speed of rotation of a ball mill is most influenced by the activation efficiency in the range of speed 60-100 rpm and the subsequent increase in speed does not significantly influencby the activation efficiency.

Table 1. Influence of ball mill loading on activation efficiency. Processing time 30 min. Speed 100 rpm

No	Mass of components of the mixture, g		Zinc content wt.%	Weight of balls, kg	Activation efficiency
	PVC	Zn			
1	50	9	15.3	1.5	0.93
2	100	18	15.3	1.5	0.95
3	50	9	15.3	2.2	0.96

In the case of an increase the degree of loading of a ball mill, both the grinding balls and the initial mixture, the efficiency of activation increases slightly. It should be borne in mind that with a greater degree of load of the mill by a mixture

of polymer with metal increases the efficiency of the use of equipment and decreases energy costs.

As a result of processing in a ball mill of a mixture of powder-like polyvinyl chloride with fine-divided zinc there is a strong interaction between the surface of the polymer and the metal-activator.

Such interaction is a prerequisite for the next stage of metallization and for the production of high-performance metal-filled polymeric composites.

The activation efficiency is largely determined by the speed, the degree of loading and the ratio of components, which allows set the optimal parameters for the process.

3. Kinetic regularities of copper plating of activated PVC surface

For obtaining metal filled polymer composites for the developed technology, the method of introducing of metal filler into a polymer matrix as a result of the metallization of the surface of the polymeric raw material is used. The main stage of such method is the process of metalizing the polymer surface, which will determine the final properties of the composite material. Therefore, the information on the kinetic regularities of metal recovery on the polymeric surface is necessary for obtaining composites with adjustable and predetermined properties.

The metallization of the activated polymeric surface was carried out in non-stabilized solutions of chemical copper plating using the following reagents: $CuSO_4$; NaOH; formaldehyde; EDTA-Na_2.

A volumetric method was used to investigate the kinetics of copper reduction in solutions of chemical metallization. This method is based on measuring the amount of hydrogen emission during copper recovery [11]. The recovery of copper ions by formaldehyde occurs according to the following scheme:

$$2\,CH_2O + Cu^{2+} + 4OH^- \rightarrow Cu\downarrow + H_2\uparrow + 2HCOO^- + 2H_2O \qquad (2)$$

1 mole of hydrogen is emission per 1 mol of recovery copper, which is the basis for studying the kinetics of copper recovery by measuring the volume of hydrogen recovered. It should be noted that in the classical technologies of copper plating to activate the polymer surface using other methods (recovery of precious metal salts on a polymeric surface) which can not affect the amount of emission hydrogen.

In the proposed technology for activating the polymer surface, a metal-activator (zinc) is used which reacts with copper sulfate, which occurs without hydrogen emission:

$$CuSO_4 + Zn \rightarrow Cu\downarrow + ZnSO_4 \qquad (3)$$

In the solution of chemical copper plating, simultaneously or successively undergo two competing chemical reactions between them, which result in the recovery of copper ions.

The results obtained during the study of the kinetics of copper recovery show a significant dependence on the nature of the resulting kinetic curves from the initial pH of the solution. The graph (Fig. 9) shows three types of kinetic copper recovery curves, which represent the averaged values of a number of studies.

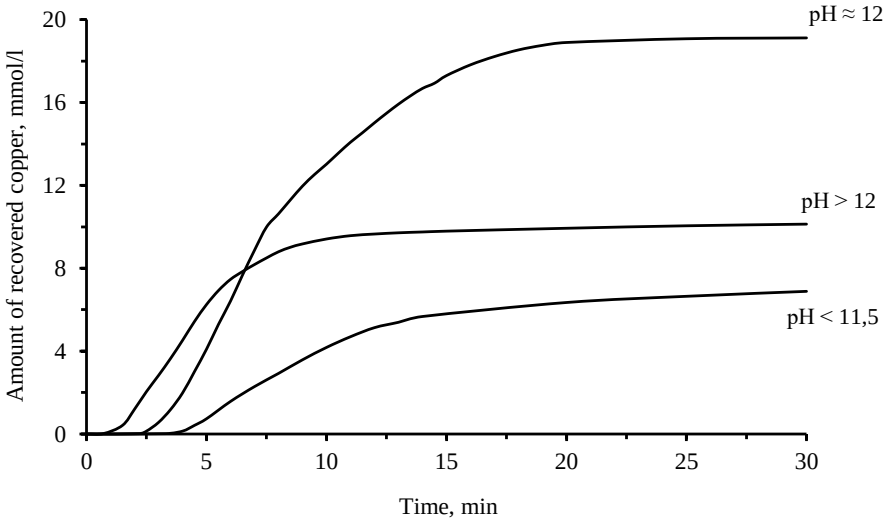

Fig. 9. Dependence of the rate of copper recovery on the activated PVC surface. The content of zinc is 15.3 wt% (a mixture of 50 g of PVC and 9 g of Zn)

Consider the recovery of copper for each of the 3 types of kinetic curves. The recovery of copper ions by formaldehyde occurs according to a scheme in which 4 moles of alkali per 1 mol of reconstituted copper is consumed.

In the case of kinetic curves of the first type (pH<11.5) at initial concentration of $CuSO_4$ at the level of 48 mmol/l, the alkaline concentration of 152.5 mmol/l is not sufficient to completely pass the reaction (at a given alkaline concentration, the initial pH of the chemical copper plating solution is 11.44). This concentration of alkali does not provide the required pH value to maintain the copper recovery reaction with formaldehyde (pH 12-12.5). In this case we see a low reaction rate and a small amount of recovered copper (by volume dedicated hydrogen), which also indicates the color blue, which remains after stopping of the reaction.

The reaction of copper recovery, which is described by the kinetic curve of the second type (pH≈12), is when the alkaline content is increased to 250-268.8 mmol/l (pH=11.92-12.06). Such a concentration of alkali is sufficient for passing the reaction, and for maintaining the required pH level. The reaction takes place with high speed and significant emission of hydrogen. The resulting solution after 20 minutes is colorless and clear.

Passage of the reaction of the third type (pH>12) occurs with a significant increase in alkaline content to 562.5-1500 mmol/l and leads to a slight increase

in pH of the solution (pH = 12.16-12.34). As a result, the growth of the reaction speed and the reduction of the time during which the solution becomes colorless and transparent (10 min).

Similar results were obtained for activated PVC containing 23.1 and 28.6 wt% of zinc (a mixture of 50 g PVC and 15 g Zn and a mixture of 50 g PVC and 20 g Zn).

Measurement of the pH of the chemical metallization solution after the end of the copper recovery reaction also showed an interesting pattern (Fig. 10).

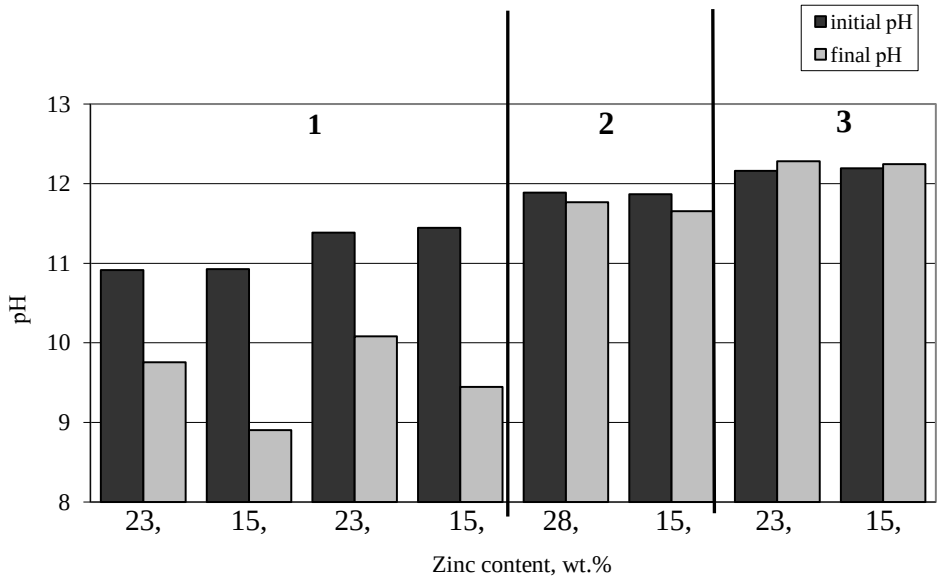

Fig. 10. The dependence of the pH of the solution upon completion of the reaction from the initial pH of the solution and the content of the metal- activator

The greatest difference between the initial and final pH is for solutions of the first type with low alkaline concentration. This feature is explained by the consumption of alkali during the copper ion copper recovery reaction. The same the dependence between the initial and final pH is observed for solutions of the second type, however, in this case, the change in the pH value is much smaller. For solutions of type 3 there is an opposite dependence, pH of solutions after the reaction is slightly higher than the initial pH of the solution. An increase of the pH of the solution can be attributed to the significant excess of alkali in the solution, which increases the pH after exhaustion of reagents that lower the pH of the solution ($CuSO_4$, formaldehyde).

In the case of low alkaline concentrations, the effect of the metal activator on the pH of the solution after the reaction is also observed. A more significant decrease of pH of the solution is observed during the copper plating of activated

PVC, which contains less amount of metal activator. That can be explained by a deeper passage of the reaction of copper recovery with the use of formaldehyde and alkali (1). On the contrary, with increasing metal-activator content, more copper is recovered as a result of exchange reaction with zinc (2). The consumption of alkali at the first reaction is less and the pH of the solution after the reaction is higher.

The confirmation of the assumptions made about the increase of metal-activator and consequently recovered copper can serve kinetic curves of copper recovery (Fig. 11).

Since the amount of the recovered copper was estimated by the volume of the isolated hydrogen, the given kinetic curves show the proportion of copper that was restored as a result of interaction with the formaldehyde by reaction (1). The amount of recovered copper by reaction (1) decreases with increasing of metal-activator content. This feature is more prominent at higher values of the pH of the solution.

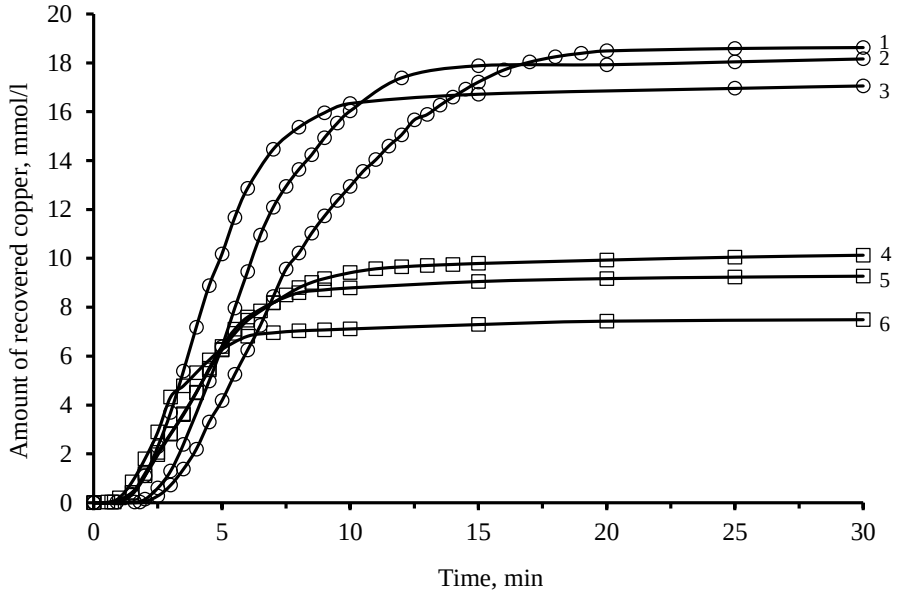

Fig. 11. Kinetic curves of copper recovery on activated PVC surface. Zinc content: 1, 4 - 15.3 wt. %; 2, 5 - 23.1 wt. %; 3, 6 - 28.6 wt. %;. 1-3 - initial pH of the solution ≈11.9; 4-6 - initial pH of the solution ≈12.2

Is necessary to note the significant effect of the pH of solutions on the mechanism of recovery of copper ions. In Fig. 12 shows the dependence of the amount of hydrogen emission from the initial pH of the solution for activated PVC.

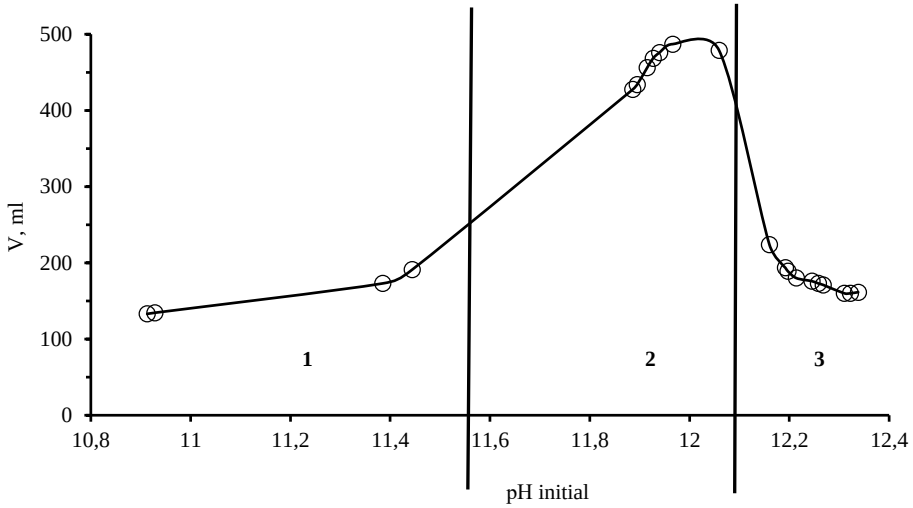

Fig. 12. Dependence of the amount of hydrogen emission from the initial pH of the solution. The content of zinc is 15.3 wt. %

Maximum hydrogen emission is observed for pH value of about 12. It can be argued that at this pH there are the best conditions for the recovery of copper ions by formaldehyde. Increasing the pH of the solution to values above 12.1 reduces the amount of copper recovered by formaldehyde and facilitates the passage of the exchange reaction with zinc.

It can be concluded that in solutions of chemical copper plating using activated PVC simultaneously there are two competing copper recovery reactions. The volumetric method of kinetics research in this case, obviously, needs to be combined with chemical or gravimetric methods, in order to account for the amount of copper recovered as a result of interaction with zinc.

The volumetric method is a convenient tool for setting the time of end of the reaction, as shown by the results of research on the termination of the emission of hydrogen means the termination of the recovery of copper.

To confirm the assumption that during copper plating of activated PVC the copper part is recovered as a result of the reaction with zinc (without hydrogen emission), a re-metallization study of the raw material on which is the copper layer (Fig. 13).

In the case of the use of already metallized raw materials, the rate of recovery and the yield of copper (determined by the amount of emissed hydrogen) are significantly higher. The yield of copper in this case reaches practically theoretically possible level, that is, all copper that was introduced into the solution in the form of $CuSO_4$ is recovered by the reaction (1) with the emission of hydrogen.

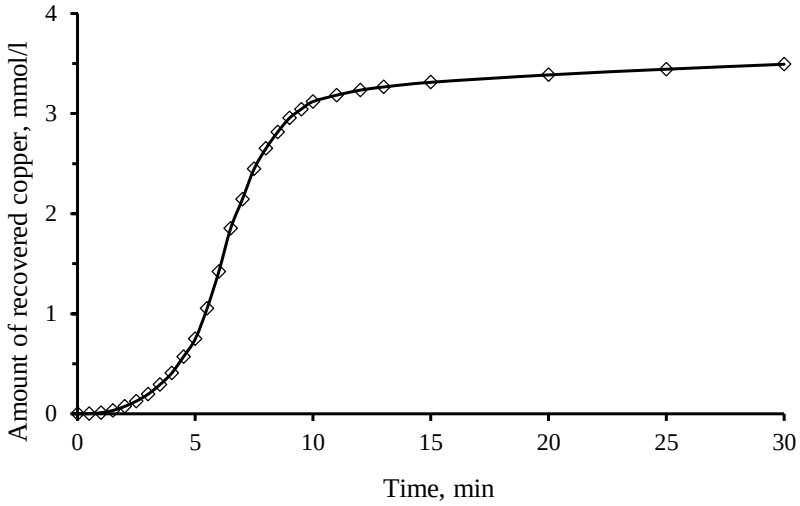

Fig. 13. Dependence of the rate of copper recovery on the copper plated surface of PVC. Initial pH = 12,11

Properties of metal filled composites obtained according to the developed technology will greatly depend on the uniformity of metallization of polymeric raw materials. The key factor that will affect this indicator is the effectiveness activating of PVC. In order to establish the impact of the activation efficiency of PVC on uniformity of copper recovery were examined samples of copper plated PVC using developed technique of research efficacy of activation (Fig. 14).

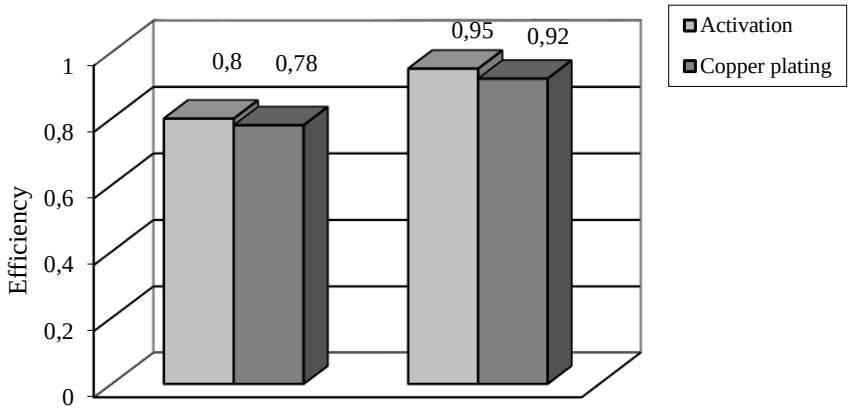

Fig. 14. Dependence of the efficiency of copper plating of activated PVC from efficiency of activation of powder-like PVC

The uniformity of metallization of mechanically activated PVC particles in solutions of chemical recovery is determined by the value of the activation efficiency of powder-like PVC and is practically equal to it. Copper recovery occurs only on activated particles of PVC with the formation of a layer of metal which is fixed on the polymeric surface.

The obtained samples of copper plated powder-like polyvinyl chloride are characterized by a high degree of coating of particles by metal, which can be observed in the microphotographs obtained using optical and electronic microscopes (Fig. 15). On microphotographs of powder-like PVC particles are identifying areas that are coated and not covered with copper.

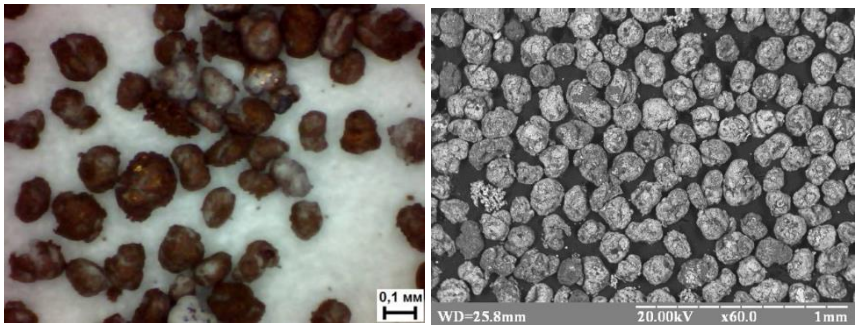

a) *b)*

Fig. 15. Optical (a) and electronic in contrast mode (b) microscopy of copper plated powder-like polyvinylchloride

The obtained results of the study of the kinetics of copper plating of active PVC show that the main parameter that determines the speed and efficiency of the metallization process is the initial pH of the chemical recovery solution.

4. Technology for the production of metallized powder-like PVC

The technological process for the production of metallized powder-like polyvinyl chloride can be realized in a periodic or semi-continuous method (Fig. 16).

By the periodic method, the measured quantities of powder-like PVC and zinc are loaded into a ball mill, which is processed for 30 minutes at a speed of rotation of 100 rpm. Further activated PVC through the intermediate capacity enters the reactor, which contains a chemical recovery solution.

In order to reduce the cooking time, the chemical recovery solution is prepared by mixing separately dissolved components. Immediately in the reactor dissolve NaOH followed by the addition of EDTA-Na_2. EDTA-Na_2 should be added after dissolution of the alkali, since its solubility in alkaline solutions is higher. On the contrary, the solubility of $CuSO_4$ in alkaline solutions is low, since the formed

copper hydroxide is a difficult soluble compound. The dissolution of $CuSO_4$ in water is carried out in a separate mixer. After dissolution, the $CuSO_4$ solution, when stirred, is merged into the copper reactor. Formalin is added to the reactor immediately before the introduction of activated PVC.

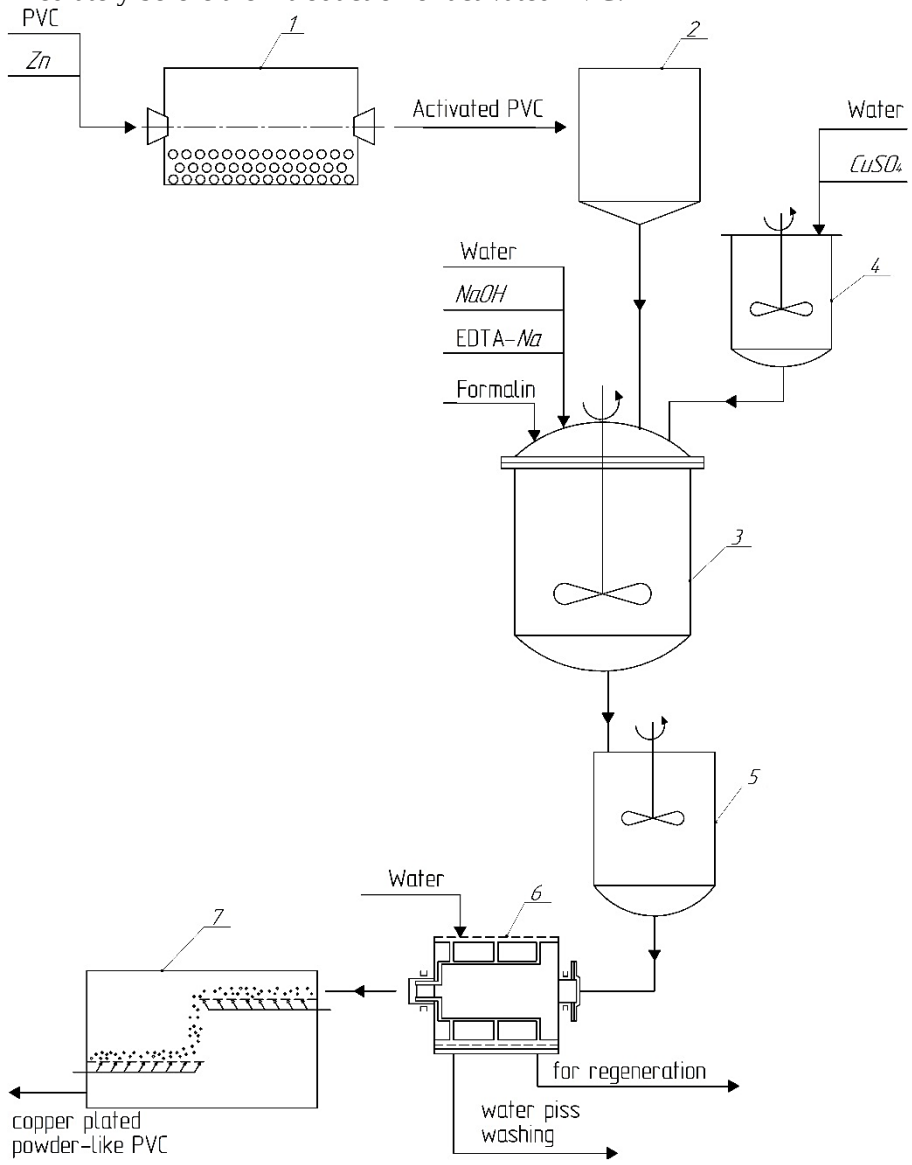

Fig. 16. Principle technological scheme for the production of metallized powder-like PVC. 1 - ball mill, 2 - intermediate storage capacity of activated PVC, 3 – copper plating reactor, 4 - mixer for dissolving $CuSO_4$, 5 - intermediate storage capacity of copper plated PVC, 6 - filter, 7 – dryer

The time of copper plating at pH of the solution 12.1-12.3 is about 10 minutes. For the separation of copper plated PVC from a metallization solution a drum filter is provided, which also includes flushing of copper PVC with water. The final operation is drying, for this purpose it is possible to use a fluidized-bed dryer or drum dryer.

In the semi-continuous method the activation of powdered PVC, the division of copper plated PVC from the metallization solution, washing and drying occurs continuously; stages of preparation of solutions and copper plating - periodically. For the possibility of implementing the process under this scheme provides for intermediate capacities, which are intended to accumulate and create the necessary stock of raw materials.

6. Conclusion

The proposed technology provides a transition from granular to powder-like activated polymeric raw material, which can significantly intensify the formation of a metal layer on the polymeric surface and increase the amount of metal that can be introduced into the final composite.

Molded on activated powder-like PVC the copper layer is not solid. This feature allows us to use plastisol technology to obtain elastic metal-containing composites, which will ensure the expansion of the range of end materials and products.

Acknowledgment

This work was supported with the project "Technology development for obtaining of constructional dispersed-filled polymer nanocomposites" (number of state registration is 0116U004410) and the European Union's Horizon 2020 research and innovation programme under the Marie Skłodowska-Curie grant agreement No 734205 – H2020-MSCA-RISE-2017.

References

[1] Los P., Lukomska A., Jeziorska R., Metal-polymer composites for electromagnetic interference shielding applications. Polimery 2016, 61, 10, 663-669.

[2] Leblanc J.L., Filled Polymers: Science and Industrial Applications. - CRC Press, Taylor & Francis Group, 2010. – 428.

[3] Delmonte J., Metal/polymer composites. – Springer, 2013. – 264.

[4] Luyt A.S., Molefi J.A., Krump H., Thermal, mechanical and electrical properties of copper powder filled low-density and linear low-density polyethylene composites. Polymer Degradation and Stability 2006, 91, 7, 1629-1636.

[5] Moravskyi V., Dziaman I., Suberliak S., Grytsenko O., Kuznetsova M., Features of the Production of Metal-filled Composites by Metallization of Polymeric Raw Materials. 2017 IEEE 7th International Conference on

Nanomaterials: Applications and Properties (NAP-2017) Vol.3. – Zatoka, Ukraine, September 10–15. – 2017. – P. 03NNSA18-1–4.
[6] Tymkiv I.A., Moravskyi V.S., Kachmarchyk I.V., Suberlyak O.V., Tekhnolohiyi metalizatsiyi polivinilkhlorydnoho plastyku ta oderzhannya kompozytu z pidvyshchenymy fizyko-mekhanichnymy vlastyvostyamy. Visnyk NU "L′vivs′ka politekhnika" 2015, 812, 414-418.
[7] Moravskyi V.S., Tymkiv I.A., Bodnarchuk P.T., Metalizatsiya polivinilkhlorydnoho plastykatu khimichnym vidnovlennyam v rozchynakh. Visnyk NU "Lvivska politekhnika" 2016, 841, 405-409.
[8] Moravskyi V.S., Dzyaman I.Z., Baran N.M., Kucherenko A.M., Dulebova L., Doslidzhennya efektyvnosti aktyvatsiyi poroshkopodibnoho polivinilkhlorydu. Visnyk NU "Lvivska politekhnika", 2017, 868, 413-418.
[9] Moravskyi V., Tymkiv I., Garbacz T., Duleba B., Metal-containing thermoplastic polyvinylchloride composites. In: Technological and design aspects of extrusion and injection moulding of thermoplastic polymer composites and nanocomposites. Vol. 3, [Red:] Sikora Janusz, Greškovič František, Suberlyak Oleh. – Lublin: Politechnka Lubelska, 2015,113-126.
[10] Moravskyi V., Tymkiv I., Bodnarchuk P., Dulebova L., Suberlyak O., Filled polymeric compositional materials. In: Technological and design aspects of extrusion and injection moulding of thermoplastic polymer composites and nanocomposites. Vol.4, [Red:] Sikora Janusz, Greškovič František. – Lublin: Politechnika Lubelska, 2016, 19-30.
[11] Moravskyi V., Dziaman I., Suberliak S., Kuznetsova M., Tsimbalista T., Dulebova L. Research into kinetic patterns of chemical metallization of powder-like polyvinylchloride. Eastern-European Journal of Enterprise Technologies 2017, 4, 88, 50-57.

Edited by : prof. Janusz W. SIKORA Ph.D., D.Sc.
Assoc. Prof. Ľudmila Dulebová, Ph.D., D.Sc.

Reviewed by: Prof. Ernest Gondár, Ph.D., D.Sc.,
Wiesław Jan Frącz, Ph.D., D.Sc.
Mykola Brailo, Ph.D., D.Sc., Assoc. Prof.

Tittle: **Technological and design aspects of the processing of composites and nanocomposites Volume I**

Publisher:
Technical University of Kosice, Fakulty of Mechanical Engineering, Letna Str. 9 , 040 01 Kosice, Slovakia, First Edition, 2018, 195 pages

Print: 100 pieces

Printed by: Technical University of Kosice, Letna Str. 9 , 040 01 Kosice

ISBN 978-80-5553-2773-0


9 788055 327730